

Development and Application of a Flow-Through Sampler for Semi-Volatile Organic Compounds in Air

by

Hang Xiao

A thesis submitted in conformity with the requirements
for the degree of Ph.D.

Department of Chemical Engineering and Applied Chemistry
University of Toronto

© Copyright by Hang Xiao 2008

Development and Application of a Flow-Through Sampler for Semi-Volatile Organic Compounds in Air

Hang Xiao

Ph.D.

Department of Chemical Engineering and Applied Chemistry
University of Toronto

2008

Abstract

The investigation of the atmospheric fate and transport of semi-volatile organic compounds (SOCs) often requires the sampling of large volumes of air ($>100 \text{ m}^3$) in a relatively short period of time. Conventionally high-volume pumps are not suitable for remote areas without access to reliable network power. We have developed a flow through sampler for such situations. It consists of a horizontally-oriented flow-tube, that can collect gaseous and particle-bound SOCs from large volumes of air by turning into the wind and having the wind blow through a porous sampling medium such as polyurethane foam. Through both indoor and outdoor experiments, we quantified its air sampling rate (through battery operated anemometers inside and outside of the flow tube), its sampling efficiency (by theoretical plate number analysis of the break-through curves for PCBs, PAHs, OCPs and PBDEs), and its accuracy (by comparison of concentrations, time trends, temperature dependences and isomer ratios with those obtained by conventional high-volume sampling) under conditions of constant and variable meteorological conditions (wind speed, temperature). The flow-through sampler was deployed to monitor SOC concentrations at a remote Chinese research station located close to Nam Co Lake, Tibet. During the campaign, fifteen 1 month-long samples were taken, corresponding to sample volumes between 5,000 and 20,000 m^3 . Despite those large sample volumes, only HCB and HCHs

experienced break-through, but application of frontal chromatograph theory allows the estimation of breakthrough-corrected air concentrations even for those relatively volatile SOCs. The pesticide levels at Nam Co are generally very low. Most pesticides had higher levels during summer, resulting in a strong temperature dependence. This is correlated with air mass origin across the Himalayas in the Gangetic plains of India and Bangladesh. The flow through sampler constitutes a feasible method for reliably and quantitatively collecting SOCs from large air volumes.

Acknowledgments

There are many people to whom I am deeply indebted and who I would like to thank. At the top of this long list is my supervisor, Dr. Frank Wania, who showed me what it is to be a dedicated, confident and thorough researcher. The project would have become a mission impossible without his inspiring guidance, generous support and patience throughout the period of my study.

Ying Lei has always been helpful with the projects, and I am grateful not only for all the effort she has put towards my thesis, but also some valuable suggestions for real life.

Thanks go also to my supervisory committee members, especially Dr. Terry Bidleman. I have been fortunate to have such a great committee. Your enthusiasm, thoughtful insight and advice were invaluable to the completion of this thesis.

Dr. Hayley Hung, Dr. Tom Harner, Dr. Mahiba Shoeib and Phil Fellin have also provided helpful suggestions and great assistance to many aspects of my work.

For the congenial atmosphere in the lab, I also would like to thank Li Shen, Yushan Su, Sung-Deuk Choi, Todd Gouin, Gillian Daly, Torsten Meyer, Junlin Zhao, Steve Hayward, Chuba Shunthirasingham, Johnny Westgate, Trevor Brown and other past and present members of Wania group. Your friendship and selfless help are much appreciated.

I would like to thank Fiona Wong, Dr. Yuan Yao, Sum Chi Lee and other “POP Stars” for their helping hand and willingness to share instruments during busy experimental time.

The Nam Co sampling campaign was completed in collaboration with Mark Loewen, Shichang Kang, Qianggong Zhang, Wenwu Han and Ciren Duoji.

I am grateful to the staff at the University workshops, especially Johnny Lo, John Ford and Jacek Jackiewicz for building the sampler.

The encouragement from Professor Guolan Huang and the help from Yinan Zhang and Yi Guo are also appreciated.

Thanks to all the reviewers of the research papers included in this thesis. Their thoughtful and helpful comments have improved the quality of my work.

Acknowledgement is also made to the NSERC and NCP for financial support.

Finally I would like to show my appreciation to my parents, my family and my mother-in-law, who have always given me unconditional love and continuous encouragement. I wouldn't have come this far on this journey if they weren't there. And special thanks to my wife, Lina, and my daughter, Claire, your love gives me a ray of sunshine during the rainy days.

Table of Contents

Acknowledgments.....	iv
Table of Contents.....	iv
List of Tables	x
List of Figures	xiii
Chapter 1 Overview	1
1 Brief	1
1.1 Persistent Organic Pollutants	1
1.2 Semivolatile Organic Compounds in the Atmosphere.....	2
1.2.1 SOCs in Tibetan Plateau	3
1.3 Sampling Techniques for SOCs in the Atmosphere	4
1.3.1 Active Air Sampling Techniques.....	4
1.3.2 Passive Air Sampling Techniques	6
1.4 Structure of This Thesis.....	9
Chapter 2 Development and Indoor Characterization of a Flow-Through Air Sampler for Semi-Volatile Organic Compounds	10
2 Brief	10
2.1 Introduction.....	10
2.2 Methods.....	12
2.2.1 Sampler Design.....	12
2.2.2 Controlled Breakthrough Experiments	14
2.2.3 Frontal Chromatographic Theory	16
2.3 Results and Discussion	19

2.3.1	Sampling Rates	19
2.3.2	Breakthrough Curves	20
2.3.3	Theoretical Plate Numbers and Breakthrough Volumes	21
2.3.4	Comparison with HiVol Samples	24
2.4	Acknowledgements.....	26
2.5	Supporting Information Available	27
Chapter 3 Field Testing a Flow-Through Sampler for Semi-Volatile Organic Compounds in		
	Air	28
3	Brief	28
3.1	Introduction.....	28
3.2	Method	29
3.2.1	Sampling Procedure	29
3.2.2	Sample Extraction and Quantification	31
3.2.3	QA/QC	31
3.3	Result and Discussion.....	32
3.3.1	Wind speed correlation	32
3.3.2	Break-through profile for different compound groups	36
3.3.3	Comparison of Flow-through samples with HiVol data.....	37
3.3.4	Effect of temperature and wind speed on the theoretical plate number.....	42
3.4	Acknowledgements.....	44
3.5	Supporting Information Available	44
Chapter 4 Validation of a Flow-Through Sampler for PBDEs and Pesticides in Air.....		
4	Brief	45
4.1	Introduction.....	45

4.2 Method	47
4.2.1 Sampling procedure and sample analysis	47
4.2.2 QA/QC	48
4.3 Result and Discussion	49
4.3.1 Break-through profile for PBDEs and OCPs	49
4.3.2 Comparison of Flow-through samples with HiVol data	51
4.3.3 Linear solvation energy relationship (LSER) prediction of the theoretical plate number, <i>N</i>	57
4.4 Acknowledgements	61
4.5 Supporting Information Available	61
Chapter 5 Seasonal Variation of Pesticides and PCBs in the Atmosphere at Nam Co, Tibet	62
5 Brief	62
5.1 Introduction.....	62
5.2 Method	64
5.2.1 Sampling site.....	64
5.2.2 Sampling Procedure	65
5.2.3 Sample Extraction and Quantification	66
5.2.4 QA/QC	67
5.2.5 Back Trajectory Analysis.....	67
5.3 Results and Discussions.....	68
5.3.1 Sampled air volumes.....	68
5.3.2 PCBs.....	68
5.3.3 Air concentration for pesticides.....	69
5.3.4 Breakthrough level estimations.....	69
5.3.5 Seasonal variation of pesticides.....	74

5.4 Acknowledgements.....	80
5.5 Supporting Information Available.....	80
Chapter 6 Synthesis, Conclusions and Outlook.....	81
6 Brief.....	81
6.1 Synthesis.....	81
6.2 Conclusions.....	82
6.3 Guidelines.....	85
6.4 Outlook.....	85
REFERENCES.....	90
Appendices.....	104
Appendix I Supporting Information for Development and Indoor Characterization of Flow-Through Air Sampler for Semi-Volatile Organic Compounds.....	104
Appendix II Supporting Information for Field Testing a Flow-Through Sampler for Semi- Volatile Organic Compounds in Air.....	114
Appendix III Supporting Information for Validation of a Flow-Through Sampler for PBDEs and Pesticides in Air.....	143
Appendix IV Supporting Information for Seasonal Variation of Pesticides and PCBs in the Atmosphere at Nam Co, Tibet.....	162

List of Tables

Table 1-1. Equations used to describe the eluting front shapes. Normalized flux (J/J_0) is represented as a function of relative retention time $\tau = t/t_R$, while φ is the normal distribution and Φ is its integral: $\varphi(x) = [1/(2\pi)^{1/2}] \exp(-x^2/2)$; $\Phi(x) = \int_{-\infty}^x \varphi(p) dp = (1/2) \operatorname{erfc}(-x/2^{1/2})$ (Lövkvist and Jönsson 1987)	5
Table 2-1. Required sampling time for 1000 m ³ of air under different wind speed conditions.	20
Table 3-1. Average temperature T, average wind speed within flow through sampler u_{in} , and sampled air volume V_{air} calculated with two different methods for each sampling period.	30
Table 3-2. Average concentrations (pg/m ³) of PCB and PAH congeners measured at Toronto urban sites.	41
Table 4-1. Comparison of concentrations (pg/m ³) of PBDEs and pesticides measured in this study with reference values for Toronto urban sites.	58
Table 5-1. Comparison of LSER predictions of PUF/air partitioning with breakthrough corrected apparent partition coefficients.	74
Table 5-2. Seasonal average OCPs concentrations (pg/m ³) at Nam Co and comparison with literature values reported in Tibetan Plateau regions.	75

Table SI 1.	Chemical amounts trapped in each P10z PUF disc in ng.	107
Table SI 2.	L_{50} from the non-linear regression equation (2-1) and its standard deviation. ...	111
Table SI 3.	The theoretical plate number N , breakthrough volume V_B , and their standard deviation for different sampled air volumes.	112
Table SI 4.	Paired two sample t-test results for nine volatile compounds before and after breakthrough level corrections. The subscript represents approximate sampling days.....	113
Table SI 5.	Field-blank corrected amounts of individual PCB congeners and individual PAHs trapped in each P10z PUF disc in nanograms.....	123
Table SI 6.	The theoretical plate number N , and their standard deviation for different sampling periods, and the temperature dependence of $\log P_L$ from references.....	130
Table SI 7.	Field-blank corrected chemical amounts trapped in HiVol samples in nanograms and their average temperature and sampled air volumes. v_i is the air volumes sampled by the FTS at the same period.	131
Table SI 8.	Average field blanks and LODs in nanograms for different sampling methods and media.	141
Table SI 9.	Field-blank corrected amounts of individual organochlorine pesticides and individual PBDEs congeners trapped in each P10z PUF disc in nanograms.	143
Table SI 10.	The theoretical plate number N , and their standard deviation for different sampling periods.	148
Table SI 11.	Field-blank corrected chemical amounts trapped in HiVol samples in nanograms and their average temperature and sampled air volumes. v_i is the air volumes sampled by the FTS at the same period.	149

Table SI 12. Average field blanks and LODs in nanograms for different sampling methods and media.	159
Table SI 13. Paired sample t-test results for comparing the differences between the FTS concentrations and weighted / unweighted average of HiVol concentrations with zero, which show only May-June concentrations derived from FTS and HiVol are significantly different from each other.	161
Table SI 14. The meteorological parameters for each flow through sampler.	163
Table SI 15. Average field blanks and LODs in nanograms for different chemicals.....	164
Table SI 16. Field-blank corrected amounts of individual PCBs congeners trapped in each P10z PUF disc in nanograms.	165
Table SI 17. Field-blank corrected amounts of individual pesticides trapped in each P10z PUF disc in nanograms.	166
Table SI 18. Breakthrough corrections for HCB, α -HCH and γ -HCH	169
Table SI 19. Concentrations and relative abundance for HCHs, Endosulfans and DDTs.	172

List of Figures

- Figure 2-1. Technical drawing and photograph of the flow-through air sampler. 13
- Figure 2-2. Vapor fronts of selected PCB congeners and anthracene for different sampling lengths. The black, red, green and blue colour represent sampling volumes of 125 m³, 368 m³, 793 m³ and 1360 m³, respectively. The upper left panel illustrates the approach to determine L_{50} and theoretical plates number N from the breakthrough curves. 17
- Figure 2-3. The breakthrough level b a function of relative breakthrough volume τ and plate numbers N 19
- Figure 2-4. Correlation between the outside windspeed and the windspeed inside the sampling tube after passage through a 17.8 cm thick PUF plug. 21
- Figure 2-5. Relationship between the sampled air volume and the L_{50} values illustrating the linear movement of PCB-18, 28, 74 and 118 vapor fronts through the PUF plugs. The breakthrough volume, V_B , is determined by extrapolating these linear relationships to the overall PUF plug length of 17.8 cm. 22
- Figure 2-6. Plots of theoretical plate number N and breakthrough volume $\log V_B$ versus vapor pressure of the subcooled liquid $\log P_L$ for PCBs (open circles) and PAHs (filled triangles). The dashed line is the regression for PCBs only. The solid line is the regression line for PCBs and PAHs. 23
- Figure 2-7. Comparison of air concentrations for PCBs and PAHs as obtained using a conventional active air sampler and the flow-through air sampler with variable sampling volume. The panel in the upper left compares air concentrations obtained by active air sampling in this study with those obtained in the same laboratory previously. The different colours represent different sampling volumes; and the dashed lines are the regression for both PCBs and PAHs.. 25

Figure 3-1. The relationship between the wind speed outside the FTS and after passage through the PUF plugs (black: August, red: November, blue: December, green: April). The bottom panel shows the fitting result from the non-linear regression equation 3-3. 33

Figure 3-2. Vapor fronts of selected PCB congeners and phenanthrene from different sampling periods. The black, red, green, blue and purple color represent samples taken during August, November, December, April and May, respectively. The upper left panel illustrates the approach to determine L_{50} and theoretical plates number N from the breakthrough curves. 34

Figure 3-3. Comparing the air concentrations of individual PCB congeners obtained using the flow through sampler with those obtained using 24-hour HiVol samples (total gas+particle concentrations) taken during the same sampling period. The bottom right panel shows the regression lines between the FTS concentrations and the weighted average of HiVol concentrations for different sampling sets. 37

Figure 3-4. Comparing the air concentrations of PAHs obtained with the FTS with the 24-hour HiVol samples taken during the same sampling period. The bottom right panel shows the regression lines between the FTS concentrations and the weighted average of HiVol concentrations for different sampling sets. 38

Figure 3-5. The relationship between the apparent theoretical plate number, N , and the vapour pressure P_L of the analytes for the five flow through samples reveals a temperature and wind speed effect on N . Average wind speed during sampling increases from November, May, August, December to April, whereas average temperature decreases from August, May, April, November to December. Panel A shows all chemicals, panel B only the gas phases compounds, and panel C the partially particle-bound chemicals. In panel C the line with the same color as the symbol represents the projection of the multi-linear regression result for different samples. 43

Figure 4-1. Vapor fronts of selected organochlorine pesticides and PBDE-47 from different sampling periods. The black, red, green, blue and purple color represent samples taken during August, November, December, April and May, respectively. The upper left panel illustrates the approach to determine L_{50} and theoretical plates number N from the breakthrough curves. 50

Figure 4-2. Comparing the air concentrations of PBDEs (black markers) and pesticides (blue markers) obtained with the flow through sampler with the 24-hour HiVol samples taken during the same sampling period. The red markers are values for PBDE-209. The bottom right panel shows the regression lines between the FTS concentrations and the weighted average of HiVol concentrations for different sampling sets (PBDEs - solid lines, pesticides - dashed lines). 51

Figure 4-3. Comparison of time trends in the air concentrations of selected chemicals as derived by FTS (bars, the two horizontal lines indicate the uncertainty introduced by the sample volume estimation) and HiVol sampler (square markers). 54

Figure 4-4. Apparent temperature dependence of air concentrations derived by FTS and active sampling for dominant pesticides and PBDE congeners. The solid and dashed lines represent the regression for HiVol samples and FTS, respectively..... 55

Figure 4-5. Comparison of Chlordane and HCH concentrations (bottom panel, the black and red color represent different isomers respectively) and TC/CC and α -/ γ -HCH ratios (top panels) as derived by FTS (bars, the two horizontal lines indicate the uncertainty introduced by the sample volume estimation) and HiVol sampler (markers). 56

Figure 4-6. Comparison between the LSER prediction of the theoretical plate number, N from equation 4-6 with the experimental results for PCBs, PAHs and pesticides. 61

Figure 5-1. Terrain maps from Google map showing the Nam Co station (point A) and surrounding. 64

Figure 5-2. Comparison of experimentally determined back to front ratios and middle plus back to front ratios of HCB, α -HCH and γ -HCH in FT samples with such ratios predicted using frontal chromatographic theory..... 71

Figure 5-3. Temperature dependence of the apparent PUF/air partition coefficient for HCB, α -HCH and γ -HCH calculated from the break-through corrected ambient air concentrations. The extrapolated values at 15°C (open markers) are compared with LSER predicted partitioning coefficients in Table 1-1. 73

Figure 5-4. Airsheds (5-day back trajectory probability maps) calculated with the HySplit model highlighting the regions where the air most likely came from during each sampling period. 77

Figure 5-5. Seasonal variation (left) and temperature dependence (right) of the atmospheric concentrations of HCB, α -HCH, γ -HCH (top), endosulfan- (middle) and DDT-related substances (bottom) at Nam Co. 78

Figure SI 1. Wind resistance for different arrangements of sampling media. 105

Figure SI 2. The correlation between the wind speed recorded by the vortex sensor on top the sampler and the windspeed recorded by the vane sensor mounted at the exit of sampling tube for four different sampling periods..... 119

Figure SI 3. Histograms showing the distribution of wind speeds measured by the vortex sensor on top of the FTS during each sampling period. The y-axis is the percentage of time. The red lines represent the percentage of the sampled air volume that was collected while u_{out} was within that particular wind speed range. 121

Figure SI 4. Observed gas/particle partition behavior of PCBs and PAHs from selected HiVol samples. 122

Figure SI 5. Example of a “spaghetti” plot showing 5-day backward trajectory for a FTS sampling period. The percentage of the lines passing through each 0.5×0.5 degree grid cells was calculated from this plot and represents the possibility of the air mass originating from this particular area..... 162

Chapter 1 Overview

1 Brief

1.1 Persistent Organic Pollutants

Since the publication of *Silent Spring* in the early 1960s (Carson 1962), the harm of organochlorine pesticide residues in the environment, such as dichlorodiphenyltrichloroethane (DDT), has aroused worldwide concern. With the advance of instrumental analytical methods, more organic compounds with similar characteristics, such as dieldrin, toxaphene, and polychlorinated biphenyls (PCBs), have been detected in virtually every environmental medium and every geographic region of the global environment. Beginning in the 1970s, more and more countries passed legislation to regulate the production and use of such compounds. In recent years, several international agreements have been negotiated with the aim to eliminate or restrict the use of these chemicals of concern. One of these agreements is the Stockholm Convention on Persistent Organic Pollutants (POPs). POPs are a class of organic compounds, which are persistent and subject to long range transport and can cause adverse effects on the environment and human beings by virtue of being both bioaccumulative and toxic (<http://www.pops.int/>).

The twelve chemicals/chemical groups initially designated by the Convention (often called the “dirty dozen”) can be classified into three categories: pesticides, industrial chemicals and unintentional by-products (Stockholm Convention on Persistent Organic Pollutants, 2005, <http://www.pops.int/>). The pesticide group includes aldrin, chlordane, DDT, dieldrin, endrin, heptachlor, hexachlorobenzene (HCB), mirex and toxaphene; the industrial chemicals are PCBs; and polychlorinated dibenzo-p-dioxins and dibenzofurans (PCDD/Fs) are the unintentional by-products. The Convention provides for the elimination of nine of those chemicals, restrictions on the production and use of DDT, and guidance on the best available techniques and best environmental practices for preventing or reducing the release of unintentional by-products (Kohler 2006). Taking measures to prevent the introduction of new POPs into commerce, the Convention defines criteria for screening of new POPs in terms of persistence, bioaccumulation, potential for long-range transport, and toxicity.

1.2 Semivolatile Organic Compounds in the Atmosphere

Once emitted into the environment, POPs partition among various environmental media such as the atmosphere, water, soil, sediments and biota. In the atmosphere, these chemicals are simultaneously present in the gas phase and associated with airborne particles (Kaupp and McLachlan 1999). Due to their multimedia environmental behaviour, the POPs belong to the group of semi-volatile organic compounds (SOCs). The vapour phase to particle phase ratio of SOCs is determined by the concentration (total suspended particles, TSP) and composition (organic matter content) of the atmospheric particles and the volatility of the chemicals, which in turn depends on temperature (Bidleman 1988). As environmental conditions change, the resulting shifts in gas/particle partitioning could significantly affect the removal rate of SOCs from atmosphere by degradation and dry and wet deposition processes, which ultimately determines their travel distance from source regions (Fernández and Grimalt 2003).

The concept of “cold condensation” was developed to explain the pervasive occurrence of SOCs in remote cold regions (Wania and Mackay 1993; Wania and Mackay 1996). It refers to SOCs transferring from the gas phase to surface media as temperature drops. This leads to the enrichment of persistent SOCs in cold regions at high latitude and altitude due to the spatial temperature gradients on a latitudinal or vertical scale. Similar to a fractionated distillation process, on their journey from warmer source regions to remote areas, the mixture SOCs will be separated (fractionated) with distance because of differences in their physico-chemical properties and ambient temperature (Wania and Su 2004). This phenomenon has been termed “global fractionation”. As a result, more volatile compounds are more likely to travel further before deposition/partitioning to surface media in colder regions, while relatively heavy compounds will be deposited and accumulate close to their source, and need more time/cycles to reach remote sinks.

The atmosphere is the major transport pathway for SOCs, and atmospheric deposition is the major means by which PCDD/Fs and pesticides (like DDT, chlordane, ect.) accumulate in pristine environments, such as the sediments of Siskiwit Lake (an isolated lake in a remote island inside Lake Superior) (Czuczwa, McVeety and Hites 1984) and in the Arctic (Su et al. 2008). It has been hypothesized that SOCs tend to volatilize from relatively warm source regions, undergo efficient atmospheric transport over considerable distances, and deposit in very remote locations

with low temperatures (Wania 1999; Wania and Mackay 1993). Such “cold condensation” effects could have strong adverse effects on the ecosystems and humans living in cold regions.

Under the Stockholm Convention, signatory countries are required to compile source inventories, identify ongoing sources, and provide environmental monitoring evidence that ambient levels of SOCs are declining. Because of the very immediate response of air concentrations to changes in emission, air monitoring is particularly well suited for these tasks. Several atmospheric SOC monitoring networks operating for a long time not only provide evidence to identify source contributions (Hoff, Muir and Grift 1992), but also illustrate atmospheric half-lives (Hung 2001).

1.2.1 SOCs in Tibetan Plateau

Remote locations without local pollution sources are ideal sites for monitoring the LRAT of SOCs. Many studies confirmed that cold-trapping and compositional shifts occur on both latitudinal (Agrell et al. 1999; Ockenden et al. 1998; Wania and Su 2004) and vertical gradients (Davidson et al. 2003; Grimalt et al. 2001). Due to the closer spatial proximity to source regions and the high precipitation rate in mountain regions, the chemical transfer efficiency from valley to mountain may be higher than that from tropical to polar regions (Blais et al. 1998).

Known as the “Third Pole on the Globe”, the Tibetan Plateau is the highest plateau on Earth, with an average elevation of 4200 m asl. The surrounding mountain areas also experience tremendous elevation gains and temperature gradients over relatively small distances. Because of the plateau’s high altitude, sparse human population, and minimal to non-existent industrial activities, LRAT is believed to be the dominant source of POPs to the area (Loewen et al. 2007). The plateau is surrounded by rapidly industrialized countries, such as China and India, which also have the largest population and intensive agricultural practices (Li and Macdonald 2005; Li et al. 1998). It has been suggested that mountain cold-trapping may be particularly pronounced in the Himalaya and the Tibetan Plateau (Daly and Wania 2005).

Compared with the long-term intensive atmospheric monitoring programs in the Arctic, studies illustrating the LRAT and the fate of POPs in the Tibetan plateau region are relatively rare. Also, most studies investigated the deposition and accumulation of SOCs in water, soil, sediments, snow/ice and biota (Wang et al. 2006; Wang et al. 2007a; Wang et al. 2007a; Wang et al. 2007b; Wang et al. 2008b; Yang et al. 2007; Yang et al. 2008; Zhang and Zhang 2003). Only a limited

number of studies focused on short-term variations in the atmospheric concentrations of pesticides (Cheng et al. 2007; Li et al. 2006). Thus a relatively long-term study focusing on the seasonal variation of atmospheric concentration of SOCs in Tibet region is needed.

1.3 Sampling Techniques for SOCs in the Atmosphere

Because of the low air concentrations of SOCs, investigating the atmospheric fate of these contaminants poses considerable challenges as to how air is being sampled for analysis. The aim of this thesis project was to develop a new sampling technique that could provide temporally resolved air concentration at very remote sites. Since two recent reviews have summarized strategies, methodologies and other aspects of air sampling for SOCs (Bohlin, Jones and Strandberg 2007; Xie and Ebinghaus 2008), here I will only briefly discuss the theory as well as the advantages and disadvantages of each category of sampling techniques.

Typically, either long-term monitoring programs or short-term intensive studies are being conducted when studying SOCs in the atmosphere. The advantages of long-term monitoring programs are the possibility to provide information on spatial and temporal variability, on the relative influence of long and short-range transport, on the regional background and on long-term temporal trends. Short-term intensive studies provide more information on the processes governing sources, transport and deposition, such as the urban/industrial influence, specific sources to an urban/industrial area and short-term fluctuations in concentrations due to meteorology, source strength and photochemical reactions (Simcik 2005). The approach taken is often determined by a compromise between monetary constraints and the desired information. In either type of studies, the methodological choices include active and passive air sampler approaches.

1.3.1 Active Air Sampling Techniques

The commonly used active air sampling techniques for monitoring SOCs utilize a pump to force air through the sampling module and a flow meter to measure the flow rate of air through the sampler. The pump and the flow meter require power by electricity or battery. Based on the flow rate, the samplers can be divided into three types: low-, medium- and high volume samplers (LowVol/MeVol/HiVol). HiVol samplers with a flow rate up to 1400 L/min are most widely used in routine monitoring networks. Airborne particle and gas phase compounds are normally

separated by downstream filters or upstream diffusion denuder devices during the sampling procedure (Bidleman 1988). A glass, quartz fibre or Teflon filter is often used to collect particle; and polyurethane foam (PUF) plugs, XAD resins, Tenax or a combination of different sorbents is utilized to trap vapour phase compounds.

Table 1-1. Equations used to describe the eluting front shapes. Normalized flux (J/J_0) is represented as a function of relative retention time $\tau = t/t_R$, while φ is the normal distribution and Φ is its integral: $\varphi(x) = [1/(2\pi)^{1/2}] \exp(-x^2/2)$; $\Phi(x) = \int_{-\infty}^x \varphi(p) dp = (1/2) \operatorname{erfc}(-x/2^{1/2})$ (Lövkvist and Jönsson 1987)

J/J_0	eq. no.
$\Phi[n^{1/2}(\tau - 1)]$	(1-1)
$\Phi[n^{1/2}(\tau - 1)] + \Phi[-n^{1/2}(\tau + 1)]$	(1-2)
$\Phi[n^{1/2}(\tau - 1)/\tau^{1/2}]$	(1-3)
$\Phi[n^{1/2}(\tau - 1)/\tau^{1/2}] + [1/2(n\tau)^{1/2}] \times \varphi[n^{1/2}(\tau - 1)/\tau^{1/2}]$	(1-4)
$\Phi[n^{1/2}(\tau - 1)/\tau^{1/2}] + \exp(2n) \times \Phi[-n^{1/2}(\tau + 1)/\tau^{1/2}]$	(1-5)

Regardless of the flow rate and the design of the apparatus, the basic goal of all pumped samplers is to quantitatively strip the chemicals of interest from the air stream. With respect to the uptake mechanism, the sampling cartridge filled with a solid sorbent constitutes a frontal chromatographic column: sample is continuously introduced to the column and subsequently blown through the column by the air flow. A long sampling duration and/or high flow rates enhances the risk of losing volatile compounds due to breakthrough. Several equations have been developed to describe the shape of an eluting front (i.e. the breakthrough curve) (see Table 1-1) (Lövkvist and Jönsson 1987). The simplest one (equation 1-1) assumes the front shape can be expressed as the integral of a Gaussian peak. But such an assumption is only valid for columns with a relatively high theoretical plate numbers, N , because it implies instantly breakthrough for lower N values, which is obviously unrealistic. When comparing these equations, Lövkvist and Jönsson concluded equation 1-5 to be most suitable to describe the vapour front curves for columns with very low plate numbers; and derived a general expression of sampling capacity as

a function of retention volume and N , which can describe the breakthrough level (Lövkvist and Jönsson 1987).

Since the late 1970s, Bidleman and co-workers expended great effort to investigate the retention efficiencies of PUF plugs for selected PCBs, PAHs and pesticides (Bidleman et al. 1984; Burdick and Bidleman 1981; Simon and Bidleman 1979; You and Bidleman 1984). A HiVol active sampler was modified and functioned as a “high volume gas chromatograph” in those studies. The N values and breakthrough volumes for those compounds under the experimental conditions were given. Guidelines of maximum safe sampling volumes for certain desired breakthrough level were also provided. Unfortunately, these guideline values were seldom followed during field sampling campaigns because the real field conditions did not necessarily resemble those in the controlled experiments. In practice, breakthrough levels were only monitored by comparing the amount on two PUF plugs in series. A lot of studies simply ignored that some SOCs may have suffered breakthrough.

Although breakthrough levels are hardly well characterized for different sampling settings and/or chemicals, active sampling techniques are considered the accepted quantitative methods in most cases because the volume of air passing through the sampler is known. Because of short sampling periods, active sampling techniques are suitable to evaluate accidental chemical exposure for risk assessment purposes.

Active sampling approaches are generally quite expensive and labor intensive. They are often not suitable for sampling in remote locations or developing countries due to their reliance on a pump and a reliable power supply. Also it is not practical to use active samplers to sample simultaneously at a large number of locations. They are therefore not suitable for investigating in detail the spatial variability of SOC air concentrations.

1.3.2 Passive Air Sampling Techniques

Responding to a growing need for inexpensive and simple monitoring of SOCs in the atmosphere, several so-called passive air sampling techniques have been developed in recent years. Passive air sampler (PAS), which are often also referred to as diffusive air sampler, can collect chemicals from the atmosphere without the help of a pump. The fundamentals of passive sampling have been described in detail by Shoeib and Harner and Bartkow *et al.* (Bartkow et al.

2005; Shoeib and Harner 2002a). Basically, a passive sampling medium can be considered a uniform sorbent for the analytes, which can pass freely through the boundary layers between the atmosphere and sorbent. The accumulation of the SOCs in the sorbent is a dynamic process, which is determined by the difference of uptake and eliminate rates. The sorbent/air partition coefficient for a chemical determines the final equilibrium distribution between these two compartments. The dynamic exchange continues until equilibrium between the gas phase and the collection medium has been established or until the sampling is stopped by the user. The resistance to uptake may be from the air boundary layer or from the rate of diffusion into the passive sampling medium. The exchange of chemicals between the passive sampler and the atmosphere undergoes three stages. Initially, the concentration inside the sampling media is close to zero, the elimination rate can be ignored and the sampling rate will be determined solely by the uptake rate. Thus the sampled amount will be linearly related to the deployment time and the atmospheric concentrations during the sampling period. As the deployment time increases, the concentration in the sampler increases as well, as does the elimination rate. The uptake enters a curvilinear stage before approaching equilibrium. Normally, PAS are operated either in the linear uptake stage or the equilibrium stage.

A sampler, which remains in this linear phase for a given compound during a deployment period, is said to be operating as a kinetic sampler. The PUF disk sampler (Jaward et al. 2004; Shoeib and Harner 2002a) and the XAD-resin (Shen et al. 2004; Wania et al. 2003) based sampler are the most widely used kinetic samplers. For this kind of sampler, the sampling rate, R_S , expressed as the air volume in contact with the sampling medium per time unit, needs to be established to determine air concentrations. Commonly, this is achieved by calibration with active sampling data or through the use of performance reference compounds (PRCs). Each method has its own advantages and limitations. The uptake of most chemicals of interest could be calibrated through comparison with active samples. However, the accuracy of the calibration could be influenced by the fact that it is hardly ever possible to cover the whole PAS deployment periods by active sampling, as well by the unquantified effects of environmental variables, such as temperature and wind speed. In contrast, PRCs are exposed to the same environmental conditions as the target analytes for the whole sampling length. Theoretically, their use should be an ideal way to account for environmental influences in the calibration. For an accurate calculation of the elimination rate of PRCs, a certain percentage range of compound is supposed to remain in the

sampling media. It is impossible to find a “gold standard” suitable for all environmental conditions. In addition, for best calibration results, the PRCs is supposed to be evenly distributed inside the sampling medium, thus the practice for spiking of PRCs still needs to optimized (Harner et al. 2006a).

Polymer-coated fibers (Khaled and Pawliszyn 2000), polymer-coated glass (Harner et al. 2003) and window films have a small sampling capacity and operate at the equilibrium stage. For this kind of sampler, the equilibrium time and partition coefficients are the most important parameters. The deployment/equilibrium time for these samplers can be as short as minutes. However, the small capacity makes them not suitable for chemicals with low atmospheric concentrations. Another drawback is that the air–sampling medium partition coefficients are not generally available. So the octanol–air partition coefficient (K_{OA}) is often used instead to estimate the air concentrations, which may cause significant errors.

Whatever stage a PAS is operating in, most of these approaches employ some kind of structure to shelter the sampling medium from sunlight, precipitation, and large particles subject to gravitational settling. Examples of such structures are Stevenson's screen boxes, cylindrical steel cans (Shen et al. 2004), and hemispherical steel bowls (Jaward et al. 2004; Shoeib and Harner 2002a). These shelters eliminate, or at least reduce, the influence of wind speed on the rate of SOC uptake in the sampling medium. Thus, it allows for the interpretation of the sampled amounts in terms of volumetric air concentrations if the sampling rate and deployment period is known. Various sampler designs have been characterized in terms of their uptake kinetics (Wania et al. 2003). These studies revealed that, in many cases, the uptake is controlled by molecular diffusion to the sampling medium (Wania et al. 2003)

Compared to active samplers, PAS are promising to address the need for spatially resolved atmospheric concentrations of SOCs, because of their capability of time-integrated sampling over extended time period, their independence from power supplies and regular maintenance, and their relatively low production and operating cost.

The main drawback of PAS designs is their limited sampling rate, typically on the order of a few m^3 of air per day (Shoeib and Harner 2002a; Wania et al. 2003). Because low air concentrations of SOCs in remote regions often necessitate large air sampling volumes on the order of 500 m^3 and higher, the low sampling rates of passive air sampling designs imply the need for long

deployment periods on the order of several months to more than a year. Variations in air concentrations on the time scale of months or shorter cannot be resolved, but are often of considerable interest.

In addition, the sampler performance and the influence of environmental variables still need further investigation. It is believed that PAS can estimate the “true concentrations” within a factor of 2-3 (Harner et al. 2006a).

1.4 Structure of This Thesis

This thesis project aimed to develop, test and apply a sampling device which has significantly higher sampling rate than existing PAS, but still does not rely on electrical power. The new sampler, called a flow through sampler (FTS), design utilizes the wind. Basically, a FTS operates as an “active” sampler, but instead of relying on electrical power, it lets the wind blow through the sampling medium. The fundamental part of this development was to characterize quantitatively the uptake mechanisms of the new sampler.

This thesis has two major parts. The first part, consisting of Chapter 2, 3 and 4, involves the development of the FTS. Chapter 2 focuses on the design of the prototype and on controlled indoor experiments. A FTS was tested under controlled conditions of constant temperature, wind speed and air concentrations and frontal chromatograph theory was applied to characterize the sampling train. Chapter 3 and 4 extends the works of Chapter 2, further testing the performance of the new sampler under field conditions during various seasons. The relationship between sampling rate and wind speed was studied. A linear solvation energy relationship (LSER) was used to investigate environmental and chemical effects on the sampling efficiency.

The second part of the thesis comprises chapter 5, and focuses on an application of the FTS. A FTS was deployed at a Chinese scientific research station near Nam Co Lake. Tibet. The performance of FTS under extreme weather conditions was tested. The seasonal variation of the atmospheric concentrations of pesticides in the Nam Co region was studied for the first time.

Chapter 2

Development and Indoor Characterization of a Flow-Through Air Sampler for Semi-Volatile Organic Compounds¹

2 Brief

By forcing the wind to blow through polyurethane foam discs, a new air sampler design achieves high sampling volume while maintaining the ability to provide volumetric air concentrations.

2.1 Introduction

The quantification of trace amounts of semivolatile organic compounds (SOCs) in the atmosphere is required for many applications, for example in efforts to assess the regional and global transport of airborne contaminants and their delivery to receptors such as the aquatic food webs in the Great Lakes or the Arctic Ocean. Conventional air sampling techniques used for SOC_s rely on pumps to pass large volumes of air through or over a sampling medium, which traps the compounds of interest either in the gas phase or sorbed to atmospheric particles. Sampling media include foams, such as polyurethane foam (PUF) plugs, resins, such as polystyrene-divinylbenzene, and glass fiber filters. The need for a pump makes such active sampling approaches generally quite expensive, labor intensive and limited in applicability to locations where network power is readily available. It is thus difficult to sample in remote locations (such as the Arctic and in mountain regions) or developing countries, and to sample simultaneously at a large number of locations, i.e., active air sampling methods are generally not practical for establishing the spatial variability of SOC air concentrations.

¹ Reproduced with permission from Xiao, H.; Hung, H.; Harner, T.; Lei, Y.D.; Johnston, G.W.; Wania, F. *Environ. Sci. Technol.*, **41** (1), 250 -256. Copyright 2007 American Chemical Society.

The sampler was designed by F. Wania, H. Hung, T. Harner, Y.D. Lei with the help of G.W. Johnston. Wind data recording unit of the sampler was modified by H. Xiao. Sampling media selection was tested by H. Xiao under the supervision of H. Hung, T. Harner, Y.D. Lei and F. Wania. Indoor controlled experiments were conducted by H. Xiao. All samples were extracted, cleaned up and quantified by H. Xiao under the supervision of H. Hung, T. Harner and Y.D. Lei. Instrumental analysis was aided by Y.D. Lei. The data were interpreted and the paper was prepared by H. Xiao in consultation with F. Wania.

Responding to a growing need for inexpensive and simple monitoring of SOCs in the atmosphere, several so-called passive air sampling techniques, that collect chemicals from the atmosphere without the help of a pump, have been developed in recent years. These samplers are promising to address the need for spatially resolved atmospheric SOC concentrations, because of their capability of time-integrated sampling over extended time periods, their independence from power supplies and regular maintenance, and their relatively low production and operating cost. The capability of passive air samplers to provide information on the large scale variability of atmospheric SOC concentrations has been shown through the results of continental sampling networks in both North America (Shen et al. 2004) and Europe (Jaward et al. 2004).

Various passive air sampling designs and sampling media have been explored in recent years. Common sampling media include semipermeable membrane devices (SPMD) (Shoeib and Harner 2002a), PUF discs (Jaward et al. 2004; Shoeib and Harner 2002a), polymer-coated fibers (Khaled and Pawliszyn 2000), polymer-coated glass (Harner et al. 2003), and XAD-resin (Shen et al. 2004; Wania et al. 2003). Most of these approaches employ some kind of structure to shelter the sampling medium from sunlight, precipitation, and large particles subject to gravitational settling. Examples of such structures are Stevenson's screen boxes, cylindrical steel cans (Shen et al. 2004), and hemispherical steel bowls (Jaward et al. 2004; Shoeib and Harner 2002a). The fact that these shelters eliminate, or at least reduce, the influence of wind speed on the rate of SOC uptake in the sampling medium is seen as an advantage, because it allows for the interpretation of the sampled amounts in terms of volumetric air concentrations if the sampling rate (i.e., the air volume in contact with the sampling medium per time unit) and deployment period is known. Various sampler designs, therefore, have been characterized in terms of their uptake kinetics (Wania et al. 2003). These studies revealed that, in many cases, the uptake is controlled by molecular diffusion to the sampling medium (Wania et al. 2003).

Molecular diffusion is a slow process and, as a result, sampling rates of passive air sampler designs are quite small, typically on the order of a few m^3 of air per day (Shoeib and Harner 2002a; Wania et al. 2003). Because low air concentrations of SOCs in remote regions often necessitate large air sampling volumes on the order of 500 m^3 and higher, the low sampling rates of passive air sampling designs imply the need for long deployment periods on the order of several months to more than a year. Variations in air concentrations on the time scale of months or shorter cannot be resolved, but are often of considerable interest. The challenge is to

significantly increase the sampling rate of air samplers, while maintaining the ability to provide quantitative information in the absence of network power. Here we present a new sampler design that seeks to address that challenge.

2.2 Methods

2.2.1 Sampler Design

The strategy adapted to greatly increase the sampling rate of an air sampler without the help of a pump is to force the ambient wind to blow through the sampling medium. The sampler consists of a horizontally oriented, aerodynamically shaped, stainless steel flow tube mounted on a post with ball bearings, which allow it to turn into the wind with the help of vanes (Figure 2-1). The sampling medium is placed into an aluminum cylinder of approximately 20 cm length and an inner diameter of 10.5 cm that is screwed into the flow tube assembly. End caps can be screwed onto the ends of the cylinder and thus allow it to be used as a sturdy, temporary, airtight storage and shipping container for samples.

By taking advantage of the wind blowing through the sampler, significantly higher sampling rates than in conventional passive air samplers can be achieved. In contrast to those samplers, however, that rate is no longer a constant but becomes dependent on wind speed. Uptake is no longer controlled by molecular diffusion, but is similar to that in active samplers. This means that it is necessary to record the sampled air volume, if the amount of SOC quantified in the sampling medium is to be converted into volumetric air concentrations or compared between locations differing in wind speed. In the new sampler, the wind speed, after passage through the sampling medium, is recorded by a data logger (MedgeTech Pulse 110, Warner, NH) with the help of a battery-operated turbine anemometer (Landtek Instruments Co. Ltd, Guangzhou, China) mounted at the exit of the flow tube (Figure 2-1). For comparison, the wind speed outside the sampler is recorded with the help of a vortex wind sensor (Inspeed.Com LLC), which is mounted on the top of the sampler (Figure 2-1). Both wind sensors have been precalibrated with a hot wire anemometer (VT-200, KIMO Instruments). The sampled air volume can be integrated from the recorded wind speed.

The wind speed dependence of the sampling rate further implies that sampling is biased toward time periods with higher wind speeds, i.e., contaminant uptake in the sampling medium is

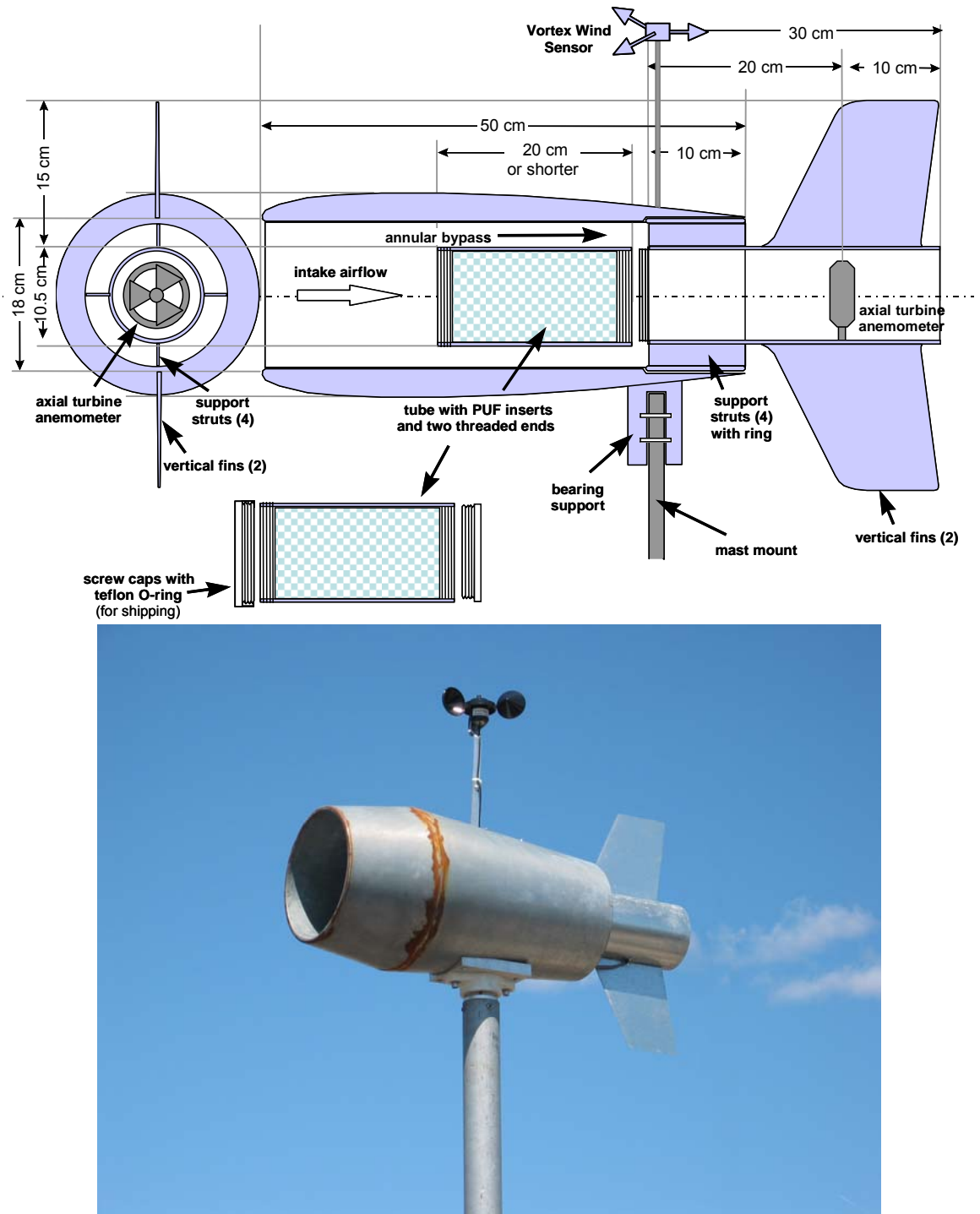


Figure 2-1. Technical drawing and photograph of the flow-through air sampler.

minimal during wind still periods, but rapid during windy days. The sampler design includes an annular bypass (Figure 2-1), which stabilizes the wind speed through the flow tube and reduces the sampling rate during periods of very high wind, thus limiting the extent of sampling bias. Such bias does not occur if SOC air concentrations are constant during the whole sampling period or are independent of wind speed, which is often the case (Hillery et al. 1997; Mandalakis and Stephanou 2002).

To allow air to pass through the flow tube and to collect the SOCs quantitatively from that air stream requires a sampling medium that ideally combines low flow resistance with high uptake efficiency. The suitability of two types of sampling medium, which have previously been used in air sampling, namely ethylene vinyl acetate (Harner et al. 2003; Shoeib and Harner 2002a) coated onto an aluminum honeycomb support structure and polyurethane foam (PUF) discs of variable density, were explored. Preliminary tests showed that the polymer-coated honeycomb displays much lower air flow resistance than the PUF discs, but suffers from low uptake efficiency. On the other hand, PUF discs with a porosity of 10 pores per inch (P10z polyester PUF, Illbruck Foamtec, Minneapolis, MN) appeared to provide both low wind resistance and low breakthrough level (see the Supporting Information for detailed experimental setup and results). Thus, P10z PUF was selected as the medium for further testing.

2.2.2 Controlled Breakthrough Experiments

The sampler was tested for breakthrough by sampling indoor laboratory air for variable lengths of time under conditions of constant wind speed, temperature and air concentrations. The samples were analyzed for a wide range of polychlorinated biphenyls (PCBs) and polycyclic aromatic hydrocarbons (PAHs). PCB concentrations in this laboratory had been measured and reported previously based on samples taken by active high volume (HiVol) pumps (Shoeib and Harner 2002a). For comparison, an additional active HiVol air sample was taken during the time period of the experiments. Most of the procedures are the same as the previous study (Shoeib and Harner 2002a). Seven P10z PUF discs of 2.54 cm thickness (i.e. one inch) with a diameter of 11 cm and a weight of approximately 7.5 g were arranged in series inside the sampling cylinder. Prior to exposure, the discs were pre-cleaned with water and by Soxhlet extraction for 24 hours using acetone and then for another 24 hours using petroleum ether (PE). PUF discs were dried in a desiccator and stored in glass jars with Teflon lined lids. To avoid contamination, sample

installation was performed in a clean lab. Air was sampled for periods of approximately 1 day, 3 days, 6 days and 11 days. A large box fan was used to generate a constant air flow inside a contaminated lab, kept at a temperature of 24 ± 1 °C. The wind speed after passage through the PUFs and outside the sampler were 0.17 ± 0.02 m/s and 3.5 ± 0.4 m/s, respectively. Based on the integration of the wind speed data, the total sampled air volumes for these four experiments were 125 ± 15 m³, 368 ± 43 m³, 793 ± 89 m³ and 1360 ± 162 m³ respectively. For each sampling period, a field blank was taken, whereby a PUF disc was sealed in aluminum foil and placed beside the flow-through sampler for the length of the experiment.

The four sets of seven PUF discs from the flow-through sampler and the front and back PUF of the pumped sample were extracted individually by Soxhlet with acetone and PE (1:1) for 24 hours. The glass fiber filter (GFF) was Soxhlet-extracted for 24 hours using dichloromethane (DCM). The extracts were reduced in a rotary evaporator under vacuum to ~5 mL, transferred to a vial and reduced under a gentle nitrogen flow to 0.5 to 1 mL, and then cleaned on a 3 g alumina column. The column was washed first with ~15 mL of 5% DCM in PE and, after application of the sample, was eluted with 15 mL of 5% DCM in PE. The sample was exchanged to isooctane and reduced again to 1 mL under a minimal nitrogen flow before instrumental analysis. Mirex (100 ng) was added as internal standard to correct for volume differences.

Samples were analyzed for 54 individual PCB congeners (8, 18, 17, 15, 16+32, 31, 28, 33, 52, 49, 44, 42, 37, 74, 70, 66, 95, 56+60, 101, 99, 87, 81, 77, 110, 151, 123, 149, 118, 114, 153, 105, 137, 138, 126, 187, 183, 128, 185, 174, 177, 171, 156, 157, 199, 180, 200, 170, 203, 195, 194, 205, 207, 206 and 209) and 16 PAHs (acenaphthylene, acenaphthene, fluorene, phenanthrene, anthracene, fluoranthene, pyrene, benzo[a]anthracene, chrysene, benzo[b]fluoranthene, benzo[k]-fluoranthene, benzo[e]pyrene, benzo[a]pyrene, indeno[1,2,3-cd]pyrene, dibenz[a,h]anthracene, benzo[g,h,i]perylene) using standard mixtures from Ultra Scientific (North Kingstown, RI) and Cambridge Isotope Laboratories (Andover, MA), respectively. Quantification was achieved with an Agilent 6890 gas chromatograph (GC) equipped with splitless injector and a mass spectrometer operating in electron impact-selected ion monitoring mode. GC conditions have been described elsewhere (Shoeib and Harner 2002a). The GC oven temperature program was modified to a 90°C hold for 0.5 min, 15°C/min to 240 °C, 20 °C/min to 290 °C, and a final hold for 5 min. The transfer line was kept at 300 °C. The target/qualifier ions were 222/224 for PCB-8 222/224 or 256/258 for tri-PCBs, 292/290 for tetra-PCBs, 326/328/324 for penta-PCBs, 360/362

for hexa-PCBs, 394/396 for hepta-PCBs, 428/430 for octa-PCBs, 464/462 for nona-PCBs, and 498/496 for PCB-209. The target/qualifier ions for PAHs have been described previously (Su et al. 2006b).

Analytical method recoveries of PCB were determined by spiking two clean PUF discs with the working standard containing all 54 PCB congeners (20 ng of each PCB congener) and treating them as real samples. Results show good recoveries ranging from 82% to 105%, which compare well with those of previous air sampling studies in the same laboratory using the same methodology (Shoeib and Harner 2002a). Recovery factors were not applied to any of the data reported below. PUF, GFF and solvent blanks were generally very low, eliminating the need for a blank correction.

2.2.3 Frontal Chromatographic Theory

In the flow-through sampler an air stream with contaminants in the gas phase is passing through a sequence of polyurethane discs. If air concentrations are constant, chemicals enter this PUF column as a front. The sampling process thus resembles frontal gas chromatography (GC) on a short column with only a few theoretical plates. In frontal GC, the quantity of a compound trapped in the stationary phase is expected to decrease along the direction of the gas flow. In the current case, this can be expressed by plotting the trapped concentration as a percentage of the first PUF plug value against the overall PU foam thickness, yielding a breakthrough curve. The theoretical plate number of the sampling assembly, N , can be determined from the thickness of foam at the 50% breakthrough point, L_{50} , and the slope of the breakthrough curve at that point (see Figure 2-2 upper left panel) (Bidleman et al. 1984; Burdick and Bidleman 1981; You and Bidleman 1984). A logistic equation was chosen to fit the data of each breakthrough curve.

$$\% \text{ of first PUF plug} = f(L) = \frac{100}{1 + (L/L_{50})^p} \quad (2-1)$$

Such a fit assures a more consistent and accurate data analysis than could be achieved by manually drawing the curves. The equation expresses the percentage of the first plug value as a function of the thickness of the PUF disc L . L_{50} and p are regression parameters. Theoretically, the percentage of first plug value equals 100 at $L = 0$, and decreases to zero with increasing L if the foam was long enough. The logistic equation (2-1) fits well into these boundary conditions,

and, more importantly, the L_{50} parameter is equal to the point where the concentration reaches half of the first plug value. It should be noted, however, that equation (2-1) is purely empirical and the shape of the vapor front may not always fit this equation, especially when N is very small.

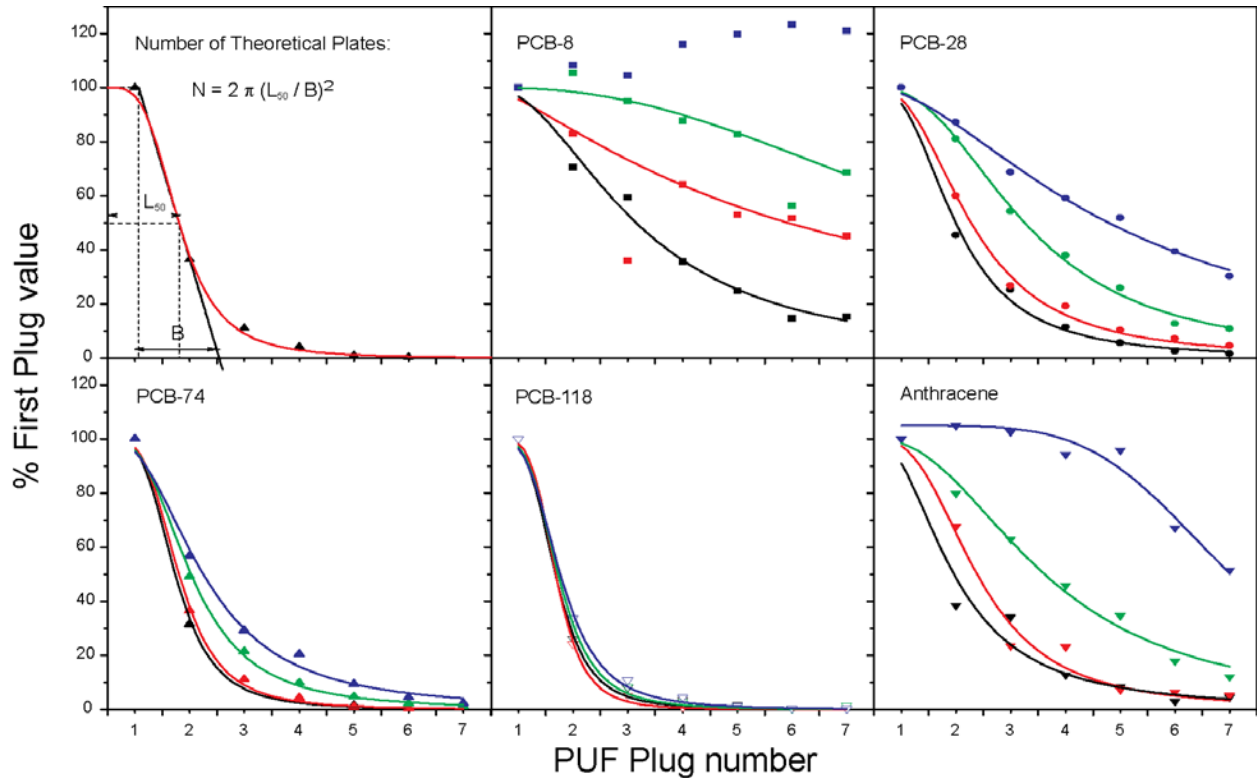


Figure 2-2. Vapor fronts of selected PCB congeners and anthracene for different sampling lengths. The black, red, green and blue colour represent sampling volumes of 125 m³, 368 m³, 793 m³ and 1360 m³, respectively. The upper left panel illustrates the approach to determine L_{50} and theoretical plates number N from the breakthrough curves.

The slope of the tangent at $L = L_{50}$ can be derived from the derivative of equation (2-1), $df(L)/dL = -25p/L_{50}$. We can further calculate the intercepts of the tangent with the lines corresponding to $f(L) = 0$ and $f(L) = 100$, and subtracting these two intercepts yields $B = 4L_{50}/p$, and the theoretical plate number,

$$N = 2\pi(L_{50}/B)^2 = \pi p^2/8 \quad (2-2)$$

Several equations have been developed to describe breakthrough curves (i.e. the shape of an eluting front) (Lövkvist and Jönsson 1987). The simplest one assumes the front shape can be expressed as the integral of a Gaussian peak. However, Lövkvist and Jönsson pointed out that this assumption applies only to columns with relatively high plate numbers (Lövkvist and Jönsson 1987). For columns with relatively few plate numbers, if the chemical flux at the column inlet, $J(0, t)$, was constant, a more general expression for the front shape can be given as follows:

$$J/J_0 = \Phi[N^{1/2}(\tau - 1)/\tau^{1/2}] + \exp(2N) \times \Phi[-N^{1/2}(\tau + 1)/\tau^{1/2}] \quad (2-3)$$

where J/J_0 is the normalized flux; N is the theoretical plate number; Φ is the integral of the normal distribution, ϕ , and τ is the relative retention time, which can also be expressed on a volume basis, $\tau = t/t_R = V/V_R$.

$$\phi(x) = [1/(2\pi)^{1/2}] \exp(-x^2/2),$$

$$\Phi(x) = \int_{-\infty}^x \phi(u) du = (1/2)[1 + \text{erf}(x/2^{1/2})]$$

$$\tau = V/V_R = V/V_B$$

where V_B is the breakthrough volume for a particular chemical, which is identical with the retention volume V_R on the same column (Reilley, Hildebrand and Ashley Jr. 1962).

The breakthrough level b , defined as the fraction of the total mass of analyte that has been eluted from a column with length L by time t , is given as a function of N and the relative retention, τ :

$$b = \frac{\int_0^t J(L, t) dt}{\int_0^t J(0, t) dt} = \frac{\tau - 1}{\tau} \Phi\left(N^{1/2} \frac{\tau - 1}{\tau^{1/2}}\right) + \frac{\tau + 1}{\tau} \exp(2N) \Phi\left(-N^{1/2} \frac{\tau + 1}{\tau^{1/2}}\right) \quad (2-4)$$

Where L is the overall length of the column, i.e. the overall length of the PUF assembly in the sampler; and Φ is the integral of the normal distribution ϕ of variable x (Lövkvist and Jönsson 1987):

Provided that the N and τ values are known for a given chemical, the sampling efficiency, $(1-b)$, can be calculated using equation (2-4). The contour profile of equation (2-4) is given in Figure 2-3. On the top and right side of the figure, the projection at $N=2$ and $\tau=2$, are also given.

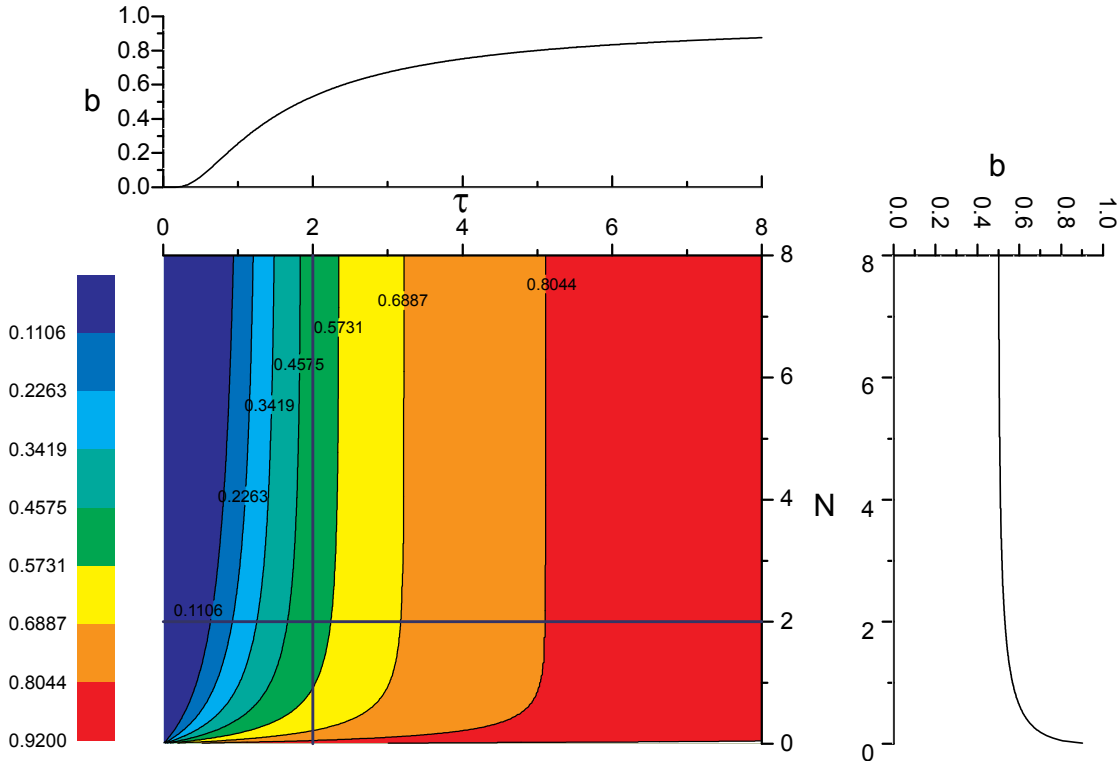


Figure 2-3. The breakthrough level b a function of relative breakthrough volume τ and plate numbers N .

2.3 Results and Discussion

2.3.1 Sampling Rates

Figure 2-4 gives the relationship between the wind speed outside the sampler and after passage through the sampling medium. Between threshold wind speeds of approximately 3 and 6.5 m/s, there is a linear relationship, which suggests that a 17.8 cm thick plug of PUF reduces the wind speed by a factor between 10 to 25. Typically an air volume of approximately 1000 m³ needs to be sampled for reliable quantification of low ambient SOC concentrations. Table 2-1 gives the approximate time needed to reach that volume using a 10.5 cm diameter sampling tube filled

with a 17.8 cm PUF plug (a stack of seven 2.54 cm discs). Even under relatively calm conditions with an average wind speed of 3 m/s, i.e., approximately 10 km/h, the new sampling design can trap approximately 86 m³ of air per day; implying a sampling time of less than 2 weeks to sample 1000 m³. During field deployment the wind speed inside the sampler is likely to be somewhat lower than the relationship of Figure 2-4 suggests, because it takes time for the sampler to rotate to face the wind. It is still safe to say that these sampling rates are more than an order of magnitude higher than those for conventional passive air samplers.

Table 2-1. Required sampling time for 1000 m³ of air under different wind speed conditions.

wind speed outside sampler	3 m/s	4 m/s	5 m/s	6 m/s
wind speed after passage through the PUF plugs	0.11 m/s	0.31 m/s	0.50 m/s	0.69 m/s
sampled air volume per day	86 m ³	231 m ³	375 m ³	520 m ³
time required for sampling 1000 m ³	12 days	4 days	3 days	2 days

2.3.2 Breakthrough Curves

Approximately 47 out of the 54 PCB congeners and only five PAHs were detected in the samples (See Table SI 1). The amount of chemicals trapped inside each 2.54 cm PUF disc was expressed as a percentage of the first PUF plug and plotted against the thickness of the PUF in Figure 2-2 for selected PCB congeners and anthracene. In those figures the spatial extension of the PUF discs is ignored and values are assigned to the center of the PUF discs. Different colors represent different sampling lengths, which in turn correspond to different sampled air volumes. Consistent with theoretical expectations and previous frontal chromatography studies (Bidleman et al. 1984; You and Bidleman 1984), the vapor front for each chemical significantly penetrates further with an increase of sampling volume. There is significant breakthrough after 11 days of sampling for volatile compounds, such as PCB-8 and anthracene, while less volatile compounds are almost stripped completely from the air stream by the seven PUF discs. The vapor front progression for

less volatile chemicals such as PCB-118 almost cannot be distinguished with the current experimental precision.

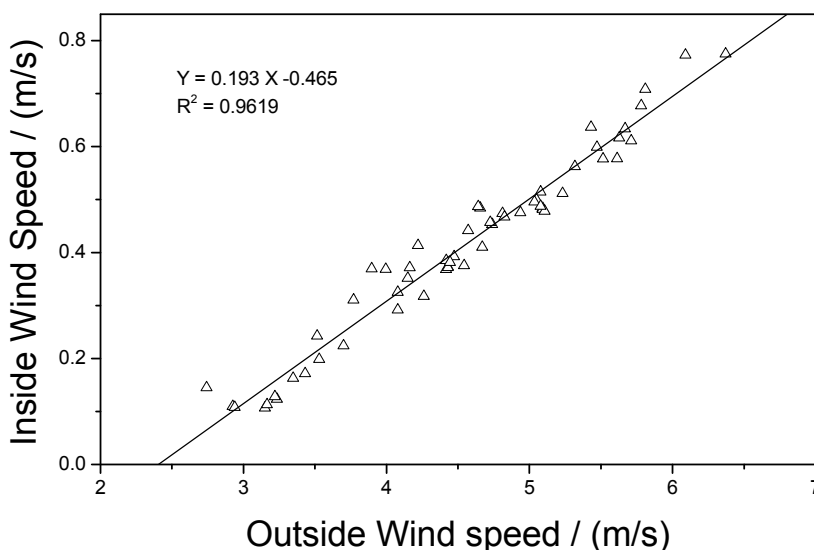


Figure 2-4. Correlation between the outside windspeed and the windspeed inside the sampling tube after passage through a 17.8 cm thick PUF plug.

2.3.3 Theoretical Plate Numbers and Breakthrough Volumes

The L_{50} and N values and their standard deviations can be calculated from the non-linear regressions based on equation (2-1). For a few chemicals, a significant outlier was excluded from the regression. Figure 2-2 includes the fitting results for selected compounds at a given air volume. It should be noted that for those chemicals which are undetectable in the last few PUF plugs, at least the first three points are necessary to obtain a reliable estimate of parameter p . However, for such cases, a straight line passing through the first two points may still give a satisfactory estimate of L_{50} . Plotting the sampled air volume against the regression parameter L_{50} , linear relationships were observed (Figure 2-5). It should be noted that $L = 0$ is represented by the entire first PUF plug, which has a finite thickness of 2.54 cm. Thus these linear regressions are not going through the origin, as might be expected from theory, but are crossing the x-axis at

a foam thickness of approximately 2.5 cm. From Figure 2-5, the breakthrough volumes, V_B , for different chemicals under current sampling conditions can be estimated by extrapolation of the linear regressions to the overall foam thickness of 17.8 cm.

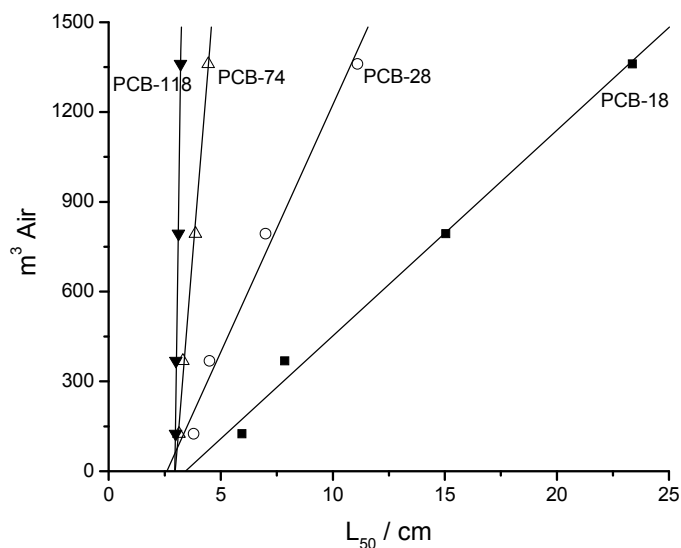


Figure 2-5. Relationship between the sampled air volume and the L_{50} values illustrating the linear movement of PCB-18, 28, 74 and 118 vapor fronts through the PUF plugs. The breakthrough volume, V_B , is determined by extrapolating these linear relationships to the overall PUF plug length of 17.8 cm.

The calculated N values and the corresponding error for individual chemicals in the four different air samples are given in Table SI 3. A paired-sample t-test shows that there is no significant difference between the N derived from the two samples with lower sampling volume ($V = 125 \text{ m}^3$ and 368 m^3) and between those derived from the two samples with higher volumes ($V = 793 \text{ m}^3$ and 1360 m^3); but the difference between these two groups is significant. Although all experiments were conducted at room temperature, this is possibly due to small changes in the average temperature between different samples. Both N and V_B are likely to decrease as temperature rises (Burdick and Bidleman 1981). However, the small change in N with sampling volume is negligible compared to the average relative error for N , which is about 30 % for all chemicals and sampling volumes. That also partly explains why most chemicals show satisfying

linearity in Figure 2-5. Thus, the average N values obtained from the four experiments represent the theoretical plate numbers of the flow-through air sampler under the current experimental conditions (temperature, wind speed, PUF plug material and length), which is about 1 theoretical plate number for volatile PCBs and 8 for much heavier compounds.

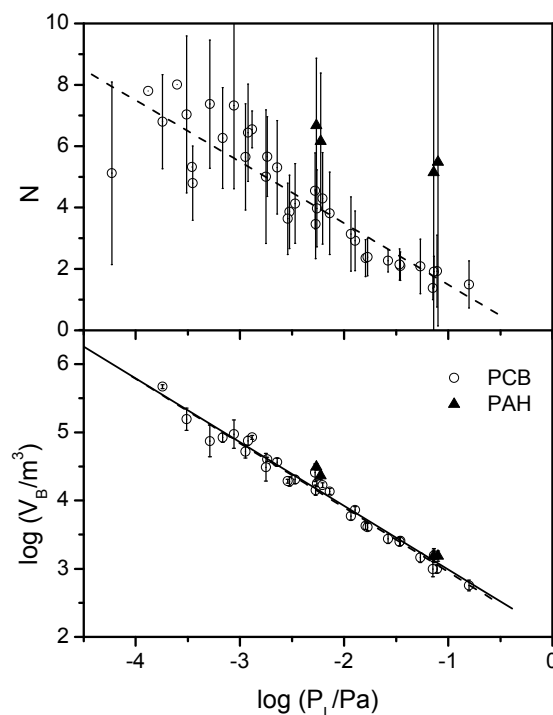


Figure 2-6. Plots of theoretical plate number N and breakthrough volume $\log V_B$ versus vapor pressure of the subcooled liquid $\log P_L$ for PCBs (open circles) and PAHs (filled triangles). The dashed line is the regression for PCBs only. The solid line is the regression line for PCBs and PAHs.

Figure 2-6 gives plots of the average theoretical plate number N and the logarithm of the breakthrough volume V_B for different chemicals against the logarithm of their sub-cooled liquid vapor pressure P_L at 25 °C, taken from references (Falconer and Bidleman 1994; Lei et al. 2002). Linear relationships were observed between both N and $\log V_B$ and $\log P_L$, which is consistent with previous studies (Bidleman et al. 1984; Pankow 1989; You and Bidleman 1984) investigating the breakthrough on PUF. Figure 2-6 also indicates that the N vs. $\log P_L$ correlations for PCBs and PAHs are different from each other. However, the data points for

PAHs are few and subject to considerable uncertainty, so the difference could be due to experimental error. For PCBs, this relationship can be fitted with the following equation,

$$N = -(2.00 \pm 0.17) \log P_L - (0.52 \pm 0.44) \quad R^2 = 0.8057, n = 36, F = 140.97, p < 0.0001 \quad (2-5)$$

The $\log V_B$ vs. $\log P_L$ relationship for the PAHs and PCBs can hardly be distinguished from each other considering the uncertainty of the V_B values. Therefore, equation (2-6) gives the relationship between breakthrough volume and P_L for both PCBs and PAHs.

$$\log V_B = -(0.93 \pm 0.03) \log P_L + (2.06 \pm 0.07) \quad R^2 = 0.9697, n = 35, F = 1054.7, p < 0.0001 \quad (2-6)$$

Pankow had suggested that the strength of the sorptive interaction of PCBs and PAHs with PUF are significantly different (Pankow 1989). These seemingly conflicting results could be due to limited sample size and experimental uncertainty. Nevertheless, our results suggest that the retention behavior for these two chemical classes can be estimated from their vapor pressures. We anticipate that for other chemical classes, this relationship can also provide an estimation of breakthrough volume with a tolerable error. Based on equations (2-5) and (2-6) above, we can safely say that the tested flow-through sampler set-up has more than one theoretical plate number for most SOCs of interest; and with a typical sampling volume of a few thousand cubic meters of air, breakthrough will be negligible for chemicals with a $\log (P_L/\text{Pa})$ value lower than -1.5 at the temperature prevalent during sampling. Whether breakthrough of an SOC will occur at other temperatures can be estimated by adjusting its vapor pressure and comparing it with this threshold. However, because N is also dependent on temperature, such estimates are somewhat uncertain.

2.3.4 Comparison with HiVol Samples

Equipped with the information on sampling and breakthrough volumes, it is possible to not only calculate the average air concentration of chemicals with low volatility, but also to estimate the breakthrough-corrected air concentration of more volatile chemicals. Figure 2-7 compares the air concentrations for selected PCBs and PAHs obtained from an active HiVol sample taken during this study with those from the flow-through sampler and those from a previous active sampler study (Shoeib and Harner 2002a). To calculate the air concentrations, the total amount of chemical sorbed to all seven PUF discs were added up and divided by the total sampled air

volume. The PUF in the flow-through sampler is expected to collect both gaseous compounds and those sorbed to atmospheric particles under such a slow wind speed. Therefore, the sum of the concentrations on GFF and two PUF plugs from the HiVol sample was used for comparison. The top left panel shows that the HiVol data from this study are slightly higher than those measured in the same laboratory earlier, but well within the same order of magnitude. Even with different sampling volumes, the four flow-through samples give almost identical concentration

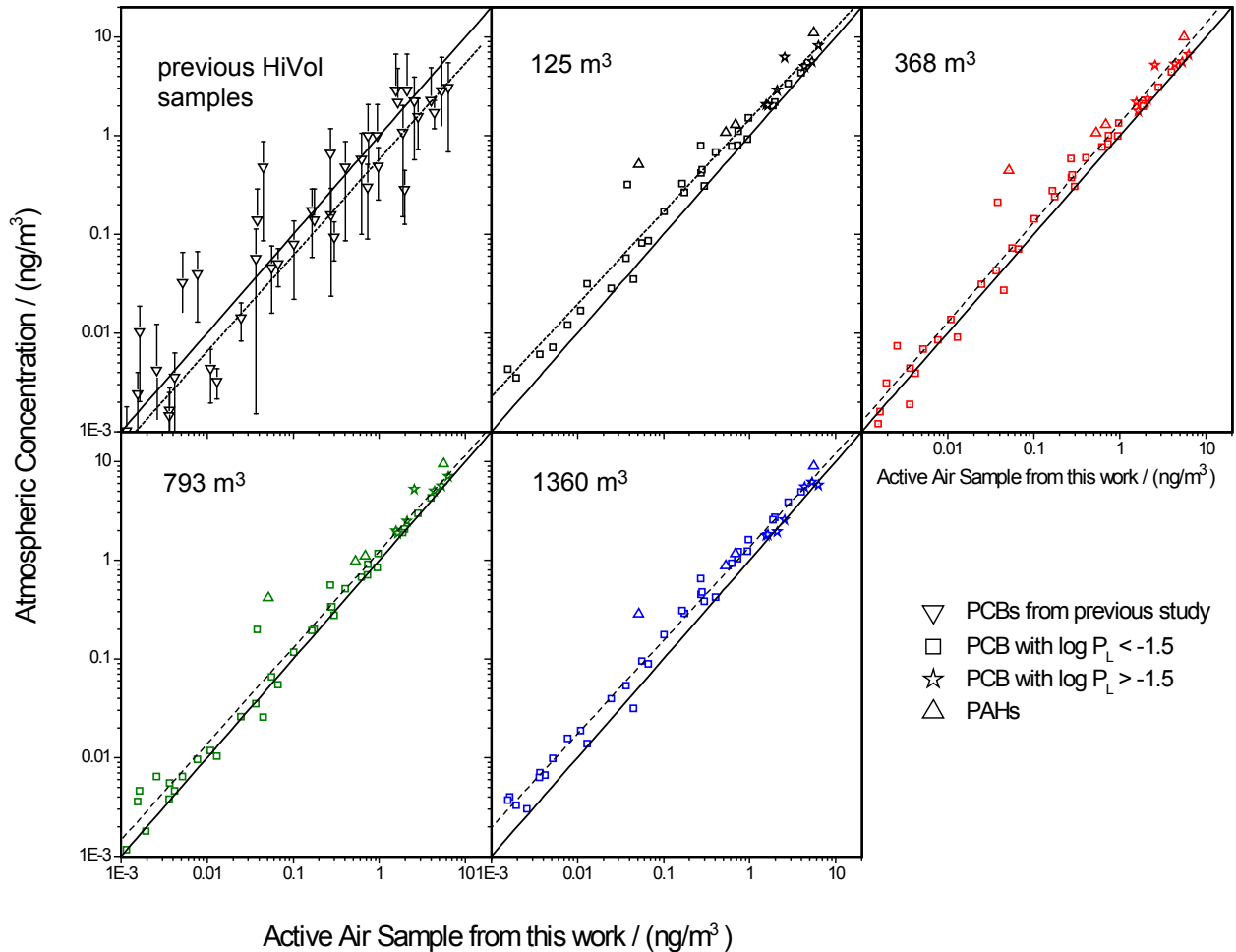


Figure 2-7. Comparison of air concentrations for PCBs and PAHs as obtained using a conventional active air sampler and the flow-through air sampler with variable sampling volume. The panel in the upper left compares air concentrations obtained by active air sampling in this study with those obtained in the same laboratory previously. The different colours represent different sampling volumes; and the dashed lines are the regression for both PCBs and PAHs.

values that also agree well with the active air sample from this work. Interestingly, the concentrations of relative volatile compounds ($\log(P_L/\text{Pa}) > -1.5$) obtained during shorter sampling periods, which experienced less breakthrough, show excellent agreement with each other. With increased sampling air volume, the non-breakthrough-corrected value given by the flow-through sampler decreases and approaches data obtained by active sampling (Figure 2-7).

We estimated the breakthrough percentage for nine volatile chemicals, which include seven PCBs and two PAHs, by substituting their N and τ values into equation 2-4. For these chemicals we can assume that the 1-day flow-through sample experienced no breakthrough. Then the ratio of the concentration from the samples with longer sampling time to those from the 1-day sample can be used to judge the breakthrough level. Table SI 4 gives the result of a paired two sample t -test which tests whether these ratios are different from 1 for the volatile compounds before and after the breakthrough-correction. The test shows that after such correction, the air concentration data no longer decrease with increasing air volume. All four samples give comparable results, which are usually slightly higher than the value given by the active air sample. This is because the active sampling also suffers from breakthrough for those compounds, but it cannot be corrected. These results, therefore, confirm that the flow-through sampler can provide reproducible and reliable quantitative air concentrations under controlled wind conditions.

The flow-through sampler developed here holds promise as a new air sampling technique for SOCs, whenever high sampling rates are required, but lack of access to reliable, sufficient or continuous power prevents the use of pumps. Examples of potential areas of application are measurements of air concentrations at relatively high temporal resolution in remote regions, especially in developing countries, or in temporary or permanent field camps in polar and high altitude environments. After having established the sampler's capability to provide reproducible, quantitative information on SOC air concentrations under conditions of constant temperature, air concentration and wind speed, the next step will be to test the sampler and to evaluate its performance by comparison with simultaneously collected pumped samples in the outdoor environment.

2.4 Acknowledgements

We are grateful to John Ford and Johnny Lo for constructing the sampler, Jacek Jackiewicz for help with the electronic components, Ryan Janzen for building the signal converter, Mahiba

Shoeib for providing air concentration data, and Terry Bidleman for helpful comments and suggestions. Thanks to the Natural Sciences and Engineering Research Council of Canada and the Northern Contaminants Program of the Canadian Department of Indian Affairs and Northern Development for funding.

2.5 Supporting Information Available

Detail on selection of sampling media (Figure SI 1), original experimental data, and mathematical and statistical results (Table SI 1, Table SI 2, Table SI 3, and Table SI 4). This material is available in Appendix I.

Chapter 3

Field Testing a Flow-Through Sampler for Semi-Volatile Organic Compounds in Air²

3 Brief

A wind-driven air sampler suffers no break-through and yields reliable time-integrated concentrations of PCBs and PAHs over two week sampling periods.

3.1 Introduction

The atmosphere plays a key role in the global cycling of semivolatile organic compounds and their delivery to both aquatic and terrestrial food chains, precipitating the need for air monitoring programs for compounds such as the polycyclic aromatic hydrocarbons (PAHs), organochlorine pesticides (OCPs), and polychlorinated biphenyls (PCBs). Conventional high volume sampling is the most widely used approach for collecting SOCs from air, but the cost, electricity-dependence, and relative complexity limits its use to sites with access to the electrical grid and to monitoring networks with relatively few sites. It is also ill-suited for sampling over extended periods of time, as would be required for time-integrated sampling. In recent years, several different passive air sampling (PAS) techniques have been developed, which are more cost-effective than active samplers for monitoring networks at the local to continental scale (Harner et al. 2004; Jaward et al. 2005; Shen et al. 2004). However, the relatively low sampling rate of most PAS constrains the temporal resolution that can be achieved. Also, the mechanism of SOC uptake in PAS and the influence of environmental variables such as wind speed and temperature on that uptake have not yet been fully characterized ((Harner et al. 2006a). Thus, calibration studies, based either on parallel active and passive sampling or performance reference compounds (PRCs), are necessary

² Reproduced with permission from Xiao, H.; Hung, H.; Harner, T.; Lei, Y.D.; Wania, F. 2008. *Environ. Sci. Technol.*, 42 (8), 2970–2975. Copyright 2008 American Chemical Society.

Field tests were conducted by H. Xiao. All samples were extracted, cleaned up and quantified by H. Xiao under the supervision of H. Hung, T. Harner and Y.D. Lei. Instrumental analysis was aided by Y.D. Lei. The data were interpreted and the paper was prepared by H. Xiao in consultation with F. Wania.

for a semiquantitative estimation of air concentrations (Harner et al. 2006a; Söderström and Bergqvist 2004) with PAS.

In an earlier publication (Xiao et al. 2007), we introduced a flow-through air sampler (FTS) that had been developed to address the need for a sampling technique that can achieve substantially faster uptake rates than typical PAS, yet still requires no access to reliable network power. This was accomplished through the use of a horizontally oriented flow-tube that rotates to face the wind, which then blows through a porous sampling medium such as polyurethane foam (PUF). The uptake mechanism in an FTS is thus similar to that in a conventional active sampler. The sampled air volume can be deduced using data on the wind speed within the flow tube after passage through the sampling medium (Xiao et al. 2007). Such data can be obtained by wind sensors and recorded by battery operated data loggers (Xiao et al. 2007). Unlike PAS, the independent determination of air sampling volumes in the FTS makes it possible to deploy it without prior calibration or the use of PRCs. Earlier indoor experiments clearly demonstrated the FTS's capability to provide reproducible, quantitative information on SOC air concentrations under conditions of constant air concentration, temperature, and wind speed (Xiao et al. 2007). Here, we describe the first test of the FTS under field conditions during different seasons. Analyses of breakthrough curves and a comparison of the results with those of an active high volume sampler (HiVol) operating at the same time allow a detailed evaluation of its performance.

3.2 Method

3.2.1 Sampling Procedure

The FTS, as described in ref (Xiao et al. 2007), consists of a horizontally oriented, aerodynamically shaped, stainless steel flow tube, which is mounted on ball bearings which allow it to turn into the wind with the help of vanes (Figure 2-1). One such FTS was deployed on a 2 m post on the roof of the science building of the University of Toronto Scarborough, (43° 47' 0.56" N, 79° 11' 16.30" W), which is located in a forested area in the Eastern suburbs of metropolitan Toronto, Ontario, Canada. As in the earlier indoor study, seven P10z PUF disks of 2.54 cm thickness (i.e., one inch) were arranged in series inside the sampling cylinder. Prior to exposure, the disks were precleaned with water and by Soxhlet extraction for 24 h using acetone and then for another 24 h using petroleum ether (PE). PUF disks were dried in a desiccator and

stored in glass jars with Teflon-lined lids. In total, five flow-through samples, each covering a sampling period of approximately two weeks (see Table 3-1), were taken between August, 2006 and June 2007, thereby including widely different seasons and weather conditions. For every sample, a field blank was taken, whereby a PUF disk was exposed to air during sample installation and sealed in the original jar and placed beside the FTS for the length of sampling.

For the first four flow-through samples, both the wind speeds outside the sampler and after passage through the sampling medium were determined by a vortex wind sensor (inspeed.com LLC) placed on the top of the sampler and a battery-operated turbine anemometer (Landtek Instruments Co. Ltd., Guangzhou, China) mounted at the exit of the flow tube. Both wind sensors have been precalibrated with a hot wire anemometer (VT-200, KIMO Instruments) (Xiao et al. 2007). During the whole sampling period, the average outside and inside wind speeds within every 5 minutes interval were recorded by two data loggers (MadgeTech Pulse 110, Warner, NH) as pulse numbers r_{out} and r_{in} , respectively, which have units of pulse numbers (or rotations) per 5 minute interval (rp5m). Air temperature was recorded every hour by a weather station near the sampling site.

Table 3-1. Average temperature T , average wind speed within flow through sampler u_{in} , and sampled air volume V_{air} calculated with two different methods for each sampling period.

Sampling period	T in °C	u_{in} in m/s ^a	V_{air} in m ³
August 11 - 25, 2006	19.9±4.6	0.0354	373±15 ^a 397 ^b
November 15 - 29, 2006	4.7±4.1	0.0201	212±8 ^a 437 ^b
December 4 - 18, 2006	2.5±5.6	0.0486	511±18 ^a 871 ^b
April 13 - 27, 2007	9.4±5.6	0.1047	1090±42 ^a 1161 ^b
May 22 - June 6, 2007	18.3±4.7	0.0267	303±15 ^a -

^a estimated using eq 3-3, ^b estimated using eqs. 3-1 and 3-2

An active HiVol sampler was set up approximately 10 m away from the FTS. A variable number of 24 h HiVol air samples was taken during each FTS sampling period. The sample train

consisted of a glass fibre filter (GFF) for collecting particle-phase compounds, followed by a double PUF plug for trapping compounds that exist in the gas-phase. Most of the procedures are the same as in an earlier study (Shoeib and Harner 2002a). Detailed information on the active HiVol samples is listed in Table SI 7 in the Appendix (S2).

3.2.2 Sample Extraction and Quantification

The five sets of seven PUF disks from the flow-through sampler and the front and back PUF of the pumped samples were extracted individually by Soxhlet with acetone and PE (1:1) for 24 h. The GFF was Soxhlet-extracted for 24 h using dichloromethane (DCM). The extracts were reduced in a rotary evaporator under vacuum to ~5 mL, transferred to a vial and reduced under a gentle nitrogen flow to 0.5 to 1 mL, and then dehydrated using a sodium sulfate column. The sample was exchanged to isooctane and reduced again to 1 mL under nitrogen prior to instrumental analysis. Mirex (100 ng) was added as internal standard to correct for volume differences.

Samples were analyzed for 54 individual PCB congeners and 16 PAHs using standard mixtures from Ultra Scientific (North Kingstown, RI) and Cambridge Isotope Laboratories (Andover, MA), respectively (Xiao et al. 2007). Quantification was achieved with an Agilent 6890 gas chromatograph (GC) equipped with splitless injector and a mass spectrometer operating in electron impact-selected ion monitoring mode. GC conditions have been described elsewhere (Shoeib and Harner 2002a). The GC oven temperature program was modified to an initial temperature of 90 °C, held for 0.5 min, 15 °C/min to 240 °C, 20 °C/min to 290 °C, and a final hold for 5 min. The transfer line was kept at 300 °C. The target/qualifier ions were 222/224 or 256/258 for tri-PCBs, 292/290 for tetra-PCBs, 326/328/324 for penta-PCBs and 360/362 for hexa-PCBs.

3.2.3 QA/QC

Analytical method recoveries of chemicals were determined by spiking two clean PUF disks with the working standard containing all 54 PCB and 16 PAH congeners (20 ng of each congener) and treating them as real samples. Results show good recoveries ranging from 85 to 108%, which compare well with those of previous air sampling studies in the same laboratory using the same methodology (Harner and Bidleman 1997; Shoeib and Harner 2002a; Xiao et al. 2007). Recovery factors were not applied to any of the data reported below. Solvent blanks and

the field blanks for PUF and GFF were typically less than 10% of sample amounts, except for some chemicals of very low abundance, such as PCB-185. All the amounts reported for the samples are corrected for field blanks. For compounds not detected in those blanks, two-thirds of the instrumental detection limit, derived as the amount at which the signal-to-noise ratio equals 3, was used for blank correction. Blank levels and limits of detection are reported in Table SI 8 in the Appendix.

3.3 Result and Discussion

3.3.1 Wind speed correlation

To calculate volumetric air concentrations, it is necessary to know the volume of air V_{air} that blew through the FTS during a deployment period t . V_{air} is the product of t , the cross-sectional area of the flow tube ($8.66 \times 10^{-3} \text{ m}^2$), and the wind speed within the flow tube u_{in} in m/s. In principle, u_{in} is measured by the vane placed within the flow tube. In contrast to the controlled indoor experiments, where the sampler always faced directly into the wind and wind speed was constant (Xiao et al. 2007), both wind speed and direction vary considerably during field deployment. In particular, under nonwindy conditions in Toronto, the vane sensor placed inside the flow tube is not sensitive enough to measure the very low wind speeds that occur after passage through the PUF disks. Based on the calibration equation for the vane sensor:

$$u_{\text{in}} = 0.000134 \cdot r_{\text{in}} + 0.0442 \quad (3-1)$$

the minimum inside wind speed required for the sensor to record pulses is about 0.04 m/s. Rather than assuming that a u_{in} of 0.04 m/s prevails whenever the sensor does not record any movement, which would result in an overestimate of V_{air} , we assume that u_{in} linearly responds to the outside wind speed until the vane sensor starts turning. The average maximum outside wind speed u_{out} during the five sampling periods while r_{in} was 0 was 2.93 m/s. Therefore,

$$u_{\text{in}} = 0.0442 / 2.93 \cdot u_{\text{out}} = 0.015 u_{\text{out}}, \quad \text{when } r_{\text{in}} = 0 \quad (3-2)$$

Although equations 3-1 and 3-2 can be used to estimate u_{in} in m/s and thus V_{air} , it would be preferable to have a single equation that would allow the estimation of u_{in} from the outside wind speed over the entire relevant wind speed range. In particular, this would then allow the deployment of an FTS without wind sensors and batter-operated data loggers at any site where wind speed at the relevant height is being recorded, because V_{air} could be deduced from those records. We, therefore, set out to derive such a relationship between u_{in} and u_{out} .

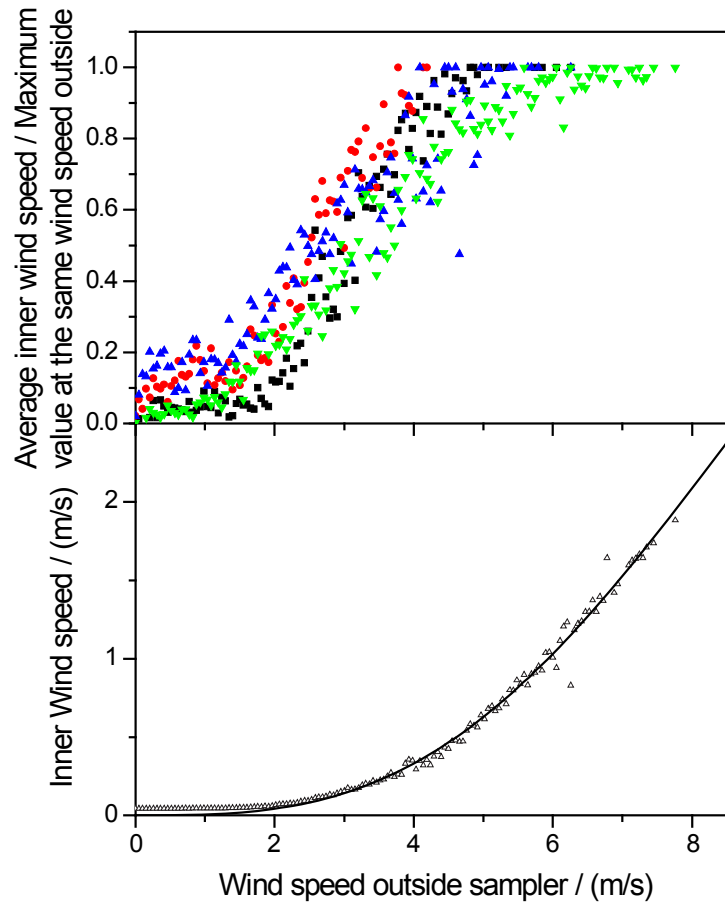


Figure 3-1. The relationship between the wind speed outside the FTS and after passage through the PUF plugs (black: August, red: November, blue: December, green: April). The bottom panel shows the fitting result from the non-linear regression equation 3-3.

A comparison of the wind speeds recorded by the two data loggers for the first four sets of FTS samples (Figure SI 2) shows that there is a maximum u_{in} for each u_{out} , and the range of the inner wind speed decreases as the wind outside the sampler becomes stronger. That can be easily explained by the fact that it takes some time for the FTS to turn to face into the wind. A relatively shorter time is needed for the sampler to align with the wind direction under stronger wind conditions; and the wind speed passing through the sampler reaches its maximum value when the sampler is directly facing into the wind. Thus, as the u_{out} gets faster, the u_{in} is more likely to be close to the maximum value applicable to a particular outside wind speed.

To mathematically solve the relationship, the maximum and average wind speeds after passage through the sampling medium were determined for a series of small outside wind speed intervals.

The top panel of Figure 3-1 plots the ratio of the corresponding average and maximum value under the same outside wind speed. It reveals that as the wind speed outside the sampler u_{out} exceeds approximately 5 m/s (corresponding to $r_{out} > 1500$ rpm), the influence of changing wind direction can be ignored. The relationships are similar for the four different data sets. Therefore, it is reasonable to assume that the unweighted average wind speed after passage through the sampling medium for the four data sets is the most likely wind speed under the corresponding outside wind conditions.

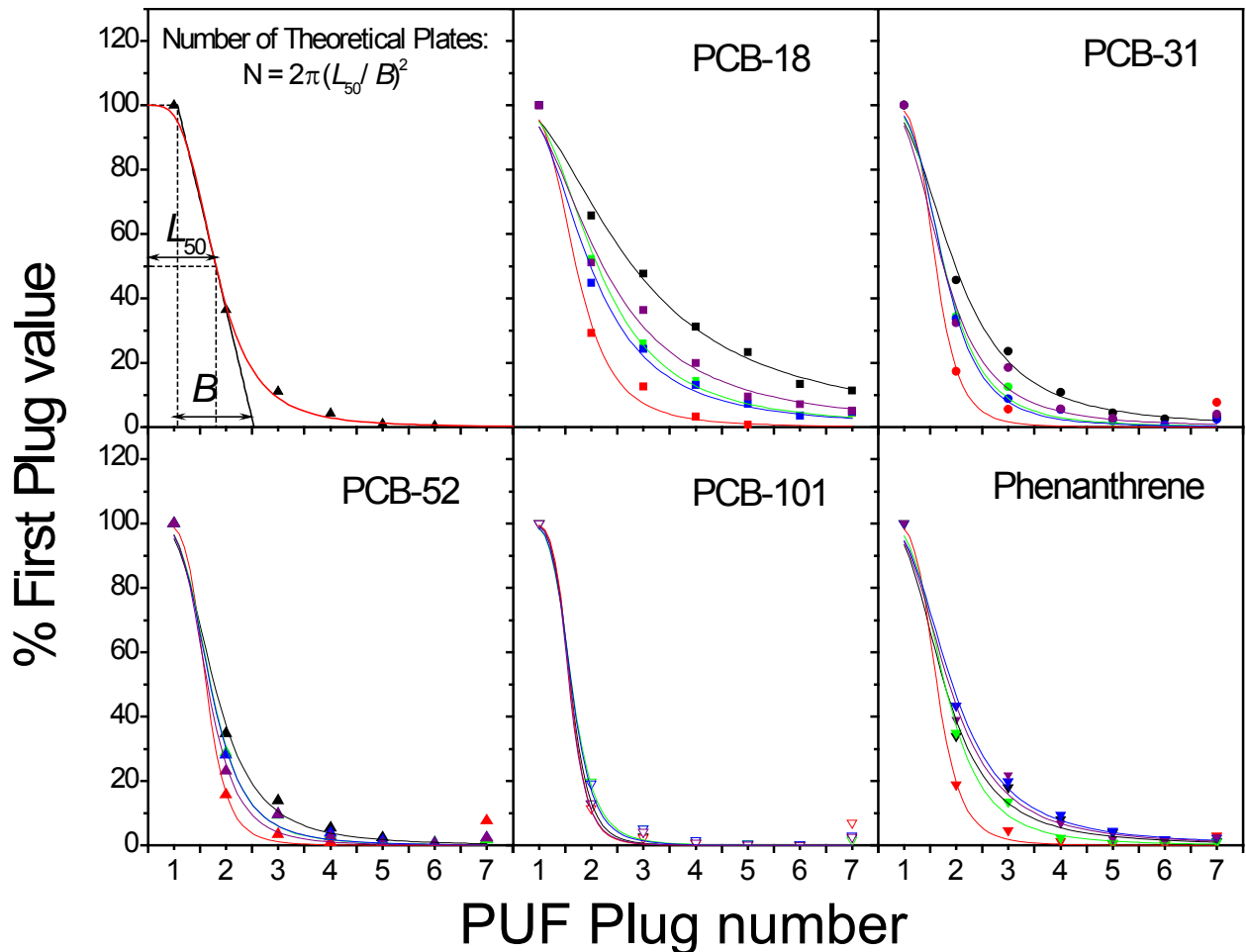


Figure 3-2. Vapor fronts of selected PCB congeners and phenanthrene from different sampling periods. The black, red, green, blue and purple color represent samples taken during August, November, December, April and May, respectively. The upper left panel illustrates the approach to determine L_{50} and theoretical plates number N from the breakthrough curves.

Plotting the un-weighted average u_{in} against the corresponding u_{out} , the bottom panel of Figure 3-2 shows that the vane sensor mounted inside the flow tube does not respond to outside wind speeds below 2 m/s ($r_{out} < 550$ rp5m). Theoretically, the u_{in} should be zero at wind still conditions, i.e. the regression curve should pass through the origin. A non-linear Langmuir-type equation with three empirical regression parameters was chosen to fit the data in Figure 3-1.

$$u_{in} = \frac{7.701 \times 6.659 \times 10^{-4} u_{out}^{3.049}}{1 + 6.659 \times 10^{-4} u_{out}^{3.049}} \quad (3-3)$$

Equation 3-3 predicts that the u_{in} would approach a maximum value of about 7.7 m/s when the wind outside the sampler became really fast, i.e. if u_{out} exceeds 30 m/s ($r_{out} > 10,000$ rp5m). However, such strong winds never occurred during these field tests and equation 3-3 should not be used for u_{out} significantly higher than 10 m/s ($r_{out} > 2500$ rp5m). Further tests under much windier condition would be required to derive an equation that is valid at higher wind speeds.

The sampled air volumes for all five samples, as well as the corresponding average wind speeds and their standard deviations are given in Table 3-1. In equations 3-2 and 3-3, u_{out} in units of m/s was used, because this makes them applicable to outside wind speeds measured with any type of anemometer. The values in Table 3-1 were calculated with versions of equation 3-2 and 3-3, which are based on r_{out} in units of rp5m, in order to avoid propagating the uncertainty introduced by the calibration equation for the outside wind sensor. For reference, those equations are given in the Appendix II. The V_{air} estimated using either equations 3-1 and 3-2 or equation 3-3 are almost identical for periods with relatively high wind speeds. Even for relatively wind still periods the difference is well within a factor of 2, while equation 3-3 could slightly underestimate V_{air} . This partially confirms the possibility of accurately estimating the sampled air volumes based on outside wind speed data and equation 3-3. For the sample taken from May 22 to June 6 2007, u_{in} was not recorded, and V_{air} was calculated using equation 3-3.

From the data listed in Table 3-1, it is safe to say the FTS can easily achieve a sampling rate of at least 15 m³ air per day, even under relatively calm wind conditions, which is a great improvement compared to current PAS designs. During windier periods, even 100 m³ per day are possible, which is comparable to sampling volumes achieved by pumped HiVol air samplers. Based on eq 3 and the outside wind speed distribution, it is possible to estimate the percentage of the total sampled air volume that was collected during periods with a specific wind speed. Such an estimation (displayed in Figure SI 3 for all five sampling periods) clearly shows that the FTS

samples mostly during time periods with intermediate wind speeds, which are more likely to occur than periods of very high wind speeds. Whereas periods of low wind speed are even more likely, they contribute little to the total sampled air volume, because u_{in} is too low. The effect of this bias toward relatively windy periods on air concentration is likely quite limited, because those wind speeds are randomly distributed during the sampling periods.

3.3.2 Break-through profile for different compound groups

Assuming the SOC air concentrations are constant during sampling, the sampling process in the FTS resembles frontal gas chromatography on a short column with only a few theoretical plates. Plotting the chemical amount trapped on each PUF as a percentage of that trapped on the first PUF plug against the overall PUF thickness, L , yields a breakthrough curve (Figure 3-2). According to frontal chromatographic theory the theoretical plate number of the sampling assembly, N , can be determined from the thickness of foam at the 50 % breakthrough point, L_{50} , and the slope of the breakthrough curve at that point (see Figure 3-2 upper left panel) (Xiao et al. 2007; You and Bidleman 1984). Earlier work (Xiao et al. 2007) had shown that the theoretical plate number is best determined by first fitting the data of each breakthrough curve with equation (3-4):

$$\% \text{ of first PUF plug} = f(L) = \frac{100}{1 + (L/L_{50})^p} \quad (3-4)$$

and then calculating N using the empirical regression parameter p ;

$$N = \pi p^2 / 8 \quad (3-5)$$

After blank correction, approximately 44 out of the 54 PCB congeners and 12 PAHs were detected in the samples (see Table SI 5). The amount of chemicals trapped inside each 2.54 cm PUF disk was expressed as a percentage of the first PUF plug and plotted against the thickness of the PUF in Figure 3-2 for selected PCB congeners and phenanthrene. In those figures different colors represent different FTS samples. Even for volatile SOCs, such as PCB-18 and phenanthrene, no significant breakthrough was observed with two-week-long sampling periods. Less volatile compounds, like the heavier PCBs and PAHs, which are partially particle bound in the atmosphere (Table SI 7), were stripped completely from the air stream by the seven PUF disks. This partly confirms the assumption that FTS can sample both gaseous and particle phase chemicals (Xiao et al. 2007) under real outdoor conditions. For all those chemicals which could

be detected in more than three 1-in P10z disks, vapor front curve were fit to equation 3-4 to estimate N (Table SI 6), which in turn were used to better understanding the uptake mechanism of FTS (see below).

3.3.3 Comparison of Flow-through samples with HiVol data

With the information on the sampled air volume and low break-through levels, the SOC air concentrations can be calculated. The total blank-corrected amounts of chemical sorbed to all seven PUF disks were added up and then divided by the total sampled air volume. The sum of the concentrations on GFF and two PUF plugs from the HiVol sample was used for comparison (see Table SI 7 for detailed information).

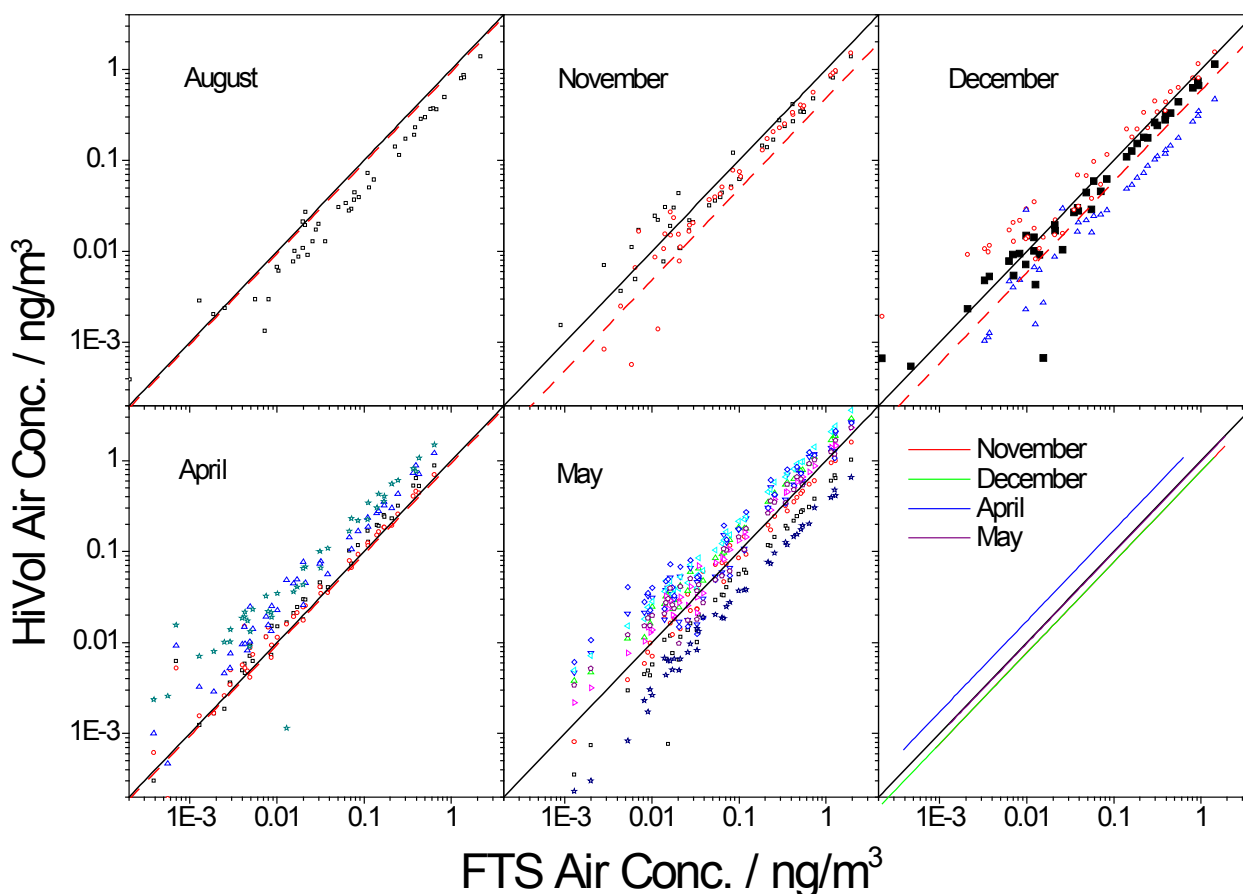


Figure 3-3. Comparing the air concentrations of individual PCB congeners obtained using the flow through sampler with those obtained using 24-hour HiVol samples (total gas+particle concentrations) taken during the same sampling period. The bottom right panel shows the regression lines between the FTS concentrations and the weighted average of HiVol concentrations for different sampling sets.

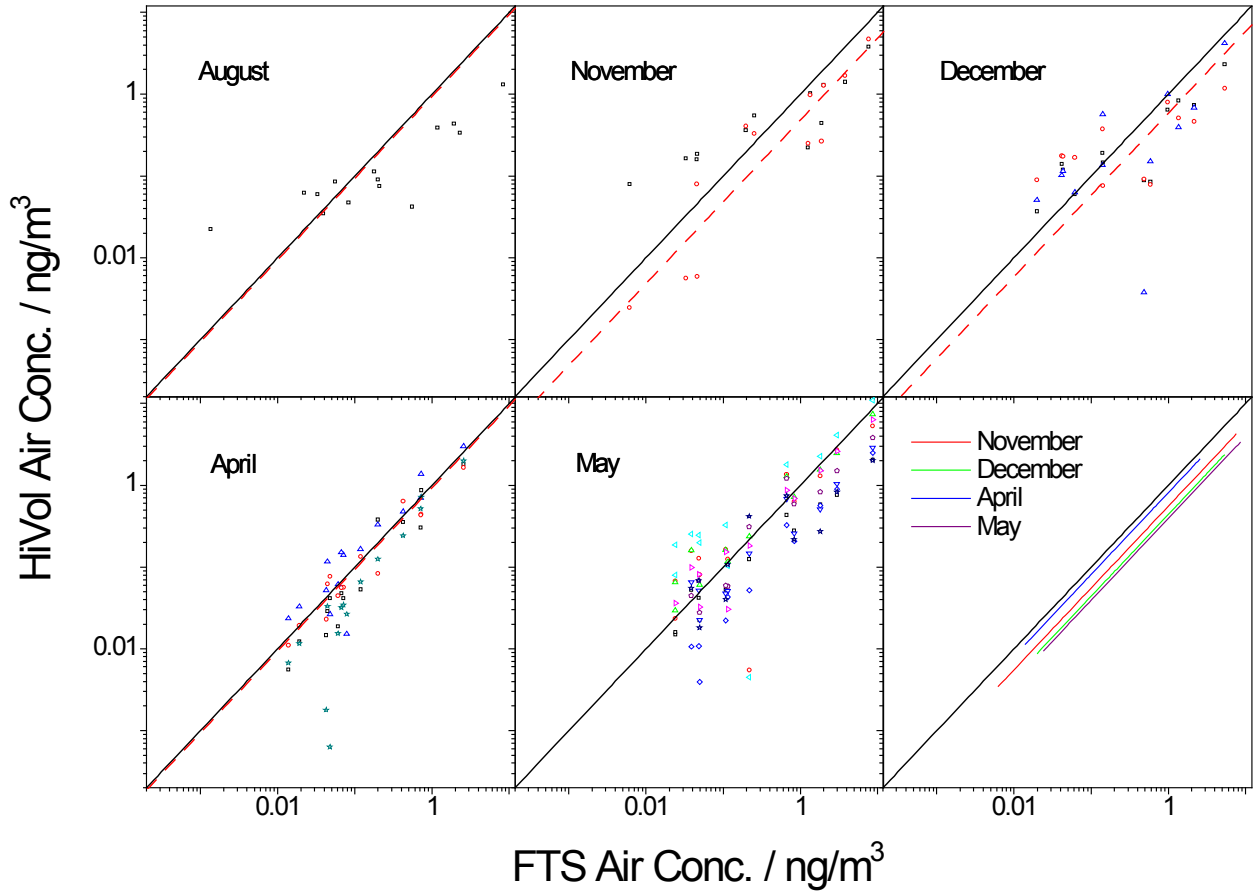


Figure 3-4. Comparing the air concentrations of PAHs obtained with the FTS with the 24-hour HiVol samples taken during the same sampling period. The bottom right panel shows the regression lines between the FTS concentrations and the weighted average of HiVol concentrations for different sampling sets.

Figure 3-3 and Figure 3-4 compare the air concentrations for PCBs and PAHs obtained from each FT sample with the concentrations obtained by HiVol samples (PUF + GFF concentrations) taken during individual 24 h periods within the FT sampling period. The sample volumes V_{air} estimated using equation 3-3 are chosen for comparison. In the figures, the black diagonal lines represent perfect agreement (1:1 ratio); and the red dashed lines indicates the shift in FTS air concentrations if V_{air} had been estimated based on equations 3-1 and 3-2. The HiVol samples are closely distributed around the FTS sampling band. Irrespective of how V_{air} is estimated, the FTS-derived air concentrations agree well with the HiVol samples taken within the same periods. Perfect agreement can not be expected because the HiVol samples only cover a fraction of the

FT sampling period and because SOC air concentration experience considerably variability on the time scale of a few days (Gouin et al. 2005a). For example, the 24 h HiVol samples taken during a two-week period show a variation within 1 order of magnitude. It thus appears, that even though the sampling by FTS is biased toward time periods with higher wind speeds (Xiao et al. 2007), the air concentrations obtained with the FTS is still representative of the average concentrations. For the flow-through sample taken from May 22 to June 6, the FTS air concentrations are fairly close to the average of all the HiVol samples taken within those days. It is therefore possible to make a reasonable estimation of the sampled air volume in the absence of any inner wind speed information. FTS-derived air concentrations for less volatile SOCs are comparable with the total concentration of those chemicals in the HiVol samples, which further confirms the capability of the FTS to capture particle-bound chemicals under relatively calm wind conditions.

To compare the FTS air concentrations more quantitatively with the HiVol concentrations, a weighted-average approach was used that takes into account the bias of the FTS toward time periods with higher wind speeds. From the stored wind speed data, it is possible to estimate the air volume, v_i , the FTS sampled during the duration of each HiVol sample (listed in Table SI 7). Then the average HiVol concentration can be calculated as,

$$\overline{C_{HiVol}} = \frac{\sum v_i \cdot c_i}{\sum v_i} \quad (3-6)$$

where c_i is the concentration in a HiVol sample taken during a flow-through sampling period.

The average HiVol concentrations calculated this way correlate strongly with the FTS results. Regression lines for different sampling sets and different chemical groups are included in the bottom right panel of Figure 3-3 and Figure 3-4. For PCBs, all of the regression lines are close to the diagonal 1:1 line, within a factor of 2, except the April HiVol sample average, which is significantly higher than the FTS-derived concentration. The April sampling period experienced the largest wind speed variation (Figure SI 2), with an average outside wind speed range from 0 to 8 m/s, and the four HiVol samples were taken during periods of particularly low wind speed. The air sampled by the FTS during those four days corresponds to only 15% of the total FTS sampling volume. Several studies have noted a negative correlation between wind speed and atmospheric SOC concentrations (Haugen, Wania and Lei 1999; Lohmann, Northcott and Jones

2000; Simcik et al. 1999), which could be due to a dilution effect and the higher atmospheric boundary layer associated with higher wind speed. In other words, the PCB air concentrations during April days without active HiVol sampling, when the wind speeds was significantly higher, were likely to be lower than during the days with HiVol sampling, resulting in the discrepancy between the concentrations derived by FTS and active HiVol.

The correlations for PAHs do not show significant bias toward one direction. Only the December and May data show relatively high variations. A careful look at the data reveals that the relative abundance of different PAHs varies widely between HiVol samples taken within a single FTS sampling period. This could be due to the wide variety of PAH sources, many of which are stronger in winter. As PAHs in the atmosphere are mainly a result of incomplete combustion of carbonaceous material, vehicle traffic, residential heating, and other local activities will strongly influence not only the total PAH amount but also levels of individual PAHs (Hafner, Carlson and Hites 2005). The PCBs, on the other hand, have a common source and have been banned in North America for many decades leading to smaller short-term variations in PCB air concentrations and congeneric compositions. In summary, despite occasional discrepancies, the concentrations derived from the two methods are all within a factor of 2, which is good considering the overall experimental uncertainty and the fact, that the HiVol samples did not cover the entire two weeks of a FT sampling period.

The active air sampling data provide information on the gas/particle partitioning behavior for the SOCs, which can be used to better understand how particle-bound chemicals interact with the PUF in the FTS. Figure SI 4 plots the fraction of the total amount of a chemical in air that is sorbed to particles, ϕ , against the subcooled liquid–vapor pressure P_L (Falconer and Bidleman 1994; Lei et al. 2002; Odabasi, Cetin and Sofuoglu 2006) of that chemical at the sampling temperature. Irrespective of the total suspended particle concentration, the ϕ value of a chemical starts increasing when its $\log(P_L/\text{Pa})$ is smaller than -2.5 . Chemicals become totally particle bound when their $\log(P_L/\text{Pa})$ is less than -5 . Those thresholds are comparable with those from a previous study (Su et al. 2006b).

Table 3-2 lists the mean and standard deviation of PCB and PAH concentrations derived from the FTS as well as some literature values reported for the Toronto area in recent years

Table 3-2. Average concentrations (pg/m³) of PCB and PAH congeners measured at Toronto urban sites.

	This work		Motelay-Massei et al. 2005	Farrar et al. 2005	Gouin et al. 2005	Harner et al. 2004
	8. 2006-6. 2007	HiVol	7. 2000-6. 2001	10. 2001	7. 2002- 6. 2003	7 -10. 2000
31	88±36	87±56	43±27		80	35
28	52±24	49±28	38±27	140	70	41
52	1100±410	990±480	68±45		140	69
49	280±110	280±150	29±23	30	40	27
44	450±180	420±220	32±23		70	31
95	950±370	930±470	60±46		130	89
101	1600±600	1700±850	56±48	10	160	64
110	1100±390	1100±630	33±24		110	46
149	360±140	440±260	33±34			43
118	510±190	560±360	23±18		50	23
153	270±110	340±230	29±27	3.6		40
138	180±73	220±170	26±25		80	31
180	11±5.8	23±19	5.2±6.2		30	7.8
∑13 PCB	6900±2600	7100±3900	480±370			547
	This work		Motelay-Massei et al. 2005	Farrar et al. 2005	Wong et al. 2004	
	FTS	HiVol	7. 2000-6. 2001	10. 2001	HiVol	
acenaphthylene	570±740	140±140	1800±2400			
acenaphthalene	650±380	550±520	3900±3300			
fluorene	2300±1100	1400±970	5300±4200	3300	2280	1930
phenanthrene	6500±2500	3600±2500	9800±7200	2700		
anthracene	150±80	140±160	270±240			
fluoranthene	1600±620	840±540	1600±530	1500		
pyrene	950±350	560±280	1200±430	600	1700	1470
B(a)A	60±15	62±55	86±71		220	180
chrysene	150±38	160±120	160±85		260	250
B(b)F	33±16	100±87	120±92		400	360
B(k)F	10±13	53±57	48±34		160	130
B(e)P			94±80		350	210
B(a)P	26±15	50±46	67±51		270	170
Indeno	43±16	96±67	63±33		1190	200
d(a,h)A	15±8	25±19	14±5		340	
B(ghi)P	52±9	93±65	68±30		1220	280
∑16 PAH	13000±5100	7866±5599	25000±18000	20000		

(Farrar et al. 2005; Gouin et al. 2005a; Harner et al. 2004; Motelay-Massei et al. 2005; Wong et al. 2004). The PCB values in this study are significantly higher than earlier reports; but the PAH levels are similar. Such differences could be due to the different source strengths in the vicinity of the sampling sites, differences in temperature/weather conditions and/or temporal changes of the chemicals.

3.3.4 Effect of temperature and wind speed on the theoretical plate number

Equipped with the information on average wind speed, temperature, and the apparent theoretical plate number N , it is possible to study the effect of temperature and wind speed on the sampling efficiency. Figure 3-5 plots the apparent theoretical plate number of PCBs and PAHs from the different sampling sets against their $\log P_L$ at the average sampling temperature. The figure is divided into three parts based on $\log P_L$, i.e. the gas/particle partitioning behavior of a chemical. For gas phase compounds with $\log (P_L/\text{Pa}) \geq -2.5$, temperature (i.e., volatility) influences the break-through level. As temperature and therefore P_L increase, chemicals escape more easily from the PUFs and N decreases. Multilinear regression confirms that the effect of wind speed on N is not significant ($p = 0.051$) within the experimental wind speed range investigated here.

$$N = -3.128 \cdot \log P_L - 1.485, \text{ when } \log P_L \geq -2.5 \quad (3-7)$$

$$(r^2 = 0.586, n=65, F = 90.744, p = 0.000)$$

Figure 3-5 B shows the linear regression of equation 3-7, including confidence and prediction limits.

Wind plays a relatively more important role for chemicals which are partially particle bound, i.e. those with $-5 \leq \log (P_L/\text{Pa}) \leq -2.5$. N -values for these chemicals are significantly lower during sampling periods with relatively high wind speeds (April and December, Figure 3-5). This is because the gaseous fraction of the SOCs is presumably more easily trapped by the PUF plugs than the particulate fraction. When winds get stronger, particles penetrate further into the PUF plugs, causing N to decrease. Multivariate linear regression also demonstrates the significant influence of wind speed (u) on N :

$$N = -(3.1 \pm 0.5) \cdot \log P_L - (57 \pm 10) \cdot u - (4.7 \pm 1.7), \text{ when } -5 < \log (P_L/\text{Pa}) < -2.5 \quad (3-8)$$

$$(r^2 = 0.431, n=96, F = 35.627, p = 0.000)$$

Figure 3-5 C, plotting the partial regression results from equation 3-8 for different wind speeds/sampling sets, shows a reasonable good fit of the experimental data.

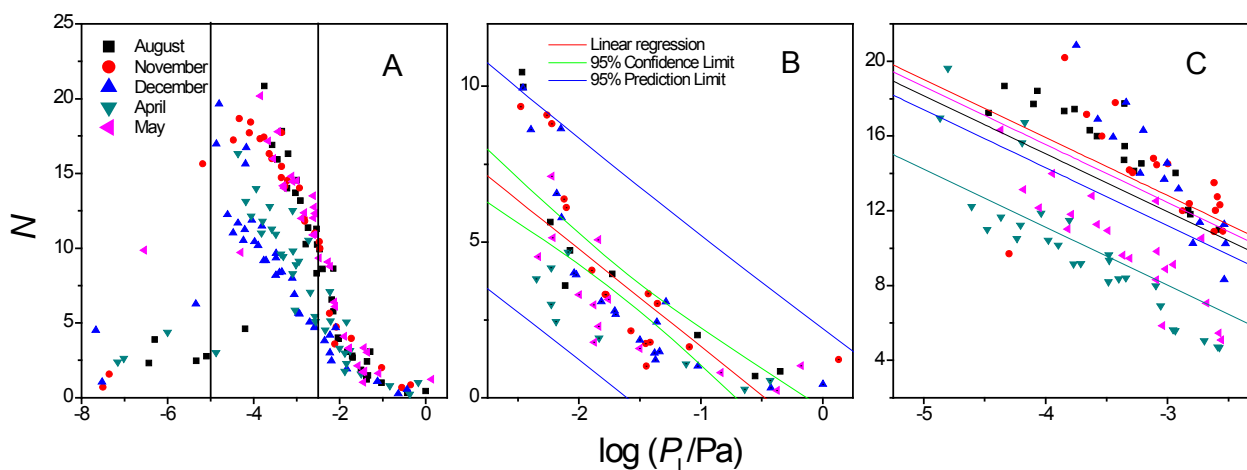


Figure 3-5. The relationship between the apparent theoretical plate number, N , and the vapour pressure P_L of the analytes for the five flow through samples reveals a temperature and wind speed effect on N . Average wind speed during sampling increases from November, May, August, December to April, whereas average temperature decreases from August, May, April, November to December. Panel A shows all chemicals, panel B only the gas phases compounds, and panel C the partially particle-bound chemicals. In panel C the line with the same color as the symbol represents the projection of the multi-linear regression result for different samples.

For nonvolatile compounds with $\log(P_L/\text{Pa}) \leq -5$, the break-through is neither temperature dependent nor chemical-specific, but is presumably controlled by how far the particles can penetrate through the sampling medium under certain wind conditions.

Both the controlled indoor experiments (Xiao et al. 2007) and the field test have demonstrated that the flow-through sampler can provide reproducible, quantitative information on SOC air concentrations. With a significantly higher sampling rate compared to PAS, this technique can provide air concentration information at a much higher temporal resolution. Even in the absence of reliable power supply, the FTS should be suitable for obtaining air samples sufficiently large to determine very low SOC concentrations at a seasonal or even monthly resolution.

3.4 Acknowledgements

We thank the Natural Sciences and Engineering Research Council of Canada and the Northern Contaminants Program of the Canadian Department of Indian Affairs and Northern Development for funding.

3.5 Supporting Information Available

Original concentration data and additional figures. This material is available in Appendix II.

Chapter 4

Validation of a Flow-Through Sampler for PBDEs and Pesticides in Air³

4 Brief

A flow-through air sampler is shown to provide similar absolute air concentrations and seasonal time trends as a classical HiVol sampler for both gas phase and particle bound substances. An empirical LSER equation predicts the sampling efficiency of the sampler for different chemicals and environmental conditions.

4.1 Introduction

There is a growing concern about semi-volatile organic compounds (SVOCs) in the environment, especially those which are persistent, display toxic effects at low concentrations, bioaccumulate and have long-range transport (LRT) potential. The 2005 Stockholm Convention on Persistent Organic Pollutants (<http://www.pops.int/>) aims to reduce or eliminate the use, discharges and emissions of such persistent organic pollutants. Besides the polychlorinated biphenyls (PCBs), and the polychlorinated dibenzo-dioxins and -furans, the initial set of twelve persistent organic pollutants designated by the Convention includes the nine organochlorine pesticides (OCPs) aldrin, dieldrin, dichlorodiphenyltrichloroethane (DDT), endrin, chlordane, mirex, heptachlor, hexachlorobenzene, and toxaphene (Eckley 2001). In addition to these identified “dirty dozen”, some “emerging” substances of concern, such as the polybrominated diphenyl ethers (PBDEs), are being considered for inclusion in the Convention (Hites 2004; Stock et al. 2004).

PBDEs are a group of flame retardants that are used in various polymers in commercial and household products to reduce their flammability (WHO 1994). PBDEs have been detected in

³ Xiao, H.; Hung, H.; Lei, Y.D.; Wania, F. Submitted to *Atmos. Environ.*

Field tests were conducted by H. Xiao. All samples were extracted, cleaned up and quantified by H. Xiao under the supervision of H. Hung and Y.D. Lei. Instrumental analysis was aided by Y.D. Lei. The data were interpreted and the paper was prepared by H. Xiao in consultation with F. Wania.

numerous environmental samples and their concentrations are often observed to increase over time, even in remote regions (Alaee and Wenning 2002; Ikonomou et al. 2002; Luross et al. 2002; Su et al. 2007). Meanwhile evidence is emerging as to their persistence, bioaccumulation potential, and potential to cause adverse effects on wildlife and humans (Eriksson, Jakobsson and Fredriksson 2001; Viberg, Fredriksson and Eriksson 2002; Zhou et al. 2002). Compared with the large number of studies reporting PBDEs in sediments, fish, marine mammals, and human samples (Hites 2004), relatively few investigations have reported concentrations in the atmosphere (Gouin et al. 2002; Gouin et al. 2005b; Jaward et al. 2004; Shen et al. 2006; Strandberg et al. 2001; Su et al. 2007; Wilford et al. 2004). Due to low volatility, concentrations of PBDEs in atmospheric samples tend to be fairly low.

Conventional high volume (HiVol) samplers, which have been used in several international, long-term monitoring programs (e.g. Northern Contaminants Program in Canada, European Monitoring and Assessment Program, and the Canada-US Integrated Atmospheric Deposition Network), can provide useful data for assessing temporal trends of SVOCs. However, high cost and the requirement for a reliable power source make large scale air monitoring networks relying exclusively on pumped HiVol samplers unrealistic. In contrast, passive air samplers (PAS) not only are small, relatively inexpensive, simple to deploy and do not require electricity, but they also can provide time integrated air concentration information. Their usefulness has been demonstrated in several studies investigating spatial distribution patterns at the local, regional, and continental scale (Harner et al. 2004; Jaward et al. 2004; Pozo et al. 2006; Shen et al. 2004). However, the limited sampling rate of PAS makes the detection of SVOCs with low atmospheric concentrations very challenging, in particular if a target analyte is present in blank samples. The most commonly used PAS designs also lack the ability to effectively capture particles and thus to quantitatively determine the concentrations of particle-bound SVOCs.

In previous studies (Xiao et al. 2008; Xiao et al. 2007), we have developed a flow-through sampler (FTS) for SVOCs in air, which can sample a large volume of air in a relatively short period of time even in the absence of power. In both indoor experiments and field tests, the FTS has been shown to be a feasible method for reliably and quantitatively collecting PCBs and PAHs from air. In this study, we tested the performance of FTS for chemicals with a larger range of properties, mainly slightly more polar substance like the OCPs and less volatile compounds

like the PBDEs. The intention is to investigate the breakthrough behaviour for all compounds of interest and thereby to identify the chemical applicability range for the sampler.

4.2 Method

4.2.1 Sampling procedure and sample analysis

The FTS, as described in detail in an earlier publication (Xiao et al. 2007), consists of a horizontally-oriented, aerodynamically-shaped, stainless steel flow tube, which is mounted on ball bearings which allow it to turn into the wind with the help of vanes (Figure 2-1). In the earlier field test, a FTS was deployed on a 2 m post on the roof of the science building of the University of Toronto Scarborough, (43° 47' 0.56" N, 79° 11' 16.30" W), which is located in a forested area in the Eastern suburbs of metropolitan Toronto, Ontario, Canada (Xiao et al. 2008). Five two-week-long flow-through samples were taken between August, 2006 and June 2007. Seven P10z PUF disks of 2.54 cm thickness (i.e., one inch) were arranged in series inside the sampling cylinder and were extracted and analyzed separately. An active HiVol sampler was set up approximately 10 meters away from the FTS. A variable number of 24-hour HiVol air samples was taken during each FTS sampling period. The PUFs from both FTS and HiVol, were extracted by Soxhlet for 24 hours with acetone and PE (1:1); GFFs were also Soxhlet-extracted for 24 h using DCM. The extracts were rotary evaporated, dehydrated and solvent exchanged to isooctane. All samples were blown down to 1 ml and 100 ng of Mirex was added as internal standard for volume correction. The detailed sampling procedure, extraction and sample preparations are documented in the earlier paper, as are the PCBs and PAHs concentration in the samples (Xiao et al. 2008). It should be noted that the May to June sample utilized a PUF/XAD sandwich as the sampling medium, for which breakthrough levels are expected to be minimal.

In this study, the extracts from both FTS and HiVol were analyzed for PBDEs and selected pesticides. All instrumental analyses were achieved with an Agilent 6890 GC equipped with splitless injector and a 5973D mass selective detector. Helium was used as the carrier gas. The mass spectrometer was run on the negative chemical ionization (NCI) mode, with methane as the reagent gas.

Fourteen PBDE congeners (BDEs 17, 28, 71, 47, 66, 100, 99, 85, 154, 153, 138, 183, 190 and 209) were quantified using an internal standard method (mirex). The quantification was done

with a 15m DB5 column with a 0.25 mm id and 0.25 μm film thickness (J&W Scientific, Rancho Cordova, CA). The GC oven temperature program was modified to 90°C for 2 min, 20°C/min to 160 °C, 5 °C/min to 290 °C, and a final hold for 11.5 minute. Sample injection volume was 1 μL in splitless mode. The injector, transfer line, source and quadrupole temperatures were 250, 280, 230, and 106 °C, respectively. Masses 79 (PBDEs) and 404 (Mirex) were monitored for quantification, plus 81 and 402 for confirmation. For BDE-209, mass 486.6 was used for quantification, and ions 79, 81, and 488.5 were used for confirmation. Compounds were identified and quantified by comparison with a series of standard solutions of known concentration (from Cambridge Isotope Laboratories, Andover, MA).

Twenty-four organochlorine pesticides (α -HCH, β -HCH, γ -HCH, δ -HCH, HCB, chlorothalonil, aldrin, dieldrin, chlorpyrifos, dacthal, heptachlor, heptachlor epoxide, trans-chlordane, cis-chlordane, trans-nonachlor, α -endosulfan, β -endosulfan, endosulfan sulphate, o,p'-DDE, o,p'-DDD, o,p'-DDT p,p'-DDE, p,p'-DDD and p,p'-DDT) as well as trifluralin, dimethoate, malathion, metribuzin, and pendimethalin were analysed with a 60m DB-5 MS column with 0.25 mm id and 0.25 μm film thickness (J&W Scientific, Rancho Cordova, CA). The initial temperature of 70 °C was held for 0.5 min, then ramped 15 °C/min to 160 °C, 2 °C/min to 250 °C, finally increased to 270 °C with 20 °C/min and held for 5 minutes.

4.2.2 QA/QC

Analytical method recoveries of PBDEs and OCPs were determined by spiking two clean PUF discs with the working standard containing all chemicals (20 ng of each PBDE congener and OCPs) and treating them as real samples. Results show good recoveries ranging from 70% to 115%. Recovery correction was not applied to any of the data reported below.

Field blanks collected from both the active and flow-through samplers and solvent blanks were analyzed. The field blanks for the PUF plugs and PUF disks have slightly higher levels of both the PBDEs and OCPs than was found in the solvent blanks, while little difference was observed between method blanks and field blanks of the GFFs. Concentrations of PBDEs and OCPs in the samples were blank corrected. For compounds not detected in blanks, two-thirds of the instrumental detection limit, derived as the amount at which the signal-to-noise ratio equals 3, was used for blank correction. Blank levels and limits of detection are reported in Table SI 12 in the Appendix.

4.3 Result and Discussion

4.3.1 Break-through profile for PBDEs and OCPs

Earlier research (Xiao et al. 2007; You and Bidleman 1984) had shown that the PUF plugs in the FTS could be treated as a short frontal gas chromatography column with only a few theoretical plates. Plotting the chemical amount trapped on each PUF as a percentage of that trapped on the first PUF plug against the overall PUF thickness, L , yields a breakthrough curve (Figure 4-1). The theoretical plate number of the sampling assembly, N , can be determined from the thickness of foam at the 50 % breakthrough point, L_{50} , and the slope of the breakthrough curve at that point (see Figure 4-1 upper left panel). The theoretical plate number can be determined from the empirical regression parameter p in the non-linear logistic regression (equation 4-1) fitting the breakthrough curve (Xiao et al. 2007):

$$\% \text{ of first PUF plug} = f(L) = \frac{100}{1 + (L/L_{50})^p} \quad (4-1)$$

$$N = \pi p^2 / 8 \quad (4-2)$$

After blank correction, ten out of the 14 PBDE congeners and 17 pesticides were detected in at least some of the samples (see Table SI 9). The amount of chemicals trapped inside each 2.54 cm PUF disk was expressed as a percentage of the first PUF plug and plotted against the thickness of the PUF in Figure 4-1 for selected pesticides and PBDE congeners. In those figures different colors represent different FTS samples. As expected, volatile pesticides, such as HCB, experienced some breakthrough during two-week-long sampling periods. Based on the integration of the logistic regression curves, the breakthrough for HCB ranged from 39% to 66%, which is comparable to values found in HiVol samples (see Table SI 11). Less volatile compounds, like the PBDEs and the larger pesticides, were stripped completely from the air stream by the seven PUF disks. In general, most chemicals of interest other than HCB had tolerable breakthrough levels. Interestingly, trifluralin and α -HCH suffered less breakthrough than HCB, even though they are more volatile. This suggests that volatility alone may not be controlling sorption to PUF and therefore breakthrough.

For some PBDE congeners, the last PUF plug sometimes had slightly higher amount than the two plugs in front of it. This could be due to uptake by molecular diffusion during wind still time periods, or to changes in wind directions that occur faster than the ability of the FTS to align

itself. Theoretically, this phenomenon should be observed for all chemicals, but it becomes much important and obvious for chemicals with lower atmospheric concentrations. The vapor front curves for all those chemicals which could be detected in more than three PUF disks, were fitted to equation 4-2 to estimate N . Only the N with a relative standard deviation smaller than 100% were listed in Table SI 10 and those N values were used to better understand the uptake mechanism of the FTS and the molecular interactions between the target chemicals and the P10z PUF plugs (see below).

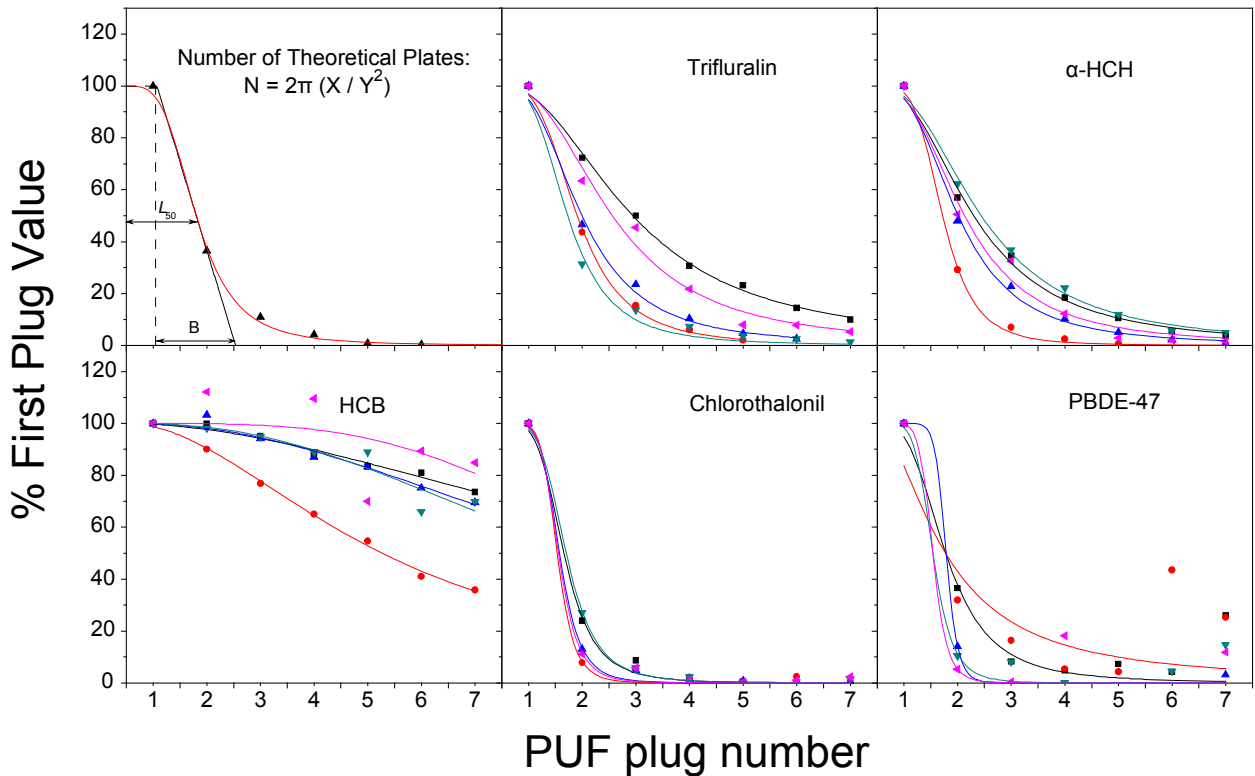


Figure 4-1. Vapor fronts of selected organochlorine pesticides and PBDE-47 from different sampling periods. The black, red, green, blue and purple color represent samples taken during August, November, December, April and May, respectively. The upper left panel illustrates the approach to determine L_{50} and theoretical plates number N from the breakthrough curves.

4.3.2 Comparison of Flow-through samples with HiVol data

In the earlier publication, we already described the estimation of the sampled air volumes for each flow-through sample based on wind speed measured by the vortex sensor on top of the sampler (Xiao et al. 2008). PBDE and pesticide air concentrations can be calculated by adding the total blank-corrected amounts of chemical sorbed to all seven PUF disks and then dividing by the total sampled air volume. The sum of the concentrations on GFF and two PUF plugs from the HiVol sample was used for comparison (see Table SI 11 for detailed information).

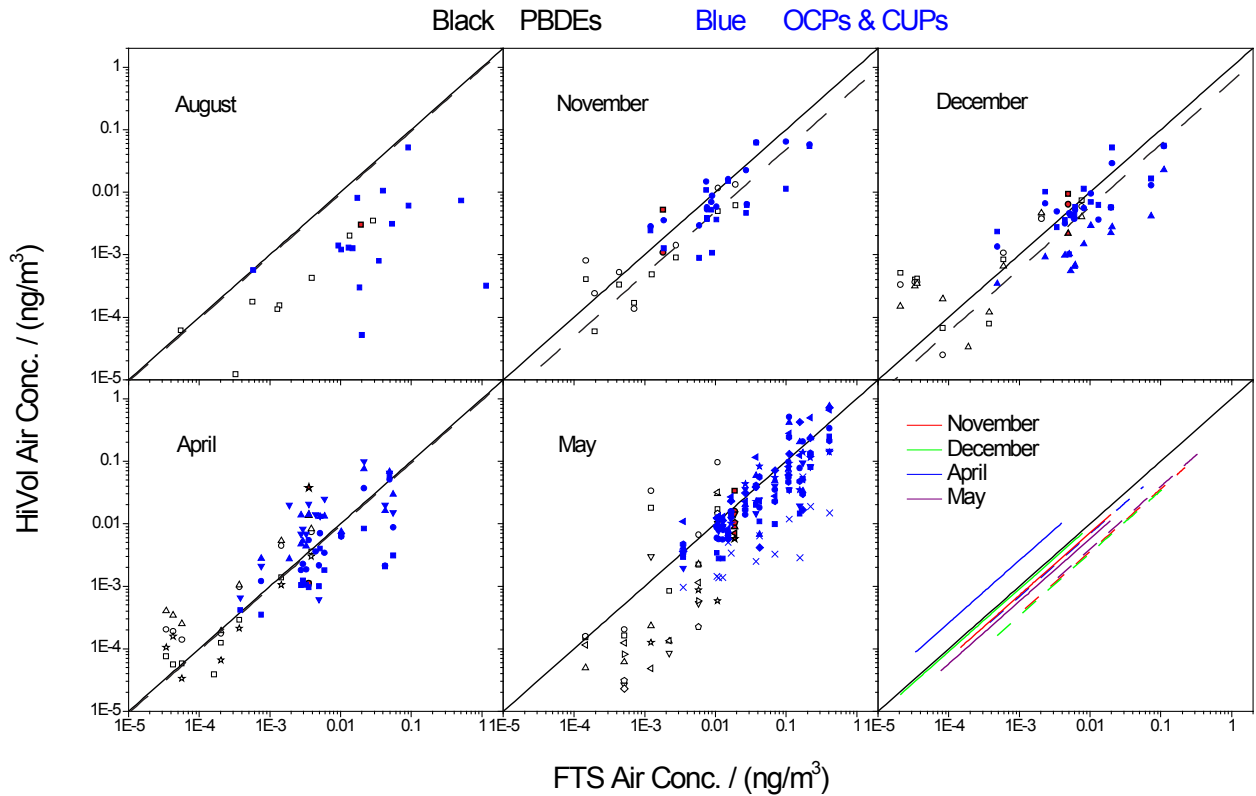


Figure 4-2. Comparing the air concentrations of PBDEs (black markers) and pesticides (blue markers) obtained with the flow through sampler with the 24-hour HiVol samples taken during the same sampling period. The red markers are values for PBDE-209. The bottom right panel shows the regression lines between the FTS concentrations and the weighted average of HiVol concentrations for different sampling sets (PBDEs - solid lines, pesticides - dashed lines).

Figure 4-2 compares the air concentrations for PBDEs and pesticides obtained from each FT sample with the concentrations obtained by HiVol samples (PUF + GFF concentrations) taken during individual 24 h periods within the FT sampling period. The sample volumes V_{air} estimated from the outside wind speed are chosen for comparison, while the black dashed lines in Figure 4-2 represent the concentrations calculated from the sampling volume estimated from inside wind speed. In the figures, different symbols represent the different HiVol samples within a particular FT sampling period; and black and blue color represent PBDEs and pesticides, respectively. Pesticide levels are substantially higher than those of the PBDEs. The black diagonal lines represent perfect agreement (1:1 ratio). Such agreement cannot be expected when comparing two sampling techniques covering different time scales, because air concentrations experience considerably variability on a scale of a few days (Gouin et al. 2005a). Indeed, the 24-h HiVol samples taken during a two-week FTS sampling period show a variation within one order of magnitude. Nevertheless, except for August, when only one HiVol sample was taken, the FTS-derived air concentrations agree well with the HiVol samples taken within the same periods, as is evident by the clustering of the data points around the diagonal. The air concentrations in the FT sample taken from May 22 to June 6 are fairly close to the average of all the HiVol samples taken during those days. Even for mostly particle-bound chemicals, such as PBDE-209 (indicated by red colour in Figure 4-2), the FTS-derived air concentrations are comparable with those from the HiVol samples. It thus appears, that even though the sampling by FTS is biased toward time periods with higher wind speeds (Xiao et al. 2007), the levels obtained with the FTS are still representative of the average air concentrations.

The weighted-average approach introduced in the previous study to correct for the bias of the FTS toward time periods with higher wind speeds (Xiao et al. 2008) was used to compare the data from the two sampling methods more quantitatively. The FTS sampled air volumes during the duration of each HiVol sample, v_i , were treated as weighting factors (listed in Table SI 11). Then the average HiVol concentration can be estimated as,

$$\overline{C}_{\text{HiVol}} = \frac{\sum v_i \cdot c_i}{\sum v_i} \quad (4-3)$$

where c_i is the concentration in a HiVol sample taken during a flow-through sampling period. The average HiVol concentrations calculated this way correlate strongly with the FTS results. In the bottom right panel of Figure 4-2, linear regression lines for different sampling sets and

different chemical groups are included. Generally, the slopes of the regression lines range from 0.343 to 2.62. This translates to discrepancies of up to a factor of 3 for compounds present at higher concentrations. It seems that for pesticides with higher atmospheric concentrations, mainly HCB and chlorothalonil, FT-derived concentrations are always higher than the average HiVol values. It is hard to judge whether this is because those compounds experience less breakthrough in the FTS than during HiVol sampling or because of the “selective” placement of the HiVol sampling periods. We further compared the FTS concentrations with the weighted and un-weighted average of the HiVol values using paired two sample t-tests (Table SI 13). Except for the pesticides in the May to June samples, when FTS results were slightly higher than the weighted-average HiVol concentrations; there was no significant difference between the concentrations derived from the two sampling techniques. In summary, despite occasional discrepancies, the concentrations derived from the two methods are within a factor of 3, which is good considering the overall experimental uncertainty, including the uncertainty in the sampled air volume, and the fact, that the HiVol samples did not cover the entire two weeks of a FT sampling period.

To further evaluate the performance of the FTS relative to the HiVol sampler, Figure 4-3 compares the time trends obtained with either sampler for selected chemicals occurring at higher concentration. Both FTS and HiVol samples show that chlorothalonil, HCB, α -endosulfan and chlorpyrifos were the dominant pesticides in the Toronto atmosphere during the whole sampling campaign, while sharp temporary concentration peaks were observed for malathion, dacthal, and pendimethalin during the spring season. PBDE-47 and PBDE-209 were the most abundant PBDE congeners (see Table SI 9 and Table SI 11 for detail). Except for the FTS samples from August when only one HiVol sample was taken, the FTS captures the concentration variations with time well. The HCB concentrations did not show any significant seasonal change, while the two-week average (FTS-derived) concentrations ranged from 49 to 215 pg/m^3 and daily concentrations changed from 22.7 to 96.8 pg/m^3 . The other chemicals show large seasonal variability, with spring and summer concentrations measured by FTS and HiVol more than one and two orders of magnitude higher than those measured in winter and early spring, respectively. Figure 4-4 plots the natural logarithm of the concentrations against the reciprocal of the average temperature during each sampling period for both FTS and HiVol samples. It confirms that while HCB concentrations are independent of temperature, those of the other chemicals are relatively

strongly correlated with temperature. The slopes of the regressions in Fig. 4-4 are similar for FTS and HiVol samples. Although it should be noted that the apparent temperature dependence of the concentrations of current use pesticides is likely the result of seasonal usage patterns, the comparison shows that the FTS is suitable for investigations of the time trends and temperature dependence of SOC air concentrations, even for fully particle-bound compounds like PBDE-209.

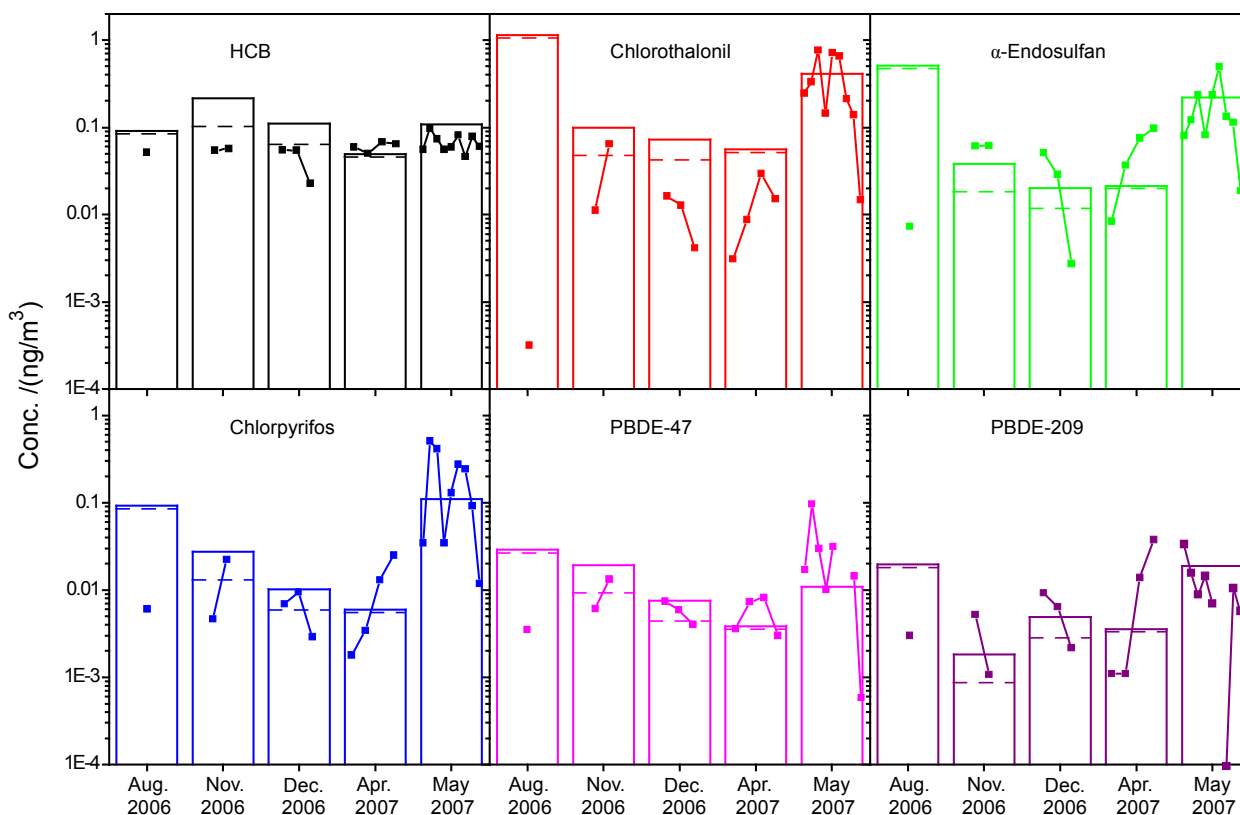


Figure 4-3. Comparison of time trends in the air concentrations of selected chemicals as derived by FTS (bars, the two horizontal lines indicate the uncertainty introduced by the sample volume estimation) and HiVol sampler (square markers).

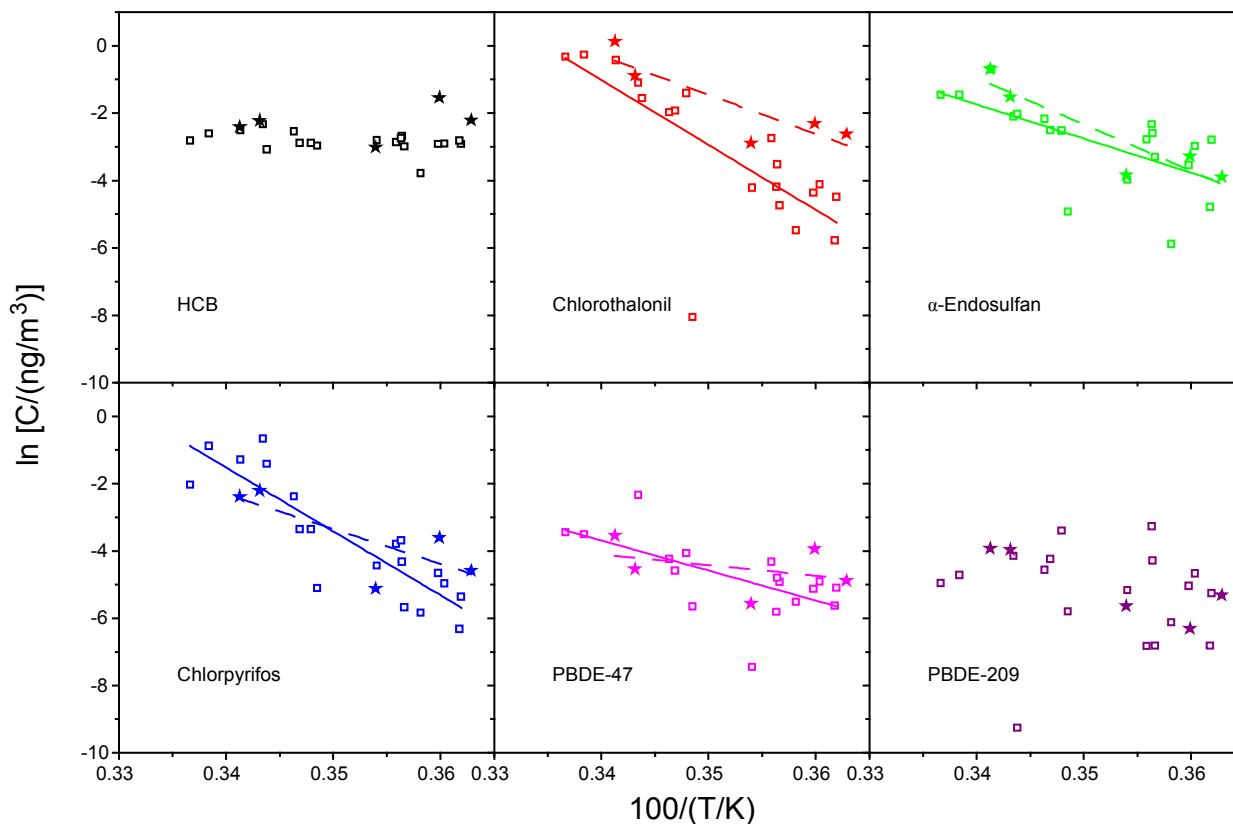


Figure 4-4. Apparent temperature dependence of air concentrations derived by FTS and active sampling for dominant pesticides and PBDE congeners. The solid and dashed lines represent the regression for HiVol samples and FTS, respectively.

Isomer ratios, such as α -HCH/ γ -HCH, TC/CC and DDT/DDE ratios, have been widely used as indicators of source characteristics (Bidleman et al. 2002; Hoff, Muir and Grift 1992; Shen et al. 2005). Figure 4-5 compares the FTS and HiVol-derived concentration for Chlordane and HCH isomers as well as their ratios. Both sampling techniques achieved similar absolute concentration values and temporal trends for the two chlordane isomers and therefore also similar TC/CC ratios (Left side of Figure 4-5). However, the α / γ -HCH ratios of 1 to 2.4 obtained with the FTS are significantly higher than those obtained from the HiVol samples which range from 0.25 to 1.7 (right side of Figure 4-5). The discrepancy is mainly due to differences in the α -HCH concentrations obtained with the two techniques, because the γ -HCH concentrations from both methods are quite consistent. One possible explanation for the discrepancy is a higher breakthrough loss of α -HCH from the HiVol samples, which use polyether PUF, compared to

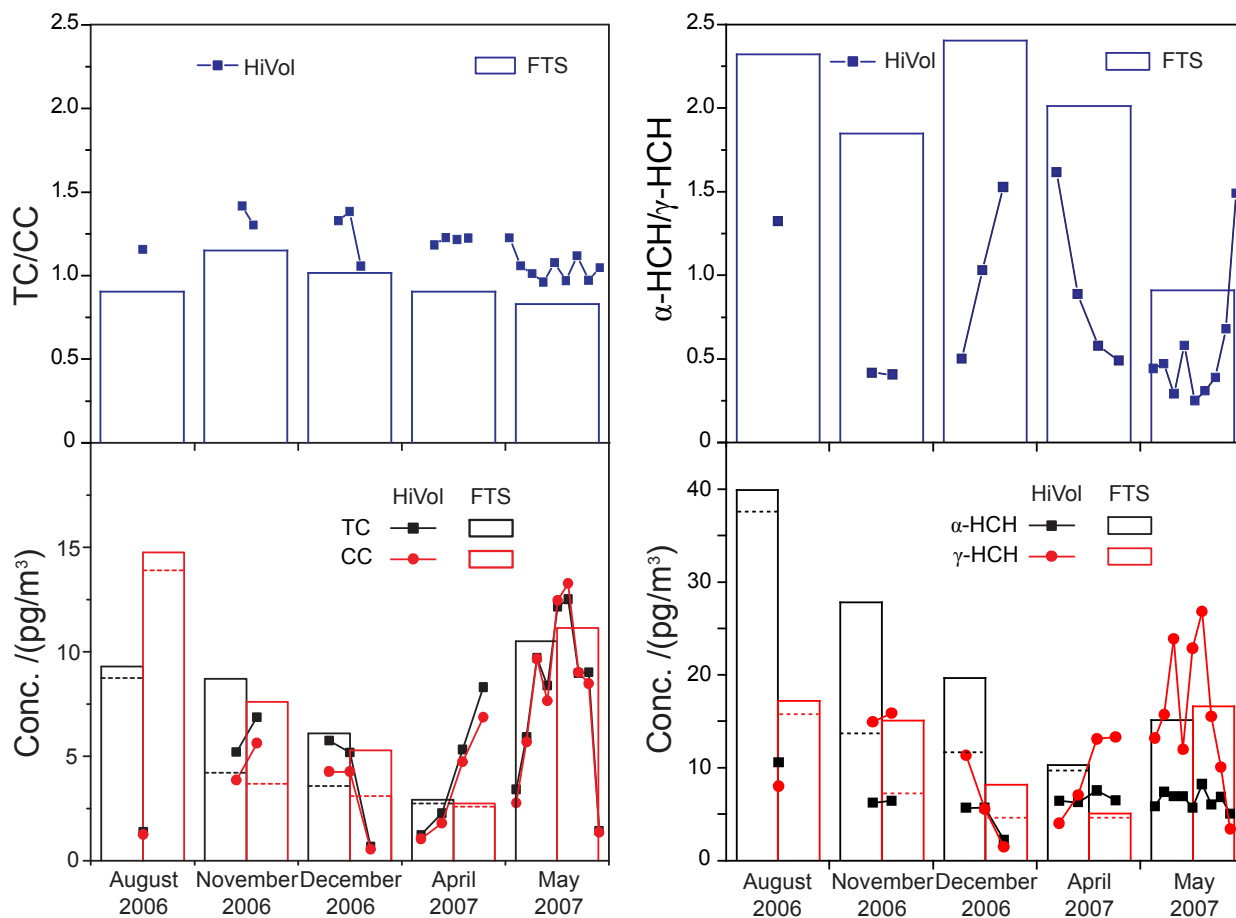


Figure 4-5. Comparison of Chlordane and HCH concentrations (bottom panel, the black and red color represent different isomers respectively) and TC/CC and α -/ γ -HCH ratios (top panels) as derived by FTS (bars, the two horizontal lines indicate the uncertainty introduced by the sample volume estimation) and HiVol sampler (markers).

the FTS, which uses polyester PUF. Actually, the α / γ -HCH ratios in the FTS samples taken during May to June, was within the range of ratios in the HiVol samples, which relied on PUF/XAD sandwiches as active sampling medium during that time period. Although the FTS-derived α -HCH concentration was still about two times higher than the average HiVol values, it may simply be due to the fact that the sampled air volume may have been underestimated based on the outside wind speeds for relatively wind still periods. Using linear solvation energy relationships reported by Kamprad et al. (2007), the sorption of the HCHs to polyester-PUF is estimated to be approximately 1.5 to 6.3 times higher than to polyether-PUF, which would be consistent with a higher break through in the HiVol samples. The same linear solvation energy relationships also predict that sorption of γ -HCH to PUF is about 2.7 time higher than that of α -

HCH. This is in agreement with observations. The breakthrough level for the FTS estimated by integrating the vapor front curves for α -HCH ranges from 0.3 to 12%, while the corresponding value for γ -HCH is 0.0 to 1.2%. It is difficult to estimate a precise breakthrough levels for the HiVol samples, but based on back-to-front PUF ratios α -HCH also suffers a higher rate of breakthrough than γ -HCH in the HiVol samples. However, overall that breakthrough is still quite small and it is unlikely to be sufficiently large to explain the differences in α -HCH concentrations measured by FTS and HiVol. Without a quantitative understanding of differences in the sampling efficiencies of even closely related congeners, the uncertainties of the ratios could easily be underestimated, especially for relatively volatile compounds such as the HCHs.

Table 4-1 compares the PBDE and pesticide concentrations measured in this study with some literature values for the Toronto area (Farrar et al. 2005; Gouin et al. 2005a; Gouin et al. 2007; Harner et al. 2004; Harner et al. 2006b; Moreau-Guigon et al. 2007; Motelay-Massei et al. 2005). Even though the studies were conducted in different locations, seasons and years using different sampling methods, most of the reported levels are well within the same order of magnitude. HCB, endosulfans, PBDE-47, 99, 100 and 209 are commonly reported SVOCs in the Toronto atmosphere.

4.3.3 Linear solvation energy relationship (LSER) prediction of the theoretical plate number, N

Previously, we have learned that wind speed, temperature, and volatility play an important role in determining the sampling efficiency of the FTS, quantitatively expressed by the apparent theoretical plate number N (Xiao et al. 2008). However, as pointed out earlier, properties other than vapor pressure may also influence the retention of organic chemicals on the PUF. When describing and/or predicting the partitioning behavior of a broad variety of neutral organic compounds, poly-parameter linear free energy relationships (pp-LFER) have significant advantages over single parameter regressions (sp-LFER). pp-LFERs have therefore been proposed as the method of choice for obtaining consistent partition coefficients over a broad variety of environmentally relevant partitioning systems and compounds (Goss and Schwarzenbach 2001). One of the most prominent pp-LFERs is the linear solvation energy relationship (LSER) method, introduced by Kamlet and Taft (Kamlet and Taft 1979) and subsequently developed by Abraham (Abraham 1993), which characterizes the interaction of a solute molecule with its environment through a correlation in the form of equation (4-4).

Table 4-1. Comparison of concentrations (pg/m³) of PBDEs and pesticides measured in this study with reference values for Toronto urban sites.

	This work		Harner et al. 2006		Gouin et al. 2005			
	FTS	HiVol	2000-2001		7. 2002-6. 2003			
PBDE-17	0.20±0.18	0.04	0.28±0.13					
PBDE-28	0.54±0.51	4.54±11.8	0.78±0.48		1.5			
PBDE-71			0.04±0.01					
PBDE-47	14.1±10.0	15.4±22.6	7.59±3.62		20			
PBDE-66	0.17±0.11	0.10±0.09	0.23±0.11					
PBDE-100	1.77±1.51	3.91±9.02	0.90±0.39					
PBDE-99	6.71±5.30	3.20±2.84	3.27±1.32		6			
PBDE-85	0.05	0.12±0.08	0.11±0.07		1.6			
PBDE-154	0.19±0.22	0.27±0.20	0.21±0.12		0.4			
PBDE-153	0.48±0.54	0.19±0.15	0.25±0.12		0.4			
PBDE-138		0.05±0.02	0.03±0.00					
PBDE-183	1.19±0.91	0.28±0.23	0.23±0.14					
PBDE-209	9.73±8.71	9.81±10.6						
	This work		Harner et al. 2004	Farrar et al. 2005	Gouin et al. 2005	Moreau-Guigon et al. 2007	Gouin et al. 2007	Motelay-Massei et al. 2005
	FTS	HiVol	7-10, 2000	10. 2001	7.2002-6.2003	30 m	7.2002-6.2003	7. 2000-6. 2001
trifluralin	22.3±23.6	13.1±21.6						
α-HCH	22.6±11.7	6.4±1.6	45.8±8.1	340	23±9.4	24.7±21.4		
HCB	115±61.3	60.4±15.5						58.3±17.4
γ-HCH	12.4±5.4	12.5±6.9	35.6±14.5	292	57.0	30.5±31.7		
chlorothalonil	356±462	179±257						
metribuzin	3.4±4.3	0.5±0.1						
HEPT	1.9±1.4	2.3±1.5						
malathion	79.4±108	74.4±119						
chlorpyrifos	49.1±48.5	96.8±152.2						
dacthal	32.3±26.1	19.5±21.2						
pendimethalin	64.1±93.7	46.9±58.9						
TC	7.5±3.0	6.0±3.6	21.2±13.7	7.4		16.0±10.0	39±31	
Endo I	161±211	102±116	394±21.1		430	293±344		
CC	8.3±4.8	5.5±3.8	19.7±12.3	4.5		17.3±12.1	37±33	389±370
TN	8.0±3.7	5.4±3.7	13.9±6.2			13.7±9.5	25±25	21.0±16.2
dieldrin	13.2±8.2	15.9±13.4	27.1±8.1		83	67.1±53.7		52.1±46.9
Endo II	14.1±14.8	22.9±27.4				84.4±98.7		
Endo SO ₄	1.3±1.2	2.9±2.3				18.5±11.6		16.4±14.1

$$SP = l \cdot \log L_{16} + e E + s S + a A + b B + c \quad (4-4)$$

Here SP represents a property, such as a partitioning equilibrium, of a solute in a particular environment. The system constants l , e , s , a , b and c are characteristic of the medium, while the parameters $\log L_{16}$, E , S , A , and B are empirical descriptors of the solute, called Abraham parameters. The first three parameters represent non-specific interactions of the solute with the system, that is, interactions that do not depend on a particular orientation of the solute with surrounding molecules. $\log L_{16}$ is generally considered a measure of cavitation and generalized dispersion interactions. E is the excess molar refraction of the solute; and R is a measure of the solute's dipolarity/polarizability, which characterizes the interaction of the solute with the surrounding medium through non-specific dipole–dipole or dipole-induced dipole interactions. The specific (orientation-dependent) interactions are characterized by parameters A and B , which respectively represent the sums of the hydrogen bond donor and hydrogen bond acceptor characteristics of the solute.

Here we try to identify the molecular interactions influencing the theoretical plate number, $\ln N$, of P10z PUF plugs. Phase equilibria between a solvent or sorbent (S) and the gas phase (A) are usually highly dependent on temperature, whereby this dependence is often quantified using an enthalpy of phase transfer $\Delta_{S/A}H$. Typically, $\Delta_{S/A}H$ is obtained by invoking a form of the van't Hoff equation, for example:

$$\ln K_{S/A} = -\Delta_{S/A}H / RT + c = a/T + c \quad (4-5)$$

Assuming that the enthalpy is not directly related to the Abraham parameters, we can add a reciprocal temperature term into the LSER to form an empirical equation that includes the temperature effect. We can do the same for wind speed, u . The $\ln N$ values from this study as well as those for PCBs and PAHs reported earlier (Xiao et al. 2008) were regressed against Abraham parameters from refs. (Abraham and Al-Hussaini 2005; Shunthirasingham, Lei and Wania 2007; Stovall et al. 2005; Yang and Holmén 2007). Values for T and u used in the regression were the arithmetic average during the FTS sampling period. The regression excludes the PBDEs because of their highly uncertain solute descriptors, low atmospheric concentrations and large relative standard deviation of N . Stepwise regression yields the following LSER,

$$\ln N = 1.03 \cdot \log L_{16} + 40.1 A - 1.51 S + 1790/T - 5.16 u + 0.738 E + 0.587 B - 12.1 \quad (4-6)$$

$$(r^2 = 0.655, n=205, F = 53.703, p < 0.001)$$

Figure 4-6 shows the comparison between the $\ln N$ calculated using linear regression equation 4-6 with the experimental values from this and the previous study (Xiao et al. 2008). Equation 4-6 shows that beside dispersive interactions, the excess molar refraction and especially the hydrogen bond donor property of the solute have a significant and positive impact on $\ln N$. The hydrogen bond acceptor strength of the solute is relatively not that important, i.e. the P10z PUF plugs used in the FTS is not a good hydrogen bond donor. This agrees well with the characterization of polyurethane ester foam by Kamprad and Goss. (Kamprad and Goss 2007), who used PUF from the same manufacturer but with different porosity.

Wind speed (u) and temperature are negatively correlated with $\ln N$. When winds get stronger, chemicals penetrate further into the PUF plugs, causing N to decrease. N -values for these chemicals are significantly lower during sampling periods with relatively high wind speeds and temperature. Although the empirical equation 4-6 only applies to the limited range of temperatures and wind speeds encountered during our field test, it still can provide a useful approximate estimation of N , which is valuable for evaluating the performance of FTS during field deployments or for predicting the breakthrough behavior of compounds with known solute descriptors.

Analysis of field tests for PBDEs and a large variety of pesticides has shown the flow-through sampler to be a reliable, quantitative method for sampling SVOCs from air, including relatively polar and strongly particle-bound substances. With a significantly elevated sampling rate compared to conventional PAS, this technique can provide air concentration information at a much higher temporal resolution. Even in the absence of reliable power supply, the FTS should be suitable for obtaining air samples sufficiently large to determine very low concentrations of SVOCs at a seasonal or even monthly resolution.

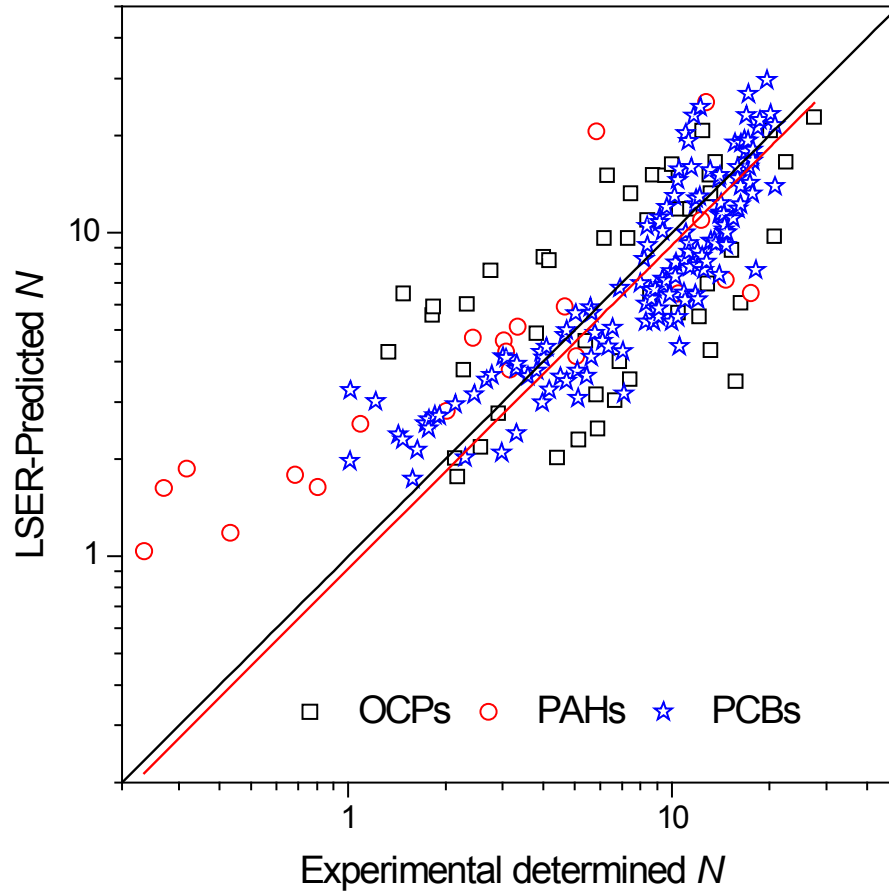


Figure 4-6. Comparison between the LSER prediction of the theoretical plate number, N from equation 4-6 with the experimental results for PCBs, PAHs and pesticides.

4.4 Acknowledgements

We thank the Natural Sciences and Engineering Research Council of Canada for funding.

4.5 Supporting Information Available

Original concentration data are listed in the Appendix III.

Chapter 5

Seasonal Variation of Pesticides and PCBs in the Atmosphere at Nam Co, Tibet⁴

5 Brief

A flow-through air sampler deployed for one year at a remote Chinese research station close to Nam Co Lake in Tibet reveals strong seasonal variations in the air concentrations of DDT, HCHs, and endosulfan, with higher summer time levels coinciding with monsoonal air mass transport across the Himalaya.

5.1 Introduction

Organochlorine pesticides (OCPs) and polychlorinated biphenyls (PCBs) are groups of semi-volatile organic compounds classified by the Stockholm Convention as persistent organic pollutants (POPs) based on their persistence in the environment, potential toxic effects on ecosystems and humans, and potential for bioaccumulation and long-range atmospheric transport (LRAT) (Stockholm Convention on Persistent Organic Pollutants, 2005, <http://www.pops.int/>). POPs can volatilize in relatively warm source regions, undergo efficient atmospheric transport over considerable distances, and deposit in very remote locations, in particular at places with low temperatures (Wania 1999; Wania and Mackay 1993). In the past decades, many studies confirmed that such cold-trapping not only occurs on the latitudinal scale, but also along altitudinal gradients (Davidson et al. 2003; Grimalt et al. 2001). Due to the closer spatial proximity of mountain regions to source regions, the chemical transfer efficiency from valley to mountain may be higher than that from tropical to polar regions. In addition, the high precipitation rate in many mountain regions, often in the form of snow, effectively scavenges the contaminants from the atmosphere to the surface (Blais et al. 1998). However, due to the sparse

⁴ Xiao, H.; Loewen, M.; Kang, S.C.; Zhang, Q.G.; Han, W.W.; Hung, H.; Lei, Y.D.; Wania, F.

Field sampling was conducted by Q.G. Zhang, C.F. Feng, Z. Wang and Ciren Duoji under the supervision of S.C. Kang. M. Loewen initiated the study and had the sampler installed at Nam Co. Weather data were provided by W.W. Han. All samples were pre-cleaned, extracted, cleaned up and quantified by H. Xiao under the supervision of H. Hung and Y.D. Lei. Instrumental analysis was aided by Y.D. Lei. The data were interpreted and the paper was prepared by H. Xiao in consultation with F. Wania.

soil and vegetation cover, terrestrial systems at high altitude tend to have low retentive capacity for POPs, and potentially focus contaminants further into alpine lakes (Blais et al. 2001; Vilanova, Fernández and Grimalt 2001).

Concerns related to POPs are particularly grave in Asia due to intensive agricultural practices and rapidly expanding industrialization. Known as the “Roof of the World” or the “Third Pole on the Globe”, the Tibetan Plateau is the largest and highest plateau on Earth, with an average elevation of 4200 m asl and an area of 2.5 million km². The plateau is surrounded by countries such as China, Nepal and India, which have a history of high organochlorine pesticide use (Li and Macdonald 2005; Li et al. 1998). Because of the plateau’s high altitude, sparse human population, and minimal to nonexistent industrial activities, LRAT is believed to be the dominant source of POPs to the area (Loewen et al. 2007) and orographic cold-trapping may be particularly pronounced in the Himalaya and the Tibetan Plateau. As the many rivers originating from the Tibetan Plateau provide fresh water for over one sixth of the world population, the plateau may play an important role in the global biogeochemical cycle of POPs, as well as in ecosystem and human health.

During recent years, several studies have been devoted to illustrating the LRAT and the fate of POPs in the Tibetan plateau region. However, most studies focused on lake water, soil, sediments, snow/ice and biota (such as fish, grass or spruce needles) (Wang et al. 2006; Wang et al. 2007a; Wang et al. 2007a; Wang et al. 2007b; Wang et al. 2008b; Yang et al. 2007; Yang et al. 2008; Zhang and Zhang 2003). Due to the extremely low atmospheric concentrations, the amounts of POPs sequestered in passive air samplers can hardly be expected to exceed detection limits; so only a limited number of active air sampling studies has investigated the short-term variation of OCPs concentrations in the plateau’s atmosphere (Cheng et al. 2007; Li et al. 2006).

In earlier publications, we introduced a flow-through sampler (FTS) that had been developed to address the need for an air sampling technique that can achieve substantially faster uptake rates than typical passive samplers, yet still requires no access to reliable network power (Xiao et al. 2008; Xiao et al. 2007). This was accomplished through the use of a horizontally-oriented flow-tube that rotates to face the wind, which then blows through a porous sampling medium such as polyurethane foam (PUF). The uptake mechanism in an FTS is thus similar to that in a conventional active sampler. The sampled air volume can be deduced from the wind speed within the flow tube after passage through the sampling medium (Xiao et al. 2008). Both indoor

experiments and field tests clearly demonstrated that the FTS can reliably and quantitatively collect both gaseous and particle-bound SOCs from large air volumes. In this study, an FTS was deployed for more than a year in central Tibet to monitor the seasonal variation of the air concentrations of OCPs and PCBs. This is the first long term atmospheric study of POPs in Tibet, which provides not only concentration information, but also direct evidence of LRAT of POPs to the plateau.

5.2 Method

5.2.1 Sampling site

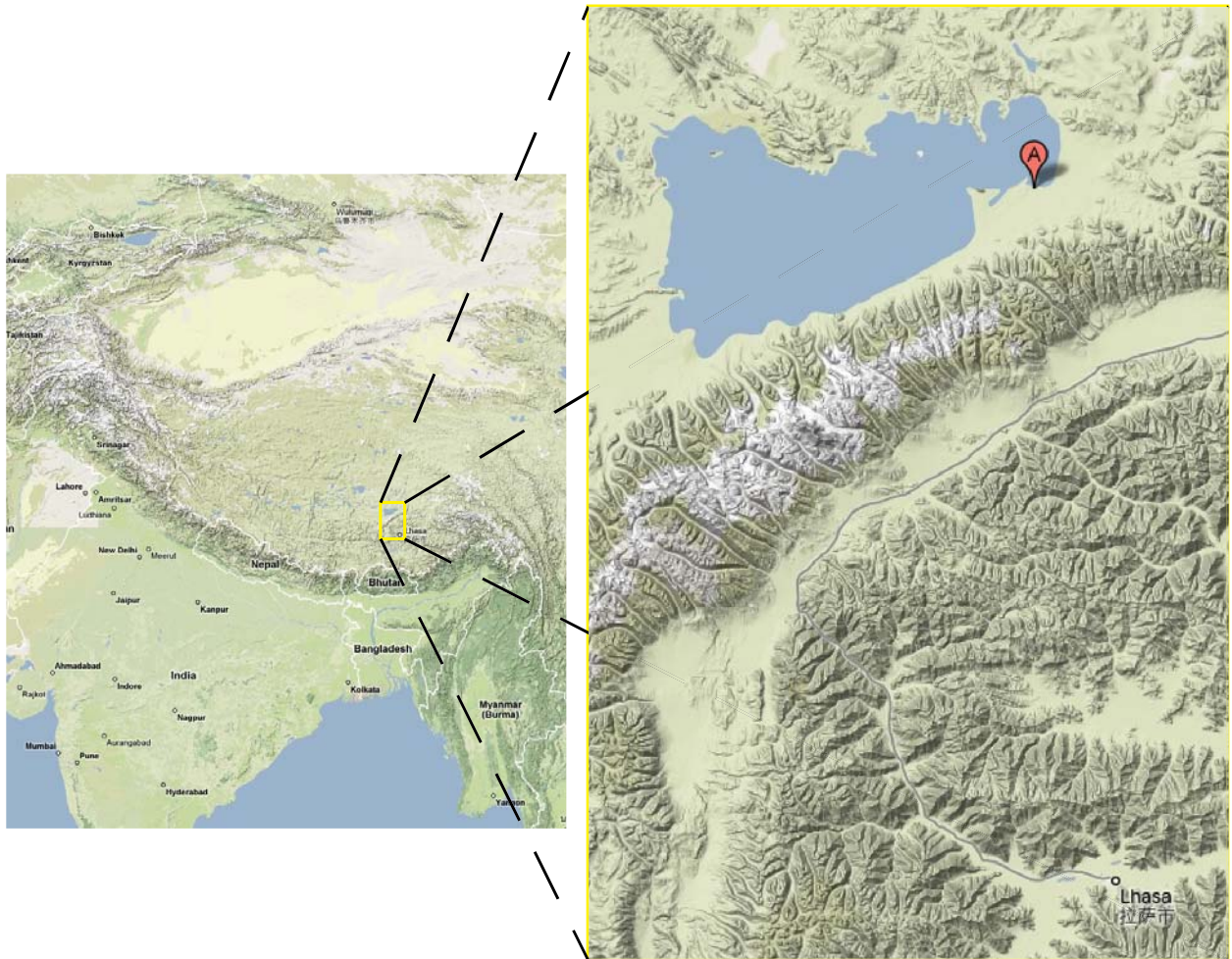


Figure 5-1. Terrain maps from Google map showing the Nam Co station (point A) and surrounding.

The FTS, as described in ref. (Xiao et al. 2007), consists of a horizontally oriented, aerodynamically shaped, stainless steel flow tube, which is mounted on ball bearings which allow it to turn into the wind with the help of vanes (See Figure 2-1). One such FTS was deployed on a 2 m post on the roof of Nam Co Comprehensive Observation and Research Station of the Institute of Tibetan Plateau Research, Chinese Academy of Sciences (briefly Nam Co Station 30°46.44'N, 90°59.31'E, 4730 m asl. See Figure 5-1). The station is located at the southeastern shore of Nam Co Lake (30°30'~30°56' N, 90°16'~91°03' E) which, lying at the foot of the Nyainqentanglha Mountains in the central part of the Plateau, is the largest saline lake in Tibet. Covering an area of 1980 km² at an elevation of 4718 meter above sea level (Cong et al. 2007) it is the highest great lake in the world. As a closed lake, the water balance of Nam Co is controlled only by precipitation, inflow and the rate of evaporation. The climate in the region is semi-arid to arid and is modified by altitude. Mean annual air temperature is low, around -1 to +3°C. Modest mean annual precipitation of 280 mm occurs mainly in the summer during the monsoonal rains (You et al. 2006).

5.2.2 Sampling Procedure

Two P10z PUF disks of 7.62 cm thickness (i.e., three inches) and one 2.54cm PUF (one inch) disk were arranged in series inside the sampling cylinder. Prior to exposure, the disks were precleaned with water and by Soxhlet extraction for 24 h using acetone and then for another 24 h using petroleum ether (PE). PUF disks were dried in a desiccator and stored in glass jars with Teflon-lined lids until sampling. In total, fifteen flow-through samples, each covering a sampling period of approximately a month, were taken between October, 2006 and February 2008, thereby including widely different seasons and weather conditions. Differently sized PUF blanks (1 and 3 inch) were taken every month, whereby a PUF disk was exposed to air during sample installation and sealed in the original jar and placed beside the FTS for the length of sampling.

The wind speed outside the sampler was determined by a vortex wind sensor (inspeed.com LLC) placed on the top of the sampler. During the whole sampling period, the outside wind speed, averaged for every 5 minutes interval, was recorded by a data logger (MADGETECH Pulse 110, Warner, NH) as pulse number r_{out} , which has units of pulse numbers (or rotations) per 5 minute interval (rp5m). Additionally, an automatic weather station at Nam Co Station was recording meteorological parameters, including air temperature, wind speed and direction, precipitation, air

pressure and relative humidity every hour during the sampling period. The meteorological parameters during each sampling periods are summarized in Table SI 14.

5.2.3 Sample Extraction and Quantification

The PUF disks from the FTS and blanks were extracted individually by Soxhlet with acetone and PE (1:1) for 24 h. The extracts were reduced in a rotary evaporator under vacuum to ~5 mL, transferred to a vial and reduced under a gentle nitrogen flow to 0.5 to 1 mL, and then dehydrated using a sodium sulfate column. The sample was exchanged to isooctane and reduced again to 1 mL under nitrogen prior to instrumental analysis. Mirex (100 ng) was added as internal standard to correct for volume differences. All instrumental analyses were achieved with an Agilent 6890 GC equipped with splitless injector and a 5973D mass selective detector with a 60m DB-5 MS column with a 0.25 mm id and 0.25 μm film thickness (J&W Scientific, Rancho Cordova, CA). Helium was used as the carrier gas.

Samples were analyzed for 54 individual PCB congeners using standard mixtures from Ultra Scientific (North Kingstown, RI) and Cambridge Isotope Laboratories (Andover, MA), respectively (Xiao et al. 2007). For PCB quantification, the mass spectrometer was operated in electron impact-selected ion monitoring mode. GC conditions have been described elsewhere (Shoeib and Harner 2002a). The GC oven temperature program was modified to an initial temperature of 90 °C, held for 0.5 min, 15 °C/min to 240 °C, 20 °C/min to 290 °C, and a final hold for 5 min. The transfer line was kept at 300 °C. The target/qualifier ions were 222/224 or 256/258 for tri-PCBs, 292/290 for tetra-PCBs, 326/328/324 for penta-PCBs and 360/362 for hexa-PCBs.

Twenty-four organochlorine pesticides (α -HCH, β -HCH, γ -HCH, δ -HCH, HCB, chlorothalonil, aldrin, dieldrin, chlorpyrifos, dacthal, heptachlor, heptachlor epoxide, trans-chlordane, cis-chlordane, trans-nonachlor, α -endosulfan, β -endosulfan, endosulfan sulphate, o,p'-DDE, o,p'-DDD, o,p'-DDT, p,p'-DDE, p,p'-DDD and p,p'-DDT) as well as trifluralin, dimethoate, malathion, metribuzin, and pendimethalin were analyzed. The initial temperature 70°C was held for 0.5 min, and then ramped 15 °C/min to 160 °C, 2 °C/min to 250 °C, finally increased to 270 °C with 20 °C/min and held for 5 minutes. The mass spectrometer was run in the negative chemical ionization-selected ion monitoring mode, with methane as the reagent gas. Details of MS condition and target/qualifying ions are described elsewhere (Pozo et al. 2004; Shoeib and

Harner 2002b). For HCHs and DDTs, the most abundant ion, Cl^- ($m/z = 71$), was used for quantification, ions 255/257, ion 246/248/283 and ion 281/283 were monitored for the identification of HCHs, o,p'-DDT and p,p'-DDT, respectively.

5.2.4 QA/QC

Analytical method recoveries of chemicals were determined by spiking two clean PUF disks with the working standard containing all 54 PCB congeners (20 ng of each congener) and treating them as real samples. Results show good recoveries ranging from 75 to 110%, which compare well with those of previous air sampling studies in the same laboratory using the same methodology (Harner and Bidleman 1997; Shoeib and Harner 2002a; Xiao et al. 2007). Recovery factors were not applied to any of the data reported below. Most of the solvent blanks and field blanks for PUF were not significantly higher than the instrumental detection limit (IDL), which was defined as the amount at which the signal-to-noise ratio equals 3. The reported amounts were corrected for field blanks. For compounds not detected in those blanks, two-thirds of the IDL was used for blank correction. Blank levels and limits of detection are reported in Table SI 15 in the Appendix IV.

5.2.5 Back Trajectory Analysis.

In order to investigate potential source regions and transport pathways of air masses, 5-day backward trajectories arriving at 20 meters above ground level at the sampling site were generated using the PC Version 4.8 of the Hybrid Single Particle Lagrangian Integrated Trajectory (HYSPLIT) model (<http://www.arl.noaa.gov/ready/hysplit4.html>) (Draxler and Hess 1998). The meteorological data fields used to run the model are the Global Data Assimilation System (GDAS) of National Center for Environmental Prediction (NCEP) data grid. NCEP is a global 2.51 latitude/longitude grid with 23 vertical levels archived every 6 h. 3D kinematic back-trajectories were generated four times daily at 00, 06, 12, 18 UTC from October 13, 2006 through February 20, 2008. This is a total of about 1900 trajectories. Each of the trajectory output files consists of latitude, longitude, and pressure/elevation every hour along the trajectory's path. Due to the limitation of meteorological data resolution and failure to account for sub-grid scale processes, an individual trajectory may have a large error. Several studies have estimated the accuracy of individual HYSPLIT trajectories at 20–30% of travel distance (Draxler and Hess 1998; Stunder 1996). Despite the uncertainty inherent in an individual trajectory, a

meaningful analysis can be performed using a large number of trajectories to interpret relatively large data sets of observations. The trajectory data were used to produce back trajectory probability maps, referred to as "air sheds", which identify where the air parcels are most frequently originating.

5.3 Results and Discussions.

5.3.1 Sampled air volumes.

In the first field test in Toronto, a relationship between the air volume sampled by the FTS and the wind speed measured by the vortex sensor on top of the sampler had been established (Xiao et al. 2008). Although on average winds in Nam Co are generally much stronger than in Toronto, the maximum ten-minute-average wind speed recorded by the automatic weather station in Nam Co, 9.9 m/s is not significantly higher than the strongest gusts recorded during the field test in Toronto (five-minute average of 7.7 m/s). Hence, it should be feasible to use the equation from Xiao et al. (2008) to estimate the sampled air volumes with tolerable accuracy, although a correlation for a wider range of wind conditions would be preferable. The average weather conditions and the calculated sampling volumes for each FT samples are listed in Table SI 14. The FTS sampled at least 5000 m³ of air over a one month period, with maximum volumes in excess of 20,000 m³/month, which is considerably higher than sampling volumes achieved with conventional active samplers. These large sample volumes make it possible to detect chemicals with exceptionally low atmospheric concentrations. As the winds at Nam Co are stronger in winter time, the FTS samples relatively less air during the summer.

5.3.2 PCBs.

In general, the PCBs amount trapped in the samples were very low. Only seven out of 56 congeners, namely PCB-18, 28, 31, 52, 95, 101, and 110, were frequently detected in the PUF plug extracts (see Table SI 16). Atmospheric concentrations for the sum of the PCBs ranged from 0.04 to 1.23 pg/m³ with higher levels during the summer season. These levels are not only much lower than those reported for the atmosphere above North America (Shen et al. 2006) and the Indian Ocean (Wurl et al. 2006), but are also lower than levels observed in Arctic (Hung 2001; Hung et al. 2005) and Antarctic Air (Kallenborn et al. 1998; Larsson, Jarnmark and Sodergren 1992; Montone et al. 2005). They are thus among the lowest atmospheric PCB concentrations ever reported. Due to such extremely low concentrations, the PCB amounts barely

exceed the instrumental quantitation limit even though a single flow-through sample represents thousands of cubic meters of air. Considering the relatively large uncertainty of data so close to the quantitation limit, we judged it inadvisable to interpret time trends and temperature dependence of the PCB concentrations in greater detail.

5.3.3 Air concentration for pesticides.

Table SI 17 reports the mass of each pesticide detected in each PUF plug during all deployment periods. Eighteen out of 29 chemicals were frequently detected in the samples. HCB, HCHs, endosulfans and DDTs are the chemical groups which are detected consistently, and are discussed in detail below with respect to seasonal variation and potential source identification. The remaining pesticides, which include dimethoate, metribuzin, heptachlor, malathion, pendimethalin, aldrin and dieldrin, were undetectable in most samples. The amounts of trifluralin, chlordanes and heptachlor epoxide were very low in all FTS samples and typically near detection limit. The corresponding individual isomer concentrations were between 1 and 100 fg/m³ and therefore orders of magnitudes lower than global background concentrations and data reported in the Chilean Andes (Estellano et al. 2008; Pozo et al. 2004; Pozo et al. 2006).

5.3.4 Breakthrough level estimations.

Comparing the amount trapped in the middle and back plugs with that in the front one (See Table SI 17), the breakthrough levels for endosulfan, DDT and their derivatives were judged to be minor. Those for HCB and HCHs, however, were so high, that it is necessary to perform a correction before investigating seasonal variations. As indicated before (Xiao et al. 2008; Xiao et al. 2007), the FTS sampling train can be seen as a frontal chromatographic column with relatively few plate numbers. Assuming that the chemical flux at the column inlet, $J(0, t)$, was constant, the front shape can be described by:

$$J/J_0 = \Phi[N^{1/2}(\tau - 1)/\tau^{1/2}] + \exp(2N) \times \Phi[-N^{1/2}(\tau + 1)/\tau^{1/2}] \quad (5-1)$$

where J/J_0 is the normalized flux, N is the theoretical plate number, and Φ is the integral of the normal distribution, φ :

$$\varphi(x) = [1/(2\pi)^{1/2}] \exp(-x^2/2),$$

$$\Phi(x) = \int_{-\infty}^x \varphi(u) du = (1/2)[1 + \operatorname{erf}(x/2^{1/2})]$$

τ is the relative retention time t/t_R , which can also be expressed on a volume basis:

$$\tau = V/V_R = V/V_B$$

where V_B is the breakthrough volume for a particular chemical, which is identical with the retention volume V_R on the same column (Bidleman et al. 1984; Burdick and Bidleman 1981). The breakthrough level b , defined as the fraction of the total mass of analyte that has been eluted from a column with length L by time t , is given as a function of N and relative retention, τ :

$$b = \frac{\int_0^t J(L,t) dt}{\int_0^t J(0,t) dt} = \frac{\tau-1}{\tau} \Phi\left(N^{1/2} \frac{\tau-1}{\tau^{1/2}}\right) + \frac{\tau+1}{\tau} \exp(2N) \Phi\left(-N^{1/2} \frac{\tau+1}{\tau^{1/2}}\right) \quad (5-2)$$

where L is the length of the column, i.e. the overall length of the PUF assembly in the sampler (Lövkvist and Jönsson 1987). In an earlier publication, we had derived a numerical solution to the breakthrough curve equation (Xiao et al. 2007) making it possible to estimate b , if N and τ for a particular chemical are known.

During indoor experiments, a strong linear relationship between the subcooled liquid vapor pressure of a chemical P_L and its breakthrough volume on the FTS sampling train (Xiao et al. 2007) had been found:

$$\log V_B = -(0.93 \pm 0.03) \log P_L + (2.06 \pm 0.07) \quad (5-3)$$

In chapter 4, a linear solvation energy relationship (LSER) provided an approximation of N from Abraham parameters, temperature and wind speeds.

$$\ln N = 1.026 \cdot \log L_{16} + 40.07 A - 1.505 S + 1794.7/T - 5.16 u + 0.74 E + 0.59 B - 12.15 \quad (5-4)$$

Although these equations were derived from data covering a relatively narrow temperature and wind speed range, they should still be able to provide relatively accurate estimation of breakthrough levels because (i) even though the prediction of V_B has a relatively large uncertainty, the absolute error for τ will be small; (ii) b , within a range from 0 to 1, cannot be highly sensitive to N and τ .

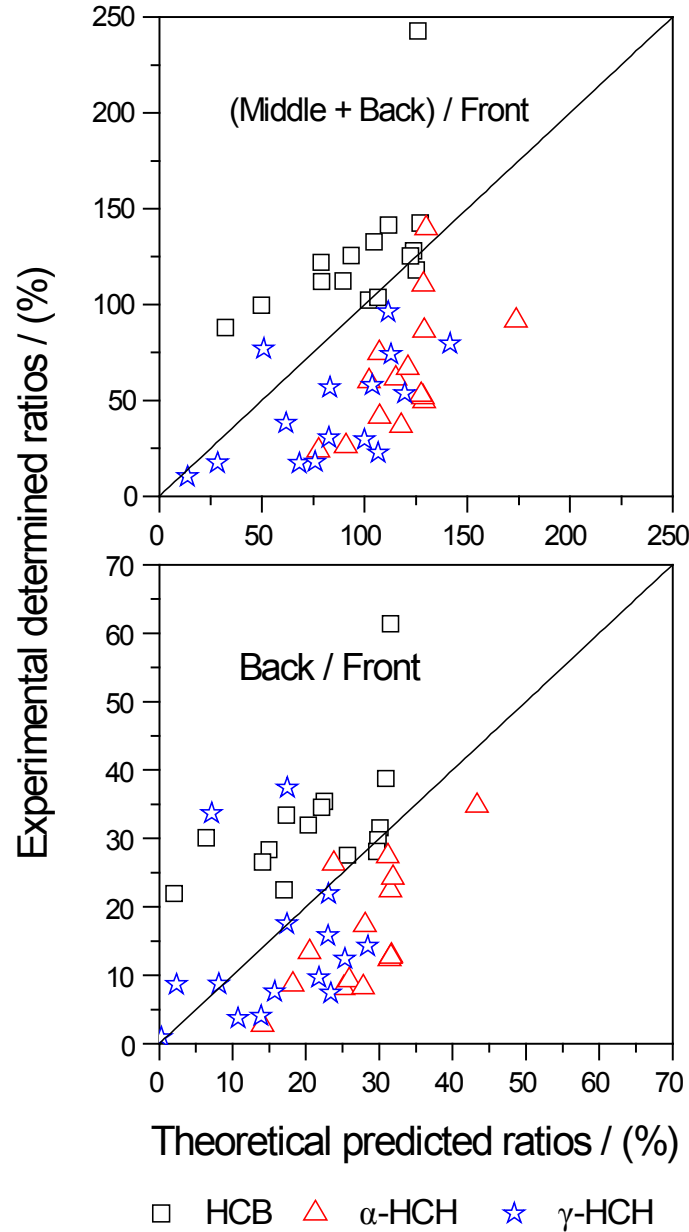


Figure 5-2. Comparison of experimentally determined back to front ratios and middle plus back to front ratios of HCB, α -HCH and γ -HCH in FT samples with such ratios predicted using frontal chromatographic theory.

Since both N and V_B are linearly related to the length of the column, breakthrough levels can be calculated from equation (1-2) for each additional plug in the sampling train. The b -values predicted for the front plug (3 inches), the first two plugs (6 inches), and the whole sampling

train (7 inches), for HCB, α -HCH and γ -HCH are listed in Table SI 18. Figure 5-2 compares the theoretically predicted and experimentally determined back to front ratio and middle plus back to front ratio for these three chemicals. It seems most of time the predicted ratios are lower than the experimental ones for HCB; whereas the opposite is true for α -HCH. There are a few reasons that could cause such an error: (i) volatility may not be the single determining factor for V_B . HCB normally suffers higher levels of breakthrough than α -HCH, i.e. penetrates much further through the column, even though it is less volatile. (ii) Uncertainties of the Abraham parameters for these two compounds. For example, the $\log L_{16}$ values for HCB and α -HCH are neither consistent with their volatilities. (iii) For compounds suffering high levels of breakthrough, the uncertainty of the non-linear fitting of N could be underestimated, which would cause equation (1-4) to predict higher number for such compounds (Figure 4-7). Generally, the prediction probably slightly underestimates the breakthrough of HCB, but overestimates the breakthrough of α -HCH. However, taking into account that equations 1-1 to 1-5 assume constant mobile phase concentrations, whereas the ambient air concentrations certainly varied during the sampling periods, the agreement is in most cases reasonable and lends support to the validity of these prediction methods. Comparing the “theoretically derived” percentages trapped in the last and last two PUF plugs with experimental values, not only gives a sense of how well we can predict N and V_B , but also allows the estimation of a range in which the “real”, i.e. break-through-corrected, concentration falls. From the amounts trapped in the first, in the first two and in all three PUF plugs and their corresponding estimated breakthrough levels, three different “ambient” atmospheric concentrations can be calculated (Table SI 18). These three values agree very well, and their average, which has a small standard deviation, is used for further discussions and figures.

Another approach to estimate average air concentrations for those volatile compounds which suffer serious breakthrough is based on the assumption that the first PUF plug (with an average weight of 22.85 g) has reached equilibrium with the ambient gas phase concentrations. Here, we used the break-through corrected air concentrations and the concentrations on the first PUF plug to calculate apparent partition coefficients $K_{\text{PUF/A}}$. Strong linear relationships were found between the logarithm of these $K_{\text{PUF/A}}$ and the reciprocal average temperature during the sampling periods (See Figure 5-3). The sorption onto the PUF becomes stronger in the sequence α -HCH, HCB to γ -HCH, which is consistent with their relative volatilities.

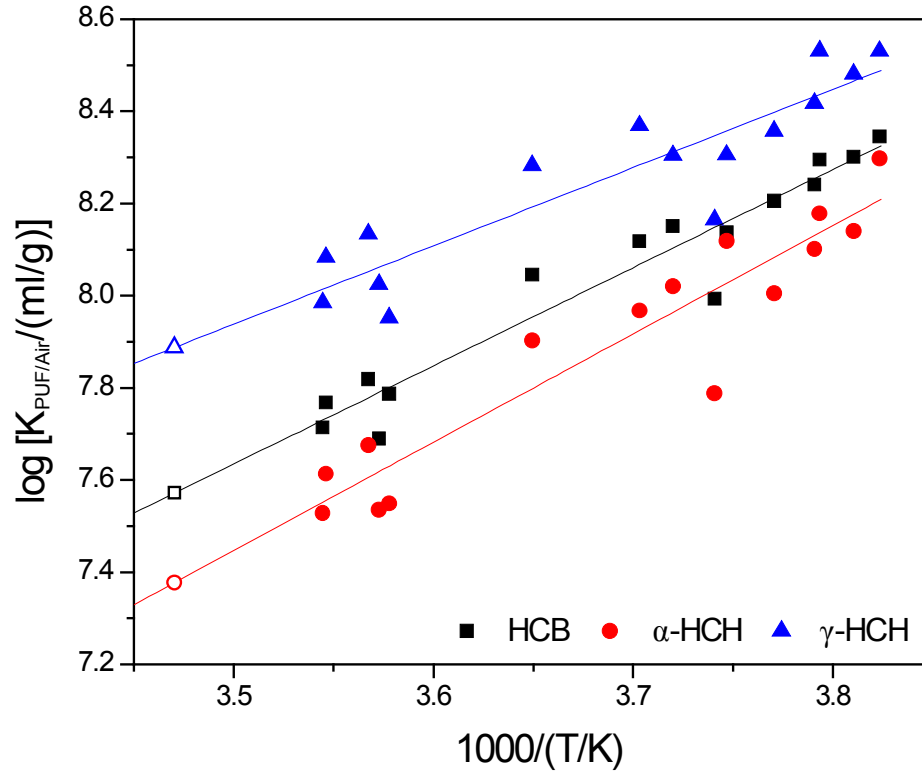


Figure 5-3. Temperature dependence of the apparent PUF/air partition coefficient for HCB, α -HCH and γ -HCH calculated from the break-through corrected ambient air concentrations. The extrapolated values at 15°C (open markers) are compared with LSER predicted partitioning coefficients in Table 1-1.

Unfortunately, no experimentally determined PUF/air partition coefficients of HCHs and HCB for P10z are available, which would allow a direct comparison with the $K_{\text{PUF/A}}$ derived from the field-exposed plugs. However, Kamprad and Goss established a series of LSERs for the $K_{\text{PUF/A}}$ of various polyester PUFs at 15 °C (Kamprad and Goss 2007). We used the relationships in Figure 5-3 to extrapolate the apparent $K_{\text{PUF/A}}$ to 15 °C. Table 5-1 compares these extrapolated values with the LSER prediction. The apparent values are all slightly lower than the LSER predicted values. However, considering the temperature variation during the sampling periods, uncertainties of the $K_{\text{PUF/A}}$ prediction and the relative humidity effect on partitioning (Kamprad and Goss 2007), such small differences are not significant, and it appears not unreasonable to assume that the first PUF plug indeed has reached an equilibrium with the ambient gas phase concentrations of HCB, α -HCH and γ -HCH. All this clearly lends credibility to the prediction of

b and the breakthrough corrected concentrations, which therefore can be used to investigate seasonal variability and temperature dependence.

Table 5-1. Comparison of LSER predictions of PUF/air partitioning with breakthrough corrected apparent partition coefficients.

	Apparent Partition coefficient			LSER predictions of $\log K_{\text{PUF}/\text{Air}} @ 15^\circ\text{C}$ for different polyester PUFs				
	m	b	$\log K_{\text{P10z}/\text{Air}} @ 15^\circ\text{C}$	P100z	ester CH	R200U	Willsorp	ester R 90% rh
HCB	2129.6	0.1811	7.57	8.06	7.60	7.42	7.87	5.76
α -HCH	2349.7	-0.7767	7.38	8.32	7.81	8.02	8.28	5.89
γ -HCH	1699.3	1.9904	7.89	8.75	8.19	8.48	8.70	6.17

5.3.5 Seasonal variation of pesticides.

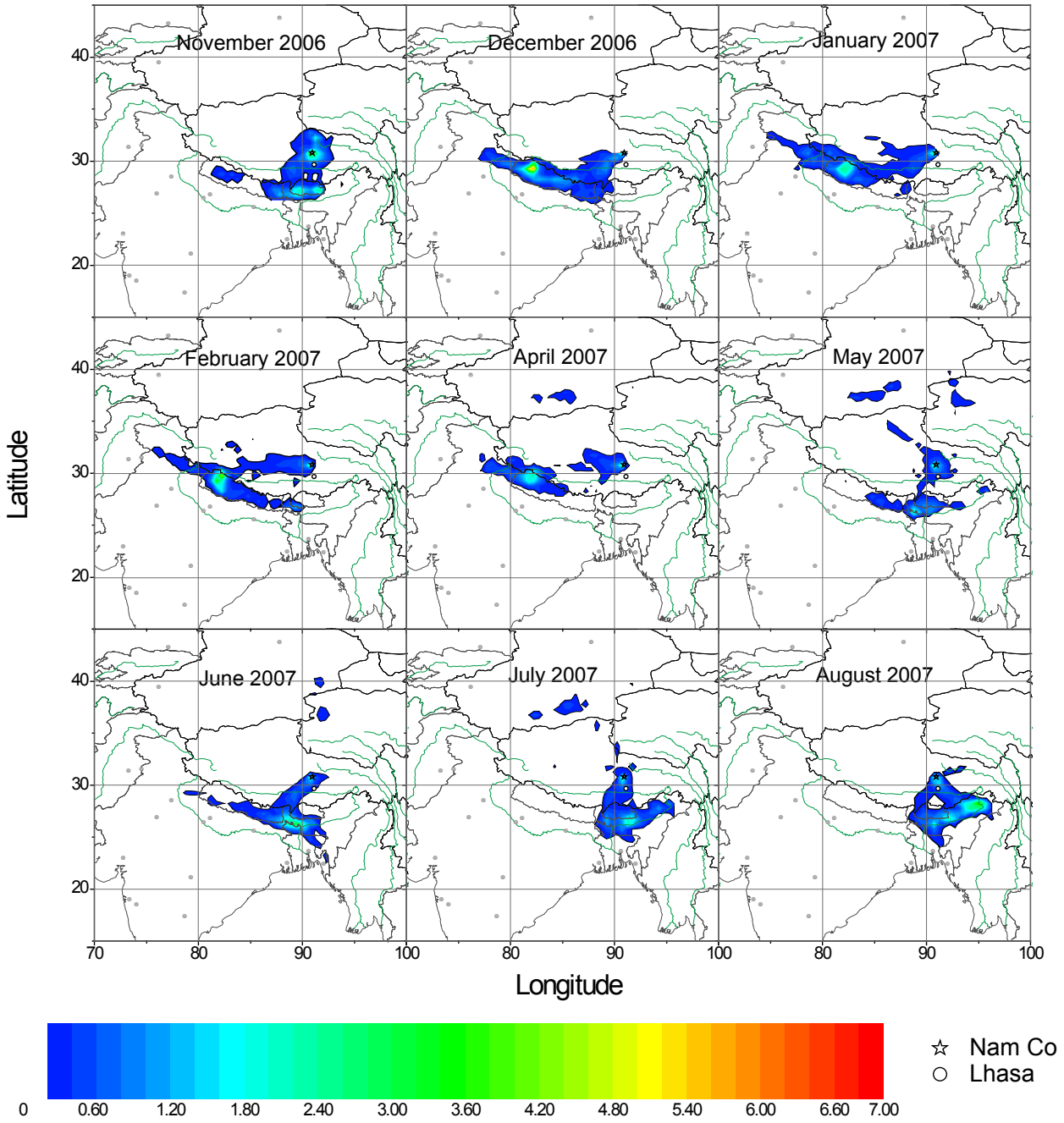
The atmospheric circulation is responsible for the transport of pollutants to the Tibetan Plateau. To identify the region of air mass origin for each of the 15 flow-through samples, the frequency of the back trajectories passing through each 0.5×0.5 degree grid cells was calculated and plotted in maps (Figure 5-4). Two distinct seasonal air-shed patterns become apparent, which are consistent with the Tibetan monsoon regime (Kang et al. 2002). From December to April, strong westerly winds blow over the plateau; and from June to November, the relatively slow moving Indian monsoon passes over the subcontinent, possibly bringing anthropogenic pollutants along with warm and moist marine air (Valsecchi et al. 1999).

After break-through correction, the most abundant pesticides in the Nam Co atmosphere are endosulfans, HCB, HCHs and DDTs. Table 5-2 lists the seasonal average concentrations for these chemicals as well as reference values reported for the Northern Tibetan Plateau (Cheng et al. 2007; Li et al. 2006) and the Mt. Everest regions (Cheng et al. 2007; Li et al. 2006). Except for γ -HCH, which probably is still in use in the Mt. Waliguan area, the concentrations are all at the same levels for the same season. Figure 5-5 plots the seasonal variation and temperature dependence of the air concentrations of these chemicals. Most pesticides had higher levels in summer, resulting in a strong temperature dependence of their air concentrations. Higher summer

time levels occur during the monsoon when air masses originate south of the Himalaya in the Gangetic plains and the Bay of Bengal. Westerly winds predominate during the winter when levels are lower.

Table 5-2. Seasonal average OCPs concentrations (pg/m³) at Nam Co and comparison with literature values reported in Tibetan Plateau regions.

	This Work				Cheng et al. 2007	Li et al. 2006
	December – February n=6	March–May n=2	June–August n=3	September– November n=4	April–May 2005 Mt. Waliguan	May–June 2002 Mt. Everest
	α -HCH	3.74±1.53	10.7±8.83	49.8±27.0	44.1±36.2	58.4
γ -HCH	0.90±0.47	2.13±1.94	8.73±2.93	5.79±4.32	139	6.88±3.29
HCB	0.42±0.23	0.26±0.04	0.81±0.66	0.79±0.91	38.4	8.45±3.28
TC	0.01±0.00	0.01±0.00	0.02±0.01	0.02±0.00	18.1	
CC	0.04±0.02	0.02±0.01	0.01±0.00	0.09±0.01	22.1	
TN	0.03±0.01	0.02±0.01	0.04±0.02	0.06±0.01		
α -Endo	9.17±5.51	15.5±16.4	46.0±43.1	79.8±57.5		27.2±22.8
β -Endo	0.10±0.06	0.42±0.00	0.60±0.31	0.44±0.24		
Endo SO ₄	0.27±0.33	0.37±0.34	0.37±0.08	0.39±0.13		
<i>o,p'</i> -DDT	0.33±0.26	3.23	6.28±4.13	5.75±4.91	17.9	4.87±2.21
<i>p,p'</i> -DDT	0.30±0.15	0.94±0.89	2.86±1.91	3.22±2.54	4.42	3.63±1.60
<i>o,p'</i> -DDE		0.18	0.35±0.05	0.40±0.02		
<i>p,p'</i> -DDE	0.10±0.04	0.15	0.35±0.16	0.46±0.33	5.12	4.62±1.78



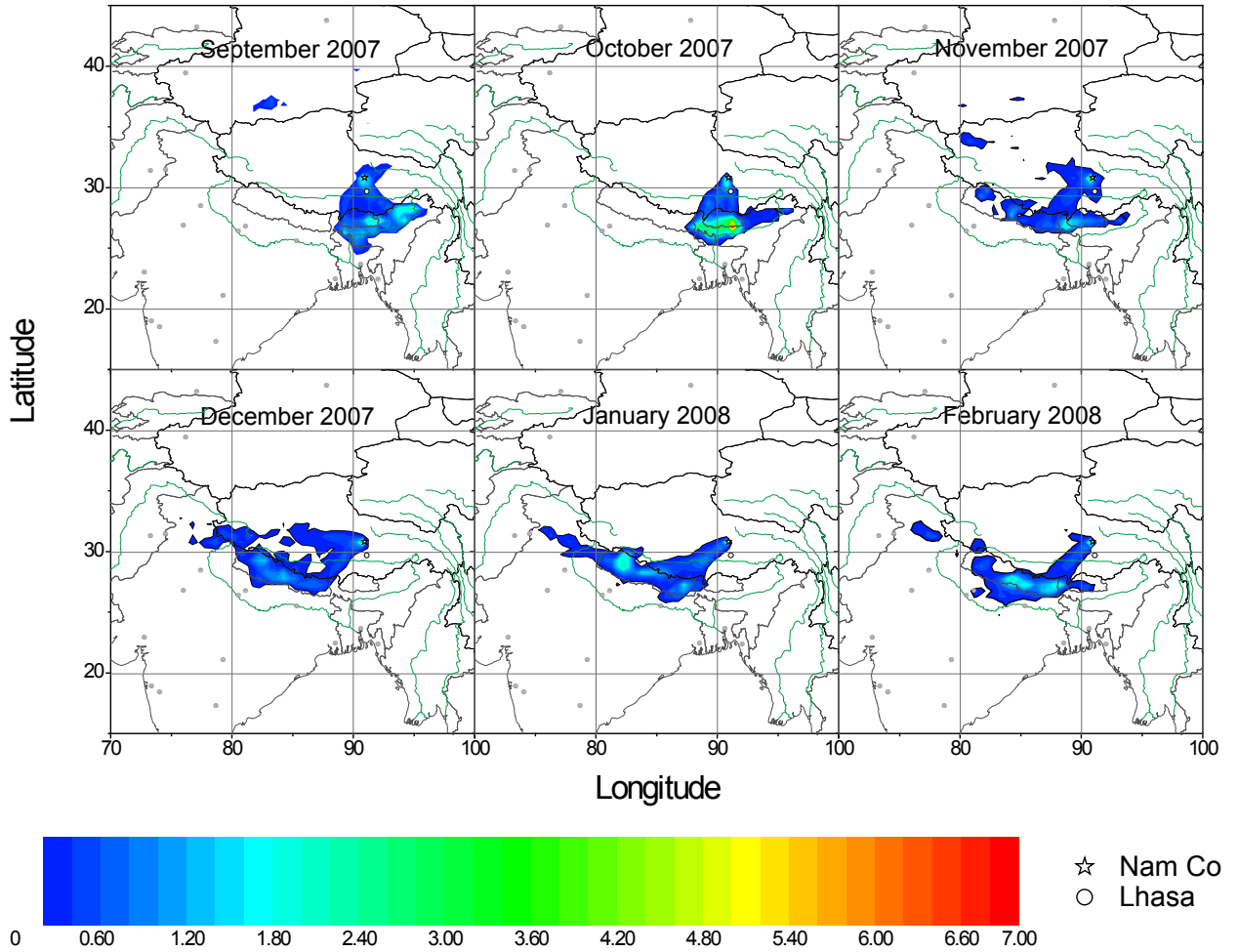


Figure 5-4. Airsheds (5-day back trajectory probability maps) calculated with the HySplit model highlighting the regions where the air most likely came from during each sampling period.

HCB displays the smallest concentration variation of all the pesticides measured in this study, ranging from 3.6 to 17.2 pg/m^3 . These values are comparable to concentrations reported for the Mr. Everest region and the southern hemisphere (Batterman et al. 2008; Li et al. 2006), but slightly lower than those found elsewhere, including in the Arctic (Shen et al. 2005; Su et al. 2006a; Wang et al. 2007b; Wang et al. 2008a).

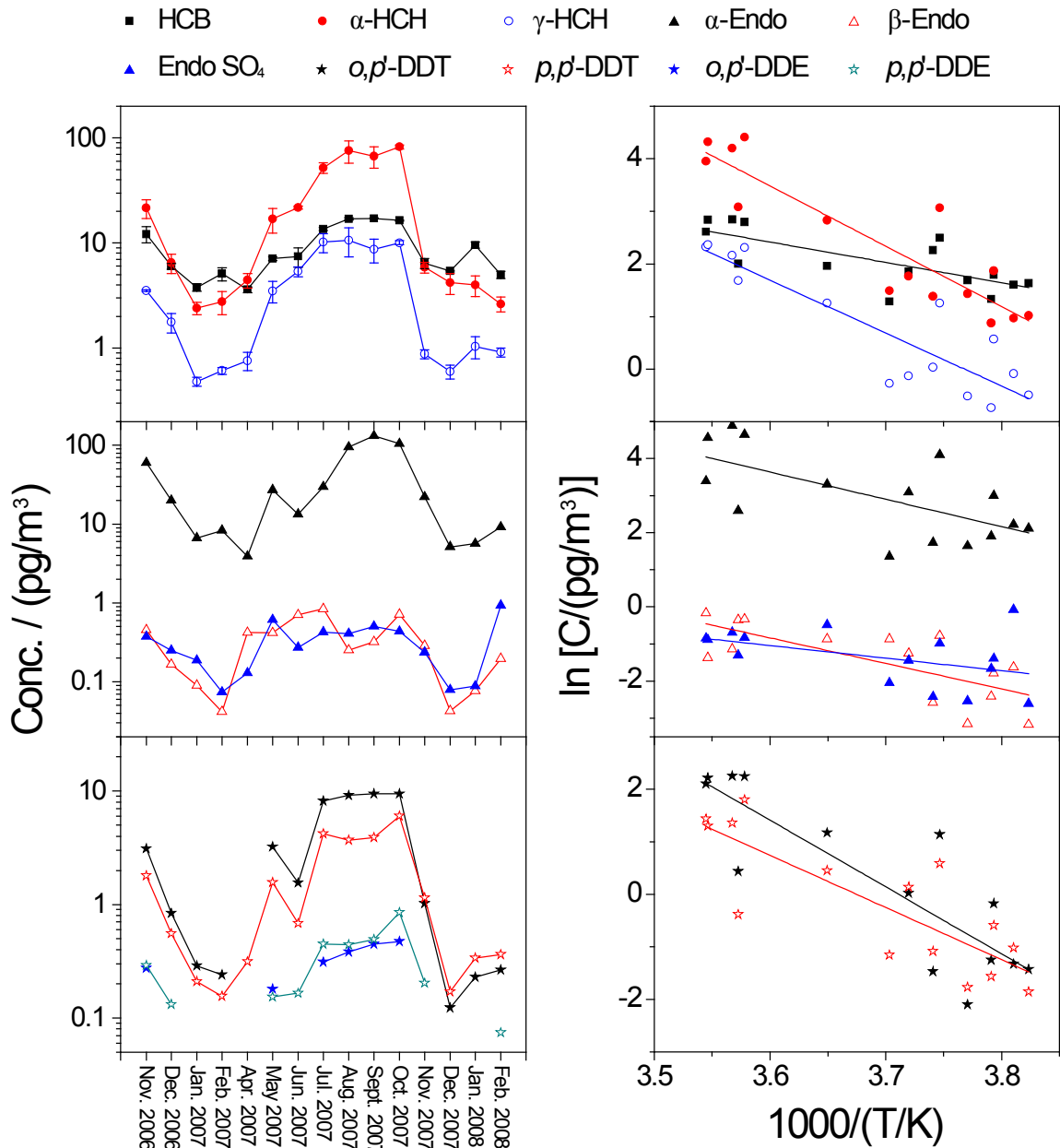


Figure 5-5. Seasonal variation (left) and temperature dependence (right) of the atmospheric concentrations of HCB, α -HCH, γ -HCH (top), endosulfan- (middle) and DDT-related substances (bottom) at Nam Co.

Although α -HCH and γ -HCH have similar volatilities as HCB, they show much stronger seasonal variations and temperature dependences. Compared with levels found at Mt. Everest during the summer 2002, the γ -HCH concentrations are similar, but the summer levels of α -

HCH at Nam Co are about 3 to 4 times higher (Li et al. 2006) and close to levels found in the Arctic and around Lake Superior (Shen et al. 2004). α -HCH always shows higher concentration than the γ - isomer, with a minimum α/γ ratio of 2.88 occurring in winter and a maximum value of 8.16 in fall (See Table SI 19). Dramatic changes in the HCHs air concentrations and in the α/γ ratio coincide with the freezing and thawing of Nam Co Lake. By no means coincident, Yang et al. also found HCH contamination and a high α/γ ratio in the muscle of fish from Nam Co Lake (Yang et al. 2007). Technical HCHs includes multiple stereoisomers and is dominated by α -HCH (~80%) and γ -HCH (10-15%), whereas lindane is almost pure γ -HCH. Since technical HCH is no longer in use, there are reasons to believe that Nam Co Lake plays the same role as a supply of α -HCH to the local atmosphere as the Arctic Ocean and Lake Superior (Bidleman et al. 1995; Jantunen et al. 2008; Shen et al. 2004). When technical HCH was still in use, the summer monsoon delivered α -HCH vapors to the Tibetan Plateau and deposited them into the cold lake. As the global atmospheric α -HCH concentration declined, the water body became oversaturated and α -HCH started to slowly re-evaporate, especially during the warmer summer months. During winter, the ice cover prevents evaporation, resulting in a low α -HCH concentration and a low α/γ -HCH ratio.

Endosulfans are a group of OCPs still used globally. The technical mixture contains two isomers, α - and β -endosulfan, at a ratio of about 2.3. In the Nam Co atmosphere, α -endosulfan is the dominant pesticide with concentrations ranging from 3.9 to 133 pg/m^3 , similar to those reported in the Mt. Everest region, higher than in the Arctic and lower than elsewhere (Estellano et al. 2008; Hung et al. 2005; Li et al. 2006; Su et al. 2008). The α/β ratio is much higher than in the technical mixture (from 9.2 to 413), and also shows a strong linear relationship with the total endosulfan concentrations (See Table SI 19). Higher level of endosulfan sulphate, the degradation product of the endosulfans, also coincide with high total endosulfan concentrations. All this suggests that endosulfan has likely undergone long range transport from source regions.

Although DDT use is heavily restricted under the Stockholm Convention, DDT-related substances are still entering the environment through DDT use for malaria prevention, DDT-containing antifouling paint of fishing ships, some mosquito-repellent incense, and impurities in commercially available dicofol (Wang et al. 2007b). Technical DDT contains about 15% *o,p'*-DDT and 85% *p,p'*-DDT, whereas the relative abundance of the two isomers is the reverse in

dicofol, yielding an average *o,p'*-DDT/*p,p'*-DDT ratio of 6.7 (Qiu et al. 2004; Qiu et al. 2005). The levels of DDT and its derivatives in the Nam Co atmosphere are generally lower than those reported elsewhere in China, and close to the levels in the Arctic and Mt. Everest (Hung et al. 2005; Li et al. 2006; Qiu et al. 2004; Su et al. 2008; Wang et al. 2007b), suggesting that LRAT plays an important role in transporting DDTs to Nam Co. High *o,p'*-DDT/*p,p'*-DDT ratios suggest usage of dicofol in the surrounding region.

The FTS performed very well under the extreme conditions of the Tibetan plateau, being exposed to very high winds and low temperatures. The very large sampling volumes of the FTS under such wind conditions make the monitoring of POPs in the air of extremely remote locations feasible. The PCBs concentrations in Nam Co are among the lowest values ever reported. Prediction of break-through level based on frontal chromatographic theory makes it possible to quantitatively analyze relatively volatile compounds. The pesticide levels at Nam Co are generally very low. Most pesticides had higher levels during summer, resulting in a strong temperature dependence. This is correlated with air mass origin across the Himalaya in the Gangetic plains of India and Bangladesh. Evaporation from cold water bodies could be an important source of α -HCH on the Tibetan Plateau. The flow through sampler constitutes a feasible method for reliably and quantitatively collecting SOCs from large air volumes.

5.4 Acknowledgements

We thank the Natural Sciences and Engineering Research Council of Canada for funding.

5.5 Supporting Information Available

Original concentration data are listed in the Appendix IV.

Chapter 6

Synthesis, Conclusions and Outlook

6 Brief

Links between the chapters and the main knowledge gain from the thesis project are provided. Future research needs are identified.

6.1 Synthesis

When quantifying concentrations of semi-volatile organic compounds (SOCs) in the atmosphere a large sampling volume is normally required to overcome the challenges of low concentrations, potential blank contamination, and limited sensitivity of current instrumental analytical methods. Conventional active sampling techniques can achieve this within a number of days, but can only be deployed in a limited number of sites because of high cost and their requirement for electricity. Several passive air samplers have been developed and applied in the determination of SOCs. The passive sampling techniques are advantageous in the monitoring of the distribution of SOCs on a large scale and in the recording of long term, i.e. inter-annual or - at best - seasonal, temporal variations. However, their relatively low sampling rates severely constrain the temporal resolution that can be achieved. Addressing the need for an improved sampling design which achieves significantly faster uptake while maintaining the capability of providing quantitative information, a new sampler has been developed that provides greatly increased sampling rates by forcing the wind to blow through the sampling medium. The sampler consists of a horizontally oriented, aerodynamically shaped, stainless steel flow tube mounted on a post with ball bearings, which turns into the wind with the help of vanes. The sampled air volume is calculated from wind speed, which is measured outside the sampler and after passage through the sampling medium using pre-calibrated vortex rotor and turbine anemometers mounted on top of the sampler and at the exit of the flow tube, respectively. Small battery-operated data loggers are used for data storage.

Basically, a flow through sampler (FTS) operates based on the same uptake mechanism as conventional active samplers, but the driving force has been changed from an electrical pump to the wind, which is less consistent and, on average, weaker. So the first challenge is how to

balance the need for both a high sampling rate and a high uptake efficiency, i.e. the selection of a sampling medium that quantitatively strips the chemicals of interest from the air stream passing through the sampling tube while at the same time posing as little resistance to the wind as possible. A low wind resistance is important for increasing the sampling rate, which is the main objective of the new sampler design. At the same time, the sampling medium should have a high uptake efficiency, which is important to eliminate break-through. The two requirements are somewhat in conflict with each other as the sampling media with higher uptake efficiency tend to also have a higher wind resistance, so a balance has to be struck. After two different sampling media were tested for their wind resistance and uptake performance, a series of polyurethane foam (PUF) discs with relatively large porosity was judged to yield the best compromise between the conflicting requirements.

After several prototypes were designed and build, the FTS was tested extensively under controlled indoor conditions and was found to provide reliable quantitative information on SOCs under conditions of constant temperature, wind speed and air concentrations (Xiao et al. 2007). The FTS was further tested under real environmental conditions during various seasons. It was found to suffer no break-through and yield reliable time-integrated concentrations for PCBs, PAHs, PBDEs and most pesticides over two week sampling periods (Xiao et al. 2008 and Chapter 4).

After both the indoor and field tests had proven the suitability of the FTS to provide reliable atmospheric concentrations, it was time to deploy it at a site which is remote, windy and scientifically important. Nam Co station met all these conditions. This field deployment not only provided an opportunity to test FTS performance under extreme weather conditions, but also to gain a systematic understanding of the seasonal variation of atmospheric concentrations of pesticides in the Nam Co region for the first time.

6.2 Conclusions.

The major conclusions that can be drawn from this project are summarized here again.

1. A novel air sampling technique that does not rely on electrical power for operation was developed and characterized. The FTS can achieve substantially faster uptake rates than typical PAS, yet still requires no access to reliable network power. The sampler aligns itself with the wind direction and utilizes the wind power to drive the air through a porous

- sampling medium such as polyurethane foam (PUF). The uptake mechanism is thus similar to that in a conventional active sampler. The sampled air volume is deduced using data on the wind speed within the flow tube after passage through the sampling medium. Unlike traditional PAS, the independent determination of air sampling volumes in the FTS makes it possible to deploy it without prior calibration or the use of performance reference compounds (PRCs). Also, a FTS can quantitatively collect compounds in both gaseous and particle phase, which makes it suitable for monitoring less volatile SOCs.
2. Frontal chromatography theory was extensively applied to investigate sampling efficiency. A numerical solution for predicting breakthrough levels was generated, which facilitates the estimation of the “real” ambient concentrations for those relatively volatile SOCs which can experience significant levels of breakthrough in both active samplers and FTS. A logistic non-linear regression was introduced to fit the vapour front curves, which makes the estimation of theoretical plate number and breakthrough volumes more accurate and consistent. In addition, the integration of this regression equation can be considered as another method to estimate the breakthrough level.
 3. The uptake efficiency of the sampling assembly was characterized in detail for a wide range of SOCs of interest. An empirical linear solvation energy relationship was developed to predict the apparent theoretical plate number, which also illustrates the effect of temperature and wind speed on FTS sampling efficiency.
 4. Quantitative relationships between the wind speed outside the sampler and after passage through the PUF were established and allow the accurate estimation of sampling volumes under conditions of low and high wind speed. Even without access to the electrical grid, FTS can easily achieve a sampling volume of hundreds of cubic meter of air per day; and under extremely windy conditions, it is even possible to sample 1000 m³ of air per day. This is a significant advantage over passive air sampling techniques; and makes the FTS comparable with conventional HiVol active samplers and suitable for monitoring SOCs with extremely low atmospheric concentrations.
 5. Through indoor controlled experiments and field tests, the performance of a FTS was extensively tested. In a constant indoor environment, a FTS can quantitatively strip both gaseous and particle-bound SOCs from large volumes of air. To test its performance under field conditions, a FTS and a traditional pumped high volume air sampler, both

using polyurethane foam (PUF) as sampling medium, were co-deployed at the campus of the University of Toronto Scarborough from August 2006 to June 2007. Polychlorinated biphenyls (PCBs), polycyclic aromatic hydrocarbons (PAHs), polybrominated diphenyl ethers (PBDEs) and pesticides were quantified in the samples taken by both air samplers. Separate analysis of 7 PUF disks arranged sequentially within the FTS, confirm that even relatively volatile SOCs do not experience serious break-through. Theoretical plate number analysis of the break-through curves yields an understanding of the effect of temperature and wind speed on FTS sampling efficiency, and reveals different behavior of gaseous and particle-bound-compounds on the PUF. Air concentrations of PCBs, PAHs, PBDEs and pesticides obtained with the FTS compare favourably with those obtained by averaging the concentrations of several 24 hour active high volume samples taken during the same time period. The time trends, temperature dependence, and even the isomer ratios show reasonable agreement between the two sampling techniques. The flow through sampler constitutes a feasible method for reliably and quantitatively collecting SOCs from large air volumes. Sampling efficiencies need to be taken into considerations when using isomer ratios to characterize the impact of different sources.

6. The flow-through sampler was deployed to monitor SOC concentrations at a remote Chinese research station located close to Nam Co Lake, Tibet. During the campaign, fifteen 1 month-long samples were taken. The collected air volume for a single 1-month sample ranged from 5,000 m³ up to 20,000 m³. The very large sampling volumes make the monitoring of SOCs in air at extremely remote location feasible. For the first time, the frontal chromatographic theory prediction of break-through level was applied to quantitatively analyze relatively volatile compounds with serious breakthrough. The flow through sampler constitutes a feasible method for reliably and quantitatively collecting SOCs from large air volumes.
7. The PCBs concentrations in Nam Co are among the lowest values ever reported. Also the pesticide levels at Nam Co are general very low. Endosulfans, HCHs, HCB and DDTs are the most abundant pesticides in the Nam Co atmosphere. Most pesticides show higher levels during summer, resulting in a strong temperature dependence. This is correlated with air mass origin across the Himalayas in the Gangetic plains of India and Bangladesh. Cold water bodies at high altitudes such as Nam Co Lake can act as a temporary sink for

HCHs during the periods of their use. As global HCH concentration decline, such water bodies become oversaturated and start to slowly release HCHs into the surrounding atmosphere, similar to what has been observed for the Arctic Ocean.

6.3 Guidelines.

All methods have advantages and limitations, and it may be worthwhile to summarize them for the FTS here briefly.

1. Selection of sampling locations

Although FTS is primarily designed for remote sites without reliable power supply, its application does not have to be limited by those locations. Due to the fact that the FTS samples more air during windy periods, a potential systematic bias may occur in samples taken in source regions. Because air concentrations in these regions are expected to correlate negatively with wind speeds, FTS derived results could underestimate the real concentrations. However, based on the experiences made during the research for this thesis and the generally random distribution of wind speed, the extent of such bias is not expected to reach significant levels. Thus, FTS can be used in both contaminated areas and remote regions.

To avoid undue influence of isolated local microenvironments, it is better to expose the FTS into the open wind field. A relatively high wind speed is preferred not only because of the correspondingly elevated sampling rate, but also for a more accurate estimation of the sampled air volume.

Setting up the FTS close to a meteorological station also has numerous benefits. The station will not only act as a backup wind speed data bank, but also allows for better experimental planning and provides additional data that could be of interest when interpreting the air concentration data.

2. Factors influencing the result

An accurate estimation of the sampled air volume is most important for obtaining the correct atmospheric concentrations. This implies the need for accurate wind speed measurements. The other important factor is the breakthrough level, which is determined by the physical-chemical properties of the compound and the sampling volume.

Therefore, it is advisable to adjust the sampling length and strategy according to the chemical of interest and the local wind scenario.

3. Chemicals

Theoretically, all chemicals with a sufficiently high sorption onto PUF disks can be sampled by FTS. However, from a practical point of view, FTS can more easily provide accurate data for chemicals with limited breakthrough levels. Thus, when dealing with relatively volatile compounds, a shorter sampling time is recommended. In case low atmospheric concentrations necessitate long sampling times, the FTS is still able to function as an equilibrium sampler provided that the gas/PUF partitioning behavior of that particular chemical has been well studied. Another option for this kind of scenario would be to replace the currently used P10z sampling train with another medium which has a much higher sorption capacity. A drawback is that the applicability of the relationship between sampled air volume and wind speed would need to be confirmed.

For fully particle bounded substances, the amount trapped at the end of the sampling train and the occurrence of extremely windy periods during sampling should be carefully monitored. As long as the instrumental quantitation limit is exceeded, shortening the sampling time can also improve the accuracy by limiting the breakthrough of the particles.

6.4 Outlooks.

The following is a list of the knowledge gaps and research needs that have been identified as a result of the research described in the thesis:

1. Wider range of wind speed and sampling volume relationship

The empirical equation (3-3) presented in chapter 3 allows the determination of the sampling volume from wind speed data collected in the vicinity of the sampler. However, it should be cautioned that the relationship should only be applied for wind speeds below 10 m/s because the wind speeds during the testing period were relatively low (Xiao et al., 2008). Thus, further tests under much windier condition would be required to derive an equation that is valid at higher wind speeds. Since many of the remote regions for which the sampler was primarily designed (e.g. polar regions and high altitudes) experience occasionally very high winds, it is imperative to obtain experimental data that allows the

extension of the empirical relationship to wind speeds above 10 m/s. Ideally, one would seek to establish an empirical equation that allows for the estimation of sampling volumes under the entire range of wind conditions encountered in the environment.

One option is to measure the air flow through the sampler during time periods of very high wind speed. The advantage of this approach is that it corresponds to the actual field sampling situation. However, periods of very high wind are not that common in the vicinity of Toronto, and if they do occur, the winds tend to be very gusty. Another option is to mount a modified sampler on a vehicle and record the air flow through the sampling tube at various driving velocities using the turbine anemometer placed at the exit of the flow tube. This has the advantage of obtaining data at high, yet reasonably constant, wind speeds.

2. Improve the sampling efficiency for more volatile compounds

In chapter 5 it was shown how to quantify the breakthrough level of volatile compounds in the FTS and therefore estimate breakthrough corrected air concentrations. However, a higher sampling efficiency is always preferable to an estimation of breakthrough, because the estimation tends to have high uncertainties, especially for more volatile compounds. Detailed analyses of the breakthrough curves in chapter 3 established that chemicals with a $\log(P_L/P_a)$ value lower than -1.5 at the temperature prevalent during sampling will not experience significant breakthrough (Xiao et al., 2007). Some atmospheric contaminants of current interest, such as many per- and polyfluorinated alkyl compounds (Shoeib et al., 2006), have a vapour pressure above that threshold. Selecting a sampling medium with higher capacity while at the same time maintaining the low wind resistance is key to achieve this goal. Several media or media combinations have such potentials, such as higher density PUF with a larger surface area per volume ratio, a layer of XAD-resin which is held in place within the flow tube using a disk-shaped stainless steel mesh cage or XAD-coated PUF disks. Recent experiments using pumped high volume air samplers suggest that the uptake capacity of PUF plugs can be greatly increased by coating them with XAD resin (Hung et al., in prep.). Experiments with XAD-coated PUF in the FTS could establish whether such an assembly would be able to increase the applicability of the sampler to higher volatilities.

3. Relative humidity effect on the sampling efficiency

Kamprad and Goss pointed out that sorption of water may significantly alter the sorption of SOCs to polyester PUF, which could possibly further affect the sampling efficiency (Kamprad and Goss 2007). This suggests that a comprehensive investigation of the relative humidity effect on the theoretical plate number of the sampling train of FTS is needed. Although recording the relative humidity during field deployment is simple, the data processing could be very complicated and challenging, because of the temporal variability in relative humidity and in other factors that affect sorption to PUF, such as temperature. A more promising way to investigate the humidity effect may be through controlled indoor experiments, in which relative humidity can be tightly controlled. Instead of a FTS, a high volume pump could be utilized as a tool for investigating the effect of relative humidity on the sorption behaviour of any kind of sampling medium.

4. Better characterization of HiVol active sampling assembly

Ever since Bidleman and coworkers applied frontal chromatography theory to investigate the collection efficiencies of PCBs and PAHs on PUF discs (Bidleman et al. 1984; You and Bidleman 1984), very few studies applying HiVol samplers sought to address the influence of environmental and operational parameters on sampling efficiencies. Ironically, as a result of the work conducted as part of this thesis, the FTS is better characterised with respect to breakthrough behaviour than the much more widely used HiVol samplers. I suggest that a better knowledge of theoretical plate numbers and breakthrough volumes for different sampler configurations would be desirable, because it would allow for a more accurate estimation of breakthrough levels. The effect of flow rate (wind speed), temperature and relative humidity on the theoretical plate number and the uptake efficiency for different chemical groups should be investigated.

5. Breakthrough correction of historical data for HCB, HCHs

There is a huge archive of historical data on HCB and HCHs in HiVol air samples. Quantitative interpretation of those data in term of volumetric air concentrations is compromised by a limited understanding of the extent of breakthrough, even though very often back and front PUF plugs had been separated and analysed individually. With a better characterization of the HiVol sampling train, it might be possible to re-analyse those historical data and gain a deeper knowledge of the geochemical fate of these compounds.

6. Using FTS to calibrate PAS

Conventionally, either PRCs or active samplers are used to obtain the sampling rate of PAS. One disadvantage of the comparison between PAS and active HiVol samplers is that samples taken by the latter typically only cover a tiny fraction of the time period that the PAS had been deployed. Since the FTS has been well characterized, it could also be used as a tool to calibrate other PAS. Compared with HiVol samplers, the FTS covers longer periods of time and thus could avoid missing any important “accidental” or application events. The FTS could also provide some information on the effect of wind speed. Unlike methods relying on performance reference compounds, which are typically limited in numbers, the FTS can provide concentration information for almost all chemicals of interest.

7. Tibet water-air exchange, chiral signatures of α -HCH.

In chapter 5, I have suggested that Nam Co Lake is a source of α -HCH to the local atmosphere. To obtain more evidence in support of this theory, the fugacity ratio between water and air should be investigated. Determination of enantiomer fractions of α -HCH could further prove whether α -HCH stems from historical or “fresh” emission.

REFERENCES

- Abraham, M.H. and Al-Hussaini, A.J.M., 2005. Solvation parameters for the 209 PCBs: Calculation of physicochemical properties. *Journal of Environmental Monitoring* 7, 295-301.
- Abraham, M.H., 1993. Scales of solute hydrogen-bonding: Their construction and application to physicochemical and biochemical processes. *Chemical Society Reviews* 22, 73-83.
- Agrell, C., Okla, L., Larsson, P., Backe, C., Wania, F., 1999. Evidence of latitudinal fractionation of polychlorinated biphenyl congeners along the baltic sea region. *Environmental Science and Technology* 33, 1149-1156.
- Alaee, M. and Wenning, R.J., 2002. The significance of brominated flame retardants in the environment: Current understanding, issues and challenges. *Chemosphere* 46, 579-582.
- Bartkow, M.E., Booij, K., Kennedy, K.E., Müller, J.F., Hawker, D.W., 2005. Passive air sampling theory for semivolatile organic compounds. *Chemosphere* 60, 170-176.
- Batterman, S.A., Chernyak, S.M., Gounden, Y., Matooane, M., Naidoo, R.N., 2008. Organochlorine pesticides in ambient air in durban, south africa. *Science of the Total Environment* 397, 119-130.
- Bidleman, T.F., Jantunen, L.M.M., Helm, P.A., Brorström-Lundén, E., Juntto, S., 2002. Chlordane enantiomers and temporal trends of chlordane isomers in arctic air. *Environmental Science and Technology* 36, 539-544.
- Bidleman, T.F., Jantunen, L.M., Falconer, R.L., Barrie, L.A., Fellin, P., 1995. Decline of hexachlorocyclohexane in the arctic atmosphere and reversal of air-sea gas exchange. *Geophysical Research Letters* 22, 219-222.
- Bidleman, T.F., 1988. Atmospheric processes. *Environmental Science and Technology* 22, 361-367.

Bidleman, T.F., Simon, C.G., Burdick, N.F., You, F., 1984. Theoretical plate measurements and collection efficiencies for high-volume air samplers using polyurethane foam. *Journal of Chromatography* 301, 448-453.

Blais, J.M., Schindler, D.W., Muir, D.C.G., Sharp, M., Donald, D., Lafrenière, M., Braekevelt, E., Strachan, W.M.J., 2001. Melting glaciers: A major source of persistent organochlorines to subalpine bow lake in banff national park, canada. *Ambio* 30, 410-415.

Blais, J.M., Schindler, D.W., Muir, D.C.G., Kimpe, L.E., Donald, D.B., Rosenberg, B., 1998. Accumulation of persistent organochlorine compounds in mountains of western canada. *Nature* 395, 585-588.

Bohlin, P., Jones, K.C., Strandberg, B., 2007. Occupational and indoor air exposure to persistent organic pollutants: A review of passive sampling techniques and needs. *Journal of Environmental Monitoring* 9, 501-509.

Burdick, N.F. and Bidleman, T.F., 1981. Frontal movement of hexachlorobenzene and polychlorinated biphenyl vapors through polyurethane foam. *Analytical Chemistry* 53, 1926-1929.

Carson, R., 1962. *Silent Spring*

Cheng, H., Zhang, G., Jiang, J.X., Li, X., Liu, X., Li, J., Zhao, Y., 2007. Organochlorine pesticides, polybrominated biphenyl ethers and lead isotopes during the spring time at the waliguan baseline observatory, northwest china: Implication for long-range atmospheric transport. *Atmospheric Environment* 41, 4734-4747.

Cong, Z.Y., Kang, S.C., Liu, X.D., Wang, G.F., 2007. Elemental composition of aerosol in the nam co region, tibetan plateau, during summer monsoon season. *Atmospheric Environment* 41, 1180-1187.

Czuczwa, J.M., McVeety, B.D., Hites, R.A., 1984. Polychlorinated dibenzo-p-dioxins and dibenzofurans in sediments from siskiwit lake, isle royale. *Science* 226, 568-569.

Daly, G.L. and Wania, F., 2005. Organic contaminants in mountains. *Environmental Science and Technology* 39, 385-398.

Davidson, D.A., Wilkinson, A.C., Blais, J.M., Kimpe, L.E., McDonald, K.M., Schindler, D.W., 2003. Orographic cold-trapping of persistent organic pollutants by vegetation in mountains of western Canada. *Environmental Science and Technology* 37, 209-215.

Draxler, R.R. and Hess, G.D., 1998. An overview of the HYSPLIT_4 modelling system for trajectories, dispersion and deposition. *Australian Meteorological Magazine* 47, 295-308.

Eckley, N., 2001. Traveling toxics: The science, policy, and management of persistent organic pollutants. *Environment* 43, 24-36.

Eriksson, P., Jakobsson, E., Fredriksson, A., 2001. Brominated flame retardants: A novel class of developmental neurotoxicants in our environment? *Environmental Health Perspectives* 109, 903-908.

Estellano, V.H., Pozo, K., Harner, T., Franken, M., Zaballa, M., 2008. Altitudinal and seasonal variations of persistent organic pollutants in the Bolivian Andes mountains. *Environmental Science and Technology* 42, 2528-2534.

Falconer, R.L. and Bidleman, T.F., 1994. Vapor pressures and predicted particle/gas distributions of polychlorinated biphenyl congeners as functions of temperature and ortho-chlorine substitution. *Atmospheric Environment* 28, 547-554.

Farrar, N.J., Harner, T., Shoeib, M., Sweetman, A., Jones, K.C., 2005. Field deployment of thin film passive air samplers for persistent organic pollutants: A study in the urban atmospheric boundary layer. *Environmental Science and Technology* 39, 42-48.

Fernández, P. and Grimalt, J.O., 2003. On the global distribution of persistent organic pollutants. *Chimia* 57, 514-521.

Goss, K.U. and Schwarzenbach, R.P., 2001. Linear free energy relationships used to evaluate equilibrium partitioning of organic compounds. *Environmental Science and Technology* 35, 1-9.

Gouin, T., Jantunen, L., Harner, T., Blanchard, P., Bidleman, T., 2007. Spatial and temporal trends of chiral organochlorine signatures in Great Lakes air using passive air samplers. *Environmental Science and Technology* 41, 3877-3883.

Gouin, T., Harner, T., Blanchard, P., Mackay, D., 2005a. Passive and active air samplers as complementary methods for investigating persistent organic pollutants in the great lakes basin. *Environmental Science and Technology* 39, 9115-9122.

Gouin, T., Harner, T., Daly, G.L., Wania, F., Mackay, D., Jones, K.C., 2005b. Variability of concentrations of polybrominated diphenyl ethers and polychlorinated biphenyls in air: Implications for monitoring, modeling and control. *Atmospheric Environment* 39, 151-166.

Gouin, T., Thomas, G.O., Cousins, I., Barber, J., Mackay, D., Jones, K.C., 2002. Air-surface exchange of polybrominated diphenyl ethers and polychlorinated biphenyls. *Environmental Science and Technology* 36, 1426-1434.

Grimalt, J.O., Fernández, P., Berdie, L., Vilanova, R.M., Catalan, J., Psenner, R., Hofer, R., Appleby, P.G., Rosseland, B.O., Lien, L., Massabuau, J.C., Battarbee, R.W., 2001. Selective trapping of organochlorine compounds in mountain lakes of temperate areas. *Environmental Science and Technology* 35, 2690-2697.

Hafner, W.D., Carlson, D.L., Hites, R.A., 2005. Influence of local human population on atmospheric polycyclic aromatic hydrocarbon concentrations. *Environmental Science and Technology* 39, 7374-7379.

Harner, T., Bartkow, M., Holoubek, I., Klanova, J., Wania, F., Gioia, R., Moeckel, C., Sweetman, A.J., Jones, K.C., 2006a. Passive air sampling for persistent organic pollutants: Introductory remarks to the special issue. *Environmental Pollution* 144, 361-364.

Harner, T., Shoeib, M., Diamond, M., Ikonou, M., Stern, G., 2006b. Passive sampler derived air concentrations of PBDEs along an urban-rural transect: Spatial and temporal trends. *Chemosphere* 64, 262-267.

Harner, T., Shoeib, M., Diamond, M., Stern, G., Rosenberg, B., 2004. Using passive air samplers to assess urban-rural trends for persistent organic pollutants. 1. polychlorinated biphenyls and organochlorine pesticides. *Environmental Science and Technology* 38, 4474-4483.

Harner, T., Farrar, N.J., Shoeib, M., Jones, K.C., Gobas, F.A.P.C., 2003. Characterization of polymer-coated glass as a passive air sampler for persistent organic pollutants. *Environmental science & technology* 37, 2486-2493.

Harner, T. and Bidleman, T.F., 1997. Polychlorinated naphthalenes in urban air. *Atmospheric Environment* 31, 4009-4016.

Haugen, J.-., Wania, F., Lei, Y.D., 1999. Polychlorinated biphenyls in the atmosphere of southern norway. *Environmental Science and Technology* 33, 2340-2345.

Hillery, B.R., Basu, I., Sweet, C.W., Hites, R.A., 1997. Temporal and spatial trends in a long-term study of gas-phase PCB concentrations near the great lakes. *Environmental Science and Technology* 31, 1811-1816.

Hites, R.A., 2004. Polybrominated diphenyl ethers in the environment and in people: A meta-analysis of concentrations. *Environmental Science and Technology* 38, 945-956.

Hoff, R.M., Muir, D.C.G., Grift, N.P., 1992. Annual cycle of polychlorinated biphenyls and organohalogen pesticides in air in southern ontario. 2. atmospheric transport and sources. *Environmental Science and Technology* 26, 276-283.

Hung, H., Blanchard, P., Halsall, C.J., Bidleman, T.F., Stern, G.A., Fellin, P., Muir, D.C.G., Barrie, L.A., Jantunen, L.M., Helm, P.A., Ma, J., Konoplev, A., 2005. Temporal and spatial variabilities of atmospheric polychlorinated biphenyls (PCBs), organochlorine (OC) pesticides and polycyclic aromatic hydrocarbons (PAHs) in the canadian arctic: Results from a decade of monitoring. *Science of the Total Environment* 342, 119-144.

Hung, H., 2001. Are PCBs in the canadian arctic atmosphere declining? evidence from 5 years of monitoring. *Environmental Science and Technology* 35, 1303-1311.

Ikonomou, M.G., Rayne, S., Fischer, M., Fernandez, M.P., Cretney, W., 2002. Occurrence and congener profiles of polybrominated diphenyl ethers (PBDEs) in environmental samples from coastal british columbia, canada. *Chemosphere* 46, 649-663.

Jantunen, L.M., Helm, P.A., Kylin, H., Bidleman, T.F., 2008. Hexachlorocyclohexanes (HCHs) in the canadian archipelago. 2. air-water gas exchange of alpha- and gamma-HCH. *Environmental Science and Technology* 42, 465-470.

Jaward, F.M., Di Guardo, A., Nizzetto, L., Cassani, C., Raffaele, F., Ferretti, R., Jones, K.C., 2005. PCBs and selected organochlorine compounds in italian mountain air: The influence of altitude and forest ecosystem type. *Environmental Science and Technology* 39, 3455-3463.

Jaward, F.M., Farrar, N.J., Harner, T., Sweetman, A.J., Jones, K.C., 2004. Passive air sampling of PCBs, PBDEs, and organochlorine pesticides across europe. *Environmental Science and Technology* 38, 34-41.

Kallenborn, R., Oehme, M., Wynn-Williams, D.D., Schlabach, M., Harris, J., 1998. Ambient air levels and atmospheric long-range transport of persistent organochlorines to signy island, antarctica. *Science of the Total Environment* 220, 167-180.

Kamlet, M.J. and Taft, R.W., 1979. Linear solvation energy relationships. part 1. solvent polarity- polarizability effects on infrared spectra. *Journal of the Chemical Society, Perkin Transactions* 2, 337-341.

Kamprad, I. and Goss, K.U., 2007. Systematic investigation of the sorption properties of polyurethane foams for organic vapors. *Analytical Chemistry* 79, 4222-4227.

Kang, S.C., Mayewski, P.A., Qin, D., Yan, Y., Hou, S., Zhang, D., Ren, J., Kruezt, K., 2002. Glaciochemical records from a mt. everest ice core: Relationship to atmospheric circulation over asia. *Atmospheric Environment* 36, 3351-3361.

Kaupp, H. and McLachlan, M.S., 1999. Atmospheric particle size distributions of polychlorinated dibenzo-p- dioxins and dibenzofurans (PCDD/Fs) and polycyclic aromatic hydrocarbons (PAHs) and their implications for wet and dry deposition. *Atmospheric Environment* 33, 85-95.

Khaled, A. and Pawliszyn, J., 2000. Time-weighted average sampling of volatile and semi-volatile airborne organic compounds by the solid-phase microextraction device. *Journal of Chromatography A* 892, 455-467.

Kohler, P.M., 2006. Science, PIC and POPs: Negotiating the membership of chemical review committees under the stockholm and rotterdam conventions. *Review of European Community and International Environmental Law* 15, 293-303.

Larsson, P., Jarnmark, C., Sodergren, A., 1992. PCBs and chlorinated pesticides in the atmosphere and aquatic organisms of ross island, antarctica. *Marine Pollution Bulletin* 25, 281-287.

Lei, Y.D., Chankalal, R., Chan, A., Wania, F., 2002. Supercooled liquid vapor pressures of the polycyclic aromatic hydrocarbons. *Journal of Chemical and Engineering Data* 47, 801-806.

Li, J., Zhu, T., Wang, F., Qiu, X.H., Lin, W.L., 2006. Observation of organochlorine pesticides in the air of the mt. everest region. *Ecotoxicology and Environmental Safety* 63, 33-41.

Li, Y.F. and Macdonald, R.W., 2005. Sources and pathways of selected organochlorine pesticides to the arctic and the effect of pathway divergence on HCH trends in biota: A review. *Science of the Total Environment* 342, 87-106.

Li, Y.F., Bidleman, T.F., Barrie, L.A., McConnell, L.L., 1998. Global hexachlorocyclohexane use trends and their impact on the arctic atmospheric environment. *Geophysical Research Letters* 25, 39-41.

Loewen, M., Kang, S.C., Armstrong, D., Zhang, Q., Tomy, G., Wang, F., 2007. Atmospheric transport of mercury to the tibetan plateau. *Environmental Science and Technology* 41, 7632-7638.

Lohmann, R., Northcott, G.L., Jones, K.C., 2000. Assessing the contribution of diffuse domestic burning as a source of PCDD/Fs, PCBs, and PAHs to the U.K. atmosphere. *Environmental Science and Technology* 34, 2892-2899.

Lövkvist, P. and Jönsson, J.Å., 1987. Capacity of sampling and preconcentration columns with a low number of theoretical plates. *Analytical Chemistry* 59, 818-821.

Luross, J.M., Alae, M., Sergeant, D.B., Cannon, C.M., Michael Whittle, D., Solomon, K.R., Muir, D.C.G., 2002. Spatial distribution of polybrominated diphenyl ethers and polybrominated biphenyls in lake trout from the laurentian great lakes. *Chemosphere* 46, 665-672.

Mandalakis, M. and Stephanou, E.G., 2002. Study of atmospheric PCB concentrations over the eastern mediterranean sea. *J. Geophys. Res.* 107, 4716-4729.

Montone, R.C., Taniguchi, S., Boian, C., Weber, R.R., 2005. PCBs and chlorinated pesticides (DDTs, HCHs and HCB) in the atmosphere of the southwest atlantic and antarctic oceans. *Marine Pollution Bulletin* 50, 778-786.

Moreau-Guigon, E., Motelay-Massei, A., Harner, T., Pozo, K., Diamond, M., Chevreuil, M., Blanchoud, H., 2007. Vertical and temporal distribution of persistent organic pollutants in toronto. 1. organochlorine pesticides. *Environmental Science and Technology* 41, 2172-2177.

Motelay-Massei, A., Harner, T., Shoeib, M., Diamond, M., Stern, G., Rosenberg, B., 2005. Using passive air samplers to assess urban-rural trends for persistent organic pollutants and polycyclic aromatic hydrocarbons. 2. seasonal trends for PAHs, PCBs, and organochlorine pesticides. *Environmental Science and Technology* 39, 5763-5773.

Ockenden, W.A., Sweetman, A.J., Prest, H.F., Steinnes, E., Jones, K.C., 1998. Toward an understanding of the global atmospheric distribution of persistent organic pollutants: The use of semipermeable membrane devices as time-integrated passive samplers. *Environmental Science and Technology* 32, 2795-2803.

Odabasi, M., Cetin, E., Sofuoglu, A., 2006. Determination of octanol-air partition coefficients and supercooled liquid vapor pressures of PAHs as a function of temperature: Application to gas-particle partitioning in an urban atmosphere. *Atmospheric Environment* 40, 6615-6625.

Pankow, J.F., 1989. Overview of the gas phase retention volume behavior of organic compounds on polyurethane foam. *Atmospheric Environment* 23, 1107-1111.

Pozo, K., Harner, T., Wania, F., Muir, D.C.G., Jones, K.C., Barrie, L.A., 2006. Toward a global network for persistent organic pollutants in air: Results from the GAPS study. *Environmental Science and Technology* 40, 4867-4873.

Pozo, K., Harner, T., Shoeib, M., Urrutia, R., Barra, R., Parra, O., Focardi, S., 2004. Passive-sampler derived air concentrations of persistent organic pollutants on a north-south transect in chile. *Environmental Science and Technology* 38, 6529-6537.

Qiu, X.H., Zhu, T., Yao, B., Hu, J.X., Hu, S.W., 2005. Contribution of dicofol to the current DDT pollution in china. *Environmental Science and Technology* 39, 4385-4390.

Qiu, X.H., Zhu, T., Li, J., Pan, H.S., Li, Q.L., Miao, G.F., Gong, J.C., 2004. Organochlorine pesticides in the air around the taihu lake, china. *Environmental Science and Technology* 38, 1368-1374.

Reilley, C.N., Hildebrand, G.P., Ashley Jr., J.W., 1962. Gas chromatographic response as a function of sample input profile. *Analytical Chemistry* 34, 1198-1213.

Shen, L., Wania, F., Lei, Y.D., Teixeira, C., Muir, D.C.G., Xiao, H., 2006. Polychlorinated biphenyls and polybrominated diphenyl ethers in the north american atmosphere. *Environmental Pollution* 144, 434-444.

Shen, L., Wania, F., Lei, Y.D., Teixeira, C., Muir, D.C.G., Bidleman, T.F., 2005. Atmospheric distribution and long-range transport behavior of organochlorine pesticides in north america. *Environmental Science and Technology* 39, 409-420.

Shen, L., Wania, F., Lei, Y.D., Teixeira, C., Muir, D.C.G., Bidleman, T.F., 2004. Hexachlorocyclohexanes in the north american atmosphere. *Environmental Science and Technology* 38, 965-975.

Shoeib, M. and Harner, T., 2002a. Characterization and comparison of three passive air samplers for persistent organic pollutants. *Environmental Science and Technology* 36, 4142-4151.

Shoeib, M. and Harner, T., 2002b. Using measured octanol-air partition coefficients to explain environmental partitioning of organochlorine pesticides. *Environmental Toxicology and Chemistry* 21, 984-990.

Shunthirasingham, C., Ying, D.L., Wania, F., 2007. Evidence of bias in air - water henry's law constants for semivolatile organic compounds measured by inert gas stripping. *Environmental Science and Technology* 41, 3807-3814.

Simcik, M.F., 2005. Air monitoring of persistent organic pollutants in the great lakes: IADN vs. AEOLOS. *Environmental Monitoring and Assessment* 100, 201-216.

Simcik, M.F., Basu, I., Sweet, C.W., Hites, R.A., 1999. Temperature dependence and temporal trends of polychlorinated biphenyl congeners in the great lakes atmosphere. *Environmental Science and Technology* 33, 1991-1995.

Simon, C.G. and Bidleman, T.F., 1979. Sampling airborne polychlorinated biphenyls with polyurethane foam - chromatographic approach to determining retention efficiencies. *Analytical Chemistry* 51, 1110-1113.

Söderström, H.S. and Bergqvist, P.A., 2004. Passive air sampling using semipermeable membrane devices at different wind-speeds in situ calibrated by performance reference compounds. *Environmental Science and Technology* 38, 4828-4834.

Stock, N.L., Lau, F.K., Ellis, D.A., Martin, J.W., Muir, D.C.G., Mabury, S.A., 2004. Polyfluorinated telomer alcohols and sulfonamides in the north american troposphere. *Environmental Science and Technology* 38, 991-996.

Stovall, D.M., Hoover, K.R., Acree Jr., W.E., Abraham, M.H., 2005. Solubility behavior of crystalline polycyclic aromatic hydrocarbons (PAHs): Prediction of fluorene solubilities in organic solvents with the abraham solvation parameter model. *Polycyclic Aromatic Compounds* 25, 313-326.

Strandberg, B., Dodder, N.G., Basu, I., Hites, R.A., 2001. Concentrations and spatial variations of polybrominated diphenyl ethers and other organohalogen compounds in great lakes air. *Environmental Science and Technology* 35, 1078-1083.

Stunder, B.J.B., 1996. An assessment of the quality of forecast trajectories. *Journal of Applied Meteorology* 35, 1319-1331.

Su, Y., Hung, H., Blanchard, P., Patton, G.W., Kallenborn, R., Konoplev, A., Fellin, P., Li, H., Geen, C., Stern, G., Rosenberg, B., Barrie, L.A., 2008. A circumpolar perspective of atmospheric organochlorine pesticides (OCPs): Results from six arctic monitoring stations in 2000-2003. *Atmospheric Environment* 42, 4682-4698.

- Su, Y., Hung, H., Sverko, E., Fellin, P., Li, H., 2007. Multi-year measurements of polybrominated diphenyl ethers (PBDEs) in the arctic atmosphere. *Atmospheric Environment* 41, 8725-8735.
- Su, Y., Hung, H., Blanchard, P., Patton, G.W., Kallenborn, R., Konoplev, A., Fellin, P., Li, H., Geen, C., Stern, G., Rosenberg, B., Barrie, L.A., 2006a. Spatial and seasonal variations of hexachlorocyclohexanes (HCHs) and hexachlorobenzene (HCB) in the arctic atmosphere. *Environmental Science and Technology* 40, 6601-6607.
- Su, Y., Lei, Y.D., Wania, F., Shoeib, M., Harner, T., 2006b. Regressing gas/particle partitioning data for polycyclic aromatic hydrocarbons. *Environmental Science and Technology* 40, 3558-3564.
- Valsecchi, S., Smiraglia, C., Tartari, G., Polesello, S., 1999. Chemical composition of monsoon deposition in the everest region. *Science of the Total Environment* 226, 187-199.
- Viberg, H., Fredriksson, A., Eriksson, P., 2002. Neonatal exposure to the brominated flame retardant 2,2a2,4,4a2,5-pentabromodiphenyl ether causes altered susceptibility in the cholinergic transmitter system in the adult mouse. *Toxicological Sciences* 67, 104-107.
- Vilanova, R.M., Fernández, P., Grimalt, J.O., 2001. Polychlorinated biphenyl partitioning in the waters of a remote mountain lake. *Science of the Total Environment* 279, 51-62.
- Wang, F., Zhu, T., Xu, B.Q., Kang, S.C., 2007a. Organochlorine pesticides in fresh-fallen snow on east rongbuk glacier of mt. qomolangma (everest). *Science in China, Series D: Earth Sciences* 50, 1097-1102.
- Wang, J., Guo, L., Li, J., Zhang, G., Lee, C.S.L., Li, X., Jones, K.C., Xiang, Y., Zhong, L., 2007b. Passive air sampling of DDT, chlordane and HCB in the pearl river delta, south china: Implications to regional sources. *Journal of Environmental Monitoring* 9, 582-588.
- Wang, X.F., Li, X.H., Cheng, H.X., Xu, X.B., Zhuang, G.M., Zhao, C.D., 2008a. Organochlorine pesticides in particulate matter of beijing, china. *Journal of Hazardous Materials* 155, 350-357.

- Wang, X.P., Yao, T.D., Wang, P.I., Wei-Yang, Tian, L.D., 2008b. The recent deposition of persistent organic pollutants and mercury to the dasuopu glacier, mt. xixiabangma, central himalayas. *Science of the Total Environment* 394, 134-143.
- Wang, X.P., Yao, T.D., Cong, Z.Y., Yan, X.L., Kang, S.C., Zhang, Y., 2007a. Distribution of persistent organic pollutants in soil and grasses around mt. qomolangma, china. *Archives of Environmental Contamination and Toxicology* 52, 153-162.
- Wang, X.P., Yao, T.D., Cong, Z.Y., Yan, X.L., Kang, S.C., Zhang, Y., 2007b. Concentration level and distribution of polycyclic aromatic hydrocarbons in soil and grass around mt. qomolangma, china. *Chinese Science Bulletin* 52, 1405-1413.
- Wang, X.P., Yao, T.D., Cong, Z.Y., Yan, X.L., Kang, S.C., Zhang, Y., 2006. Gradient distribution of persistent organic contaminants along northern slope of central-himalayas, china. *Science of the Total Environment* 372, 193-202.
- Wania, F. and Su, Y., 2004. Quantifying the global fractionation of polychlorinated biphenyls. *Ambio* 33, 161-168.
- Wania, F., Shen, L., Lei, Y.D., Teixeira, C., Muir, D.C.G., 2003. Development and calibration of a resin-based passive sampling system for monitoring persistent organic pollutants in the atmosphere. *Environmental Science and Technology* 37, 1352-1359.
- Wania, F., 1999. On the origin of elevated levels of persistent chemicals in the environment. *Environmental Science and Pollution Research* 6, 11-19.
- Wania, F. and Mackay, D., 1996. Tracking the distribution of persistent organic pollutants. *Environmental Science and Technology* 30,
- Wania, F. and Mackay, D., 1993. Global fractionation and cold condensation of low volatility organochlorine compounds in polar regions. *Ambio* 22, 10-18.
- WHO 1994. *Environmental Health Criteria 162: Brominated Diphenyl Ethers*. In: Anonymous World Health Organization, Geneva, 31-31-34.

Wilford, B.H., Harner, T., Zhu, J., Shoeib, M., Jones, K.C., 2004. Passive sampling survey of polybrominated diphenyl ether flame retardants in indoor and outdoor air in ottawa, canada: Implications for sources and exposure. *Environmental Science and Technology* 38, 5312-5318.

Wong, F., Harner, T., Liu, Q.-., Diamond, M.L., 2004. Using experimental and forest soils to investigate the uptake of polycyclic aromatic hydrocarbons (PAHs) along an urban-rural gradient. *Environmental Pollution* 129, 387-398.

Wurl, O., Potter, J.R., Obbard, J.P., Durville, C., 2006. Persistent organic pollutants in the equatorial atmosphere over the open indian ocean. *Environmental Science and Technology* 40, 1454-1461.

Xiao, H., Hung, H., Harner, T., Lei, Y.D., Wania, F., 2008. Field testing a flow-through sampler for semivolatile organic compounds in air. *Environmental Science and Technology* 42, 2970-2975.

Xiao, H., Hung, H., Harner, T., Lei, Y.D., Johnston, G.W., Wania, F., 2007. A flow-through sampler for semivolatile organic compounds in air. *Environmental Science and Technology* 41, 250-256.

Xie, Z. and Ebinghaus, R., 2008. Analytical methods for the determination of emerging organic contaminants in the atmosphere. *Analytica Chimica Acta* 610, 156-178.

Yang, R.Q., Yao, T.D., Xu, B.Q., Jiang, G.B., Zheng, X.Y., 2008. Distribution of organochlorine pesticides (OCPs) in conifer needles in the southeast tibetan plateau. *Environmental Pollution* 153, 92-100.

Yang, R.Q., Yao, T.D., Xu, B.Q., Jiang, G.B., Xin, X.D., 2007. Accumulation features of organochlorine pesticides and heavy metals in fish from high mountain lakes and lhasa river in the tibetan plateau. *Environment International* 33, 151-156.

Yang, W. and Holmén, B.A., 2007. Effects of relative humidity on chloroacetanilide and dinitroaniline herbicide desorption from agricultural PM_{2.5} on quartz fiber filters. *Environmental Science and Technology* 41, 3843-3849.

You, F. and Bidleman, T.F., 1984. Influence of volatility on the collection of polycyclic aromatic hydrocarbon vapors with polyurethane foam. *Environmental Science and Technology* 18, 330-333.

You, Q., Kang, S.C., Li, C., Li, M., Liu, J., 2006. Features of Meteorological Parameters at Nam Co Station, Tibetan Plateau. , 8-15.

Zhang, W.L. and Zhang, G., 2003. A preliminary study of organochlorine pesticides in water and sediments from two tibetan lakes. *Geochimica* 32, 363-367.

Zhou, T., Taylor, M.M., De Vito, M.J., Crofton, K.M., 2002. Developmental exposure to brominated diphenyl ethers results in thyroid hormone disruption. *Toxicological Sciences* 66, 105-116.

Appendices

Appendix I Supporting Information for Development and Indoor Characterization of Flow-Through Air Sampler for Semi-Volatile Organic Compounds

Appendix I.1 Selection of Sampling Media

To allow air to pass through the flow tube and to collect the SOC quantitatively from that air stream requires a sampling medium that ideally combines a low flow resistance with a high uptake efficiency. Two types of sampling media were explored:

- aluminium honeycomb discs of 1/8" cell size and 1" thickness, coated with a thin film of ethylene vinyl acetate (EVA). EVA has previously been used as a sampling medium in passive air samplers (Shoeib and Harner 2002a).
- polyurethane foam (PUF) discs of 1" thickness and different densities (P10z, P20z, P30z and P50z, corresponding to pore sizes of 10, 20, 30 and 50 pore per inch, respectively). PUF is regularly used as sampling medium for SOCs in both active and passive air samplers.

Honeycomb inserts were coated with EVA by the method described in reference 8. In order to improve the uptake efficiency, honeycomb inserts were separated by half-inch space rings to maximize the turbulence. A large box fan was used to generate an indoor air flow field. By changing the mass of the EVA coating, the number of inserts, flow resistance was determined by comparing the wind speed within the sampling tube and through the annular bypass under different wind scenarios. The angles between wind direction and axes of honeycomb were also adjusted to increase the wind resistance. Honeycomb samples were extracted with 400ml methanol for 1 hour twice. PUF discs were extracted by Soxhlet using acetone and PE (1:1) overnight. All the samples were cleaned-up and exchanged with iso-octane then blown down to 1ml before instrumental analysis. The extent of breakthrough was quantified as the percentage of the total chemical trapped in the last disc. The effect of sampling time and wind speeds on sampling efficiency was conducted for different sampling media.

Results (see Figure SI 1) from the flow resistance experiments showed that the EVA-coated honeycomb display much lower air flow resistance than the PUF discs and that the resistance of

the PUF discs depends on its porosity. The wind speed through 5 honeycomb units in series was only three time lower than the one through the annular bypass, whereas 5 low density PUF (P10z) discs in series decreased the wind speed by about an order of magnitude. Nevertheless, low density PUF-discs (P10z) had a wind resistance sufficiently low to allow for sampling.

PCB concentrations in multiple, serially arranged EVA-coated honey-comb discs were found to be rather uniform. Additional experiments with thicker EVA films and different physical arrangement of the honeycomb inserts did not improve the sampling efficiency. This suggests that the EVA coated honeycombs are not efficient enough to prevent substantial break-through. Despite its superiority in terms of flow resistance, the honeycomb inserts was thus judged not suitable for quantitative measurements of SOC air concentrations.

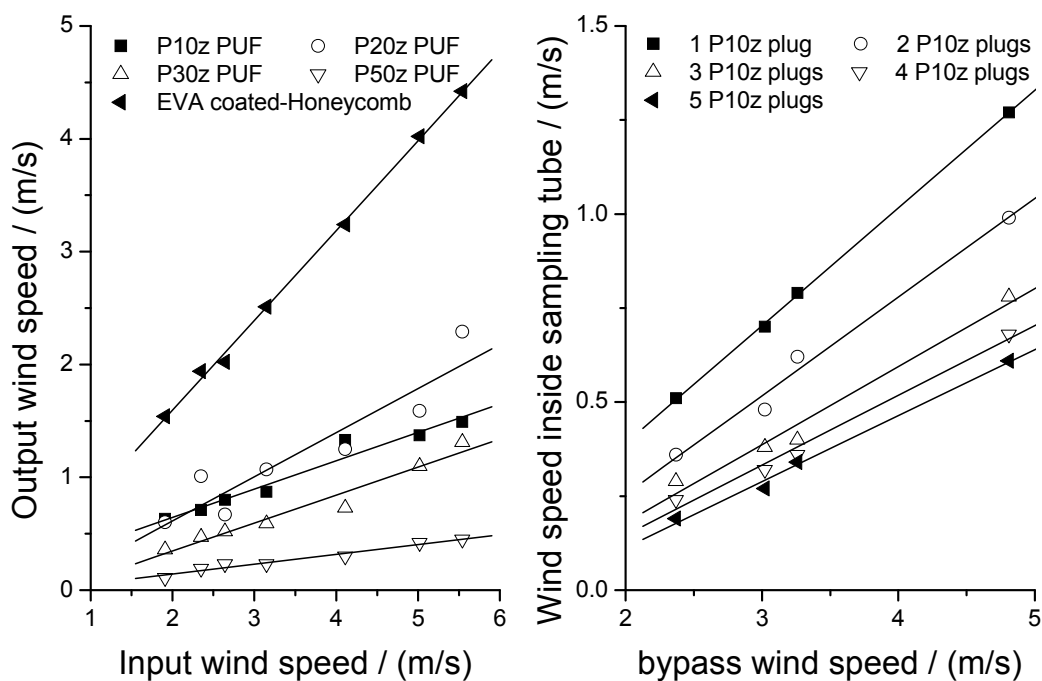
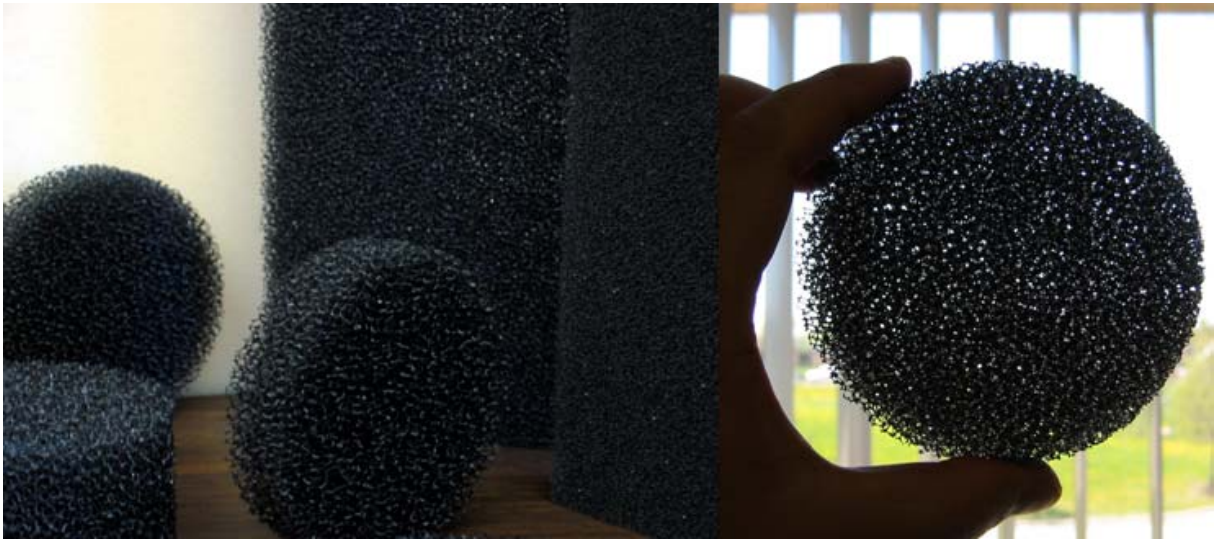


Figure SI 1. Wind resistance for different arrangements of sampling media.



P10z PUF plugs



Aluminium honeycomb discs

Appendix I.2 Original data and mathematical results

Table SI 1. Chemical amounts trapped in each P10z PUF disc in ng.

	PUF-I	PUF-II	PUF-III	PUF-IV	PUF-V	PUF-VI	PUF-VII	Blank
	125 m³							
PCB-8	2.4×10 ²	1.7×10 ²	1.4×10 ²	8.7×10 ¹	6.0×10 ¹	3.6×10 ¹	3.7×10 ¹	
PCB-18	3.5×10 ²	2.3×10 ²	1.8×10 ²	1.1×10 ²	7.1×10 ¹	4.1×10 ¹	3.4×10 ¹	
PCB-15	1.1×10 ²	5.5×10 ¹	3.9×10 ¹	2.0×10 ¹	8.1	3.4	2.0×10 ¹	
PCB-17	1.3×10 ²	8.1×10 ¹	6.4×10 ¹	3.8×10 ¹	2.5×10 ¹	1.4×10 ¹	1.1×10 ¹	
PCB-16+32	1.0×10 ²	6.1×10 ¹	4.1×10 ¹	2.2×10 ¹	1.2×10 ¹	6.1	4.3	
PCB-31	3.6×10 ²	1.7×10 ²	9.5×10 ¹	4.3×10 ¹	2.0×10 ¹	9.3	6.4	
PCB-28	3.3×10 ²	1.5×10 ²	8.3×10 ¹	3.7×10 ¹	1.8×10 ¹	7.9	5.2	
PCB-33	2.8×10 ²	1.3×10 ²	6.9×10 ¹	3.0×10 ¹	1.4×10 ¹	6.7	5.5	
PCB-52	2.3×10 ²	1.0×10 ²	4.8×10 ¹	2.1×10 ¹	1.0×10 ¹	4.4	3.9	
PCB-49	1.5×10 ²	6.6×10 ¹	3.2×10 ¹	1.3×10 ¹	6.2	2.3	1.9	
PCB-44	1.6×10 ²	5.9×10 ¹	2.4×10 ¹	9.0		1.6		
PCB-42	6.2×10 ¹	2.4×10 ¹	8.4	3.0	1.1			
PCB-74	6.7×10 ¹	2.1×10 ¹	7.5	2.6	9.7×10 ⁻¹			
PCB-70	6.5×10 ¹	2.0×10 ¹	7.4	2.8	1.2			
PCB-66	8.1×10 ¹	2.3×10 ¹	7.8	2.4				
PCB-56+60	2.7×10 ¹	8.0	3.1					
PCB-95	9.0×10 ¹	3.2×10 ¹	1.1×10 ¹	4.3				
PCB-101	1.3×10 ²	4.0×10 ¹	1.4×10 ¹	4.5				
PCB-99	3.6×10 ¹	1.1×10 ¹	3.9	1.4				
PCB-87	4.1×10 ¹	1.1×10 ¹	3.6					
PCB-77	4.4							
PCB-110	6.2×10 ¹	1.6×10 ¹	4.9	1.5				
PCB-151	7.9							
PCB-123	3.0×10 ¹	7.7	2.3					
PCB-149	2.4×10 ¹	6.9	1.6					
PCB-118	2.9×10 ¹	7.6	2.4	1.0	4.7E-01			
PCB-153	1.6×10 ¹	4.2	1.4					
PCB-105	5.4	1.8						
PCB-138	8.2	1.8	7.5×10 ⁻¹					
PCB-187	3.5							
PCB-183	3.9							
PCB-128	2.1							
PCB-185	4.4×10 ⁻¹							
PCB-174	1.5							
PCB-177	7.6×10 ⁻¹							
PCB-199	5.4×10 ⁻¹							
PCB-180	8.9×10 ⁻¹							
fluorene	1.1×10 ²	8.7×10 ¹	1.2×10 ²	8.0×10 ¹	8.2×10 ¹	6.1×10 ¹	4.6×10 ¹	2.6
phenanthrene	7.3×10 ²	3.3×10 ²	2.2×10 ²	8.0×10 ¹	4.8×10 ¹	2.0×10 ¹	1.1×10 ¹	1.0×10 ¹
anthracene	3.3×10 ¹	1.3×10 ¹	1.2×10 ¹	5.1	3.7	2.0	1.5	1.0
fluoranthene	1.3×10 ²	2.8×10 ¹	9.5	2.8	2.1	1.1	8.8×10 ⁻¹	1.4
pyrene	1.0×10 ²	2.2×10 ¹	7.0	2.2	1.7	1.7	9.4×10 ⁻¹	8.3×10 ⁻¹

	PUF-I	PUF-II	PUF-III	PUF-IV	PUF-V	PUF-VI	PUF-VII	Blank
368 m³								
PCB-8	4.4×10 ²	3.6×10 ²	1.6×10 ²	2.8×10 ²	2.3×10 ²	2.3×10 ²	2.0×10 ²	
PCB-18	7.0×10 ²	5.2×10 ²	2.7×10 ²	3.1×10 ²	2.3×10 ²	2.1×10 ²	2.0×10 ²	
PCB-15	3.1×10 ²	2.0×10 ²	8.0×10 ¹	7.6×10 ¹	5.1×10 ¹	4.4×10 ¹	3.7×10 ¹	
PCB-17	2.5×10 ²	1.9×10 ²	9.7×10 ¹	1.1×10 ²	7.9×10 ¹	7.6×10 ¹	7.0×10 ¹	
PCB-16+32	2.3×10 ²	1.5×10 ²	7.8×10 ¹	7.2×10 ¹	4.8×10 ¹	4.0×10 ¹	3.3×10 ¹	
PCB-31	9.0×10 ²	5.2×10 ²	2.4×10 ²	1.7×10 ²	9.7×10 ¹	6.6×10 ¹	4.4×10 ¹	
PCB-28	8.6×10 ²	5.1×10 ²	2.3×10 ²	1.6×10 ²	8.8×10 ¹	6.1×10 ¹	3.8×10 ¹	
PCB-33	7.4×10 ²	4.2×10 ²	1.9×10 ²	1.3×10 ²	6.8×10 ¹	4.6×10 ¹	3.0×10 ¹	
PCB-52	5.6×10 ²	2.9×10 ²	1.3×10 ²	7.5×10 ¹	3.8×10 ¹	2.5×10 ¹	1.5×10 ¹	
PCB-49	3.8×10 ²	2.0×10 ²	8.9×10 ¹	5.1×10 ¹	2.6×10 ¹	1.7×10 ¹	1.0×10 ¹	
PCB-44	4.2×10 ²	1.8×10 ²	7.0×10 ¹	3.4×10 ¹	1.5×10 ¹	7.7	4.0	
PCB-42	1.2×10 ²	5.4×10 ¹	1.8×10 ¹	9.2	4.3	2.7	7.6×10 ⁻¹	
PCB-74	2.0×10 ²	7.2×10 ¹	2.2×10 ¹	8.4	2.0	8.6×10 ⁻¹		
PCB-70	1.9×10 ²	6.4×10 ¹	1.9×10 ¹	7.1	2.5	1.4		
PCB-66	2.5×10 ²	8.4×10 ¹	2.4×10 ¹	8.4	2.1	3.2×10 ⁻¹		
PCB-56+60	7.7×10 ¹	2.5×10 ¹	6.7	2.2		2.3×10 ⁻¹		
PCB-95	2.3×10 ²	8.8×10 ¹	3.0×10 ¹	1.2×10 ¹	4.8	2.0	4.9×10 ⁻¹	
PCB-101	3.3×10 ²	1.1×10 ²	3.4×10 ¹	1.2×10 ¹	4.2	2.1	5.6×10 ⁻¹	
PCB-99	8.9×10 ¹	3.1×10 ¹	1.0×10 ¹	4.0	1.7	1.5		
PCB-87	1.1×10 ²	3.1×10 ¹	7.6	2.0				
PCB-81	3.8	7.4×10 ⁻¹						
PCB-77	8.4	1.4	2.0×10 ⁻¹					
PCB-110	1.7×10 ²	4.7×10 ¹			1.0			
PCB-151	2.0×10 ¹	5.6	1.3					
PCB-123	7.8×10 ¹							
PCB-149	6.4×10 ¹	1.8×10 ¹	4.5	1.1	1.2×10 ⁻¹			
PCB-118	7.8×10 ¹	1.9×10 ¹	4.0	6.7×10 ⁻¹				
PCB-114	1.4							
PCB-153	4.0×10 ¹	1.0×10 ¹	2.1	2.7×10 ⁻¹				
PCB-105	1.3×10 ¹	2.7	4.6×10 ⁻¹					
PCB-137	8.4×10 ⁻¹							
PCB-138	2.0×10 ¹	4.6	7.3×10 ⁻¹	3.0×10 ⁻²		2.7×10 ⁻¹		
PCB-187	8.9	2.2	3.3×10 ⁻¹					
PCB-183	2.8	5.2×10 ⁻¹						
PCB-128	4.5	5.2×10 ⁻¹						
PCB-185	1.0	1.0×10 ⁻¹						
PCB-174	3.0	1.7×10 ⁻¹						
PCB-177	1.6	2.0×10 ⁻²						
PCB-171	6.0×10 ⁻¹							
PCB-199	4.4×10 ⁻¹							
PCB-180	2.2	2.9×10 ⁻¹						
PCB-170	2.3	4.2×10 ⁻¹						
PCB-203	7.1×10 ⁻¹							
fluorene	1.4×10 ²	1.3×10 ²	2.7×10 ¹	1.3×10 ²	9.3×10 ¹	1.1×10 ²	1.4×10 ²	2.6
phenanthrene	1.6×10 ³	9.9×10 ²	3.8×10 ²	4.0×10 ²	1.9×10 ²	1.3×10 ²	8.8×10 ¹	1.0×10 ¹
anthracene	7.1×10 ¹	4.9×10 ¹	1.8×10 ¹	1.7×10 ¹	6.2	5.5	4.8	1.0
fluoranthene	3.6×10 ²	9.5×10 ¹	2.1×10 ¹	8.0	2.9	1.8	1.4	1.4
pyrene	3.0×10 ²	7.4×10 ¹	1.6×10 ¹	5.2	2.6	2.4	1.6	8.3×10 ⁻¹

	PUF-I	PUF-II	PUF-III	PUF-IV	PUF-V	PUF-VI	PUF-VII	Blank
	793 m³							
PCB-8	7.0×10 ²	7.3×10 ²	6.6×10 ²	6.1×10 ²	5.8×10 ²	3.9×10 ²	4.8×10 ²	
PCB-18	1.1×10 ³	1.1×10 ³	9.1×10 ²	8.0×10 ²	7.1×10 ²	4.4×10 ²	5.2×10 ²	
PCB-15	4.3×10 ²	3.7×10 ²	2.6×10 ²	1.9×10 ²	1.4×10 ²	7.5×10 ¹	8.9×10 ¹	
PCB-17	3.9×10 ²	3.8×10 ²	3.2×10 ²	2.8×10 ²	2.5×10 ²	1.6×10 ²	1.8×10 ²	
PCB-16+32	3.5×10 ²	3.2×10 ²	2.5×10 ²	2.0×10 ²	1.6×10 ²	9.5×10 ¹	9.9×10 ¹	
PCB-31	1.4×10 ³	1.1×10 ³	7.5×10 ²	5.2×10 ²	3.7×10 ²	1.8×10 ²	1.6×10 ²	
PCB-28	1.2×10 ³	1.0×10 ³	6.7×10 ²	4.7×10 ²	3.2×10 ²	1.5×10 ²	1.3×10 ²	
PCB-33	1.1×10 ³	8.6×10 ²	5.6×10 ²	3.8×10 ²	2.5×10 ²	1.2×10 ²	1.0×10 ²	
PCB-52	8.7×10 ²	6.1×10 ²	3.7×10 ²	2.3×10 ²	1.5×10 ²	6.7×10 ¹	5.4×10 ¹	
PCB-49	6.0×10 ²	4.3×10 ²	2.6×10 ²	1.7×10 ²	1.1×10 ²	4.7×10 ¹	3.8×10 ¹	
PCB-44	6.6×10 ²	4.0×10 ²	2.1×10 ²	1.1×10 ²	6.2×10 ¹	2.5×10 ¹	1.6×10 ¹	
PCB-42	1.9×10 ²	1.2×10 ²	6.5×10 ¹	3.4×10 ¹	1.9×10 ¹	5.1	3.4	
PCB-74	3.0×10 ²	1.5×10 ²	6.3×10 ¹	2.9×10 ¹	1.4×10 ¹	6.5	3.8	
PCB-70	3.0×10 ²	1.4×10 ²	5.7×10 ¹	2.4×10 ¹	1.2×10 ¹	2.2	2.2	
PCB-66	3.8×10 ²	1.7×10 ²	6.9×10 ¹	2.8×10 ¹	1.2×10 ¹	3.6	3.4	
PCB-56+60	1.3×10 ²	5.6×10 ¹	2.2×10 ¹	6.5	3.4	1.6	1.8	
PCB-95	3.7×10 ²	1.9×10 ²	8.8×10 ¹	4.1×10 ¹	2.0×10 ¹	6.7	4.0	
PCB-101	5.3×10 ²	2.4×10 ²	9.6×10 ¹	3.9×10 ¹	1.7×10 ¹	5.7	3.8	
PCB-99	1.5×10 ²	6.6×10 ¹	2.9×10 ¹	1.1×10 ¹	5.3	5.0	3.1	
PCB-87	1.7×10 ²	6.3×10 ¹	2.3×10 ¹	5.0	2.6			
PCB-81	8.3	2.8	1.1					
PCB-77	1.3×10 ¹	5.2	1.7	7.8×10 ⁻¹				
PCB-110	2.7×10 ²	9.4×10 ¹	3.1×10 ¹	1.1×10 ¹	3.6	1.4		
PCB-151	3.3×10 ¹	1.3×10 ¹	4.6	1.7				
PCB-123	1.1×10 ²	3.3×10 ¹	9.1	2.7	7.2×10 ⁻¹		6.5×10 ⁻¹	
PCB-149	1.0×10 ²	3.7×10 ¹	1.3×10 ¹	4.4	1.8			
PCB-118	1.1×10 ²	3.2×10 ¹	9.0	2.9	1.3	3.2×10 ⁻¹	1.5	
PCB-114	2.7	9.2×10 ⁻¹						
PCB-153	6.4×10 ¹	2.0×10 ¹	6.4	2.1				
PCB-105	2.0×10 ¹	5.7	1.8	2.6×10 ⁻¹				
PCB-137	2.6							
PCB-138	3.1×10 ¹	8.8	2.2	1.2				
PCB-187	1.5×10 ¹	4.4	1.5					
PCB-183	5.5	1.8	8.7×10 ⁻¹					
PCB-128	7.3	2.0						
PCB-185	1.0	3.8×10 ⁻¹						
PCB-174	5.8	1.5	3.4×10 ⁻¹					
PCB-177	3.3	1.0						
PCB-171	3.6							
PCB-156	9.2×10 ⁻¹							
PCB-157	1.3							
PCB-199	1.7	7.6×10 ⁻¹						
PCB-180	4.1	1.0						
PCB-170	4.1	1.0						
PCB-203	2.5		5.3×10 ⁻¹					
fluorene	1.4×10 ²	2.2×10 ²	1.5×10 ²	1.7×10 ²	1.5×10 ²	1.3×10 ²	1.7×10 ²	3.9×10 ⁻¹
phenanthrene	1.9×10 ³	2.2×10 ³	1.2×10 ³	9.6×10 ²	6.0×10 ²	3.4×10 ²	3.2×10 ²	1.4
anthracene	9.4×10 ¹	7.6×10 ¹	6.0×10 ¹	4.4×10 ¹	3.3×10 ¹	1.8×10 ¹	1.2×10 ¹	1.1
fluoranthene	5.6×10 ²	2.2×10 ²	6.1×10 ¹	2.2×10 ¹	7.7	3.8	1.6	5.3×10 ⁻¹
pyrene	5.2×10 ²	1.8×10 ²	4.7×10 ¹	1.7×10 ¹	5.4	1.7	1.7	3.5×10 ⁻¹

	PUF-I	PUF-II	PUF-III	PUF-IV	PUF-V	PUF-VI	PUF-VII	Blank
1360 m³								
PCB-8	4.4×10 ²	4.8×10 ²	4.6×10 ²	5.1×10 ²	5.3×10 ²	5.4×10 ²	5.3×10 ²	
PCB-18	1.3×10 ³	1.2×10 ³	1.1×10 ³	1.2×10 ³	1.1×10 ³	1.0×10 ³	9.4×10 ²	
PCB-15	4.4×10 ²	4.4×10 ²	3.7×10 ²	3.7×10 ²	3.2×10 ²	2.5×10 ²	2.3×10 ²	
PCB-17	4.2×10 ²	4.1×10 ²	3.8×10 ²	3.7×10 ²	3.7×10 ²	3.5×10 ²	3.2×10 ²	
PCB-16+32	4.5×10 ²	4.1×10 ²	3.5×10 ²	4.2×10 ²	3.2×10 ²	2.8×10 ²	2.4×10 ²	
PCB-31	2.0×10 ³	1.7×10 ³	1.3×10 ³	1.1×10 ³	9.9×10 ²	7.3×10 ²	5.8×10 ²	
PCB-28	1.7×10 ³	1.5×10 ³	1.2×10 ³	1.0×10 ³	8.9×10 ²	6.8×10 ²	5.2×10 ²	
PCB-33	1.6×10 ³	1.4×10 ³	1.0×10 ³	1.0×10 ³	7.3×10 ²	5.3×10 ²	4.0×10 ²	
PCB-52	1.5×10 ³	1.1×10 ³	8.0×10 ²	7.9×10 ²	4.7×10 ²	3.2×10 ²	2.2×10 ²	
PCB-49	1.0×10 ³	7.9×10 ²	5.5×10 ²	5.5×10 ²	3.3×10 ²	2.3×10 ²	1.5×10 ²	
PCB-44	1.2×10 ³	8.3×10 ²	5.1×10 ²	4.4×10 ²	2.4×10 ²	1.4×10 ²	8.2×10 ¹	
PCB-42	2.9×10 ²	2.0×10 ²	1.5×10 ²	1.2×10 ²	6.7×10 ¹	3.8×10 ¹	2.2×10 ¹	
PCB-74	6.3×10 ²	3.6×10 ²	1.8×10 ²	1.3×10 ²	5.9×10 ¹	2.8×10 ¹	1.4×10 ¹	
PCB-70	6.1×10 ²	3.2×10 ²	1.5×10 ²	9.9×10 ¹	4.3×10 ¹	2.0×10 ¹	1.0×10 ¹	
PCB-66	8.1×10 ²	4.3×10 ²	2.0×10 ²	1.3×10 ²	5.7×10 ¹	2.3×10 ¹	1.1×10 ¹	
PCB-56+60	2.9×10 ²	1.3×10 ²	5.0×10 ¹	3.3×10 ¹	1.4×10 ¹	4.5	2.0	
PCB-95	7.3×10 ²	4.1×10 ²	2.2×10 ²	1.6×10 ²	7.5×10 ¹	3.8×10 ¹	1.9×10 ¹	
PCB-101	1.1×10 ³	5.5×10 ²	2.6×10 ²	1.6×10 ²	6.8×10 ¹	3.1×10 ¹	1.4×10 ¹	
PCB-99	3.0×10 ²	1.5×10 ²	7.3×10 ¹	4.7×10 ¹	2.0×10 ¹	9.4	5.1	
PCB-87	3.8×10 ²	1.6×10 ²	6.2×10 ¹	3.0×10 ¹	1.2×10 ¹	4.2	1.7	
PCB-81	1.4×10 ¹	6.0	3.0	1.3				
PCB-77	3.2×10 ¹	1.1×10 ¹						
PCB-110	5.7×10 ²						2.1	
PCB-151	7.5×10 ¹	3.1×10 ¹	1.3×10 ¹	6.9	2.5	9.9×10 ⁻¹	3.8×10 ⁻¹	
PCB-149	2.4×10 ²	9.3×10 ¹	3.5×10 ¹	1.7×10 ¹	5.9	2.1		
PCB-118	2.8×10 ²	9.4×10 ¹	3.0×10 ¹	1.3×10 ¹	3.8	1.4	7.1×10 ⁻¹	
PCB-114	6.7	2.3						
PCB-153	1.6×10 ²	5.3×10 ¹	1.8×10 ¹	7.4	2.5	8.0×10 ⁻¹		
PCB-105	5.0×10 ¹	1.5×10 ¹	4.5	2.1	1.1			
PCB-137	6.6	1.5						
PCB-138	8.2×10 ¹	2.4×10 ¹	7.4	2.9	1.1	3.0×10 ⁻¹	2.9	
PCB-187	3.7×10 ¹	1.2×10 ¹	3.4	1.3	2.1×10 ⁻¹			
PCB-183	1.3×10 ¹	3.8	1.3	3.8×10 ⁻¹	9.0×10 ⁻²			
PCB-128	1.8×10 ¹	5.3	2.1					
PCB-185	2.8	1.2	6.4×10 ⁻¹					
PCB-174	1.5×10 ¹	4.3	1.3	6.6×10 ⁻¹	1.2×10 ⁻¹			
PCB-177	7.2	1.8	4.2×10 ⁻¹					
PCB-171	4.3	1.2						
PCB-156	2.4	8.1×10 ⁻¹						
PCB-157	7.2×10 ⁻¹							
PCB-199	3.7	1.1	2.4×10 ⁻¹					
PCB-180	1.0×10 ¹	2.6	5.8×10 ⁻¹	1.8×10 ⁻¹				
PCB-200	2.0							
PCB-170	3.2	8.9×10 ⁻¹						
PCB-203	6.2	2.4						
fluorene	1.3×10 ²	1.6×10 ²	1.7×10 ²	2.1×10 ²	2.3×10 ²	2.2×10 ²	2.2×10 ²	1.3
phenanthrene	2.0×10 ³	2.1×10 ³	1.9×10 ³	2.0×10 ³	1.8×10 ³	1.3×10 ³	1.0×10 ³	4.0×10 ⁻¹
anthracene	6.4×10 ¹	6.8×10 ¹	6.6×10 ¹	6.1×10 ¹	5.9×10 ¹	4.3×10 ¹	3.3×10 ¹	
fluoranthene	8.9×10 ²	4.1×10 ²	1.6×10 ²	7.6×10 ¹	3.3×10 ¹	1.3×10 ¹	4.9	4.4×10 ⁻¹
pyrene	7.2×10 ²	3.0×10 ²	1.1×10 ²	4.4×10 ¹	1.7×10 ¹	6.0	3.3	3.4×10 ⁻¹

Table SI 2. L_{50} from the non-linear regression equation (2-1) and its standard deviation.

	L-50 / cm			
	125 m ³	368 m ³	793 m ³	1360 m ³
PCB-8	6.74±0.34	13.80±0.69	22.77±2.83	
PCB-18	5.95±0.29	7.85±0.50	15.04±0.69	23.37±2.27
PCB-15	4.15±0.46	5.18±0.28	8.06±0.20	16.30±0.44
PCB-17	5.84±0.31	7.86±0.48	15.12±0.67	
PCB-16+32	4.79±0.24	5.45±0.39	10.46±0.23	16.98±1.09
PCB-31	3.90±0.19	4.40±0.17	7.01±0.16	10.88±0.25
PCB-28	3.79±0.20	4.51±0.17	7.00±0.16	11.10±0.27
PCB-33	3.78±0.18	4.29±0.15	6.53±0.15	10.30±0.40
PCB-52	3.63±0.16	4.00±0.13	5.64±0.13	7.73±0.58
PCB-49	3.63±0.16	4.04±0.13	5.74±0.13	7.94±0.58
PCB-44	3.36±0.21	3.61±0.11	4.66±0.12	5.76±0.40
PCB-42	3.36±0.14	3.57±0.10	4.86±0.12	6.29±0.60
PCB-74	3.14±0.17	3.31±0.10	3.87±0.11	4.44±0.19
PCB-70	3.12±0.18	3.23±0.10	3.68±0.12	4.09±0.16
PCB-66	3.06±0.21	3.23±0.10	3.65±0.11	4.14±0.16
PCB-56+60	3.08±0.34	3.20±0.11	3.59±0.10	3.70±0.14
PCB-95	3.28±0.19	3.36±0.10	4.00±0.12	4.45±0.21
PCB-101	3.11±0.20	3.23±0.10	3.65±0.11	3.96±0.16
PCB-99	3.11±0.21	3.23±0.13	3.70±0.12	4.01±0.17
PCB-87	3.04±0.28	3.10±0.14	3.33±0.14	3.51±0.12
PCB-81			3.21±0.33	3.65±0.26
PCB-77			3.49±0.14	3.71 ^a
PCB-110	3.01±0.19		3.26±0.12	
PCB-151		3.09±0.19	3.41±0.16	3.53±0.14
PCB-123	3.01±0.27		3.12±0.11	0.00±0.00
PCB-149	3.08±0.20	3.08±0.12	3.27±0.14	3.39±0.15
PCB-118	2.99±0.18	3.00±0.15	3.11±0.10	3.21±0.11
PCB-153	3.02±0.30	3.03±0.14	3.13±0.18	3.22±0.13
PCB-105		2.97±0.20	3.07±0.19	3.11±0.16
PCB-138	2.88±0.42	3.00±0.12	3.07±0.18	3.08±0.14
PCB-187		3.05±0.15	3.11±0.29	3.14±0.14
PCB-183			3.22±0.40	3.07±0.17
PCB-128				3.06±0.35
PCB-174			3.05±0.21	3.06±0.17
PCB-177				3.03±0.21
PCB-199				3.15±0.16
PCB-180				3.02±0.15
PCB-200				3.36±2.27
phenanthrene	3.80±0.26	4.54±0.31	8.61±0.71	16.41±0.59
anthracene	3.71±0.43	4.78±0.29	7.92±0.30	16.44±0.50
fluoranthene	2.91±0.14	3.05±0.09	3.41±0.07	3.68±0.11
pyrene	2.89±0.14	3.00±0.09	3.26±0.07	3.47±0.10

a. only two points for non-linear regression.

Table SI 3. The theoretical plate number N , breakthrough volume V_B , and their standard deviation for different sampled air volumes.

	N				$\log(P_L/\text{Pa})^5$	$\log(V_B/\text{m}^3)$
	125 m ³	368 m ³	793 m ³	1360 m ³		
PCB-8	1.64±0.34	0.67±0.15	2.17±0.93		-0.801	2.755 ±0.072
PCB-18	1.69±0.33	0.93±0.21	1.48±0.30	3.62±1.43	-1.108	2.993 ±0.050
PCB-15	1.68±0.64	1.58±0.26	1.74±0.21	2.66±0.50	-1.139	3.192 ±0.094
PCB-17	1.68±0.34	0.96±0.22	1.50±0.29		-1.148	2.995 ±0.103
PCB-16+32	1.99±0.38	1.34±0.34	1.65±0.19	3.35±1.52	-1.268	3.163 ±0.065
PCB-31	2.54±0.52	2.16±0.34	2.22±0.23	1.45±0.19	-1.461	3.406 ±0.060
PCB-28	2.54±0.56	2.35±0.36	2.29±0.24	1.40±0.20	-1.468	3.395 ±0.055
PCB-33	2.64±0.55	2.39±0.36	2.24±0.22	1.79±0.42	-1.578	3.439 ±0.063
PCB-52	2.93±0.60	2.67±0.39	2.25±0.22	1.56±0.47	-1.794	3.630 ±0.049
PCB-49	3.00±0.61	2.66±0.37	2.29±0.23	1.58±0.48	-1.774	3.611 ±0.047
PCB-44	3.88±1.37	3.48±0.55	2.61±0.29	1.70±0.39	-1.894	3.862 ±0.044
PCB-42	4.29±1.06	3.82±0.59	2.87±0.32	1.55±0.49	-1.934	3.773 ±0.053
PCB-74	4.94±1.58	4.94±0.99	3.12±0.43	2.25±0.39	-2.137	4.133 ±0.039
PCB-70	4.82±1.63	5.19±1.11	3.38±0.56	2.50±0.43	-2.262	4.253 ±0.045
PCB-66	5.65±2.40	5.44±1.14	3.51±0.56	2.60±0.42	-2.207	4.224 ±0.031
PCB-56+60	5.28±3.65	5.85±1.42	3.87±0.62	3.17±0.59	-2.277	4.408 ±0.118
PCB-95	4.43±1.53	4.32±0.79	2.99±0.42	2.09±0.39	-2.274	4.150 ±0.068
PCB-101	5.25±2.11	5.16±1.01	3.52±0.56	2.60±0.46	-2.470	4.308 ±0.055
PCB-99	5.03±2.09	4.68±1.11	3.20±0.53	2.52±0.44	-2.524	4.278 ±0.061
PCB-87	6.33±3.98	6.79±2.24	4.58±1.21	3.53±0.66	-2.641	4.563 ±0.052
PCB-81			4.45±2.86	2.81±1.02	-2.542	4.285 ±0.025 ⁶
PCB-110	6.57±2.75		4.74±1.08		-2.737	4.605 ±0.026
PCB-151		7.47±3.47	4.19±1.24	3.35±0.66	-2.750	4.488 ±0.185
PCB-123	6.97±4.36		6.13±1.45		-2.884	4.926 ±0.026 ^b
PCB-149	7.29±3.55	6.94±1.92	4.60±1.23	3.77±0.87	-2.947	4.717 ±0.087
PCB-118	6.28±2.33	8.63±3.07	5.95±1.34	4.88±1.04	-2.923	4.876 ±0.059
PCB-153	6.39±4.21	8.51±2.89	5.41±2.04	4.74±1.15	-3.165	4.922 ±0.063
PCB-105		10.43±5.18	6.13±2.51	5.41±1.70	-3.058	4.973 ±0.191
PCB-138	7.11±6.29	10.36±3.20	6.46±2.51	5.56±1.61	-3.289	4.873 ±0.212
PCB-187		9.98±3.96	5.46±3.38	5.65±1.62	-3.512	5.194 ±0.149
PCB-183			3.94±2.88	5.65±1.90	-3.453	
PCB-128				5.32±3.77	-3.461	
PCB-174			7.88±3.97	5.71±1.95	-3.743	5.670 ±0.026
PCB-177				8.01±4.18	-3.603	
PCB-199			3.01±1.75	7.22±2.99	-4.228	
PCB-180				7.80±2.80	-3.881	
phenanthrene	2.52 ±0.72	2.21 ±0.60	3.78 ±1.88	13.42 ±6.39	-1.097	3.185±0.075
anthracene	1.82 ±0.73	2.96 ±0.83	2.03 ±0.36	13.75 ±5.59	-1.140	3.187±0.084
fluoranthene	8.14 ±2.55	7.82 ±1.62	5.19 ±0.71	3.46 ±0.53	-2.223	4.364±0.053
pyrene	8.58 ±2.71	8.36 ±1.88	5.74 ±0.95	4.01 ±0.68	-2.266	4.492±0.047

⁵ The $\log P_L$ data for PCBs are from reference 14, for PAHs are from reference 15.

⁶ Only two points for regression to calculate V_B , the standard deviation could be underestimated.

Table SI 4. Paired two sample t-test results for nine volatile compounds before and after breakthrough level corrections. The subscript represents approximate sampling days.

		Paired Differences						
		Mean	Std. Deviation	Std. Error Mean	95% Confidence Interval of the Difference		t	Sig. (2-tailed)
					Lower	Upper		
Before b-correction	1 – C _{III} /C _I	0.089	0.096	0.032	0.015	0.162	2.759	0.025
	1 – C _{VI} /C _I	0.099	0.069	0.023	0.046	0.152	4.317	0.003
	1 – C _X /C _I	0.209	0.231	0.077	0.032	0.387	2.721	0.026
After b-correction	1 – C _{III} /C _I	0.065	0.083	0.028	0.000	0.129	2.324	0.049
	1 – C _{VI} /C _I	-0.034	0.167	0.056	-0.162	0.094	-0.607	0.561
	1 – C _X /C _I	-0.056	0.179	0.060	-0.194	0.081	-0.944	0.373

Appendix II Supporting Information for Field Testing a Flow-Through Sampler for Semi-Volatile Organic Compounds in Air

Appendix II.1 Standard operation procedure for field sampling of FTS

Setting Up the Sampler Housing:

Using the screws provided, fix the vortex rotor wind sensor on top of the Flow-through Passive Air Sampler (FT-PAS) flow tube.

Find a stable support stand for the metal post. The post tube should have an I.D. of 5.2 cm and a 2.5 cm hole at about half a meter away from the top. Set up the post upright by mounting it on the stand. Make sure the top of the post is more than 1.5 meters above the ground. Let the vane sensor cable go through the top of the metal post and the hole; then set up the FT-PAS on top of the post. Fasten the sampler to the post with two Allen screws. After connecting the signal cable to the Signal Converter case, the sampler housing is ready.

Recording the Wind Speed Data:

Install the MadgeTech Data Recorder Software onto a computer. If there is no Serial port available, the USB-to-Serial adaptor driver will also need to be installed. Note: Install the driver first before plugging the adaptor into the computer!

Connect the Pulse 110 data logger to the computer using the provided IFC 110 cable. Open the MadgeTech Data Recorder Software (the national flag symbol under the menu can be used to select the language); select the correct communication port under the “Communication → Select Comm Port” menu. (Selects “COM1” if the IFC 110 cable is directly connected to computer; it would likely to be “COM6” if the



USB-to-serial adaptor is used.)

Set the Baud rate at 57600 baud for Pulse 110 through “Communication → Select Baud Rate” menu.

Using the “Device” menu, the operator can identify and control the data loggers: includes start, stop and reset the device; and download the data.

The data loggers must be started while connected to the computer. You have the option to start them instantly or delay for a while. It is simplest to set the data loggers to start at a specific time, before heading outside to deploy the sample. Since the sample deployment takes a few minutes, “delay start” is normally selected. In general it takes less than 5 minutes to deploy the samples, plus time taken to get to the sampling site. Set up the reading rate at whatever interval you want: for one month period of sampling, select “5 minutes”. The log time will display how long it will take for the storage memory to be filled up. Finally press the “Start Device” button. Wait a few seconds until the software gives the device its starting instructions, then the data logger can be disconnected from the computer (repeat the starting instructions with the second data logger). Note: Set the two data loggers to start synchronically in order to compare the wind speed outside and passage through the sampling media. Both data loggers are now ready for recording the wind speed data during the sampling period.

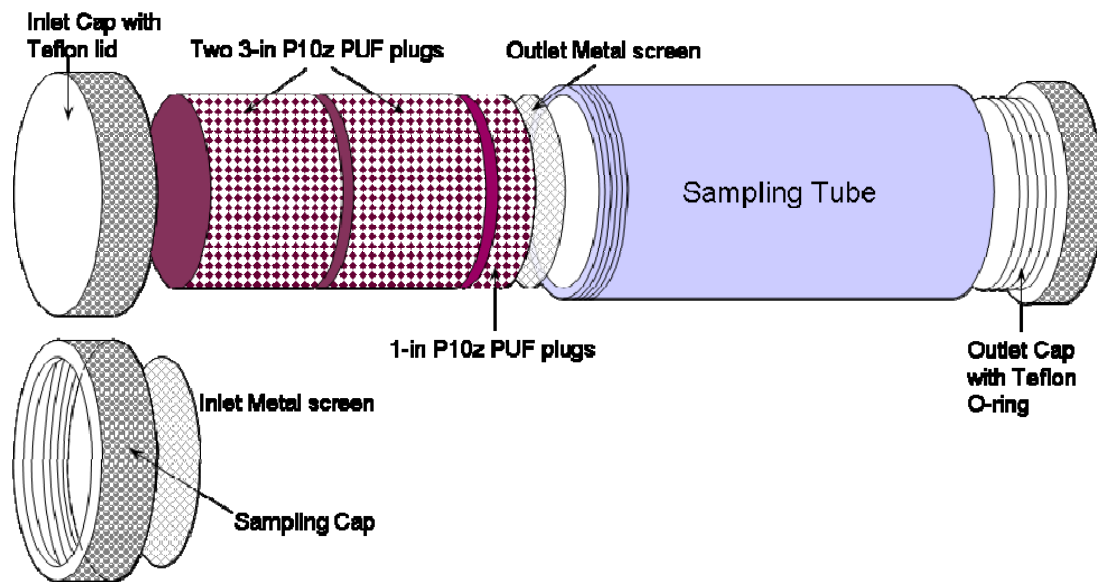
When finishing the sampling, connect the data logger to the computer again. From the Device Menu, select “Stop Device”, then “Read Device Data” to download data to the computer. Note: DO NOT Press “Reset Device” or “Start Device” buttons until you have downloaded and saved all the data, otherwise the data will be lost!!

After downloading the data from the device, the software will show available datasets on the dropdown list at the top-right corner of the composite graph. Save all of them separately and name it correspondingly (such as: inside_oct1.csv; outside_oct1.csv; inside_nov1.csv etc.) before closing the program.

Sampling:

When handling the sampling tube and PUFs, please wear nitrile gloves and use clean (solvent-rinsed) tweezers/tongs. Before starting the sampling, rinse the sampling tube, metal screens and caps with soapy water, water, then distilled water, followed by acetone then petroleum ether (or

Hexane) in sequence. Screw in the outlet cap, and then install the metal screen and sampling media as shown in the following figure, before sealing the sampling tube. After taking out the PUFs (sampling media) from their storage glass jars, leave the jars capped and seal them with Teflon tapes. If a blank sample needs to be taken, also remove a PUF plug (1-inch or 3-inch) from its jar, wrap it in aluminum foil and place in a Ziploc bag. This part of sampling preparation could be done before going to the field site, but you should be alert to the potential for contamination from the indoor environment.



Once at the sampling site, plug the signal cable from the vortex wind sensor into a started data logger and place the data logger into the holder inside the FT-PAS. Make sure the vane sensor cable is well connected to the signal converter case. Connect the other data logger with the converter circuit. Ensure the connection between the battery, converter circuit and data logger is good; also check the battery inside the case is fully charged ($>5.5V$). It would be best, if possible, to leave the charger always plugged in to AC/solar panel. Close the case properly to prevent the rain and snow.



Open the outlet cap, and then fit the sampling tube (with the sampling media inside) into the sampler housing by screwing the tube in front of the vane sensor. Note: NO need to be too tight otherwise it may be difficult to disassemble them. At approximately the time the data loggers start recording wind speed data, open the Inlet Cap and replace it with Sampling Cap and Inlet Metal Screen. The sampler is then completely functional.

For blank samples, open the Ziploc bag and unwrap then aluminum foil which contain the PUF plug and expose the PUF to the air during the time you are installing the sampling tube, then close and bring the sample back for storage as for all other samples.

During the sampling, caps and other materials should be carefully stored inside a Ziploc bag.



Please make sure the vane sensor cable doesn't twist too much during the sampling. If it is possible release the twist by rotating the signal converter case.

When it is time to stop the sampling, replace the Sampling Cap and Inlet Metal Screen with Inlet Cap (with Teflon lid). Then disconnect the two signal cables from the data loggers to prevent the data logger recording any more data. After that, disassemble the Sampling Tube from the sampler and seal it with the Outlet Cap (with O-ring).

On arrival at the lab, transfer all PUF samples (including blank samples) into storage jars separately, and seal them properly with Teflon tapes. Label the samples carefully; please at least include the starting (or ending) date and the relative position (Front, middle, back; or 1, 2, 3; or blank). Leave the storage jars in the fridge.

Remember to connect the data loggers into the computer to download the wind speed data.

Please check the battery of the data logger regularly (whether the LEDs are flashing every five minutes during the sampling). If you need to replace the battery, peel off the label (the side without LED) of the data logger, unscrew the nut to open the data logger, and then replace it with a new one.

Appendix II.2 Wind speed correlation under field conditions

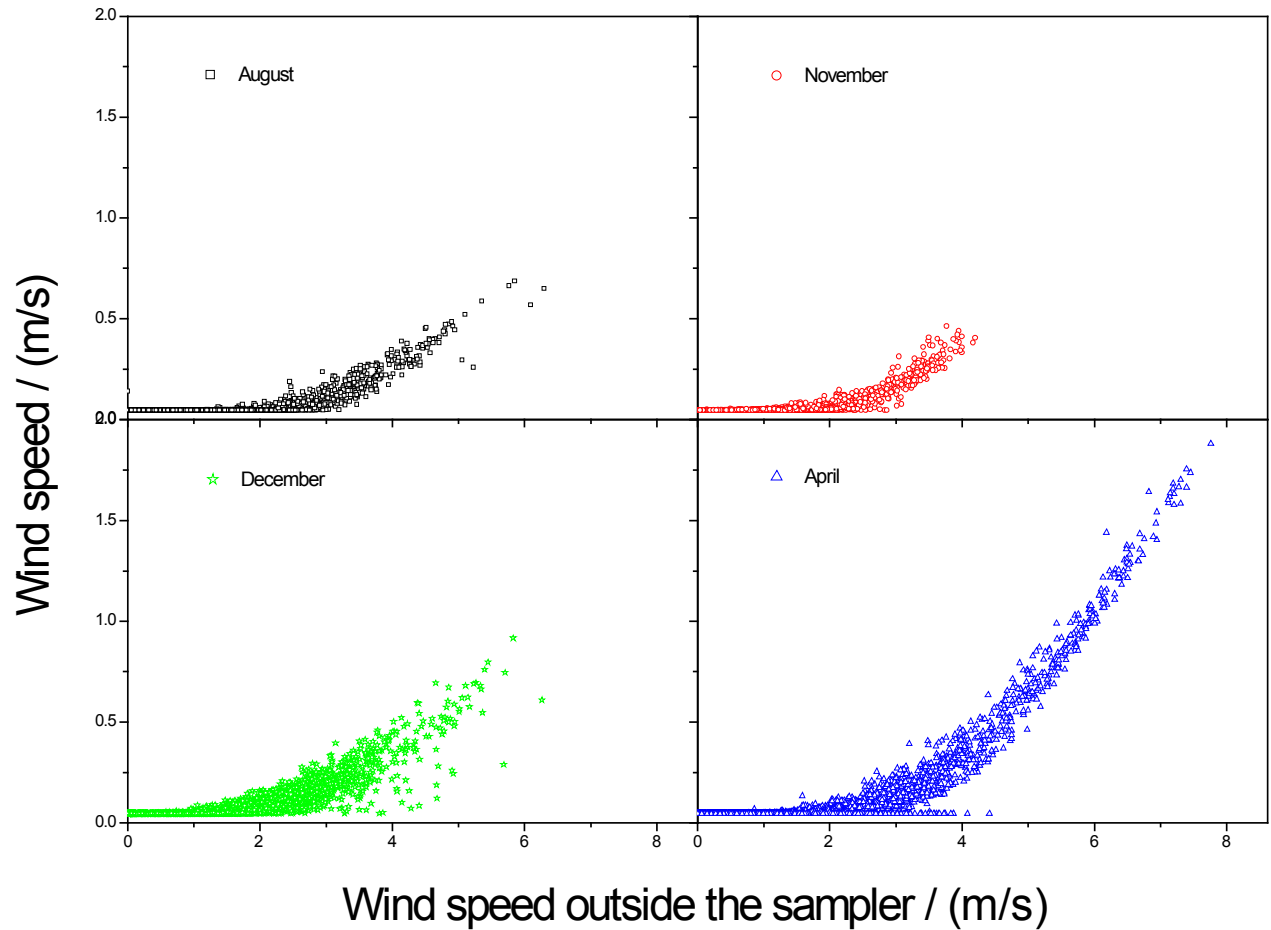


Figure SI 2. The correlation between the wind speed recorded by the vortex sensor on top the sampler and the windspeed recorded by the vane sensor mounted at the exit of sampling tube for four different sampling periods.

The calibration equation for the outside wind sensor (u_{out} in m/s, r_{out} in rp5m) is

$$u_{out} = 0.00345 r_{out} \quad (1')$$

These are the versions of equations (2) and (3), which use r_{out} instead of u_{out} , in order to avoid the error introduced by calibration equation (1')

$$u_{in} = 0.0442 / 848.5 \cdot r_{out} = 5.21 \cdot 10^{-5} \cdot r_{out}, \quad \text{when } r_{in} = 0 \quad (2')$$

$$u_{in} = \frac{7.701 \times 2.046 \times 10^{-11} r_{out}^{3.049}}{1 + 2.046 \times 10^{-11} r_{out}^{3.049}} \quad (3')$$

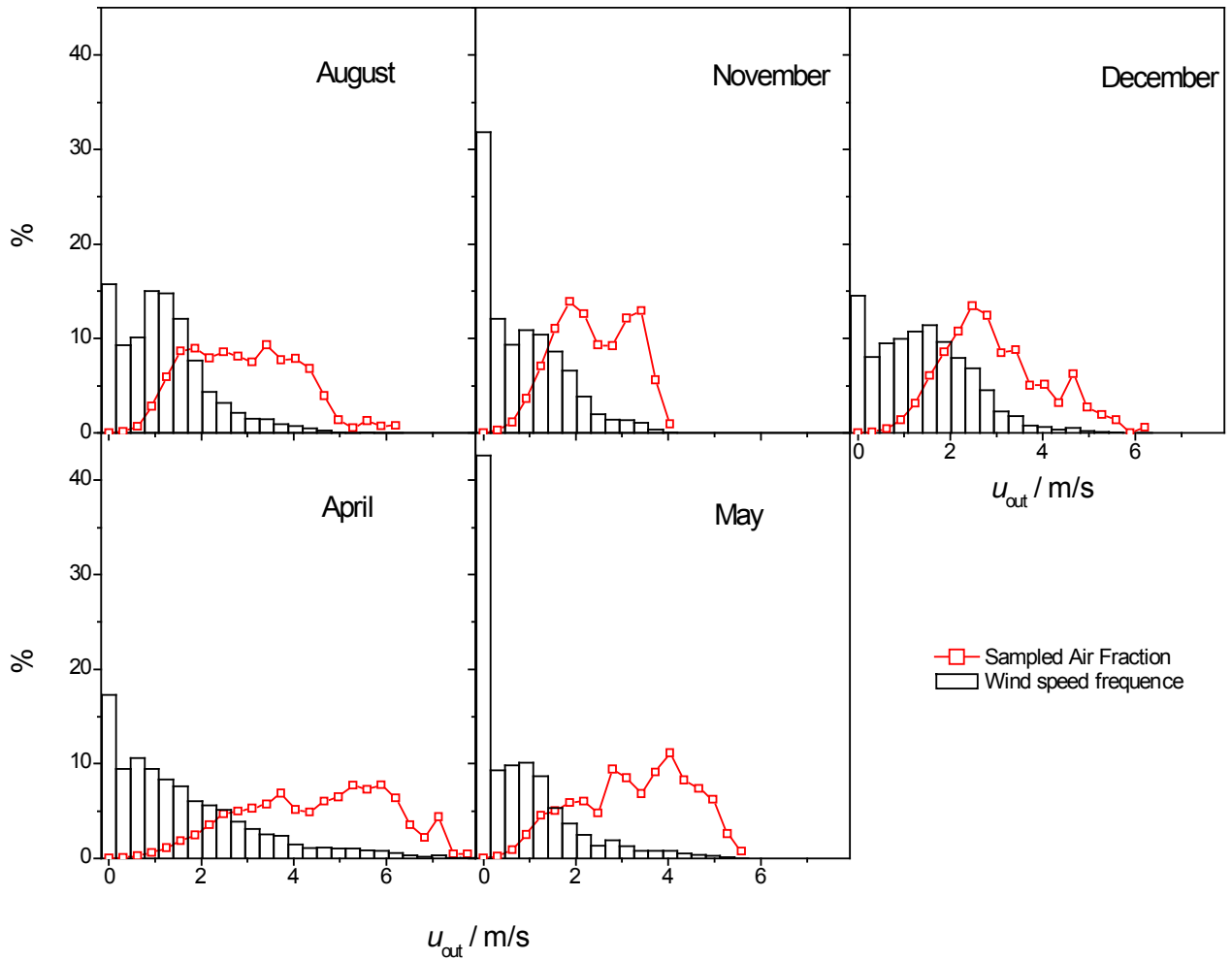


Figure SI 3. Histograms showing the distribution of wind speeds measured by the vortex sensor on top of the FTS during each sampling period. The y-axis is the percentage of time. The red lines represent the percentage of the sampled air volume that was collected while u_{out} was within that particular wind speed range.

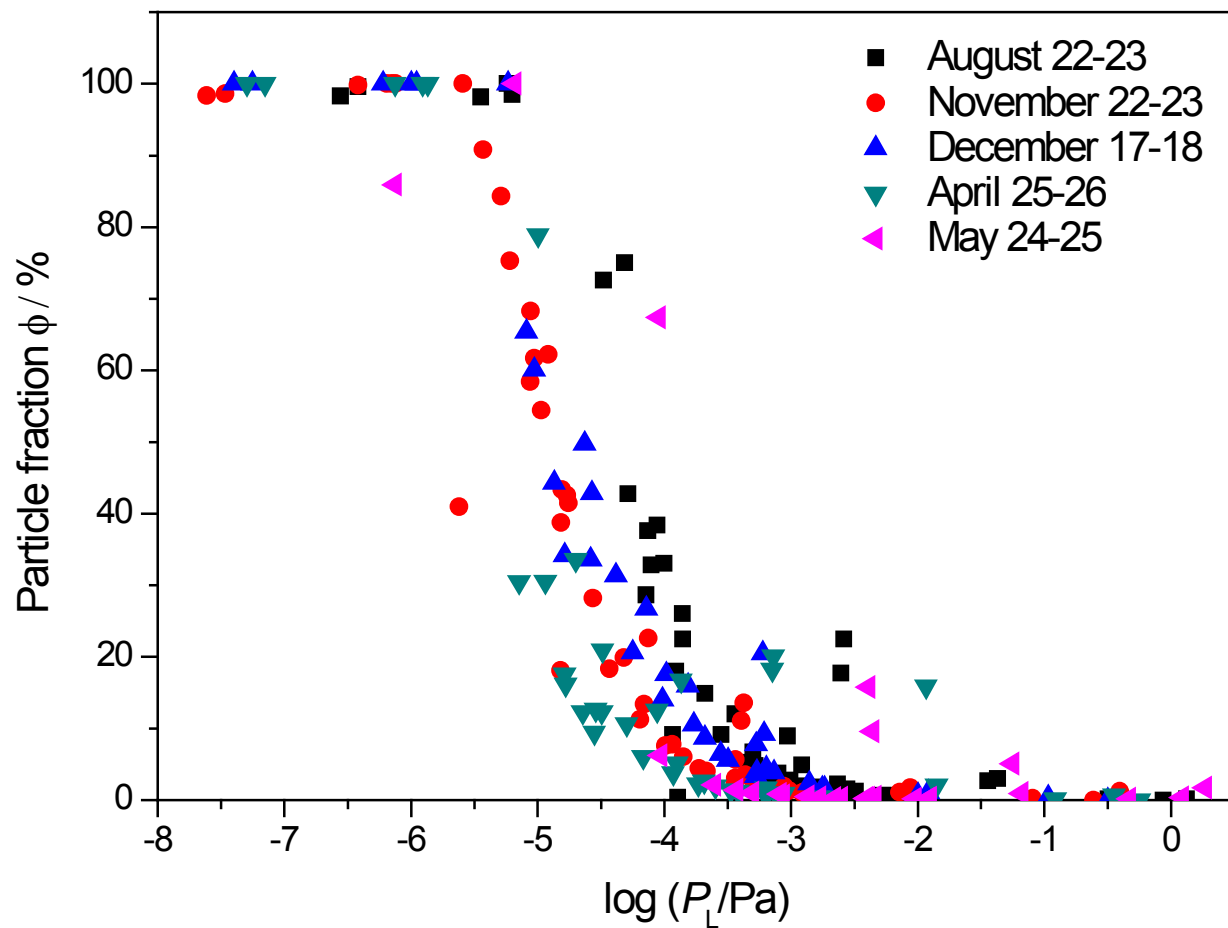


Figure SI 4. Observed gas/particle partition behavior of PCBs and PAHs from selected HiVol samples.

Table SI 5. Field-blank corrected amounts of individual PCB congeners and individual PAHs trapped in each P10z PUF disc in nanograms.

August 11 – 25, 2006							
Congener	PUF-I	PUF-II	PUF-III	PUF-IV	PUF-V	PUF-VI	PUF-VII
PCB-8	5.8	5.3	4.1	3.4	3.2	2.5	2.4
PCB-18	11	7.4	5.3	3.5	2.6	1.5	1.3
PCB-15	4.5	2.2	1.6	1.1	0.76	0.46	0.57
PCB-17	3.1	2.0	1.7	1.0	0.74	0.45	0.43
PCB-16+32	3.4	2.0	1.3	0.67	0.47	0.22	0.33
PCB-31	22	10	5.3	2.4	0.98	0.56	0.74
PCB-28	15	6.9	3.4	1.2	0.95	0.43	0.68
PCB-33	13	5.4	2.5	1.0	0.45	0.24	0.41
PCB-52	330	110	46	18	7.9	2.9	6.0
PCB-49	89	32	13	5.1	2.3	0.87	1.6
PCB-44	160	45	15	5.0	1.8	0.51	2.7
PCB-42	14	3.5	1.2	0.26			0.019
PCB-37	6.1	1.1	0.47				0.23
PCB-74	64	14	3.5	1.2	0.43	0.20	1.2
PCB-70	130	24	5.9	1.7	0.44	0.11	2.4
PCB-66	87	16	4	1.4	0.53	0.20	1.8
PCB-56+60	24	3.8	0.97	0.26	0.056		0.49
PCB-95	370	77	22	6.8	2.4	0.63	7.5
PCB-101	650	120	22	6.6	1.6	0.41	12
PCB-99	170	31	7.7	2.1	0.56	0.14	3.7
PCB-87	260	37	8.1	2.0	0.16		5.7
PCB-81	7.4						
PCB-77	11	1.1			0.23		0.62
PCB-110	450	57	12	3.1	0.59	0.31	9.8
PCB-151	35	4.9	0.99	0.068			0.53
PCB-123	7.1	0.76					
PCB-149	160	21	4.4	1.1	0.24		3.8
PCB-118	220	25	4.6	1.1			4.5
PCB-114	3.7	0.053					
PCB-153	120	14	2.7	0.78	0.11	0.042	2.6
PCB-105	42	4.6	0.66	0.24	0.065		1.1
PCB-137	5.5	0.31					
PCB-138	82	9.1	1.6	0.53	0.030	0.08	1.8
PCB-126	0.94						
PCB-187	9.8	0.67					
PCB-183	5.6	0.40					
PCB-128	23	2.0	0.31				
PCB-185	0.48						
PCB-174	7.0	0.43					
PCB-177	3.9						
PCB-171	2.1						
PCB-156	2.7	0.30					
PCB-157	0.70						
PCB-180	6.2	0.37					
PCB-170	2.7						

November 15 – 29, 2006

Congener	PUF-I	PUF-II	PUF-III	PUF-IV	PUF-V	PUF-VI	PUF-VII
PCB-8	2.2	1.2	0.44				
PCB-18	12	3.4	1.5	0.38	0.076		0.51
PCB-15	5.8						
PCB-17	3.5	1.2	0.58	0.13			0.24
PCB-16+32	3.1	0.76	0.34				0.24
PCB-31	17	3.0	0.95				1.3
PCB-28	10	1.6	0.6				0.76
PCB-33	8.8	1.4	0.41				0.61
PCB-52	210	34	7.3	1.9	0.62	0.69	16
PCB-49	55	8.7	2.1	0.39	0.039	0.26	4.4
PCB-44	91	12	2.5	0.56	0.059	0.17	6.8
PCB-42	5.4	0.62					0.24
PCB-37	3.3						0.18
PCB-74	35	4.3	1.0	0.41	0.31		3.3
PCB-70	72	8.3	1.9	0.69			5.1
PCB-66	42	5.4	1.3				3.2
PCB-56+60	11	1.1	0.11				0.96
PCB-95	190	24	4.7	1.1	0.35	0.53	15
PCB-101	330	38	7.6	1.9	0.73	1.1	23
PCB-99	89	10	1.6	0.34	0.059	0.089	6.0
PCB-87	130	13	2.4	0.23			8.3
PCB-77	3.5						
PCB-110	210	23	4.3	0.93	0.12	0.45	13
PCB-151	16	1.4					0.56
PCB-123	4.5						
PCB-149	74	7.6	1.5	0.14			3.6
PCB-118	100	10	1.7	0.17			4.9
PCB-114	1.4						
PCB-153	53	5.3	0.89	0.032			2.2
PCB-105	19	1.7	0.085				0.91
PCB-137	2.8	0.074					
PCB-138	33	3.6	0.64	0.09		0.13	1.5
PCB-187	4.2	0.085					
PCB-183	2.4	0.060					
PCB-128	9.0	0.69					
PCB-174	3.0						
PCB-177	1.5						
PCB-171	0.60						
PCB-156	0.93						
PCB-157	0.19						
PCB-180	2.3	0.02					
PCB-170	1.2						

December 4 – 18, 2006

Congener	PUF-I	PUF-II	PUF-III	PUF-IV	PUF-V	PUF-VI	PUF-VII
PCB-8	5.6	0.60	1.7	1.4	0.96	0.40	
PCB-18	14	7.1	3.6	2.0	1.0	0.51	0.61
PCB-15	8.3	2.3	1.3	1.4			
PCB-17	3.8	2.1	0.70	0.33	0.18		0.035
PCB-16+32	3.8	1.7	0.63	0.28	0.044		
PCB-31	24	8.4	3.1		0.43		
PCB-28	14	4.0	1.8		0.38		
PCB-33	12	4.5	1.3				0.27
PCB-52	330	96	31	10	3.8	1.7	5.7
PCB-49	87	25	8.4	2.6	0.86	0.40	1.4
PCB-44	150	36	11	3.1	1.0	0.42	2.2
PCB-42	8.4	2.0	0.53				
PCB-37	4.4	0.58	0.061				
PCB-74	63	13	3.6	1.3	0.39	0.30	1.3
PCB-70	130	25	6.3	2.1	0.56	0.34	2.1
PCB-66	72	15	4.5	1.2	0.59	0.41	1.1
PCB-56+60	19	3.6	1.0	0.15			0.6
PCB-95	310	67	19	5.7	1.8	0.91	5.2
PCB-101	570	110	30	8.4	2.9	1.6	9.3
PCB-99	160	32	8.0	2.0	0.57	0.20	2.2
PCB-87	220	41	10	2.7	0.99	0.44	3.6
PCB-81	6.6	0.95	0.35				
PCB-77	6.2						
PCB-110	380	67	17	4.5	1.5	0.84	6.4
PCB-151	25	4.2	0.82	0.038			0.11
PCB-123	4.6	0.60					
PCB-149	120	21	5.6	1.5	0.47	0.25	2.0
PCB-118	180	31	7.5	2.1	0.43	0.13	2.8
PCB-114	3.1	0.49					
PCB-153	90	15	3.7	0.93	0.32	0.082	1.5
PCB-105	35	5.7	1.2	0.015			0.3
PCB-137	4.4	0.56					
PCB-138	59	9.4	2.2	0.55	0.19	0.07	0.89
PCB-187	5.5	0.74					
PCB-183	2.9	0.33					
PCB-128	17	2.4	0.36				
PCB-185	0.11						
PCB-174	3.8	0.40					
PCB-177	1.9						
PCB-171	1.1						
PCB-156	1.9						
PCB-157	0.24						
PCB-180	3.1	0.44					
PCB-170	1.7						

April 13 – 27, 2007

Congener	PUF-I	PUF-II	PUF-III	PUF-IV	PUF-V	PUF-VI	PUF-VII
PCB-8	6.2	2.9	2.0	1.2	0.76	0.19	0.79
PCB-18	11	5.0	2.7	1.4	0.80	0.40	0.54
PCB-15	5.3	1.7	1.2	1.2			
PCB-17	3.0	1.2	0.53	0.26	0.16	0.10	0.095
PCB-16+32	3.2	1.2	0.59	0.2	0.10		0.014
PCB-31	23	7.7	2.0	1.2	0.56	0.17	0.56
PCB-28	13	4.3	0.8	0.31	0.12		0.15
PCB-33	11	3.3	1.6	0.42	0.082		0.23
PCB-52	300	83	29	11	4.4	1.7	7.1
PCB-49	80	22	7.4	3.1	5.9	0.36	2.0
PCB-44	130	33	9.7	3.3	1.1	0.27	3.1
PCB-42	9.0	1.6	0.41				
PCB-37	4.4	0.26					
PCB-74	57	11	2.9	0.93	0.21		2.0
PCB-70	120	22	5.7	1.9	0.63		4.3
PCB-66	69	14	3.7	1.3	1.7		3.6
PCB-56+60	19	3.1	0.62				0.29
PCB-95	300	64	18	6.0	2.0	0.71	8.7
PCB-101	540	100	27	8.6	2.6	1.8	16
PCB-99	150	28	7.1	1.9	0.39	0.11	3.9
PCB-87	210	37	8.6	2.4	0.47	0.25	6.4
PCB-81		0.76					
PCB-77	8.6	0.68	0.055				
PCB-110	370	61	15	4.1	0.88	0.47	12
PCB-151	28	4.5	0.85				0.48
PCB-123	8.7						
PCB-149	130	21	5.3	1.5	0.20	0.21	4.1
PCB-118	180	29	7.2	1.6	0.18		6.0
PCB-114	3.2						
PCB-153	98	16	3.5	0.92	0.13		3.0
PCB-105	35	5.0	0.95	0.015			0.83
PCB-137	4.8	0.22					
PCB-138	64	9.4	2.0	0.43			1.7
PCB-187	7.4	0.75					
PCB-183	4.0	0.33					
PCB-128	19	2.7	0.23				
PCB-185	0.42						
PCB-174	5.6	0.21					
PCB-177	3.2						
PCB-171	1.4						
PCB-156	2.1						
PCB-157	0.61						
PCB-180	4.5	0.21					
PCB-170	2.7						

May 22 – June 6, 2007

Congener	PUF-I	PUF-II	PUF-III	PUF-IV	PUF-V	PUF-VI	PUF-VII
PCB-8	4.3	3.2	2.7	1.6			
PCB-18	10	5.3	3.8	2.1	0.99	0.75	0.54
PCB-15	4.0	2.7	2.2			1.0	
PCB-17	3.0	1.9	1.2	0.66	0.36	0.39	0.33
PCB-16+32	3.3	1.4	0.83	0.44	0.28		
PCB-31	21	6.9	4.0	1.2	0.58		0.83
PCB-28	12	3.9	1.9	0.9	0.34		0.58
PCB-33	11	3.9	1.6				
PCB-52	280	64	26	7.0	1.6	0.95	6.2
PCB-49	75	17	7.6	2.2	0.65	0.40	1.6
PCB-44	130	23	8.7	2.0	0.48	0.28	2.6
PCB-42	8.4	1.5	0.62				
PCB-37	4.3						
PCB-74	51	8.5	3.3	0.79	0.40		1.5
PCB-70	110	14	4.7	1.4	0.44		2.9
PCB-66	63	9.0	3.4	1.1			1.6
PCB-56+60	18	2.1	0.74				0.70
PCB-95	280	42	14	2.9	0.59	0.34	6.7
PCB-101	490	64	20	3.7	0.45	0.23	12
PCB-99	130	18	5.8	1.1	0.12		3.1
PCB-87	190	21	6.6	1.3			4.8
PCB-81	5.5						
PCB-77	8.9	0.78					0.41
PCB-110	330	35	11	1.9	0.11		8.8
PCB-151	26	2.8	0.85	0.068			0.46
PCB-123	4.0	0.41					
PCB-149	120	14	3.8	0.61	0.084		3.1
PCB-118	170	17	4.8	1.1		0.066	4.2
PCB-114	2.9						
PCB-153	94	9.8	2.8	0.41			2.5
PCB-105	32	3.0	0.78				1.0
PCB-137	4.8	0.45					
PCB-138	61	5.9	1.7	0.27			1.5
PCB-187	7.8	0.63					
PCB-183	4.5	0.21					
PCB-128	18	1.7	0.25				
PCB-185	0.39						
PCB-174	6.0	0.43					
PCB-177	3.0	0.013					
PCB-171	1.6						
PCB-156	2.3	0.22					
PCB-157	0.61						
PCB-180	4.7	0.23					
PCB-170	2.7						

August 11 – 25, 2006

Congener	PUF-I	PUF-II	PUF-III	PUF-IV	PUF-V	PUF-VI	PUF-VII
acenaphthylene	10	13	12	10	10	9.7	9.1
acenaphthalene	31	30	29	29	28	30	29
fluorene	140	110	100	96	95	87	79
phenanthrene	1900	630	340	150	75	33	23
anthracene	40	18	9.9	5.0	2.4	1.5	1.3
fluoranthene	750	74	20	6.3	3.3	2.3	5.7
pyrene	380	37	11	4.2	2.7	2.3	3.9
B(a)A	14	4.6	3.3	2.4	2.4	2.0	2.1
chrysene	40	8.1	5.3	3.5	3.1	2.9	3.1
B(a)P	7.0	3.7	2.1	0.87	0.47	0.40	
Indenopyrene	7.9	2.8	1.4	0.13			
B(ghi)P	11	4.0	2.4	0.91	0.83	0.95	0.74

November 15 – 29, 2006

Congener	PUF-I	PUF-II	PUF-III	PUF-IV	PUF-V	PUF-VI	PUF-VII
acenaphthylene	110	84	65	54	47	38	
acenaphthalene	56	47	41	36	32	27	26
fluorene	320	200	120	68	48	26	17
phenanthrene	1300	240	59	16	5.4	2.2	37
anthracene	42	9.5	1.6	0.073			
fluoranthene	370	36	6.9	2.1	1.2	1.1	9.5
pyrene	250	23	4.5	1.5	1.3	0.76	6.8
B(a)A	9.0	0.62					
chrysene	34	3.8	1.4	0.83	0.57	0.53	1.1
B(a)P	1.3						
Indenopyrene	3.4	1.0	0.64	0.56	0.45	0.54	0.30
B(ghi)P	3.8	1.2	1.2	0.98	0.93	0.99	0.64

December 4 – 18, 2006

Congener	PUF-I	PUF-II	PUF-III	PUF-IV	PUF-V	PUF-VI	PUF-VII
acenaphthylene	57	47	45	33	33	33	
acenaphthalene	61	44	46	40	36	36	35
fluorene	300	230	190	120	100	100	69
phenanthrene	1800	630	240	40	14	14	18
anthracene	50	22			0.25	0.25	
fluoranthene	530	100	31	11	3.0	3.0	6.2
pyrene	390	70	21	7.8	2.1	2.1	3.5
B(a)A	22	4.5	2.0	2.6	0.11	0.11	
chrysene	49	10	4.8	4.8	0.83	0.83	0.98
B(a)P	8.9	1.3					
Indenopyrene	14	3.3	1.5	2.7			
B(ghi)P	15	3.7	1.8	1.5	0.20	0.20	

April 13 – 27, 2007

Congener	PUF-I	PUF-II	PUF-III	PUF-IV	PUF-V	PUF-VI	PUF-VII
acenaphthylene	23	16	15	9.2	10	8.2	4.1
acenaphthalene	37	33	33	26	31	27	29
fluorene	190	140	130	98	93	66	69
phenanthrene	1500	670	310	140	68	29	34
anthracene	24	17	6.3	2.8	1.4	0.12	
fluoranthene	530	140	44	25	13	8	12
pyrene	310	84	28	17	9.1	5.9	8.4
B(a)A	38	15	4.8	4.2	2.2	1.0	0.88
chrysene	72	26	11	8.4	5.3	3.3	2.9
B(a)P	28	11	3.1	3.0	1.1		
Indenopyrene	41	16	6.7	5.7	3.2	2.2	1.9
B(ghi)P	39	14	6.6	5.3	3.7	2.8	2.0

May 22 – June 6, 2007

Congener	PUF-I	PUF-II	PUF-III	PUF-IV	PUF-V	PUF-VI	PUF-VII
acenaphthylene	12	10	13	9.6	6.1	6.9	7.8
acenaphthalene	22	19	34	33	25	31	36
fluorene	130	140	220	160	89	100	73
phenanthrene	1500	590	330	100	27	18	34
anthracene	17	11	5.7	1.5			
fluoranthene	450	59	21	5.3	1.9	1.6	9.3
pyrene	210	26	9.5	2.7	0.83	0.73	4.1
B(a)A	11	2.0	0.9	0.42	0.071	0.071	0.14
chrysene	26	3.8	1.9	0.78	0.027	0.087	0.32
B(a)P	7.2						
Indenopyrene	11	0.45					
B(ghi)P	12	1.6	1.1	0.17			

Table SI 6. The theoretical plate number N , and their standard deviation for different sampling periods, and the temperature dependence of $\log P_L$ from references.

Average Temperature in °C	August	November	December	April	May	m_L	b_L
	19.9±4.6	4.7±4.1	2.5±5.6	9.4±5.6	18.3±4.7		
PCB 8	1.01±0.22	3.97±1.64	1.91±0.59	1.58±0.37	1.63±0.59	-3769	11.84
PCB 18	1.48±0.22	4.72±2.09	2.45±0.54	2.29±0.60	1.77±0.40	-3935	12.09
PCB 15	1.22±0.36		3.00±0.83	1.77±0.50	1.02±0.29	-3971	12.18
PCB 17	1.43±0.32	3.59±1.35	4.18±1.12	2.98±0.91	1.73±0.38	-3935	12.05
PCB 16+32	1.85±0.34	5.63±2.95	3.82±1.15	3.31±1.11	2.14±0.58	-3935	11.93
PCB 31	2.67±0.60	9.97±9.24	4.68±1.86	5.13±2.38	3.30±1.07	-4058	12.15
PCB 28	2.78±0.63	10.4±9.8	4.73±1.84	7.11±4.53	3.32±1.08	-4075	12.2
PCB 33	3.08±0.75	11.0±11.7	5.04±2.17	4.52±1.87	4.09±1.74	-4075	12.09
PCB 52	4.01±1.20	12.0±15.0	5.64±2.45	5.45±2.64	6.37±3.35	-4220	12.36
PCB 49	3.95±1.17	11.8±14.2	5.59±2.40	5.09±2.31	6.10±3.06	-4229	12.41
PCB 44	5.78±2.36	14.0±22.1	6.91±3.62	7.05±4.40	8.79±6.34	-4229	12.29
PCB 42	6.55±3.04	18.1±43.5	7.99±2.79	10.5±10.8	9.08±6.79	-4229	12.25
PCB 37	8.63±2.83					-4242	12.33
PCB 74	8.61±3.02	14.5±18.9	8.41±2.93	9.12±3.67	9.35±3.68	-4382	12.56
PCB 70	10.2±4.5	15.5±22.8	9.35±3.72	9.83±4.30	12.0±6.5	-4431	12.6
PCB 66	9.94±4.14	14.1±17.7	8.37±2.87	8.88±3.40	10.9±5.0	-4349	12.38
PCB 56+60	11.3±5.5	17.7±32.0	9.65±3.92	12.5±8.1	13.5±8.5	-4382	12.42
PCB 95	8.32±2.76	14.7±20.0	8.20±2.78	8.30±2.98	10.9±5.2	-4399	12.48
PCB 101	11.4±5.9	16.0±25.3	9.17±3.55	9.45±3.94	12.4±7.0	-4514	12.67
PCB 99	10.3±4.4	16.3±27.0	9.16±3.60	9.61±4.14	12.0±6.5	-4533	12.68
PCB 87	13.2±8.2	17.4±31.4	10.2±4.5	10.9±5.6	14.5±10.4	-4562	12.66
PCB 81			11.5±5.5			-4598	12.88
PCB 110	14.6±8.6	17.3±31.9	10.4±3.5	11.3±6.0	14.5±9.7	-4522	12.43
PCB 151	13.7±7.6		11.9±4.9	12.8±8.6	14.8±11.0	-4681	12.95
PCB 123			16.7±14.4			-4688	12.84
PCB 149	14.0±7.8	17.7±23.9	10.5±3.6	11.0±5.6	14.2±9.8	-4689	12.78
PCB 118	16.3±11.9	18.4±27.9	11.2±4.2	11.8±5.7	14.0±8.8	-4664	12.72
PCB 114			15.6±13.7			-4688	12.82
PCB 153	15.9±11.1	18.7±29.0	11.0±3.9	12.2±6.3	16.0±13.0	-4775	12.85
PCB 105	17.8±16.0		11.7±4.6	14.0±9.2	17.8±17.8	-4758	12.9
PCB 137			17.0±15.0			-4816	12.61
PCB 138	16.9±13.1	17.2±22.9	12.2±5.19	13.1±7.7	17.2±15.8	-4800	12.81
PCB 128	20.9±24.8		19.6±18.2	16.3±15.7	20.2±28.7	-4881	12.91
Acenaphthylene		0.85±0.31	0.55±0.32	1.02±0.26	1.22±1.97	-2855	9.93
Acenaphthalene	0.43±1.57	0.69±0.27	0.27±0.16	0.23±0.17		-2979	10.17
Fluorine	0.32±0.19	2.01±0.58	1.09±0.38	0.80±0.23		-3233	10.61
Phenanthrene	3.07±1.46	10.5±13.7	4.67±2.98	3.15±1.05	3.02±0.71	-3726	11.43
Anthracene	2.43±0.98			5.07±1.45	3.34±0.77	-3780	11.54
Fluoranthene					12.3±10.5	-4382	12.47
Pyrene				5.85±3.28	12.7±11.3	-4164	11.7
B(a)A	1.27±0.43			3.65±1.37	8.21±4.14		
chrysene	4.60±2.62	15.6±34.4	6.28±4.85	3.02±1.01	9.70±5.68	-5294	13.87
B(a)P	2.45±0.97			4.37±1.85		-5252	12.59
Indenopyrene	3.88±2.25	1.57±0.46	1.04±0.34	2.64±0.82		-5691	13.13
B(ghi)P	2.30±0.93	0.70±0.19	4.50±2.71	2.39±0.71	9.87±5.56	-5737	13.15

Table SI 7. Field-blank corrected chemical amounts trapped in HiVol samples in nanograms and their average temperature and sampled air volumes. v_i is the air volumes sampled by the FTS at the same period.

Method	Aug. 22-23			Nov 22-23			Nov 27-28		
		PS2			PS2			PS2	
V/m ³		972			911			972	
T/ °C		17.98			3.14			7.87	
v_i /m ³					2.52 m ³			22.54 m ³	
	GFF	PUF I	PUFII	GFF	PUF I	PUFII	GFF	PUF I	PUFII
PCB 8		27	1.0		28			23	
PCB 18		38			47			46	2.6
PCB 15		20			20			19	
PCB 17		12			15			14	1.9
PCB 16+32		8.8			9.9			7.6	
PCB 31		49			59			64	
PCB 28		36			36			41	
PCB 33		33			33			38	
PCB 52	3.8	830	4.0	8.7	850	4.7	32	870	31
PCB 49	1.1	220	1.0	2.5	210	0.87	6.4	230	5.3
PCB 44	2.2	360	1.7	4.5	330	0.80	9.6	360	4.8
PCB 42	0.19	29		0.37	19			20	
PCB 37		26			17			26	
PCB 74	1.7	130	0.91	3.5	120		11	150	2.7
PCB 70	3.7	270	1.9	7.6	240		16	290	5.3
PCB 66	2.6	160	1.1	5.5	150	0.68	11	190	4.1
PCB 56+60	0.98	42	0.39	2.3	37	1.5		48	0.84
PCB 95	8.6	770	4.1	19	740	1.7	30	800	14
PCB 101	24	1300	8.2	51	1200	3.3	76	1400	26
PCB 99	7.1	350	2.1	14	300	0.73	23	360	6.6
PCB 87	13	470	3.4	26	410	1.2	33	500	9.6
PCB 81	1.0	20							
PCB 77	1.1	11						15	
PCB 110	30	760	6.0	57	670	3.0	62	810	17
PCB 151	2.5	68	0.15	8.4	100		4.6	71	

	GFF	PUF I	PUFII	GFF	PUF I	PUFII	GFF	PUF I	PUFII
PCB 123	0.69	18		2.2	7.6			11	
PCB 149	15	270	1.6	43	330	0.68	26	300	4.8
PCB 118	24	330	2.2	42	270	1.0	40	340	7.8
PCB 114	0.32	6.3			4.5			6.4	
PCB 153	17	170	1.1	46	200	0.56	23	200	3.9
PCB 105	7.2	52	0.48	11	45		10	62	1.2
PCB 137	0.69	6.8		1.3	5.7		1.2	9.2	
PCB 138	17	94	0.79	37	93	1.1	17	110	2.2
PCB 126		2.3							
PCB 187	3.0	14		15	24		2.2	13	
PCB 183	2.2	7.6		8.6	12		1.4		
PCB 128	7.1	20		12	17		7.9	28	
PCB 185	0.010	2.8		1.1	1.5				
PCB 174	3.1	7.6		16	12		2.1	13	
PCB 177	2.0	4.0		9.7	5.9		1.2	15	
PCB 171	1.1	1.8		4.4	2.1		0.81		
PCB 156	1.1	1.8		1.8	1.5			2.4	
PCB 157	0.65	1.3		0.87	0.54				
PCB 180	3.6	4.9		17	5.5		3.1	5.3	
PCB 170	0.94	0.35		9.2	0.93		0.55		
acenaphthylene	0.19	69	19	4.9	260	140	1.6	160	97
acenaphthalene		22	19		120	83		130	110
fluorene	0.69	380	40	3.3	910	370	2.2	820	810
phenanthrene	38	1200	8.9	59	3400	3.6	44	4500	59
anthracene	2.0	69	1.7	5.4	490		4.1	310	
fluoranthene	74	250	3.5	130	1100	1.1	120	1100	2.9
pyrene	67	300	14	130	800	1.2	120	820	4.0
B(a)A	36	7.1	3.1	120	24	0.25	49	28	0.15
chrysene	83	21	6.2	280	51	1.0	280	110	2.1
B(a)P	33	0.63		72	0.15			2.4	
Indeno	58	0.24		150	1.3	0.78		5.5	
B(ghi)P	82	1.1	0.37	170	1.7	1.1		5.7	

Sampling method	Dec. 11 - 12			Dec. 12 - 13			Dec. 17 - 18		
	PS2	PS2	PS2	PS2	PS2	PS2	PS2	PS2	PS2
V/m ³	925			877			932		
T/°C	4.33			4.8			6.06		
v _i /m ³	12.05			24.49			18.70		
	GFF	PUF I	PUFII	GFF	PUF I	PUFII	GFF	PUF I	PUFII
PCB 8		13	4.6		13			8.1	
PCB 18		27			29	4.0		15	
PCB 15		9.6			14			24	3.6
PCB 17		8.4			7.7	1.8		5.8	
PCB 16+32		4.0			6.4	0.77		1.5	
PCB 31		41	1.8		48			23	
PCB 28		24	1.3		27			19	
PCB 33		24	1.1		25				
PCB 52	1.9	560	46	5.1	650	62	5.2	310	12
PCB 49	0.48	150	11	1.3	180	19	1.3	79	
PCB 44	0.97	240	18	2.0	290	21	2.6	110	
PCB 42		14	1.3		19				
PCB 37		14			26			27	
PCB 74	0.74	110	7.6	1.7	140	13	2.0	48	0.37
PCB 70	1.7	200	16	3.3	260	32	4.1	98	1.1
PCB 66	1.3	130	9.7	2.6	180	14	2.7	56	0.82
PCB 56+60	1.5	36	3.2	1.2	54	4.4	1.6	18	0.74
PCB 95	3.3	540	43	7.0	650	49	8.3	240	1.5
PCB 101	9.4	980	74	18	1300	87	24	410	3.0
PCB 99	2.7	270	20	5.5	350	25	7.8	110	0.69
PCB 87	5.7	370	28	11	520	32	14	150	0.94
PCB 81			0.62		13			2.5	
PCB 77		8.5	0.81		16				
PCB 110	14	620	48	24	910	78	30	250	2.2
PCB 151	0.72	51	2.6	1.3	78	5.0	3.6	19	
PCB 123					13				
PCB 149	7.4	220	14	9.6	360	24	13	81	0.54

	GFF	PUF I	PUFII	GFF	PUF I	PUFII	GFF	PUF I	PUFII
PCB 118	16	260	23	19	450	26	24	110	0.56
PCB 114		5.0			11				
PCB 153	8.2	150	9.2	11	270	15	14	54	0.22
PCB 105	4.0	50	3.6	5.7	89	7.9	7.1	19	
PCB 137	0.41	6.0	0.17	0.65	11			2.2	
PCB 138	8.9	87	5.7	11	170	8.8	14	31	
PCB 187	1.5	11	0.24	1.4	29		3.1	3.1	
PCB 183	0.78	6.4	0.080	0.72	14		1.5	2.9	
PCB 128	4.8	21	1.5	5.9	54		6.6	8.8	
PCB 185		0.61			1.7				
PCB 174	1.7	7.0	0.016	1.4	17	0.96	2.0	2.5	
PCB 177	0.97	3.9		0.85	9.4			1.2	
PCB 171	0.39	1.8		0.36	7.7				
PCB 156	0.68	2.1		0.81	7.8		0.36	0.69	
PCB 157	0.14	0.36		0.02					
PCB 180	2.5	6.0		2.5	16		2.2	1.5	
PCB 170	2.5	2.0		2.6	6.7		0.96		
acenaphthylene		14	67		52	28	3.5		
acenaphthalene		8.0	70		43	25		59	81
fluorene	2.1	290	390	4.1	270	140	2.6	320	320
phenanthrene	39	2100	19	77	620	340	42	3800	97
anthracene	2.0	130	0.35	7.4	21	38	3.9	520	11
fluoranthene	81	690	3.7	170	210	59	75	290	1.4
pyrene	65	520	8.4	150	240	300	86	830	12
B(a)A	35	20	0.18	83	22	42	42	14	2.1
chrysene	110	69	0.98	150	72	100	83	38	6.0
B(a)P	34			78			47		
Indeno	130			150			95		
B(ghi)P	110			150	0.46	1.6	110		

Sampling method	April 13-14			April 17-18			April 25-26			April 26-27		
	PS2			PS2			PS2			PS2		
V/m ³	1066			1105			843			949		
T/°C	3.255			7.26			7.43			7.48		
v _i /m ³	45.87			30.77			25.40			51.49		
	GFF	PUF I	PUFII	GFF	PUF I	PUFII	GFF	PUF I	PUFII	GFF	PUF I	PUFII
PCB 8	0.10	17	0.95		13	4.3		41				1.1
PCB 18		30	1.9		27			65			41	
PCB 15		16			10			21			18	
PCB 17		9.8	0.69		9.8			21			12	
PCB 16+32		7.4	0.16		4.6			8.6			8.6	
PCB 31		42	1.7		38			65			62	
PCB 28		25	0.87		23			42			39	
PCB 33		22			21			37			34	
PCB 52	1.9	650	29	1.8	500	3.3	2.3	730	11	1.4	720	
PCB 49	0.67	170	7.5	0.58	140		0.75	200	2.2	0.78	210	
PCB 44	1.0	260	8.0	1.1	200		1.4	290	1.5	1.0	330	0.74
PCB 42		16			13			19			33	
PCB 37		6.2			17			12			18	
PCB 74	1.1	100	3.1	0.68	87		1.1	120	1.1	0.79	160	0.50
PCB 70	2.0	200	7.0	1.5	160	1.4	2.2	220	1.9	1.2	290	0.71
PCB 66	1.5	120	4.8	1.2	100		1.4	140	1.4	0.98	210	0.50
PCB 56+60	0.22	31	0.69	0.37	27		0.63	37		0.40	64	
PCB 95	3.9	550	16	3.0	450	1.7	4.5	610	3.6	2.2	770	1.0
PCB 101	12	910	27	8.9	760	3.1	12	1000	7.3	5.7	1400	2.2
PCB 99	3.7	240	8.2	2.0	200	0.75	3.8	270	2.1	2.0	380	0.57
PCB 87	7.5	320	9.4	4.5	280	0.94	7.0	350	2.9	3.3	570	0.37
PCB 81		6.6			5.8			7.8			15	
PCB 77		7.8			7.6			11			20	
PCB 110	17	530	15	10	470	2.5	16	580	4.8	7.6	1000	1.3
PCB 151	0.88	47	0.92	1.1	44		1.4	60	0.23	0.47	94	
PCB 123	7.4	8.4		6.8	7.9	1.7	2.2	11		3.9	17	
PCB 149	9.2	190	5.1	7.5	170	1.2	8.9	220	1.6	4.1	400	0.60

	GFF	PUF I	PUFII	GFF	PUF I	PUFII	GFF	PUF I	PUFII	GFF	PUF I	PUFII
PCB 118	12	230	6.7	8.1	200	0.69	13	240	2.7	6.2	520	0.87
PCB 114		3.9			3.8			4.4			9.6	
PCB 153	8.4	120	2.8	6.8	120		9.6	150	0.93	4.4	320	0.34
PCB 105	3.6	39	0.57	2.4	37		6.0	42		2.3	100	
PCB 137		5.0		0.23	5.1		0.65	6.2			17	
PCB 138	8.1	69	1.5	5.8	67		9.5	79	0.59	4.8	210	0.24
PCB 187	0.89	11		2.1	11		2.1	14		0.49	30	
PCB 183	0.34	4.9		0.49	5.8		0.99	7.0		0.22	17	
PCB 128	3.7	15		2.2	17		4.6	17		2.5	59	
PCB 185		0.32			0.68			0.84			2.2	
PCB 174	0.98	5.7		1.4	6.7		2.1	9.7		0.57	21	
PCB 177	0.52	3.2		0.64	4.9		0.78	5.6		0.35	13	
PCB 171		1.3			1.7		0.44	2.3			6.7	
PCB 156	0.22	1.6		0.11	1.7		0.81	1.6		0.20	7.4	
PCB 157		0.091			0.21			0.39			2.4	
PCB 180	1.3	3.7		1.4	4.3		2.5	5.6		1.3	19	
PCB 170	0.83	1.2		0.61	2.3		1.2	2.7		1.3	8.3	
acenaphthylene									13			25
acenaphthalene		160	250	3.2	39	50	2.0	62	210		70	48
fluorene	0.86	610	310	1.7	290	200	2.4	750	400	1.9	480	200
phenanthrene	21	1800	110	30	1700	36	52	2500	3.8	23	1900	3.6
anthracene	0.81	43		1.9	78	4.7	3.6	19		0.60		
fluoranthene	38	280	7.1	62	400	11	110	480	0.26	47	440	0.12
pyrene	36	330	8.3	51	570	86	81	320		33	200	
B(a)A	17	3.0		27	17	5.4	47	5.1		11	3.6	
chrysene	44	12	0.097	83	52	13	110	30		35	28	
B(a)P	16			25			44			1.7		
Indeno	44			62			120			32		
B(ghi)P	51			61	0.55		130			30		

Sampling method	May 22 – 23		May 23 – 24		May 24 – 25		May 27 – 28		June 1 – 2		
	PS1		PS1		PS1		PS1		PS1		
	377		299		343		417		412		
T/ °C	14.26		18.02		22.37		15.13		23.9		
v _i /m ³	5.99		1.44		5.02		37.89		5.47		
	GFF	PUF/XAD	GFF	PUF/XAD	GFF	PUF/XAD	GFF	PUF/XAD	GFF	PUFI/XAD	PUFII
PCB 8		7.0		18		16		13		24	1.0
PCB 18		18		35		46		28		57	5.8
PCB 15		3.8		7.0				6.6		15	1.1
PCB 17		5.2		10		13		7.4		17	1.6
PCB 16+32		2.4		8.5		8.3	0.31	6.7		15	1.4
PCB 31		24		44		62	0.59	45		89	3.3
PCB 28		13		22		32	0.40	25		50	0.73
PCB 33		11		21		29	0.51	22		42	1.1
PCB 52	3.8	250	0.69	340	0.92	640	0.64	530	1.2	920	11
PCB 49	1.0	71		96	0.54	190	0.43	160		270	2.8
PCB 44	1.7	110	2.0	140	0.50	270	0.54	250	0.73	400	2.0
PCB 42		7.7		15		22	0.39	20		35	
PCB 37		4.0		5.5		9.1		7.5		15	
PCB 74	0.77	44		58		120	0.50	130		190	0.025
PCB 70	1.6	81	0.64	110	0.73	210	0.74	230	1.0	330	
PCB 66	1.3	53	0.74	72	0.66	150	0.70	170	0.88	240	
PCB 56+60	0.48	15		22		44	0.40	52	0.37	68	
PCB 95	5.9	220	1.0	280	1.5	570	0.86	580	1.6	850	1.3
PCB 101	11	370	2.1	480	3.0	1000	2.1	1100	3.4	1500	0.92
PCB 99	3.1	100	0.59	130	0.73	260	0.77	300	1.2	400	0.20
PCB 87	5.1	140	0.90	180	1.5	370	1.0	490	1.8	580	0.63
PCB 81				5.4		10		13		16	
PCB 77		5.2		7.0		14		19		22	
PCB 110	11	230	2.1	300	3.2	630	2.4	850	3.9	980	0.34
PCB 151	0.84	20		25		63	0.32	73	0.3	89	
PCB 123		2.5				11		16		20	

	GFF	PUF/XAD	GFF	PUF/XAD	GFF	PUF/XAD	GFF	PUF/XAD	GFF	PUFI/XAD	PUFII
PCB 149	5.3	86	1.1	120	2.2	270	1.2	340	3.3	380	
PCB 118	8.1	110	1.7	160	2.0	310	2.4	460		510	
PCB 114		1.6		2.9		5.6		8.4		9.3	
PCB 153	5.9	61	1.3	82	2.1	200	1.4	290	1.9	300	
PCB 105	2.0	20	0.42	27		61	0.72	96	0.91	100	
PCB 137	0.40	2.5		3.7		7.9	0.17	14	0.15	14	
PCB 138	5.7	38	1.2	50	1.7	120	1.5	210	2.0	200	0.12
PCB 187	0.49	5.7	0.18	6.5		20	0.25	28	0.37	29	
PCB 183	0.29					11	0.10	17		17	
PCB 128	2.5	10	0.28	14	0.71	33	0.53	64	0.9	54	
PCB 185		0.13		0.24		1.3	0.04	1.9		2.0	
PCB 174	0.41	3.9		4.2		14	0.20	22	0.20	21	
PCB 177	0.15	2.0		2.1		8.5	0.03	13		12	
PCB 171		1.1		1.2		3.8		8.7		6.2	
PCB 156	0.50	1.2		1.8		3.9	0.26	8.6	0.27	7.2	
PCB 157		0.28				1.6		3.2		3.0	
PCB 180	0.97	3.5	0.37	4.5	0.79	12	0.45	21	0.58	19	
PCB 170	0.68	1.2		2.3		6.3	0.22	13	0.34	9.8	
acenaphthylene	1.0	46	1.7		1.4	79		62	1.9		
acenaphthalene		160	2.0	400	1.7	440		280	12	720	8.7
fluorene	0.58	290	1.4	810	1.7	840	0.40	440	17	1600	41
phenanthrene	9.3	750	22	1600	24	2500	6.8	1200	140	4100	280
anthracene	0.26	22	1.7	36	2	38	0.35	21	11	31	
fluoranthene	18	200	48	340	51	480	13	200	210	720	
pyrene	14	91	37	150	39	210	11	98	150	280	
B(a)A	6.9	1.5	19	5.5	18	3.3	5.3	4.2	72	9.9	
chrysene	14	5.4	37	12	37	18	8.7	11	98	36	
B(a)P	5.6		20		22				76		
Indeno	14	5.7	36	11	47	7.7	18	8.9	100		
B(ghi)P	16		38				22		100		

Sampling method	June 2 - 3		June 3 - 4		June 4 - 5		June 5 - 6	
	PS1	PS1	PS1	PS1	PS1	PS1	PS1	PS1
V/m ³	258	480	480	480	359	359	399	399
T/°C	19.81	17.72	17.72	17.72	15.6	15.6	9.28	9.28
v _i /m ³	1.20	10.49	10.49	10.49	80.29	80.29	63.19	63.19
	GFF	PUF/XAD	GFF	PUF/XAD	GFF	PUF/XAD	GFF	PUF/XAD
PCB 8		9.0		9.0		9.8	1.9	5.6
PCB 18		27		26		22		11
PCB 15		5.5		5.9		6.4		5.7
PCB 17		6.6		7.3		6.3		3.1
PCB 16+32		7.0		7.2		3.5		2.0
PCB 31		42		49		38		15
PCB 28		22		26		19		7.5
PCB 33		19		23		18		8.1
PCB 52	0.64	390	0.87	510	0.81	420	0.57	190
PCB 49	0.39	110		160	0.43	120		50
PCB 44	0.45	170	0.60	260	0.62	190	0.51	76
PCB 42		18		26		16		5.3
PCB 37		6.1		11		7.5		2.7
PCB 74		74		150	0.69	94		31
PCB 70	0.62	130	0.73	250	0.86	170	0.71	58
PCB 66		97	0.67	200	0.93	120	0.65	38
PCB 56+60		27	0.31	65	0.36	37		9.9
PCB 95	0.80	360	1.2	620	1.2	440	0.92	160
PCB 101	1.5	590	1.8	1200	2.7	820	1.8	260
PCB 99	0.44	160	0.75	350	1.0	220	0.66	69
PCB 87	0.71	220	1.2	550	1.5	370	1.2	120
PCB 81		5.1		16		8.5		2.6
PCB 77		8.1		25		13		3.3
PCB 110	1.9	380	2.4	1000	3.5	590	2.3	160
PCB 151	0.13	34		85	0.33	51	0.20	14
PCB 123		8.3		23		9.8		1.7
PCB 149	1.2	150	1.3	410	1.9	240	1.1	61

	GFF	PUF/XAD	GFF	PUF/XAD	GFF	PUF/XAD	GFF	PUF/XAD
PCB 118	2.5	190	2.9	590	4.1	330	1.8	78
PCB 114		3.3		11		5.5		1.2
PCB 153	0.77	120	1.0	380	2.1	190	1.4	46
PCB 105	0.45	37	0.47	130	1.0	63	0.45	15
PCB 137		5.2		19		9.2		2.0
PCB 138	1.0	72	1.1	290	2.0	130	1.2	28
PCB 187		11		39	0.44	18		3.8
PCB 183		6.0		24		11		2.5
PCB 128	0.52	21	0.77	91	0.79	37		7.3
PCB 185		0.56		2.9		1.2		0.092
PCB 174		8.1	0.04	32	0.27	15		2.6
PCB 177		3.5		19	0.16	7.0		1.1
PCB 171		2.0		20		4.4		0.33
PCB 156		2.7	0.20	13	0.23	5.2		0.91
PCB 157		0.82		5.1		1.9		0.12
PCB 180	0.14	7.3	0.23	35	0.57	14	0.30	2.2
PCB 170		3.8	0.15	17	0.24	6.4		0.68
acenaphthylene	0.93	46		25		110		170
acenaphthalene	0.62	220		160	0.62	430		300
fluorene	0.35	670	0.13	430	0.06	530	0.14	330
phenanthrene	9.9	1600	4.4	1200	6.3	1400	6.5	800
anthracene		7.8		21		21	4.0	39
fluoranthene	22	370	7.8	260	12	280	8.9	100
pyrene	16	160	5.7	94	9.1	200	7.9	79
B(a)A	4.7	3.7	1.3	0.58	5.8	4.2	5.0	2.3
chrysene	16	23	3.8	6.9	9.7	12	10	5.9
B(a)P	9.3							
Indeno	25		5.1		16		22	
B(ghi)P	21		5.2		23	1.1	27	

Table SI 8. Average field blanks and LODs in nanograms for different sampling methods and media.

	2/3 of IDL	1-inch P10z PUF blank for FTS	LOD for FTS	GFF blank for HiVol Samples PS1	LOD for GFF PS1	PUF/XAD blank for HiVol samples PS1	LOD for PUF/XAD PS1	GFF blank for HiVol Samples PS2	LOD for GFF PS2	PUF blank for HiVol samples PS2	LOD for PUF PS2
PCB 8	0.12	0.23	0.97			1.0	1.1			0.39	2.7
PCB 18	0.19					0.51	1.9				
PCB 15	0.22										
PCB 17	0.17					0.33	1.0				
PCB 16+32	0.086										
PCB 31	0.10	0.14	0.36								
PCB 28	0.11	0.14	0.32			0.76	0.84				
PCB 33	0.15	0.18	0.38			0.41	1.5				
PCB 52	0.075	0.48	2.11	0.17	0.59	2.5	4.4	0.27	0.83	0.27	0.81
PCB 49	0.15	0.2	0.55			1.0	1.2				
PCB 44	0.078	0.21	0.76			0.45	2.0				
PCB 42	0.12	0.22	0.89								
PCB 37	0.26	0.28	0.38								
PCB 74	0.11					0.72	1.0				
PCB 70	0.060	0.30	1.93							0.085	0.30
PCB 66	0.078					0.47	2.1				
PCB 56+60	0.094					0.33	1.3			0.11	0.26
PCB 95	0.11	0.33	1.32			0.75	1.7			0.18	0.52
PCB 101	0.13	0.52	2.17			1.3	2.9			0.21	0.62
PCB 99	0.17	0.19	0.31			0.33	0.98				
PCB 87	0.21					0.30	0.71				
PCB 81	0.11										
PCB 77	0.11										
PCB 110	0.25	0.44	1.23			0.86	1.4			0.30	0.76
PCB 151	0.11										
PCB 123	0.25										
PCB 149	0.11					0.52	1.5				
PCB 118	0.22	0.29	0.81			0.47	1.5				
PCB 114	0.22										

	2/3 of IDL	1-inch P10z PUF blank for FTS	LOD for FTS	GFF blank for HiVol Samples PS1	LOD for GFF PS1	PUF/XAD blank for HiVol samples PS1	LOD for PUF/XAD PS1	GFF blank for HiVol Samples PS2	LOD for GFF PS2	PUF blank for HiVol samples PS2	LOD for PUF PS2
PCB 153	0.12					0.24	0.78				
PCB 105	0.14										
PCB 137	0.20										
PCB 138	0.070					0.12	0.36				
PCB 187	0.22										
PCB 183	0.15										
PCB 128	0.17										
PCB 185	0.14										
PCB 174	0.15										
PCB 177	0.27										
PCB 171	0.30										
PCB 156	0.076										
PCB 157	0.17										
PCB 180	0.11										
PCB 170	0.24										
acenaphthylene	0.088					0.75	3.6			0.38	2.4
acenaphthalene	0.090			0.47	2.1	9.0	15	0.86	4.1	0.96	4.1
fluorene	0.12	0.54	2.3	0.19	0.32	22	34	0.22	0.62	0.72	3.4
phenanthrene	0.12	2.0	6.1	0.35	0.60	70	120	0.41	1.6	2.6	11
anthracene	0.23	0.23								0.37	1.6
fluoranthene	0.091	0.27	1.1			15	31			0.36	2.2
pyrene	0.089	0.40	2.5			6.8	21			0.58	4.0
B(a)A	0.13	0.15	0.27			0.40	1.5				
chrysene	0.14					0.50	2.0				
B(a)P	1.2										
Indeno	0.56	0.67	1.4			4.8					
B(ghi)P	0.56	0.75	2.0								

Appendix III Supporting Information for Validation of a Flow-Through Sampler for PBDEs and Pesticides in Air

Table SI 9. Field-blank corrected amounts of individual organochlorine pesticides and individual PBDEs congeners trapped in each P10z PUF disc in nanograms.

August 11 – 25, 2006							
Congener	PUF-I	PUF-II	PUF-III	PUF-IV	PUF-V	PUF-VI	PUF-VII
trifluralin	6.64	4.80	3.32	2.04	1.54	0.96	0.66
α -HCH	6.48	3.70	2.24	1.20	0.69	0.36	0.24
HCB	5.45	5.44	5.18	4.80	4.54	4.41	4.01
γ -HCH	4.41	1.31	0.48	0.17	0.06	0.01	
chlorothalonil	318	76.3	27.7	1.39	1.48	0.30	0.26
HEPT	0.20	0.01					
chlorpyrifos	26.6	5.41	1.60	0.53	0.11		
dacthal	9.72	2.22	0.97	0.08	0.09		
pendimethalin	4.77	1.42	0.54	0.19			
TC	2.71	0.59	0.17				
Endo I	136	35.6	11.5	3.74	1.31	0.42	
CC	2.79	0.56	0.13	2.03			
TN	3.03	0.59	0.17	0.07			
dieldrin	4.86						
Endo II	5.98	1.12	0.34				
Endo SO ₄	0.19	0.07	0.00				
November 15 – 29, 2006							
Congener	PUF-I	PUF-II	PUF-III	PUF-IV	PUF-V	PUF-VI	PUF-VII
trifluralin	0.75	0.33	0.12	0.05	0.02		
α -HCH	4.21	1.23	0.30	0.11	0.03		0.03
HCB	9.83	8.86	7.55	6.39	5.38	4.04	3.52
γ -HCH	2.70	0.35	0.06				0.10
chlorothalonil	17.86	1.41	0.97	0.39	0.06	0.44	0.01
HEPT	0.39						
chlorpyrifos	5.18	0.52	0.05				0.01
dacthal	1.94	0.20	0.03	0.00			0.02
TC	1.57	0.22	0.05				0.01
Endo I	7.31	0.72	0.02				
CC	1.46	0.14	0.01				
TN	1.33	0.24	0.05				
dieldrin	1.90						
Endo II	1.45	0.12					
Endo SO ₄	0.24	0.01					

December 4 – 18, 2006

Congener	PUF-I	PUF-II	PUF-III	PUF-IV	PUF-V	PUF-VI	PUF-VII
trifluralin	1.39	0.65	0.33	0.15	0.07	0.04	
α -HCH	5.31	2.55	1.21	0.55	0.27	0.12	0.05
HCB	9.18	9.48	8.65	7.99	7.65	6.90	6.38
γ -HCH	2.99	0.82	0.29	0.09			0.01
chlorothalonil	30.88	4.04	1.55	0.50	0.26	0.06	0.03
HEPT	1.18	0.36	0.18				
chlorpyrifos	4.51	0.59	0.10				
dacthal	1.95	0.26	0.04				0.00
HEPX	2.72						
TC	2.44	0.50	0.15	0.02			0.01
Endo I	8.71	1.36	0.30				
CC	2.27	0.37	0.06				
TN	2.40	0.48	0.13	0.05			0.03
dieldrin	6.68						
Endo II	1.05	0.13	0.01				
o,p'-DDT		5.65					
Endo SO ₄	0.21	0.03					

April 13 – 27, 2007

Congener	PUF-I	PUF-II	PUF-III	PUF-IV	PUF-V	PUF-VI	PUF-VII
trifluralin	3.36	1.06	0.46	0.25	0.13	0.09	0.05
α -HCH	4.59	2.86	1.69	1.02	0.55	0.27	0.23
HCB	8.85	8.69	8.38	7.88	7.87	5.84	6.18
γ -HCH	3.60	1.20	0.45	0.18	0.07	0.02	0.07
chlorothalonil	44.25	11.94	2.61	1.05	0.15	0.16	0.67
metribuzin	0.42						
malathion	3.00						
chlorpyrifos	5.25	0.88	0.26	0.06			0.02
dacthal	36.48	6.44	1.54	0.70	0.45	0.08	0.67
pendimethalin	1.50	0.24	0.32				
TC	2.30	0.63	0.20	0.06			0.01
Endo I	17.61	4.01	1.27	0.35	0.04		0.10
CC	2.25	0.54	0.16	0.04			
TN	2.53	0.70	0.19	0.08	0.03		0.04
dieldrin	4.84						
Endo II	3.23	0.45	0.11	0.03			0.03
Endo SO ₄	0.66	0.11	0.03	0.01			

May 22 – June 6, 2007

Congener	PUF-I	PUF-II	PUF-III	PUF-IV	PUF-V	PUF-VI	PUF-VII
trifluralin	5.08	3.23	2.31	1.11	0.41	0.40	0.27
α -HCH	2.27	1.15	0.74	0.28	0.07	0.05	0.04
HCB	4.62	5.18	6.60	5.06	3.23	4.13	3.92
γ -HCH	3.61	0.90	0.38	0.09			0.07
chlorothalonil	102.49	11.38	5.87	1.01	0.45	1.00	2.38
metribuzin	1.01			0.13	0.77		0.07
malathion	44.35	1.92	0.47				0.52
chlorpyrifos	27.76	3.51	1.22	0.43	0.07	0.08	0.34
dacthal	16.77	2.82	0.96	0.20	0.02	0.00	0.19
pendimethalin	38.05	9.06	3.36	0.93	0.23	0.12	0.32
TC	2.57	0.45	0.12	0.02			0.03
Endo I	53.36	9.30	2.89	0.55	0.06		0.61
CC	2.81	0.41	0.15				
TN	3.03	0.55	0.17	0.05			0.07
dieldrin	7.87	0.16					
Endo II	9.78	0.97	0.26	0.07	0.18	0.02	0.11
Endo SO ₄	0.90	0.09	0.03	0.00		0.02	0.00

August 11 – 25, 2006

Congener	PUF-I	PUF-II	PUF-III	PUF-IV	PUF-V	PUF-VI	PUF-VII
PBDE-28	0.48						0.02
PBDE-47	5.75	2.10	0.48	0.28	0.42	0.25	1.50
PBDE-66	0.12						
PBDE-100	0.70	0.30	0.14	0.03	0.06	0.02	0.17
PBDE-99	2.64	1.08	0.67	0.10	0.10	0.02	0.43
PBDE-85	0.02						
PBDE-154	0.14	0.04	0.04				
PBDE-153	0.22	0.07	0.09	0.04	0.03	0.03	0.04
PBDE-183	0.48						
PBDE-209	7.29						

November 15 – 29, 2006

Congener	PUF-I	PUF-II	PUF-III	PUF-IV	PUF-V	PUF-VI	PUF-VII
PBDE-17	0.09						
PBDE-28	0.12	0.00					0.02
PBDE-47	1.81	0.58	0.30	0.10	0.08	0.79	0.46
PBDE-66	0.04						
PBDE-100	0.17	0.09	0.06	0.02	0.02	0.13	0.07
PBDE-99	0.64	0.41	0.23	0.12	0.10	0.53	0.27
PBDE-154	0.02	0.01				0.01	
PBDE-153	0.02				0.06	0.01	0.01
PBDE-183					0.27		
PBDE-209					0.39		

December 4 – 18, 2006

Congener	PUF-I	PUF-II	PUF-III	PUF-IV	PUF-V	PUF-VI	PUF-VII
	0.08	0.01					
PBDE-28	0.16	0.02	0.00				
PBDE-47	3.31	0.47					0.11
PBDE-66	0.04						
PBDE-100	0.27	0.02					0.00
PBDE-99	0.91	0.09				0.02	0.04
PBDE-154	0.02						
PBDE-153	0.02						
PBDE-183	0.01		0.01				
PBDE-209	2.02	0.49					

April 13 – 27, 2007

Congener	PUF-I	PUF-II	PUF-III	PUF-IV	PUF-V	PUF-VI	PUF-VII
	0.17						0.00
PBDE-28	0.17	0.01					0.03
PBDE-47	3.04	0.32	0.25	0.01		0.14	0.45
PBDE-66	0.06						
PBDE-100	0.26	0.03	0.03	0.00		0.03	0.03
PBDE-99	1.06	0.12	0.10	0.03	0.01	0.15	0.12
PBDE-154	0.04						
PBDE-153	0.04					0.01	
PBDE-209	2.17	0.50	0.04	0.31	0.88		

May 22 – June 6, 2007

Congener	PUF-I	PUF-II	PUF-III	PUF-IV	PUF-V	PUF-VI	PUF-VII
PBDE-28							0.02
PBDE-47	2.41	0.13	0.01	0.44			0.29
PBDE-66	0.05						
PBDE-100	0.22	0.00	0.00	0.08			0.05
PBDE-99	0.74	0.05	0.07	0.50		0.04	0.36
PBDE-154	0.01			0.04			
PBDE-153	0.01			0.15			
PBDE-183				0.68			
PBDE-209	0.80	2.22	2.64	0.07			

Table SI 10. The theoretical plate number N , and their standard deviation for different sampling periods.

	August	November	December	April	May
Average Temperature in °C	19.9±4.6	4.7±4.1	2.5±5.6	9.4±5.6	18.3±4.7
trifluralin	1.82±0.17	4.01±0.76	2.75±0.58	3.80±1.16	2.33±0.52
α-HCH	2.14±0.33	6.65±1.55	2.91±0.48	2.18±0.27	2.56±0.70
HCB	1.33±0.30	1.48±0.12	1.83±0.55	2.27±1.26	
γ-HCH	5.14±1.57		5.82±2.17	4.42±1.10	5.89±2.71
chlorothalonil	6.89±2.31	16.3±13.6	12.2±5.8	7.41±1.73	13.2±8.3
chlorpyrifos	8.55±3.61			10.5±4.9	12.9±6.2
dacthal	6.55±3.23	18.5±10.2		10.4±4.0	9.98±3.99
pendimethalin	5.01±2.25				6.55±2.17
TC	8.39±5.85		8.71±3.66	6.16±2.14	10.5±4.73
Endo I	6.31±2.00			7.45±2.61	9.97±4.18
CC				7.30±3.32	11.4±11.2
TN	9.12±4.86		9.14±3.84	6.50±1.83	9.63±4.90
Endo II	9.53±7.50		20.1±8.4	13.2±6.5	16.8±9.8
Endo SO4	17.4±0.6			10.1±6.0	15.3±10.7
PBDE-28			14.8±9.0		
PBDE-47	3.81±3.53	1.20±1.19			
PBDE-100	2.27±1.41				
PBDE-99	2.59±1.30				
PBDE-153	1.04±0.59				

Table SI 11. Field-blank corrected chemical amounts trapped in HiVol samples in nanograms and their average temperature and sampled air volumes. v_i is the air volumes sampled by the FTS at the same period.

Method	Aug. 22-23			Nov 22-23			Nov 27-28		
	GFF	PUF I	PUFII	GFF	PUF I	PUFII	GFF	PUF I	PUFII
V/m ³									
T/ °C									
v_i /m ³					2.52 m ³			22.54 m ³	
trifluralin	0.04	2.96		0.02	0.78	0.01	0.03	2.77	0.06
α -HCH	0.03	10.23	0.02	0.23	5.39	0.02		6.01	0.24
HCB	0.12	46.39	3.79	0.09	34.83	14.74	0.32	30.23	24.79
γ -HCH		7.74	0.03		13.58		0.13	15.13	0.16
chlorothalonil	0.31			6.35	3.87		41.41	20.81	0.16
HEPT		0.55			1.14			3.41	
malathion				2.24			5.39	0.97	
chlorpyrifos	1.11	4.79		0.72	3.51		1.11	20.72	
dacthal	0.40	0.37		1.14	2.14	0.01	0.40	5.23	
pendimethalin	0.29							1.68	
TC	0.07	1.29		0.24	4.50		0.39	6.30	
Endo I	0.07	7.05		0.51	55.14		2.94	57.30	
CC	0.06	1.16		0.19	3.32		0.37	5.10	
TN	0.07	1.11		0.19	3.15	0.02	0.37	4.78	
dieldrin		1.25			0.97			8.41	
Endo II	0.05			6.36	3.46	0.02	7.09	7.07	0.10
Endo SO ₄				1.94	0.25	0.01	2.31	0.40	0.03

Method	Aug. 22-23			Nov 22-23			Nov 27-28		
V/m ³									
T/°C									
v _i /m ³					2.52 m ³			22.54 m ³	
	GFF	PUF I	PUFII	GFF	PUF I	PUFII	GFF	PUF I	PUFII
PBDE-28					0.13	0.02		0.13	
PBDE-47	2.60	0.80		2.24	2.13	1.20	3.04	9.78	
PBDE-66		0.01			0.03	0.02		0.23	
PBDE-100	0.41			0.49	0.09	0.23	0.37	1.01	
PBDE-99	1.96			2.73	0.47	1.31	7.89	3.32	
PBDE-85	0.06			0.15	0.01	0.03	0.12	0.04	
PBDE-154	0.17			0.25	0.03	0.08	0.72	0.06	
PBDE-153	0.15			0.16	0.04	0.10	0.51		
PBDE-138	0.03			0.06					
PBDE-183	0.13			0.44					
PBDE-209	2.93			2.94	1.84		1.05		

Sampling method	Dec. 11 - 12			Dec. 12 - 13			Dec. 17 - 18		
	PS2	PS2	PS2	PS2	PS2	PS2	PS2	PS2	PS2
V/m ³	925			877			932		
T/ °C	4.33			4.8			6.06		
v _i /m ³	12.05			24.49			18.70		
	GFF	PUF I	PUFII	GFF	PUF I	PUFII	GFF	PUF I	PUFII
trifluralin	0.03	0.91	0.01	0.03	3.60	0.38		0.94	0.02
α-HCH		5.12	0.11		4.48	0.51		2.02	0.07
HCB	0.07	26.12	24.65	0.13	28.55	18.88	0.09	11.00	10.08
dimethoate								3.44	
γ-HCH		10.19	0.28		4.43	0.42		1.37	
chlorothalonil	0.23	14.94		10.98		0.23	0.42	3.46	
metribuzin				0.46					
HEPT		2.53			4.29				
malathion	1.92								
chlorpyrifos	0.30	6.11	0.01	0.90	6.94	0.44	0.63	2.08	
dacthal	0.27	3.03	0.03	0.57	2.06	0.12	0.32	0.60	
pendimethalin	0.41			1.64					
TC	0.16	5.17		0.25	4.10	0.20	0.06	0.58	
op-DDE		0.62							
Endo I	0.66	46.71		0.85	22.85	1.51	0.10	2.47	
CC	0.11	3.84		0.16	3.43	0.15		0.51	
TN	0.15	3.87		0.23	2.89	0.18	0.06	0.55	
dieldrin		5.74			3.19				
Endo II	3.74	5.63	0.02	2.77	2.84	0.19	0.65	0.21	
Endo SO ₄	1.73	0.42		0.99	0.19		0.32		

Sampling method	Dec. 11 - 12			Dec. 12 - 13			Dec. 17 - 18		
PS2									
V/m ³									
T/ °C									
v _i /m ³									
	GFF	PUF I	PUFII	GFF	PUF I	PUFII	GFF	PUF I	PUFII
PBDE-17								0.03	
PBDE-28		0.07						0.11	
PBDE-47	2.94	3.88		3.13	2.05		2.97	0.78	
PBDE-66		0.06			0.02		0.14	0.04	
PBDE-100	0.68	0.09		0.93			0.61		
PBDE-99	3.79	0.08		3.26			4.29		
PBDE-85	0.13			0.19			0.16		
PBDE-154	0.37			0.32			0.29	0.00	
PBDE-153	0.38			0.32			0.32		
PBDE-138	0.06			0.05			0.05		
PBDE-183	0.47			0.29			0.14		
PBDE-209	8.60			4.52	1.11		2.03		

Sampling method	April 13-14			April 17-18			April 25-26			April 26-27		
	PS2			PS2			PS2			PS2		
V/m ³	1066			1105			843			949		
T/ °C	3.255			7.26			7.43			7.48		
v _i /m ³	45.87			30.77			25.40			51.49		
	GFF	PUF I	PUFII	GFF	PUF I	PUFII	GFF	PUF I	PUFII	GFF	PUF I	PUFII
trifluralin		0.97	0.10		2.29	0.10	0.02					0.59
α-HCH		6.44	0.41		6.73	0.17		6.35			6.07	0.07
HCB	0.10	42.55	21.02	0.05	34.36	21.57	0.09	35.89	21.54	0.06	33.22	28.02
dimethoate												0.68
β-HCH											4.12	
γ-HCH		4.07	0.18		7.78			11.02			12.59	
chlorothalonil	0.08	3.20	0.02	0.07	9.55	0.04	9.93	14.96		1.88	12.51	
metribuzin		0.44										0.62
HEPT		0.27			0.49			1.29			3.78	
malathion							11.59					
chlorpyrifos	0.31	1.60		0.07	3.70		0.42	10.66		0.58	23.03	
dacthal	0.78	1.41	0.02	0.15	2.20		1.98	11.62	0.01	1.85	16.81	
pendimethalin							2.31			18.79		
TC	0.12	1.19	0.01	0.04	2.48		0.15	4.34		0.09	7.79	
Endo I	0.88	7.98	0.08	0.24	40.55		1.42	61.75		0.81	91.70	
CC		1.11			2.00		0.15	3.84			6.51	
TN		1.12		0.05	2.01		0.14	3.56		0.11	6.34	
pp-DDE												
dieldrin					3.96						13.29	
Endo II	0.77	0.25		1.53	4.51		8.21	3.63		5.16	14.46	
Endo SO ₄	0.34	0.03		1.02	0.30		2.12	0.22		1.36	0.61	

Sampling method	April 13-14			April 17-18			April 25-26			April 26-27		
	PS2			PS2			PS2			PS2		
V/m ³	1066			1105			843			949		
T/ °C	3.255			7.26			7.43			7.48		
v _i /m ³	45.87			30.77			25.40			51.49		
	GFF	PUF I	PUFII	GFF	PUF I	PUFII	GFF	PUF I	PUFII	GFF	PUF I	PUFII
PBDE-17		0.04										
PBDE-28	0.04	0.09		0.08	0.11	0.00	0.08	0.08				0.06
PBDE-47	1.99	1.83		2.88	4.18	1.03	3.91	3.01		0.98		1.86
PBDE-66	0.04	0.02		0.08	0.06	0.01	0.18	0.03				0.03
PBDE-100	0.31			0.48	0.32	0.27	0.75	0.13		0.20		0.00
PBDE-99	1.47			2.46	0.93	1.50	4.43	0.07		1.00		
PBDE-85	0.04			0.09		0.03	0.19			0.04		
PBDE-154	0.08			0.16		0.06	0.34			0.10		
PBDE-153	0.06			0.16		0.05	0.29			0.15		
PBDE-183	0.06			0.19	0.00		0.36			0.18		
PBDE-209	1.17			1.22			11.62			35.88		

	May 22 – 23		May 23 – 24		May 24 – 25		May 27 – 28		June 1 – 2		
Sampling method	PS1		PS1		PS1		PS1		PS1		
V/m ³	377		299		343		417		412		
T/°C	14.26		18.02		22.37		15.13		23.9		
v _i /m ³	5.99		1.44		5.02		37.89		5.47		
	GFF	PUF/XAD	GFF	PUF/XAD	GFF	PUF/XAD	GFF	PUF/XAD	GFF	PUFI/XAD	PUFII
trifluralin	0.02	4.07	0.02	5.35		2.32		10.11		1.69	0.02
α-HCH		2.19		2.21		2.37		2.88		1.85	0.50
HCB	0.04	20.98	0.05	28.94	0.07	25.14	0.07	23.10	0.05	24.02	0.47
γ-HCH		4.96		4.70		8.18		4.98		8.11	1.30
chlorothalonil	39.69	52.98	10.47	89.23	14.76	247.02	21.91	38.75	6.98	289.02	
HEPT		0.12		0.86		1.25		1.03		1.74	
malathion	5.46		8.18	14.94		69.40		8.01		172.91	
chlorpyrifos	0.14	12.88	68.92	83.59	0.91	141.20	0.64	13.80	0.14	53.63	
dacthal	0.07	3.61	0.14	10.33	0.05	16.33	0.05	16.57	0.07	29.25	
pendimethalin	12.89	6.77	48.18	13.58	2.94	8.46	9.41	30.16		6.85	
TC	0.03	1.26	0.03	1.75		3.33		3.50		5.01	
Endo I	0.51	29.71	0.22	36.40	0.12	80.43	0.07	33.84	0.42	96.52	
CC		1.04		1.70		3.31		3.19		5.13	
TN	0.03	1.02		1.68		3.29		3.64		4.65	
dieldrin				4.19		7.00		14.84		12.75	
Endo II	2.97	4.55	2.26	8.97	0.48	19.59	0.25	5.80	0.83	15.12	
Endo SO ₄	0.94	0.16	0.37	0.61	0.09	1.35	0.09	0.72	0.20	1.30	

	May 22 – 23		May 23 – 24		May 24 – 25		May 27 – 28		June 1 – 2		
Sampling method	PS1		PS1		PS1		PS1		PS1		
V/m ³	377		299		343		417		412		
T/ °C	14.26		18.02		22.37		15.13		23.9		
v _i /m ³	5.99		1.44		5.02		37.89		5.47		
	GFF	PUF/XAD	GFF	PUF/XAD	GFF	PUF/XAD	GFF	PUF/XAD	GFF	PUFI/XAD	PUFII
PBDE-28				12.03				5.54			
PBDE-47	0.41	6.05	0.13	28.62	0.45	9.82	0.04	4.19		13.06	
PBDE-100	0.13	6.57	0.07	10.01	0.08		0.01	1.23	0.02		
PBDE-99	0.83		0.49	1.50	0.78		0.22		0.47		
PBDE-85			0.00		0.04						
PBDE-154	0.06		0.05		0.02				0.05		
PBDE-153	0.06		0.06		0.02		0.01		0.05		
PBDE-183	0.32				0.05		0.04		0.06		
PBDE-209	11.37	1.21	2.45	2.25	3.05		4.78	1.23	1.67	0.84	0.39

Sampling method	June 2 - 3		June 3 - 4		June 4 - 5		June 5 - 6	
	GFF	PUF/XAD	GFF	PUF/XAD	GFF	PUF/XAD	GFF	PUF/XAD
PS1								
V/m ³	258		480		359		399	
T/ °C	19.81		17.72		15.6		9.28	
v _i /m ³	1.20		10.49		80.29		63.19	
trifluralin		5.91		26.95		29.65		2.55
α-HCH		2.12	0.06	2.83		2.45		2.01
HCB	0.03	21.08	0.04	22.18	0.06	28.26	0.06	24.07
γ-HCH		6.91		7.45		3.61		1.35
chlorothalonil	3.18	165.72	0.69	101.45	2.68	47.25	2.25	3.67
metribuzin							0.14	
HEPT		0.62		0.81		0.85		
malathion		31.76		22.80	4.54	7.98	1.14	
aldrin								
chlorpyrifos	1.02	69.82	0.24	115.87	0.19	32.85		4.72
dacthal	0.05	7.12	0.03	10.86	0.07	19.59	0.08	1.22
pendimethalin	7.64	5.21	4.87	9.30	7.75	41.69	2.97	19.25
TC		3.23		4.32		3.24		0.58
Endo I	0.11	127.75	0.16	63.78	0.17	40.60	0.06	7.42
CC		3.42		4.33		3.04		0.54
TN		3.33		3.86		3.33		0.55
dieldrin		5.83		8.04		15.53		
Endo II	0.90	28.64	0.48	19.31	0.63	7.52	0.40	0.59
Endo SO ₄	0.45	2.33	0.39	1.85	0.23	0.99	0.26	0.12

	June 2 - 3		June 3 - 4		June 4 - 5		June 5 - 6	
Sampling method	PS1		PS1		PS1		PS1	
V/m ³	258		480		359		399	
T/ °C	19.81		17.72		15.6		9.28	
v _i /m ³	1.20		10.49		80.29		63.19	
	GFF	PUF/XAD	GFF	PUF/XAD	GFF	PUF/XAD	GFF	PUF/XAD
PBDE-47					5.19		0.05	0.18
PBDE-100							0.05	
PBDE-99	0.15				0.08		0.35	
PBDE-85							0.01	
PBDE-153	0.02		0.01		0.01		0.00	
PBDE-209			0.05		3.74		2.28	

Table SI 12. Average field blanks and LODs in nanograms for different sampling methods and media.

	2/3 of IDL	1-inch P10z PUF blank for FTS	LOD for FTS	GFF blank for HiVol Samples PS1	LOD for GFF PS1	PUF/XAD blank for HiVol samples PS1	LOD for PUF/XAD PS1	GFF blank for HiVol Samples PS2	LOD for GFF PS2	PUF blank for HiVol samples PS2	LOD for PUF PS2
trifluralin	0.02					0.13	0.19				
α-HCH	0.03										
HCB	0.00	0.05	0.11	0.02	0.03	1.48	2.67	0.04	0.07	0.09	0.28
dimethoate	4.43										
β-HCH	0.10										
γ-HCH	0.03					0.07	0.23				
δ-HCH	0.13										
chlorothalonil	0.02	0.03	0.05	0.04	0.06	2.63	4.39	0.06	0.09	0.03	0.07
metribuzin	0.07									0.09	
HEPT	0.24										
malathion	0.27										
aldrin	1.36										
chlorpyrifos	0.09					0.32	0.42				0.11
dacthal	0.03					0.28	0.53			0.03	0.08
pendimethalin	0.12					0.27	0.88				
HEPX	0.15										
TC	0.03					0.06	0.12				
o,p'-DDE	0.86										
Endo I	0.20					0.89	1.67				0.25
CC	0.06										0.28
TN	0.01					0.06	0.14				
p,p'-DDE	2.91										
dieldrin	1.49										
o,p'-DDD	2.56										
Endo II	0.03					0.13	0.26			0.03	0.07
p,p'-DDD	9.41										
o,p'-DDT	7.62										
Endo SO ₄	0.02										

	2/3 of IDL	1-inch P10z PUF blank for FTS	LOD for FTS	GFF blank for HiVol Samples PS1	LOD for GFF PS1	PUF/XAD blank for HiVol samples PS1	LOD for PUF/XAD PS1	GFF blank for HiVol Samples PS2	LOD for GFF PS2	PUF blank for HiVol samples PS2	LOD for PUF PS2
PBDE-17	0.21					1.24	1.41				
PBDE-28	0.24					1.49	2.74				
PBDE-71	0.16										
PBDE-47	0.22	0.74	3.58	4.40	4.61	18.79	35.82	4.45	4.91	2.32	7.27
PBDE-66	0.22									0.40	1.62
PBDE-100	0.12	0.41	1.50	0.38	0.38	2.77	5.46	0.58	0.88	0.46	1.83
PBDE-99	0.17	0.76	1.83	0.74	0.97	8.74	17.24	0.79	1.57	1.66	4.99
PBDE-85	0.16										
PBDE-154	0.11					0.35	0.82			0.30	1.34
PBDE-153	0.09	0.16	0.21							0.30	1.56
PBDE-138	0.25										
PBDE-183	0.07					0.48	0.58				
PBDE-190	0.16										
PBDE-209	1.09					1.29	3.09			0.96	1.83

Table SI 13. Paired sample t-test results for comparing the differences between the FTS concentrations and weighted / unweighted average of HiVol concentrations with zero, which show only May-June concentrations derived from FTS and HiVol are significantly different from each other.

			Mean	Std. Deviation	Std. Error Mean	95% Confidence Interval of the Difference		t	df	Sig. (2-tailed)
						Lower	Upper			
FTS-unweighted average HiVol	November	PBDEs	0.00149	0.00327	0.00109	-0.00102	0.00401	1.36897	8	0.20821
		Pesticides	0.01655	0.04353	0.01124	-0.00756	0.04066	1.47253	14	0.16300
	December	PBDEs	-0.00022	0.00100	0.00031	-0.00093	0.00050	-0.68699	9	0.50940
		Pesticides	0.01050	0.02231	0.00576	-0.00186	0.02285	1.82153	14	0.08996
	April	PBDEs	-0.00151	0.00322	0.00107	-0.00399	0.00096	-1.41192	8	0.19567
		Pesticides	-0.00042	0.01651	0.00401	-0.00891	0.00807	-0.10390	16	0.91854
	May-June	PBDEs	-0.00202	0.00815	0.00308	-0.00956	0.00551	-0.65718	6	0.53544
		Pesticides	0.01745	0.03897	0.00974	-0.00331	0.03822	1.79128	15	0.09344
FTS-weighted average HiVol	November	PBDEs	0.00106	0.00226	0.00075	-0.00068	0.00280	1.40991	8	0.19624
		Pesticides	0.01392	0.04233	0.01093	-0.00952	0.03737	1.27399	14	0.22341
	December	PBDEs	-0.00016	0.00100	0.00032	-0.00087	0.00056	-0.50007	9	0.62903
		Pesticides	0.01098	0.02221	0.00573	-0.00132	0.02328	1.91462	14	0.07620
	April	PBDEs	-0.00159	0.00391	0.00130	-0.00460	0.00142	-1.21961	8	0.25735
		Pesticides	0.00066	0.01643	0.00399	-0.00779	0.00911	0.16577	16	0.87041
	May-June	PBDEs	0.00169	0.00348	0.00116	-0.00099	0.00436	1.45497	8	0.18376
		Pesticides	0.04697	0.07266	0.01817	0.00825	0.08569	2.58552	15	0.02069

Appendix IV Supporting Information for Seasonal Variation of Pesticides and PCBs in the Atmosphere at Nam Co, Tibet

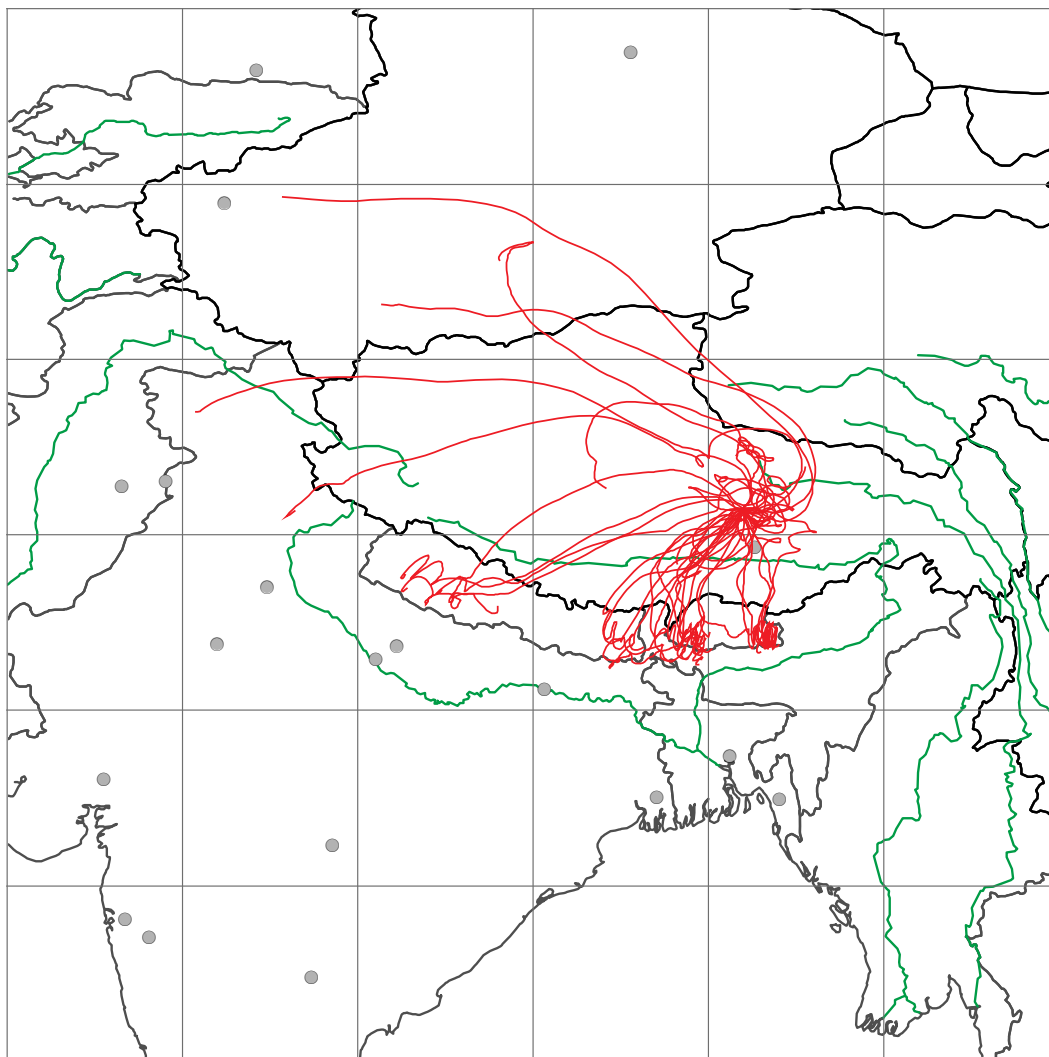


Figure SI 5. Example of a “spaghetti” plot showing 5-day backward trajectory for a FTS sampling period. The percentage of the lines passing through each 0.5×0.5 degree grid cells was calculated from this plot and represents the possibility of the air mass originating from this particular area.

Table SI 14. The meteorological parameters for each flow through sampler.

No.	Sampling period	t/°C	V/m ³	u/(m/s)
1	10.13. 2006-11.12.2006	-6.25	5138	0.226
2	11.13. 2006-12.13.2006	-9.53	12808	0.570
3	12.13. 2007-1.9.2007	-9.36	10061	0.565
4	1.9. 2007-2.10.2007	-11.60	9358	0.412
5	3.17. 2007-4.16.2007	-3.11	11027	0.493
6	4.16. 2007-5.16.2007	0.86	7451	0.345
7	5.16. 2007-6.17.2007	6.75	11603	0.499
8	6.17. 2007-7.17.2007	8.97	11309	0.501
9	7.17. 2007-8.19.2007	8.83	7382	0.301
10	8.19. 2007-9.23.2007	7.16	7680	0.293
11	9.23. 2007-10.21.2007	6.34	12773	0.613
12	10.21. 2007-11.20.2007	-4.32	7911	0.352
13	11.20. 2007-12.21.2007	-7.95	18402	0.789
14	12.21. 2007-1.20.2008	-5.83	21175	0.949
15	1.20. 2008-2.20.2008	-10.71	15442	0.665

Table SI 15. Average field blanks and LODs in nanograms for different chemicals.

	2/3 of IDL	1-inch P10z PUF blank for FTS	3-inch P10z blank for FTS		2/3 of IDL	1-inch P10z PUF blank for FTS	3-inch P10z blank for FTS
trifluralin	0.03	0.06		PCB-8	0.02	0.33	
α -HCH	0.06	0.60		PCB-18	0.03	0.32	
HCB	0.00	0.28	0.06	PCB-15	0.04	0.12	
dimethoate	1.66			PCB-17	0.03	0.24	
β -HCH	0.18	0.52		PCB-16+32	0.01		
γ -HCH	0.10	0.36		PCB-31	0.01	0.43	1.68
δ -HCH	0.23			PCB-28	0.02	0.40	
chlorothalonil	0.15			PCB-33	0.02	0.10	
metribuzin	0.24			PCB-52	0.02		
HEPT	0.08			PCB-49	0.02		
malathion	3.71			PCB-44	0.02	0.08	
aldrin	0.16			PCB-42	0.03		
chlorpyrifos	0.20	0.25		PCB-37	0.05	0.06	
dacthal	0.08			PCB-74	0.03		
pendimethalin	0.08			PCB-70	0.01		
HEPX	0.03			PCB-66	0.02		
TC	0.10			PCB-95	0.02	0.06	
o,p'-DDE	0.36			PCB-56+60	0.01	0.01	
Endo I	0.18			PCB-101	0.04	0.08	
CC	0.21			PCB-99	0.03		
TN	0.16			PCB-87	0.04		
p,p'-DDE	0.31			PCB-81	0.01		
dieldrin	0.70			PCB-110	0.04		
o,p'-DDD	1.39			PCB-77	0.03		
Endo II	0.03		0.04	PCB-151	0.03		
p,p'-DDD	1.03			PCB-123	0.03		
o,p'-DDT	0.63			PCB-149	0.03		
Endo SO ₄	0.02			PCB-118	0.04		
p,p'-DDT	0.50			PCB 114	0.17		
PCB 185	0.14			PCB 153	0.12		
PCB 174	0.15			PCB 105	0.14		
PCB 177	0.27			PCB 137	0.20		
PCB 171	0.30			PCB 138	0.070		
PCB 156	0.076			PCB 187	0.22		
PCB 157	0.17			PCB 183	0.15		
PCB 180	0.11			PCB 128	0.17		
PCB 170	0.24						

Table SI 17. Field-blank corrected amounts of individual pesticides trapped in each P10z PUF disc in nanograms.

No.	1			2			3		
	Front	Middle	Back	Front	Middle	Back	Front	Middle	Back
trifluralin					0.01		0.01	0.01	
α -HCH	64.39	13.54	1.79	22.34	7.46	1.81	6.94	3.23	0.93
HCB	37.93	24.99	8.33	27.09	24.29	6.09	15.03	12.55	4.26
β -HCH	1.34			1.62			0.84	0.2	
γ -HCH	16.24	1.51	0.15	13.69	1.84	0.51	2.87	0.84	0.25
δ -HCH				0.59			0.27		
chlorothalonil	0.27	0.04	0.02	0.11	0.02		0.03		
chlorpyrifos				0.09			0.05		
dacthal	0.03	0.01		0.05			0.02	0.01	
HEPX	0.38			0.58			0.22		
TC	0.11			0.18	0.04		0.08	0.03	
o,p'-DDE	1.41								
Endo I	285.73	21.97	1.55	222.27	27.36	6.25	53.27	11.55	2.69
CC	0.4			0.84	0.11	0.03	0.29	0.1	
TN	0.29			0.49	0.07		0.22	0.05	
p,p'-DDE	1.49			1.68					
Endo II	2.16	0.16	0.03	1.89	0.18	0.06	0.78	0.12	
o,p'-DDT	15.97			10.74			2.89		
Endo SO ₄	1.71	0.17	0.03	2.81	0.27	0.1	1.44	0.34	0.11
p,p'-DDT	8.37	0.87		6.42	0.67		2.1		

No.	4			5			6		
	Front	Middle	Back	Front	Middle	Back	Front	Middle	Back
trifluralin		0.01		0.06	0.01	0.01	0.06	0.03	0.05
α -HCH	12.54	2.2	1.09	9.41	4.92	0.87	30.9	8.76	2.55
HCB	25.8	17.9	7.75	10.79	10.49	3.82	18.02	12.17	6.22
β -HCH	1.65		0.46	0.88			1.42		
γ -HCH	4.73	0.41	0.41	4.07	0.93	0.31	15.33	2.11	0.62
δ -HCH	0.43			0.27			0.29		
chlorothalonil	0.08	0.03	0.02	0.63	0.16	0.03	0.37		
chlorpyrifos	0.13		0.06	0.15			0.36	0.11	0.11
dacthal	0.02			0.05	0.03		0.06	0.06	0.02
HEPX	0.22								
TC	0.11			0.08			0.09		
o,p'-DDE							1.34		
Endo I	70.2	5.09	2.67	36.12	5.66	1.06	181.02	18.61	2.61
CC	0.3			0.23			0.21		
TN	0.19			0.14	0.03		0.2	0.03	
p,p'-DDE							1.14		
Endo II	0.31	0.08		4.46		0.18	3.11		
o,p'-DDT	2.24						24.08		
Endo SO ₄	0.5	0.13	0.06	1.12	0.21	0.09	4.05	0.4	0.12
p,p'-DDT	1.46			1.13	1.64	0.69	10.69	0.98	

No.	7			8			9		
	Front	Middle	Back	Front	Middle	Back	Front	Middle	Back
trifluralin					0.11	0.02			0.02
α -HCH	17.08	19.21	4.68	40.25	25.71	9.03	70.89	25.97	9.14
HCB	8.33	15.1	5.11	16.13	16.7	6.25	22.83	19.71	7.2
β -HCH	1.03			2.19			2.77		
γ -HCH	12.98	7.99	1.61	22.51	8.87	3.21	29.45	4.46	2.18
δ -HCH	0.16			0.4					
chlorothalonil				0.97		0.4	0.14		
chlorpyrifos	0.33	0.19		0.47	1.22	0.2		0.08	0.07
dacthal	0.12	0.04		0.15	0.09	0.04	0.04		
HEPX							0.65		
TC	0.07	0.04		0.14	0.1		0.14	0.03	0.03
o,p'-DDE				3.51			2.83		
Endo I	108.33	39.73	6.68	266.27	52.13	18.17	602.72	59.99	37.44
CC	0.15				0.14				
TN	0.13	0.04		0.36	0.08		0.43	0.04	
p,p'-DDE	1.92			5.06			3.27		
dieldrin		3.25					1.83		
o,p'-DDD	2.37			3.25			2.01		
Endo II	6.47	1.7		9.51			1.69	0.08	0.09
o,p'-DDT	16	1.94		81.54	7.17	3.45	60.94	3.47	3.04
Endo SO ₄	2.53	0.5	0.13	4.23	0.37	0.22	2.74	0.13	0.15
p,p'-DDT	6.86	1.04		43.23	3.09	1.36	24.63	1.13	1.42

No.	10			11			12		
	Front	Middle	Back	Front	Middle	Back	Front	Middle	Back
trifluralin									
α -HCH	72.41	28.4	8.96	66.36	57.22	16.1	14.06	6.8	3.7
HCB	25.85	25.33	7.71	22.92	22.27	6.43	20.71	19.75	5.5
β -HCH	1.05			0.68	0.56		0.74		0.32
γ -HCH	27.08	5.4	2.62	20.58	15.27	4.52	4.04	1.75	1.36
chlorothalonil				0.34	0.17		0.07		
chlorpyrifos							0.1		
dacthal	0.03		0.01						
HEPX	0.51			0.73	0.29		0.32		
TC	0.16			0.16	0.12	0.03	0.07		0.03
o,p'-DDE	3.45			3.31	2.74				
Endo I	795.31	146.32	76.53	703.7	489.73	142.08	105.44	36.82	32.02
CC	0.7			0.77	0.43	0.14	0.38	0.17	0.16
TN	0.4	0.07	0.04	0.33	0.23	0.07	0.23	0.09	0.09
p,p'-DDE	3.25	0.51		6.68	3.06	1.1	0.97		0.63
o,p'-DDD	1.84			3.62	8.39	3.78			
Endo II	2.06	0.23	0.17	5.14	3.13	0.86	1.4	0.4	0.46
p,p'-DDD				2.72	3.19	1.69			
o,p'-DDT	58.76	7.69	6.2	73.84	37.34	8.91	6.19		1.88
Endo SO ₄	3.19	0.4	0.27	2.88	2.12	0.59	1.16	0.34	0.37
p,p'-DDT	24.91	3.07	1.93	46.82	24.88	5.42	5.19	2.06	1.83

No.	13			14			15		
	Front	Middle	Back	Front	Middle	Back	Front	Middle	Back
trifluralin	0.01								
α -HCH	9.67	3.87	1.23	5.58	3.18	1.94	8.31	4.12	1.44
HCB	19.84	15.07	5.46	21.54	23.26	7.19	22.7	21.25	7.25
β -HCH	0.63			0.45			0.5		
γ -HCH	3.1	1.3	0.49	3.45	1.45	1.29	6.33	2.47	1.11
δ -HCH	0.62						0.25		
chlorothalonil		0.04					0.12	0.14	
chlorpyrifos								0.18	
dacthal	0.02	0.01							
HEPX	0.33			0.45			1.08		
TC	0.12	0.05	0.02	0.1	0.04	0.05	0.11	0.07	
Endo I	64.57	23.07	7.25	72.15	22.86	25	97.69	31.6	12.75
CC	0.46	0.27	0.07	0.37	0.15	0.18	0.42	0.15	0.08
TN	0.27	0.11	0.04	0.24	0.08	0.11	0.27	0.1	0.05
Endo II	0.49	0.23	0.06	0.82	0.4	0.39	1.83	0.83	0.36
o,p'-DDT	2.26			4.86			4.08		
Endo SO ₄	0.96	0.36	0.13	1.01	0.48	0.37	8.89	3.86	1.56
p,p'-DDT	2.44	0.7		3.87	1.42	1.86	2.94	1.74	0.9

Table SI 18. Breakthrough corrections for HCB, α -HCH and γ -HCH

HCB

No.	$\log P_L$	V_B	Total Length			First plug			First two plugs			(M+B)/F		B/F		C	ΔC	$\log K_{PUF/A}$
			N_T	b_T	C_T	N_1	b_1	C_1	N_2	b_2	C_2	Pred.	Exp.	Pred.	Exp.			
1	-2.256	14395	2.92	0.01	13.98	1.25	0.25	9.84	2.50	0.02	12.54	32.17	87.85	2.05	21.96	12.12	2.10	8.14
2	-2.420	20462	0.54	0.28	6.26	0.23	0.62	5.60	0.46	0.35	6.15	89.51	112.14	17.06	22.48	6.00	0.36	8.30
3	-2.412	20089	0.55	0.22	4.06	0.24	0.57	3.43	0.47	0.29	3.84	79.06	111.84	15.02	28.34	3.78	0.32	8.24
4	-2.527	25684	1.28	0.05	5.80	0.55	0.37	4.36	1.10	0.09	5.14	49.89	99.42	6.42	30.04	5.10	0.72	8.35
5	-2.102	10350	0.68	0.40	3.81	0.29	0.71	3.36	0.58	0.47	3.63	104.62	132.62	22.50	35.40	3.60	0.23	8.12
6	-1.913	6902	1.33	0.33	7.27	0.57	0.67	7.26	1.14	0.40	6.77	102.04	102.05	22.16	34.52	7.10	0.29	8.05
7	-1.642	3861	0.52	0.71	8.54	0.22	0.87	5.64	0.45	0.75	8.15	126.09	242.62	31.54	61.34	7.44	1.58	7.69
8	-1.542	3121	0.49	0.75	14.05	0.21	0.89	13.18	0.42	0.79	13.67	127.14	142.28	30.90	38.75	13.63	0.44	7.71
9	-1.548	3162	1.38	0.60	16.91	0.59	0.82	17.49	1.19	0.65	16.69	125.36	117.87	30.09	31.54	17.03	0.41	7.77
10	-1.623	3713	1.50	0.56	17.25	0.64	0.80	16.97	1.28	0.61	17.30	124.08	127.81	29.84	29.83	17.17	0.18	7.82
11	-1.660	4018	0.29	0.75	16.39	0.13	0.89	16.19	0.25	0.79	16.55	122.55	125.22	29.67	28.05	16.38	0.18	7.79
12	-2.161	11743	1.45	0.17	6.96	0.62	0.53	5.61	1.24	0.23	6.65	78.83	121.92	14.13	26.56	6.41	0.71	8.15
13	-2.341	17254	0.17	0.59	5.40	0.07	0.80	5.49	0.14	0.64	5.34	106.75	103.48	25.68	27.52	5.41	0.08	8.21
14	-2.235	13764	0.07	0.76	10.20	0.03	0.89	8.94	0.06	0.78	9.57	111.68	141.36	17.33	33.38	9.57	0.63	7.99
15	-2.481	23287	0.34	0.37	5.30	0.15	0.68	4.54	0.29	0.44	5.08	93.47	125.55	20.38	31.94	4.97	0.39	8.30

α -HCH

No.	$\log P_L$	V_B	Total Length			First plug			First two plugs			(M+B)/F		B/F		C	ΔC	log $K_{\text{PUF/A}}$
			N_T	b_T	C_T	N_1	b_1	C_1	N_2	b_2	C_2	Pred.	Exp.	Pred.	Exp.			
1	-1.98	8011	1.37	0.16	18.41	0.59	0.53	26.39	1.17	0.22	19.55	77.51	23.81	14.14	2.78	21.45	4.32	8.12
2	-2.15	11351	0.25	0.55	5.50	0.11	0.78	8.05	0.22	0.61	5.90	107.31	41.50	25.15	8.10	6.48	1.37	8.18
3	-2.14	11146	0.26	0.50	2.20	0.11	0.75	2.78	0.22	0.55	2.24	102.33	59.94	20.54	13.40	2.41	0.32	8.10
4	-2.25	14218	0.60	0.28	2.34	0.26	0.62	3.54	0.51	0.35	2.41	90.84	26.24	18.25	8.69	2.76	0.67	8.30
5	-1.83	5778	0.32	0.65	3.91	0.14	0.84	5.21	0.27	0.69	4.19	115.20	61.53	25.87	9.25	4.43	0.68	7.97
6	-1.64	3868	0.62	0.59	13.83	0.27	0.81	22.04	0.53	0.64	14.89	117.78	36.60	27.82	8.25	16.92	4.47	7.90
7	-1.37	2176	0.25	0.84	21.91	0.11	0.93	21.00	0.21	0.86	22.45	129.94	139.87	31.16	27.40	21.79	0.73	7.54
8	-1.28	1762	0.23	0.86	48.10	0.10	0.94	59.18	0.20	0.88	49.06	129.22	86.31	31.54	22.43	52.12	6.14	7.53
9	-1.28	1785	0.65	0.77	63.11	0.28	0.90	96.65	0.56	0.80	66.92	129.01	49.53	31.66	12.89	75.56	18.37	7.61
10	-1.36	2093	0.70	0.75	56.21	0.30	0.89	84.66	0.60	0.78	59.85	128.34	51.60	31.40	12.37	66.91	15.48	7.68
11	-1.39	2263	0.14	0.86	79.05	0.06	0.94	85.90	0.12	0.88	81.26	128.72	110.49	31.86	24.26	82.07	3.49	7.55
12	-1.89	6548	0.68	0.45	5.61	0.29	0.73	6.64	0.58	0.51	5.38	107.01	74.68	23.84	26.32	5.88	0.67	8.02
13	-2.07	9586	0.08	0.77	3.53	0.03	0.90	5.26	0.07	0.80	3.76	127.54	52.74	31.64	12.72	4.18	0.94	8.01
14	-1.96	7664	0.03	0.86	3.51	0.01	0.95	5.02	0.03	0.88	3.42	173.72	91.76	43.36	34.77	3.98	0.90	7.79
15	-2.21	12903	0.16	0.62	2.36	0.07	0.83	3.12	0.14	0.67	2.42	121.10	66.91	28.05	17.33	2.63	0.42	8.14

γ -HCH

No.	$\log P_L$	V_B	Total Length			First plug			First two plugs			(M+B)/F		B/F		C	ΔC	log $K_{PUF/A}$
			N_T	b_T	C_T	N_1	b_1	C_1	N_2	b_2	C_2	Pred.	Exp.	Pred.	Exp.			
1	-2.65	33542	1.56	0.00	3.49	0.67	0.12	3.60	1.34	0.00	3.47	13.70	10.22	0.30	0.92	3.52	0.07	8.31
2	-2.83	49495	0.29	0.18	1.52	0.12	0.51	2.19	0.25	0.23	1.58	68.19	17.17	10.73	3.73	1.76	0.37	8.53
3	-2.82	48498	0.29	0.14	0.46	0.13	0.47	0.53	0.25	0.18	0.45	61.67	37.98	8.16	8.71	0.48	0.05	8.42
4	-2.95	63646	0.69	0.01	0.60	0.29	0.23	0.66	0.59	0.03	0.57	28.54	17.34	2.36	8.67	0.61	0.05	8.53
5	-2.48	23287	0.36	0.28	0.67	0.16	0.60	0.93	0.31	0.34	0.69	82.58	30.47	15.71	7.62	0.76	0.15	8.37
6	-2.27	14874	0.71	0.18	2.96	0.31	0.54	4.43	0.61	0.25	3.11	76.02	17.81	13.86	4.04	3.50	0.81	8.28
7	-1.97	7824	0.28	0.60	4.91	0.12	0.81	6.01	0.24	0.65	5.18	112.81	73.96	25.29	12.40	5.37	0.57	8.02
8	-1.86	6183	0.26	0.65	8.82	0.11	0.84	12.59	0.23	0.70	9.19	119.48	53.67	28.41	14.26	10.20	2.08	7.98
9	-1.87	6273	0.74	0.43	8.52	0.32	0.72	14.37	0.63	0.49	9.02	106.73	22.55	23.40	7.40	10.64	3.24	8.08
10	-1.95	7492	0.80	0.37	7.28	0.34	0.69	11.24	0.69	0.44	7.56	99.96	29.62	21.78	9.68	8.70	2.21	8.13
11	-1.99	8175	0.16	0.68	9.81	0.07	0.85	10.58	0.13	0.71	9.78	111.55	96.16	23.07	21.96	10.05	0.45	7.95
12	-2.55	26777	0.78	0.07	0.97	0.33	0.38	0.83	0.66	0.11	0.83	50.81	76.98	7.14	33.66	0.88	0.08	8.31
13	-2.74	40986	0.09	0.51	0.54	0.04	0.76	0.70	0.08	0.56	0.55	103.69	57.74	23.00	15.81	0.60	0.09	8.36
14	-2.63	31921	0.04	0.70	0.97	0.02	0.88	1.30	0.03	0.72	0.83	141.63	79.42	17.49	37.39	1.03	0.25	8.16
15	-2.90	57108	0.18	0.26	0.87	0.08	0.60	1.02	0.16	0.33	0.85	83.18	56.56	17.41	17.54	0.91	0.09	8.48

Table SI 19. Concentrations and relative abundance for HCHs, Endosulfans and DDTs.

No.	t/°C	α -HCH / γ -HCH	Σ Endo	Endo SO ₄	α -/ β - Endo	o,p'- DDT	p,p'- DDT	o,p'/p,p'
1	-6.25	6.1	61	0.37	132	3.11	1.80	1.73
2	-9.53	3.7	20	0.25	120	0.84	0.55	1.51
3	-9.36	5.0	7.0	0.19	75	0.29	0.21	1.38
4	-11.60	4.5	8.4	0.07	200	0.24	0.16	1.53
5	-3.11	5.8	4.4	0.13	9		0.31	
6	0.86	4.8	28	0.61	65	3.23	1.57	2.06
7	6.75	4.1	14	0.27	19	1.55	0.68	2.27
8	8.97	5.1	31	0.43	35	8.15	4.22	1.93
9	8.83	7.1	96	0.41	376	9.14	3.68	2.48
10	7.16	7.7	133	0.50	414	9.46	3.89	2.43
11	6.34	8.2	106	0.44	146	9.40	6.04	1.56
12	-4.32	6.7	23	0.24	77	1.02	1.15	0.89
13	-7.95	7.0	5.3	0.08	122	0.12	0.17	0.72
14	-5.83	3.9	5.8	0.09	75	0.23	0.34	0.68
15	-10.71	2.9	10	0.93	47	0.26	0.36	0.73